



From the journal:

MedChemComm

Selected aryl thiosemicarbazones as a new class of multi-targeted monoamine oxidase inhibitors†



[Bijo Mathew](#),  ^{†*a} [Seung Cheol Baek](#),  ^{†b} [Della Grace Thomas Parambi](#), ^c [Jae Pil Lee](#), ^b [Monu Joy](#),  ^d [P. R. Annie Rilda](#), ^a [Rugma V. Randev](#), ^a [P. Nithyamol](#), ^a [Vijitha Vijayan](#), ^a [Sini T. Inasu](#), ^a [Githa Elizabeth Mathew](#), ^e [Krishnakumar K. Lohidakshan](#), ^f [Girish Kumar Krishnan](#) ^g and [Hoon Kim](#) ^{*b}

Author affiliations

* Corresponding authors

^a Division of Drug Design and Medicinal Chemistry Research Lab, Department of Pharmaceutical Chemistry, Ahalia School of Pharmacy, Palakkad-678557, Kerala, India

E-mail: bijovilaventgu@gmail.com

^b Department of Pharmacy and Research Institute of Life Pharmaceutical Sciences, Suncheon National University, Suncheon-57922, Republic of Korea

E-mail: hoon@sunchon.ac.kr

^c Department of Pharmaceutical Chemistry, Jouf University, Al Jouf-2014, Sakaka, Saudi Arabia

^d School of Pure & Applied Physics, M.G. University, Kottayam, Kerala, India

^e Department of Pharmacology, Grace College of Pharmacy, Palakkad, India

^f Department of Pharmaceutical Chemistry, Nirmala College of Health Science, Chalakudy-680311, India

^g Department of Pharmaceutical Chemistry, College of Pharmaceutical Sciences, Government Medical College Trivandrum, India

Abstract

Log in

Using your institution credentials

Sign in

With your membership or subscriber account

Supplementary files

Supplementary information

PDF (669K)

Supplementary information

PDF (368K)

Supplementary information

PDF (780K)

Supplementary information

RTF (57K)

Crystal structure data

CIF (18K)

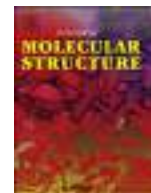
Publication details

The article was received on 14 Aug 2018, accepted on 23 Sep 2018 and first published on 25 Sep 2018



Contents lists available at ScienceDirect

Journal of Molecular Structure

journal homepage: <http://www.elsevier.com/locate/molstruc>

Do hydrogen bonding and noncovalent interactions stabilize nicotinamide-picric acid cocrystal supramolecular assembly?



U. Likhitha ^{a, b}, B. Narayana ^{a, b, *}, B.K. Sarojini ^a, Anupam G. Lobo ^c, Gopal Sharma ^d,
Surbhi Pathania ^d, Rajni Kant ^d

^a Department of Industrial Chemistry, Mangalore University, Mangalagangothri, 574199, India

^b Department of Studies in Chemistry, Mangalore University, Mangalagangothri, 574199, India

^c School of Chemical Sciences, Mahatma Gandhi University, Kottayam, 686560, India

^d Department of Physics, University of Jammu, Jammu Tawi, 180 006, India

ARTICLE INFO

Article history:

Received 21 November 2018

Received in revised form

26 March 2019

Accepted 11 June 2019

Available online 14 June 2019

Keywords:

Crystal structure
Direct methods
Hydrogen bonding
Hirshfeld surface
Molecular dynamics

ABSTRACT

A 1:1 stoichiometric cocrystal of nicotinamide with picric acid ($C_{12}H_8N_5O_8$) has been synthesised successfully by solvent assisted grinding method and structure of the cocrystal is established by single crystal X-ray diffraction studies. The compound crystallizes in the orthorhombic space group *Pbca* with unit cell parameters: $a = 7.7608$ (11), $b = 14.5110$ (14), $c = 24.751$ (3) Å and $Z = 8$. The crystal structure was solved by direct methods and refined to $R = 0.0723$ for 1755 observed reflections. Current study has primarily focused on hydrogen bonding which is the driving force for the formation of cocrystal. Hirshfeld surfaces and fingerprint plots indicate that the structures are stabilized by O...H, N...H intermolecular interactions. In order to make a better understanding supercell model of nicotinamide-picric acid cocrystal (NICPIC) is created with crystallographic data. Based on this hydrogen bonding population, radial distribution function (RDF) and bulk properties are simulated via Molecular Dynamics (MD). Furthermore, DSC/TGA analysis indicates that the NICPIC maintains its crystallinity up to 195 °C, suggesting its higher stability compared to individual components.

© 2019 Elsevier B.V. All rights reserved.

1. Introduction

The cocrystallisation tend to enhance the physicochemical properties of APIs and great impetus is being generated in the recent past. A cocrystal alludes to two or more than two molecules combined into the same crystal lattice via intermolecular interactions such as hydrogen bonding, π - π stacking and van der Waals forces with a fixed stoichiometric ratio, which forms a special multicomponent supramolecular crystal structure [1]. Its extensive applications in pharmaceutical industry were well documented and also attracted much attention in other fields, such

acids were carried out by Fábíán and co-workers. Their investigation resulted that well known acid–aromatic nitrogen heterosynthons would provide sufficient driving force for cocrystallisation [3]. Examples of various cocrystals of nicotinamide with respect to those of pure acids, have also been reported by Kaup et al.

In their work they could control the formation of stoichiometric variations by adjusting the reaction mixture composition using mechanochemical process which in turn helped to manifest the mechanism of formation for the hydrogen bonded cocrystals. Interconvertibility of different stoichiometric variations by liquid assisted grinding was explored by them and it also offered quali-



Reduced Graphene Oxide/ZnO Nanorods Nanocomposite: Structural, Electrical and Electrochemical Properties

Swati Chaudhary¹ · Leo Sam James¹ · A. B. V. Kiran Kumar¹  · CH. V. V. Ramana^{2,3} · D. K. Mishra⁴ · Sabu Thomas⁵ · Daewon Kim²

Received: 7 February 2019 / Accepted: 23 April 2019
© Springer Science+Business Media, LLC, part of Springer Nature 2019

Abstract

The present research work aimed to development of reduced graphene oxide (rGO) and ZnO nanorods based rZN nanocomposite with different molar ratios. This nanocomposite was prepared using a simple, one-step thermal reaction method. The morphology, phase identification and crystalline properties of the nanocomposites were studied using SEM, TEM, SAED and XRD techniques. Further, EDS analysis was used for elemental conformation of the nanocomposite. Films of the nanocomposite were deposited on a substrate by the cost-effective spin coating technique and the resistivity was measured by a Hall measurement system, which shows a decrease in resistivity value. The electrochemical properties studied by measuring the specific capacitance using cyclic voltammetry (CV) and galvanostatic charge–discharge techniques in 3 M KOH solution. These CV studies indicated that the positive synergistic effect of rGO and ZnO nanorods has shown excellent performance. The best results were obtained from the 1:2 ratio of rGO: ZnO, which demonstrated a specific capacitance of 472 F/g, an energy density of 2.62 Wh/kg, and a power density of 32.24 W/kg. These results concluded that rZN nanocomposites are promising electrode materials for supercapacitor applications.

Keywords Zinc oxide (ZnO) nanorods · rGO · Nanocomposite · Hall measurement · Galvanostatic charge–discharge · Hybrid supercapacitor

Electronic supplementary material The online version of this article (<https://doi.org/10.1007/s10904-019-01172-6>) contains supplementary material, which is available to authorized users.

✉ A. B. V. Kiran Kumar
bharanichem@gmail.com

✉ Daewon Kim
daewon@khu.ac.kr

¹ Amity Institute of Nanotechnology, Amity University, Sector-125, Noida 201 303, Uttar Pradesh, India

² Department of Electronic Engineering, Institute for Wearable Convergence Electronics, Kyung Hee University, 1732 Deogyong-daero, Giheung-gu, Yongin 17104, Republic of Korea

1 Introduction

With the increasing modernization and mechanization over the past few years, the demands for energy storage devices for consumer and industrial power management systems also increasing. To counteract these requirements, it is necessary to develop flexible, light-weight, fast charging/discharging, long life cycle, wide operating range, high energy density and environment friendly energy storage devices such as supercapacitors [1–3]. Supercapacitors are considered as one of the efficient among all the energy storage devices such as batteries and capacitors for fast energy storage and delivery applications. Supercapacitors are basically energy storage



Advanced
**Synthesis &
Catalysis**

Accepted Article

Title: RECENT TRENDS IN THE SILVER-CATALYZED SYNTHESIS OF NITROGEN HETEROCYCLES

Authors: Radhakrishnan Sreedevi, Salim Saranya, and Gopinathan Anilkumar

This manuscript has been accepted after peer review and appears as an Accepted Article online prior to editing, proofing, and formal publication of the final Version of Record (VoR). This work is currently citable by using the Digital Object Identifier (DOI) given below. The VoR will be published online in Early View as soon as possible and may be different to this Accepted Article as a result of editing. Readers should obtain the VoR from the journal website shown below when it is published to ensure accuracy of information. The authors are responsible for the content of this Accepted Article.

To be cited as: *Adv. Synth. Catal.* 10.1002/adsc.201900599

Link to VoR: <http://dx.doi.org/10.1002/adsc.201900599>

DOI: 10.1002/adsc.201900599

RECENT TRENDS IN THE SILVER-CATALYZED SYNTHESIS OF NITROGEN HETEROCYCLES

Radhakrishnan Sreedevi^a, Salim Saranya^a, Gopinathan Anilkumar^{a*}

^a School of Chemical Sciences, Mahatma Gandhi University, Priyadarsini Hills P O., Kottayam, Kerala, INDIA 686560;
Email: anilgi1@yahoo.com

((will be filled in by the editorial staff))

Abstract: Heterocycles are generally biologically active compounds and are the main basic scaffolds in many natural and non-natural moieties. Recently, silver-catalyzed syntheses have shown remarkable progress in the field of synthetic heterocyclic chemistry. This review summarizes the recent trends in the silver-catalyzed synthesis of nitrogen-containing heterocyclic compounds.

Keywords: Silver, catalysis, nitrogen-heterocycles.

1 Introduction

Heterocyclic chemistry is one of the most complex and intriguing branches of organic chemistry and constitutes the largest and most varied family of organic compounds. Many broader aspects of heterocyclic chemistry are recognized as disciplines of general significance that impinge on almost all aspects of modern organic chemistry, medicinal chemistry and biochemistry. Derivatives of heterocycles constitute inevitable part of a wide variety of biologically active natural and pharmaceutically important compounds. Development of new strategies for the synthesis of heterocycles has always been a hot research area in organic synthesis. Nitrogen-containing heterocyclic compounds are very important because these are the basic scaffolds in many natural products^[1], pharmaceuticals^[2] and materials of importance^[3].

Transition metal catalysis is an emerging tool in the field of heterocyclic chemistry, where palladium is the

This review focuses on the silver-catalyzed construction of nitrogen-containing heterocycles. To the best of our knowledge, this is the first review exclusively dealing with the synthesis of nitrogen-containing heterocycles by silver-catalysis^[4] covering literature up to 2019; however, a brief discussion on Ag-catalyzed heterocyclic synthesis has been described under the general topic 'Coinage metal-assisted synthesis of heterocycles'^[5].

For simplicity and brevity, the N-heterocycles are categorized based on the size of the ring as well as the number of N atom in the ring.



Accepted Manuscript



Salim Saranya was born in 1990 in Kerala, India. She received her B. Sc. and M. Sc. degrees from Christian College, Chengannur in 2012 and 2014 respectively. She qualified the CSIR-UGC National Eligibility Test in 2015 with a research fellowship and currently pursuing her doctoral research under the guidance of Dr. G. Anilkumar in School of Chemical Sciences, Mahatma Gandhi University.



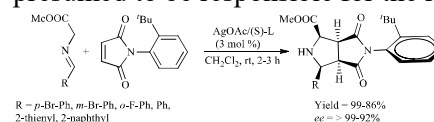
Gopinathan Anilkumar was born in Kerala, India and took his Ph. D in 1996 from Regional Research Laboratory (renamed as National Institute for Interdisciplinary Science and Technology NIIST-CSIR), Trivandrum with Dr. Vijay Nair. He did postdoctoral studies at University of Nijmegen, The Netherlands (with Professor Binne Zwanenburg), Osaka University, Japan (with Professor Yasuyuki Kita), Temple University, USA (with Professor Franklin A. Davis), Leibniz-Institut für Organische Katalyse (IfOK), Rostock, Germany (with Professor Matthias Beller) and Leibniz-Institut für Katalyse an der Universität (LIKAT), Rostock, Germany (with Professor Matthias Beller). He was a senior scientist at AstraZeneca (India). Currently he is Professor in Organic Chemistry at the School of Chemical Sciences, Mahatma Gandhi University in Kerala, India. His research interests are in the areas of organic synthesis, medicinal chemistry, heterocycles and catalysis, particularly on Ruthenium, Iron, Zinc, Copper, Manganese, Cobalt and Nickel catalyzed reactions. He has published more than 75 papers in peer-reviewed journals, 7 patents and one book chapter. He has

2.1 Five membered N-heterocycles

2.1.1. Five membered heterocycles containing one N atom

(a) Synthesis of Pyrroles

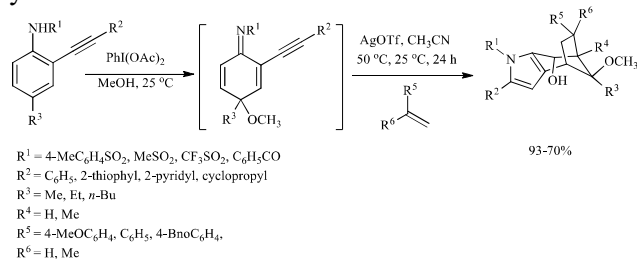
Ag(I)-catalyzed atroposelective desymmetrization of *N*-(2-*t*-butylphenyl)maleimides were reported via 1,3-dipolar cycloaddition of azomethine ylides [6]. This reaction furnishes a series of biologically relevant and enantio-enriched octahydropyrrolo[3,4-*c*]pyrrole derivatives in excellent yields having high levels of diastereo-/enantioselectivities (**Scheme 1**). A model reaction of imino ester and prochiral *N*-(2-*t*-butylphenyl)maleimide using Ag(I)-chiral TF-BiphamPhos complex as the catalyst and Et₃N as the base at room temperature in 0.2 h afforded the desired cycloadduct in good yield and enantioselectivity with excellent diastereoselectivity. After optimizing the reaction conditions, the substrate scope of imino esters was explored and observed that non- α -substituted imino esters having differently substituted phenyl rings, heteroaromatic and fused rings reacted well with *N*-(2-*t*-butylphenyl)maleimide. The formation of a stabilized transition state via hydrogen bonding between the NH₂ group of the chiral ligand and a carbonyl moiety of *N*-(2-*t*-butylphenyl)maleimide is presumed to be responsible for the reaction.



Scheme 1. Substrate scope study of Ag-catalyzed desymmetrization of *N*-(2-*t*-butylphenyl)maleimide.

The sequential multicomponent synthesis of polysubstituted pyrroles via the Hantzsch pyrrole synthesis involving the coupling of α -iodoketone with the aid of high speed vibration milling under solvent-free conditions was reported for the first time [7]. The reaction used ketones, primary amines and β -dicarbonyl compounds as the building blocks with the formation of one C–C and two C–N bonds in the

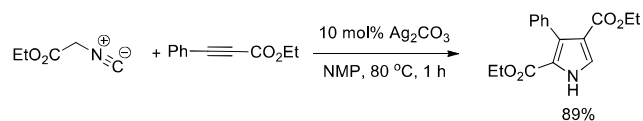
Wang and co-worker developed another Ag-catalyzed strategy for the construction of pyrrole derivatives^[8]. The dearomatization of *para*-substituted *o*-alkynylanilines on furnishes 2-alkynyl cyclohexadienimines, which reacts with electron-rich styrenes (**Scheme 3**). Various protected nitrogen atom of aniline showed different effects on this reaction. Ts and Ms groups showed best results compared to Tf and Bz groups. The presence of aryl groups, thiophene, cyclopropyl, pyridine etc. on alkynyl group tolerated well with this reaction and gave the expected product in moderate to excellent yields.



Scheme 3. Construction of derivatives of pyrroles from *p*-substituted *o*-alkynylanilines.

Martin and co-workers disclosed a protocol for the synthesis of 1,1'-dimethyl-2,2'-bipyrroles using silver promoted cyclization^[9]. This silver-catalyzed cyclization strategy provides a way to access 2,2'-bipyrroles and its derivatives by simply treating it with NBS or NCS or with both.

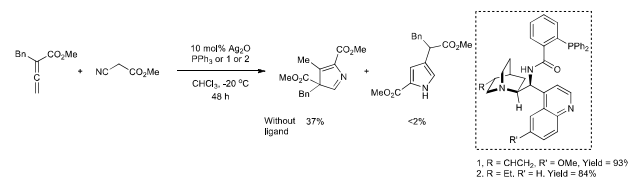
A novel protocol for the synthesis of pyrroles via a [3+2] cycloaddition of isocyanide with alkyne was reported by Lan *et al*^[10]. The reaction of ethyl 2-isocyanoacetate with phenylacetylene in presence of 10 mol% of Ag_2CO_3 in NMP at 80 °C for 1 h delivered ethyl 3-phenyl-1*H*-pyrrole-2-carboxylate in 89% yield (**Scheme 4**).



Scheme 4: Silver catalyzed [3 + 2] cycloaddition of ethyl 2-isocyanoacetate and ethyl 3-phenylpropiolate.

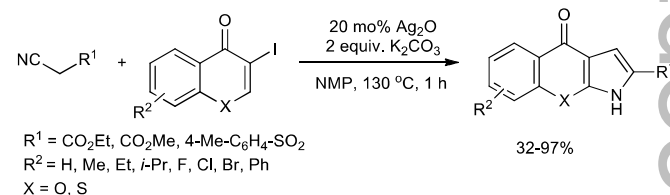
Scheme 5: Competitive experiments between internal alkyne and terminal alkynes with isocyanide for pyrrole synthesis.

The [3+2] cyclization of allenates with activated isocyanides delivered 3*H*- or 1*H*-pyrroles^[11]. The reaction of methyl 2-benzylbuta-2,3-dienoate with methyl 2-cyanoacetate in presence of 10 mol% of Ag_2CO_3 without any ligand afforded 1*H*-pyrrole and 3*H*-pyrrole in 37:<2% yield in 24 h at 0 °C (**Scheme 6**). But when PPh_3 was used as the ligand, the yield increased to 55% with 3*H*-pyrrole as the exclusive product. Further optimization studies disclosed that the yield could be increased to 90% when CHCl_3 was used as the solvent. The cinchona derived alkaloids as ligands were efficient for this protocol yielding 3*H*-pyrroles in good to excellent yields with excellent enantioselectivity.



Scheme 6: Ag-catalyzed synthesis of 1*H*- and 3*H*-pyrroles.

A new protocol for chromeno[2,3-*b*]pyrrol-4(1*H*)-ones using silver catalyst has been reported^[12]. The silver oxide-catalyzed cascade cyclization of ethyl 4-(2-hydroxybenzoyl)-5-iodo-2*H*-pyrrole-2-carboxylate formed from 3-iodochromone and ethyl isocyanoacetate resulted in chromeno[2,3-*b*]pyrrol-4(1*H*)-one in 87% yield (**Scheme 7**). 3-Iodochromone with electron-donating and electron-withdrawing substituents on the aromatic rings gave the corresponding products in good to excellent yields.





Contents lists available at ScienceDirect

Applied Surface Science

journal homepage: www.elsevier.com/locate/apsusc

Full length article

Sol-gel synthesized plasmonic nanoparticles and their integration into dye sensitized solar cells



K.V. Arun Kumar^{a,b}, Arya Balu^{a,b}, Athira Ramachandran^{a,b}, N.V. Unnikrishnan^c, Nivas Babu Selvaraj^{d,*}

^a Department of Physics, C M S College, Kottayam 686001, Kerala, India

^b Nanotechnology and Advanced Materials Research Centre, C M S College, Kottayam 686001, Kerala, India

^c School of Pure & Applied Physics, Mahatma Gandhi University, Kottayam, India

^d Department of Materials and Ceramic Engineering, CICECO – Aveiro Materials Institute, University of Aveiro, Portugal

ARTICLE INFO

Keywords:

Plasmonic nanoparticles

DSSC

Sol-gel

ABSTRACT

In the present study, we synthesized silver nanoparticles in titanosilicate matrix through low cost non-hydrolytic sol-gel method using titanium isopropoxide (TIP), tetraethylorthosilicate (TEOS, $(\text{Si}(\text{OC}_2\text{H}_5)_4)$ and ethanol ($\text{C}_2\text{H}_5\text{OH}$) as solvents. These were investigated for the plasmonic effect of nanoparticles in dye sensitized solar cells (DSSC). The fabricated dye-sensitized solar cells with Ag: SiO_2 - TiO_2 films coated in fluorine doped tin oxide (FTO) glass plate with dye of amaranthus red shows an improved output voltage. The samples were optically and structurally well studied by absorption spectroscopy, Fourier transform infrared spectroscopy (FTIR), X-Ray diffraction (XRD) and transmission electron microscopy (TEM). The XRD studies confirmed the crystalline nature of TiO_2 and Ag.

1. Introduction

Noble metal nanoparticles research has attracted a lot of attention due to a wide range of potential applications in plasmonic solar cells, surface enhanced Raman scattering, surface enhanced fluorescence and metamaterial absorbers to count a few [1–13]. Plasmonics is one of the most important fields that make use of the nanoscale properties of noble metals. It extracts the surface plasmon resonance properties of nanoparticles. In plasmonic solar cells, plasmonic structure excites more electrons due to increased light absorption and scattering and the plasmon-polaritons trapped more incident light within the structure. These factors favor the enhancement of efficiency of plasmonic DSSCs compared to normal DSSCs. [14–17]. Due to increasing energy consumption, there is a great need for new inexpensive sources of renewable energy. Sunlight is plentiful, inexhaustible and eco-friendly source of energy and therefore trapping of solar energy is established as one of the interesting research areas [18–20]. The energy harvesting may be improved by plasmonic nanoparticles (NPs) in two ways (i) by adopting

the plasmonic NPs, and by choosing the right surrounding medium, one can also enhance the aforesaid aspects [21–24]. Further broad band optical absorption has tremendous potential for solar energy harvesting and it is a necessary condition for improving the efficiency of solar cells [25–27]. One of the factors that determines the performance of solar cells is the efficiency of the light absorption process that generates electron-hole pairs, as well as the subsequent extraction of these charge carriers. DSSCs with incorporation of plasmonic nanoparticles are promising alternatives to traditional solar cells [18,28–30]. Recently solar cells such as DSSCs and organic solar cells (OSC) have received promising role for renewable energy exploration due to low cost, simple fabrication techniques, flexibility, and low toxicity. One of the main disadvantages is the lower energy-conversion efficiency compared to other solar cells [31–33].

Researchers have reported many methods for the synthesis of NPs like sol-gel techniques, melt-quenching, ion exchange, ion implantation etc. Sol-gel method is one of the important techniques used for nano scale synthesis and it has several advantages over other methods such as



Contents lists available at ScienceDirect

Journal of Alloys and Compounds

journal homepage: <http://www.elsevier.com/locate/jalcom>

Novel white light emitting dysprosium oxalate nanocrystals: Competing luminescence quenching by the features of Dy-Oxalate layered structure



Dinu Alexander, Kukku Thomas, R.J. Manju Gopinath, Monu Joy¹, P.R. Biju, N.V. Unnikrishnan, Cyriac Joseph*

School of Pure and Applied Physics, Mahatma Gandhi University, Kerala, 686560, India

ARTICLE INFO

Article history:

Received 20 February 2019

Received in revised form

13 June 2019

Accepted 18 June 2019

Available online 21 June 2019

Keywords:

Nanostructured materials
Rare earth alloys and compounds
Crystal structure
Optical properties
Luminescence

ABSTRACT

Novel white light emitting dysprosium oxalate nanocrystals were prepared via microwave assisted coprecipitation method and the photoluminescence characteristics were elucidated on the basis of crystal structure. X-ray powder diffraction and transmission electron microscopy analyses were employed to identify the structure and morphology of the synthesized nanocrystals. Under 364 nm excitation dysprosium oxalate nanocrystals emit blue (480 nm), yellow (572 nm) and red (655 nm) light with chromaticity co-ordinate (0.35, 0.39) which lies in the near white light region. The efficient luminescence exhibited by dysprosium oxalate negating the probable luminescence limiting factors is further investigated by single crystal structure analysis. The crystal structure of dysprosium oxalate facilitates well separated Dy³⁺ centres thereby minimizing the energy migration between the luminescent centres, allowing higher concentration of Dy³⁺ ions in oxalate matrix without substantial luminescence quenching. The other crystallographic features promoting the luminescence emission of Dy³⁺ in oxalate matrix are also discussed in detail in view of the structural features.

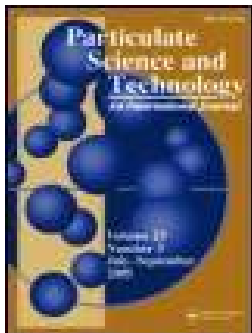
© 2019 Elsevier B.V. All rights reserved.

1. Introduction

Rare earth based phosphor materials have assumed a key role in lighting and display devices due to their characteristic sharp emission lines originating from 4f–4f transitions spanning over the entire visible region. They became an indispensable component of white light emitting diodes (WLEDs) in which suitable combinations of near ultra violet (NUV) excitable blue, green and red emitting phosphors are employed [1–4]. Even though tri-colour WLEDs have fairly good colour rendering index, the luminescence efficiency is relatively low due to the re-absorption of blue light. Moreover, fabricating a single illuminating system with multiple

are the features of single component white light emitting phosphors [6,7].

Trivalent dysprosium (Dy³⁺) ion is a promising candidate to achieve white light emission more easily due to its intra configurational 4f⁹ → 4f⁹ transitions yielding strong emission lines in the blue, yellow and red spectral regions corresponding to the transitions ⁴F_{9/2} → ⁶H_{15/2}, ⁴F_{9/2} → ⁶H_{13/2} and ⁴F_{9/2} → ⁶H_{11/2} respectively. Among these, intensity of the electric dipole transition (⁴F_{9/2} → ⁶H_{13/2}) strongly depends on crystalline field of the host lattice. Therefore by the proper choice of host lattice and concentration of Dy³⁺, the intensity ratio (yellow to blue) can be controlled and tune the emission colour of the material to white region. Recent reports



Particulate Science and Technology

An International Journal



ISSN: 0272-6351 (Print) 1548-0046 (Online) Journal homepage: <http://www.tandfonline.com/loi/upst20>

Green synthesis of silver nanoparticles using *Nervalia zeylanica* leaf extract and evaluation of their antioxidant, catalytic, and antimicrobial potentials

Remya Vijayan, Siby Joseph & Beena Mathew

To cite this article: Remya Vijayan, Siby Joseph & Beena Mathew (2018): Green synthesis of silver nanoparticles using *Nervalia zeylanica* leaf extract and evaluation of their antioxidant, catalytic, and antimicrobial potentials, *Particulate Science and Technology*, DOI: [10.1080/02726351.2018.1450312](https://doi.org/10.1080/02726351.2018.1450312)

To link to this article: <https://doi.org/10.1080/02726351.2018.1450312>



Published online: 03 May 2018.



Submit your article to this journal 



View related articles 



View Crossmark data 



Green synthesis of silver nanoparticles using *Nervalia zeylanica* leaf extract and evaluation of their antioxidant, catalytic, and antimicrobial potentials

Remya Vijayan^a, Siby Joseph^b, and Beena Mathew^a

^aSchool of Chemical Sciences, Mahatma Gandhi University, Kottayam, Kerala, India; ^bDepartment of Chemistry, St. George's College, Aruvithura, Kottayam, Kerala, India

ABSTRACT

Here we report a simple, one-pot, inexpensive, and eco-friendly method for the synthesis of silver nanoparticles. The leaf extract of a medicinal plant *Nervalia zeylanica* was used as reducing and stabilizing agent for the synthesis of nanoparticles by microwave-assisted strategy. The nanoparticles show characteristic surface plasmon peak at 468 nm in UV-vis absorption spectrum. The involvement of phytochemicals in the reduction and stabilization of nanoparticles was confirmed by FTIR analysis. Using X-ray diffraction analysis, the crystalline nature of the nanoparticles was demonstrated. Transmission electron microscopic analysis shows that the nanoparticles were in spherical shape with average particle size of 34.2 nm. The antioxidant studies were performed by the 1,1-diphenyl-2-picryl hydrazyl method. The nanoparticles show excellent scavenging activities than the leaf extract. The IC₅₀ values of silver nanoparticles and the leaf extract, respectively, were 15.20 and 92.83 µg mL⁻¹. The catalytic activities of synthesized nanoparticles were examined by using them in the reduction of organic dyes. The nanoparticles show excellent catalytic activities and follow pseudo-first-order kinetics. The antimicrobial activities of nanoparticles were analyzed by an agar well diffusion method against six microbial strains and found that the nanoparticles were highly toxic against all the tested microbial strains.

KEYWORDS

Antimicrobial; antioxidant; catalysis; microwave; *Nervalia zeylanica*; silver nanoparticles

1. Introduction

Nanotechnology is one of the latest and emerging areas of research in modern material science. Nanoparticles exhibit new and superior properties than their larger counterparts. They have unique physical and chemical properties and major use in various fields such as medicine, biology, biotechnology, magnetic, catalysis, electronics, chemistry, physics, material sciences, optoelectronics, optics, and sensors (Li et al. 2003; Cruz et al. 2010; Ahmed et al. 2016; Varadavenkatesan, Selvaraj, and Vinayagam 2016; Keshavamurthy, Srinath, and Rai 2017).

Because of the wide application in various fields, silver nanoparticles (AgNPs) occupy special importance in nanotechnology industry (Shukla et al. 2012; Nayak et al. 2016). Researchers use different methods such as chemical, physical, electrochemical, photochemical, and biological techniques for producing silver nanoparticles (Sun et al. 2002; Yin et al. 2003; Zhang et al. 2008; Alias Antonysamy et al. 2017). Most of these methods are quite expensive or potentially hazardous to the

several biomolecules act as reducing and protecting agents. Biosynthesis of silver nanoparticles can be done using microorganisms (Shahverdi et al. 2007; Nanda and Saravanan 2009; Saravanan and Nanda 2010) and plant extract (Joseph and Mathew 2015a; Francis et al. 2017a; Kasithevar et al. 2017a; Vijayan, Joseph, and Mathew 2017a). Since microbe-mediated synthesis requires highly aseptic conditions and its maintenance, its use in industry is limited. Using plant extracts for the synthesis of nanoparticles is advantageous than others, because, it is rapid, less biohazards (Prakash et al. 2013), and eliminates the complicated process of maintaining the cell cultures. If plant-mediated biosynthesis performed in normal conditions, it will take more time than chemical methods. The microwave-assisted synthesis overcomes this problem. In microwave synthesis method, heat energy can be directly applied to the reaction and heating the vessel is not required. This leads to a fast rise in temperature, faster reaction, and clean product formation (Roberts and Strauss 2005; Kappe and Dallinger 2006). Microwave synthesis is eco-friendly as it does not produce



Contents lists available at ScienceDirect

Electrochimica Acta

journal homepage: www.elsevier.com/locate/electacta

Influence of MOF ligands on the electrochemical and interfacial properties of PEO-based electrolytes for all-solid- state lithium batteries



Deepa Elizabeth Mathew^{a, c}, Sivalingam Gopi^{a, c}, Murugavel Kathiresan^{a, c},
A. Manuel Stephan^{a, c, *}, Sabu Thomas^{b, **}

^a CSIR- Central Electrochemical Research Institute, Karaikudi, 630 003, India

^b International and Inter University Centre for Nanoscience and Nanotechnology, Mahatma Gandhi University, Kottayam, 686560, Kerala, India

^c Academy of Scientific and Innovative Research (AcSIR), CSIR-CECRI Campus, Karaikudi, India

ARTICLE INFO

Article history:

Received 4 February 2019

Received in revised form

20 May 2019

Accepted 26 June 2019

Available online 27 June 2019

Keywords:

All-solid- state lithium batteries

Composite polymer electrolyte

Metal organic frameworks

Interfacial properties

ABSTRACT

Magnesium-1,4-benzenedicarboxylic acid (Mg-TPA) and magnesium- 1,3,5-benzene tricarboxylic acid (Mg-TMA) MOFs were synthesized and successfully incorporated in a poly (ethylene oxide) (PEO) matrix as filler for different proportions of LiN(CF₃SO₂)₂ (LiTFSI) as salt. The membranes prepared were thermally stable up to 360 °C. The ionic conductivity of the polymer electrolytes was enhanced upon addition of MOF and a maximum conductivity of $7.02 \times 10^{-4} \text{ S cm}^{-1}$ was achieved for CPE containing 10 wt % of Mg-TPA as filler. The interfacial properties of the CPEs with lithium metal anode were analysed by compatibility, Fourier transform infrared (FT-IR) and XPS analyses. Li/NCPE/Li symmetric cells were assembled and the dendrite growth was also studied. The lithium transference numbers (t_{Li^+}) was measured as 0.58 and 0.52 for the CPE containing Mg-TPA and Mg-TMA, respectively which is appreciable for battery applications. The influence of different organic ligands on the electrochemical and interfacial properties of solid polymer electrolytes was investigated and discussed.

© 2019 Elsevier Ltd. All rights reserved.

1. Introduction

Although lithium-ion batteries (LIBs) were commercialized in 1991 by Sony, Japan for consumer electronics (e.g. laptop, mobile) their applications in hybrid electric vehicles still require improvements in terms of energy density, cycle life and better safety [1,2]. LIBs also face critical safety issues since it contains organic liquid electrolytes which have low thermal stability and flash point that lead to poor safety issues [3]. In order to overcome these challenges, new types of solid electrolytes with better safety, excellent flexibility and outstanding electrochemical properties are being

electrolyte by solid polymer electrolytes (SPE) in conjunction with Li- metal anode [4]. Although inorganic solid electrolyte possesses high thermal stability the poor electrode/electrolyte contact hampers it from practical application [5,6]. Obviously, by virtue of its advantages, SPEs have been identified as a potential candidate for all-solid-state lithium batteries. The basic requirements for solid polymer electrolyte are; (i) high ionic conductivity ($10^{-4} \text{ S cm}^{-1}$ at ambient temperature) with negligible electronic conductivity, (ii) appreciable mechanical integrity and compatibility with electrodes and (iii) chemical and electrochemical stability. However, identifying a SPE with appreciable ionic conductivity at ambient tem-



Contents lists available at ScienceDirect

Sensors and Actuators B: Chemical

journal homepage: www.elsevier.com/locate/snb

Polypyrrole based core-shell structured composite based humidity Sensor operable at room temperature



B. Chethan^a, H.G. Raj Prakash^a, Y.T. Ravikiran^{b,*}, S.C. Vijayakumari^c, S. Thomas^d

^a Department of Physics, VTU Research centre, JNN College of Engineering, Shivamogga, Karnataka, India

^b Department of PG Studies and Research in Physics, Government Science College, Chitradurga, Karnataka, India

^c Department of Physics, SJM College of Arts, Science and Commerce, Chitradurga, Karnataka, India

^d International and Inter University Centre for Nanoscience and Nanotechnology, Mahatma Gandhi University, Kottayam, Kerala, India

ARTICLE INFO

Keywords:

Polypyrrole
Tantalum pentoxide
Mechanical mixing
Humidity sensing response
Limit of detection
Linearity

ABSTRACT

The present work explores the humidity sensing performance of core-shell structured Polypyrrole/Tantalum pentoxide (PTO) composite. For the study, Polypyrrole (PPy) prepared by chemical oxidative polymerization was mixed mechanically with different mass ratios of Tantalum pentoxide (Ta_2O_5) to form four PTO composites. The compositional properties of PTO composites were studied by FTIR and XRD techniques. The SEM and TEM morphological studies revealed core-shell structures of the composites. For the sensing studies, the film of PPy and each of PTO composites were prepared by implanting each sample on a glass plate using simple spin coating technique. Of all the samples prepared, the PTO-4 composite, as an epitome of near perfect sensing, has shown humidity sensing response of 99.99% and has recorded a good response and recovery times of 6 s and of 7 s respectively. It has also recorded a good real sensitivity, limit of detection (LOD), linearity, hysteresis and has shown good sensing stability over a period of two months. As compared to PPy, the porosity, water content and degree of swelling of PTO-4 composite has remarkably enhanced. The humidity sensing mechanism of the composite has been discussed as due to the formation of chemisorption and physisorption layers followed by capillary condensation process.

1. Introduction

In a modern world, the demand for smart technical devices like humidity sensors has correspondingly increased and so they are gaining economical importance in the field of medical industry, food production and storage industry, meteorological industry, agriculture, libraries, museums, nuclear power plants [1,2]. The Industrially fabricated humidity sensors devised using established sensing materials such as ceramics, alumina thin films and metal oxides are less advantageous because of the stumbling blocks such as high power consumption, more complexity in device fabrication, high operating temperature and high cost [3,4]. To prevail over these disadvantages, conducting polymer based sensors were developed which have many advantages like simple fabrication, room temperature operability, hygroscopicity and possibility of miniaturization [5-6]. Also, the electrical and mechanical prop-

and in chemical sensors [8] because of its special transport properties, great workability, low cost and light weight [9]. However, with all the aforementioned favorable properties of pure PPy, humidity sensors based on it need to be improved in many ways; water adsorption capacity needs to be improved to enhance their sensitivity, response and recovery time need to be shortened to increase their efficiency [10,11].

In this direction, PPy/metal oxide based sensors are being extensively studied by many researchers. Among them, some are reviewed here: W. Delin et al. have synthesized and examined sensing response of PPy/Graphene composite in the RH range of 12 to 90%, and have reported 82% sensing response with response time of 15 s and recovery time of 20 s respectively [12]. R. Najjar et al. have studied the sensing properties of the PPy/ZnO composite and have accounted a sensing performance of 98% with response time of 180 s and recovery time of 60 s [13]. PPy/Zinc Oxide has shown a sensing performance of 46% in



Contents lists available at ScienceDirect

Materials Science & Engineering C

journal homepage: www.elsevier.com/locate/msec

Yttrium oxide nanoparticle loaded scaffolds with enhanced cell adhesion and vascularization for tissue engineering applications

Robin Augustine^{a,b,*}, Yogesh B. Dalvi^c, Yadu Nath V.K.^d, Ruby Varghese^c, Varun Raghuveeran^{e,f}, Anwarul Hasan^{a,b}, Sabu Thomas^{d,g}, Neelakandapillai Sandhyarani^f

^a Department of Mechanical and Industrial Engineering, College of Engineering, Qatar University, Doha 2713, Qatar

^b Biomedical Research Center, Qatar University, Doha 2713, Qatar

^c Pushpagiri Research Centre, Pushpagiri Institute of Medical Sciences, Tiruvalla, Kerala 689 101, India

^d International and Inter University Centre for Nanoscience and Nanotechnology, Mahatma Gandhi University, Kottayam, Kerala 686 560, India

^e MIMS Research Foundation, Malabar Institute of Medical Sciences (Aster MIMS), Kozhikode, Kerala 673016, India

^f Nanoscience Research Laboratory, School of Materials Science and Engineering, National Institute of Technology Calicut, Kozhikode, Kerala 673 601, India

^g School of Chemical Sciences, Mahatma Gandhi University, Kottayam, Kerala 686 560, India



ARTICLE INFO

Keywords:

Yttrium oxide
Tissue engineering
Electrospinning
Angiogenesis
Cell adhesion

ABSTRACT

In situ tissue engineering is emerging as a novel approach in tissue engineering to repair damaged tissues by boosting the natural ability of the body to heal itself. This can be achieved by providing suitable signals and scaffolds that can augment cell migration, cell adhesion on the scaffolds and proliferation of endogenous cells that facilitate the repair. Lack of appropriate cell proliferation and angiogenesis are among the major issues associated with the limited success of *in situ* tissue engineering during *in vivo* studies. Exploitation of metal oxide nanoparticles such as yttrium oxide (Y_2O_3) nanoparticles may open new horizons in *in situ* tissue engineering by providing cues that facilitate cell proliferation and angiogenesis in the scaffolds. In this context, Y_2O_3 nanoparticles were synthesized and incorporated in polycaprolactone (PCL) scaffolds to enhance the cell proliferation and angiogenic properties. An optimum amount of Y_2O_3 -containing scaffolds (1% w/w) promoted the proliferation of fibroblasts (L-929) and osteoblast-like cells (UMR-106). Results of chorioallantoic membrane (CAM) assay and the subcutaneous implantation studies in rats demonstrated the angiogenic potential of the scaffolds loaded with Y_2O_3 nanoparticles. Gene expression study demonstrated that the presence of Y_2O_3 in the scaffolds can upregulate the expression of cell proliferation and angiogenesis related biomolecules such as VEGF and EGFR. Obtained results demonstrated that Y_2O_3 nanoparticles can perform a vital role in tissue engineering scaffolds to promote cell proliferation and angiogenesis.

1. Introduction

There has been a steady progress in translating various approaches in tissue engineering to produce viable and functional tissue engineered constructs [1]. Bioactive polymeric tissue engineering scaffolds that display bioactivity, biodegradability and cytocompatibility are being developed to generate such functional engineered tissues [2]. However, the clinical translation of traditional methods of tissue engineering has relatively been slow due to the difficulties associated with the use of

using a cell free scaffolding technique which reduces the cost and labour associated with *in vitro* cell culture. A key challenge in such *in situ* tissue engineering approaches is the lack of rapid formation of functional vascular bed through the scaffolds to ensure the survival of migrating and proliferated cells within the scaffolds [7]. Lack of vascularization in tissue engineering scaffolds can result in insufficient cell integration within the scaffolds or cell death [8]. Use of growth factors in scaffolds can significantly enhance cell proliferation and angiogenesis. However, the low stability of growth factors *in vivo*, their short

Contents lists available at [ScienceDirect](https://www.sciencedirect.com)

Progress in Organic Coatings

journal homepage: www.elsevier.com/locate/porgcoat

Review

Bio-epoxy resins with inherent flame retardancy

Elaheh Rohani Rad^a, Henri Vahabi^{b,c,*}, Agustin Rios de Anda^d, Mohammad Reza Saeb^{b,c,*}, Sabu Thomas^{e,**}

^a Faculty of Health and Medical Sciences, The University of Adelaide, SA, Adelaide, Australia

^b Université de Lorraine, CentraleSupélec, LMOPS, F-57000 Metz, France

^c Laboratoire Matériaux Optiques, Photoniques et Systèmes, CentraleSupélec, Université Paris-Saclay, 57070, Metz, France

^d Institut de Chimie et des Matériaux Paris-Est, UMR 7182 CNRS – Université Paris-Est Créteil Val-de-Marne, 2, rue Henri Dunant, 94320 Thiais, France

^e School of Chemical Sciences, MG University, Kottayam 686560, Kerala, India



ARTICLE INFO

Keywords:

Bio-based epoxy resin
Flame retardancy
Thermoset composites
Flame retardants

ABSTRACT

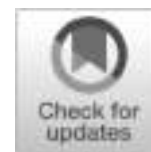
Nowadays, roughly 90% of worldwide epoxy resin materials are made from diglycidyl ether of bisphenol A (DGEBA). This resin offers unique features such as outstanding mechanical properties, chemical resistance, and shape stability. By contrast, the growing awareness of environmental issues, global warming, and depletion of petroleum reservoir suggest search for using bio-epoxy resin from sustainable resources. Indeed, DGEBA is a petroleum-based monomer obtained from bisphenol A and epichlorohydrin, two potential precursors harmful for the environment and human health as well. The problem deepens when it comes to the high flammability of such materials, which restricts their use in strategic applications. Although the introduction of flame retardant (FR) additives to epoxy matrices has been a major strategy to induce flame retardancy, negative impact on mechanical properties and migration of FRs to the materials' surface remained unresolved issues. Tailoring epoxy chains with chemically bonded reactive flame retardants to epoxy resins would be the solution to avoid migration of FRs to surface, along with protecting mechanical properties of resin. With the rapid development of reactive bio-based FRs and epoxy resins, production of flame retardant bio-epoxy with high biomass content has become a promising strategy to address these issues. This concise review encompasses latest progress in flame retardant bio-epoxy resins made of different resources, with inherent chemical structures of either epoxy monomers or embedded reactive flame retardant elements.

1. Bio-epoxy versus conventional petroleum-based epoxy

Epoxy resins offer versatile integrated features such as outstanding mechanical properties, chemical resistance, and shape integrity in harsh conditions. These properties are the result of a crosslinked 3D network obtained by the chemical reaction between an epoxy monomer and a curing agent [1,2]. The use of epoxy thermosets has been surged over the last decade in a wide range of applications such as coatings, adhesives, solar cells, electronic apparels, as well as in automotive and aerospace industries [3,4]. Such applications are expected to receive more attention in the near future. Petroleum-based diglycidyl ether bisphenol A (DGEBA) accounts for ca. 90% of the epoxy resin worldwide usage. This monomer is produced from the reaction between bi-

properties, the use of epoxy monomers brings about some problems [6] summarized as follows:

- (I) It has been proved that DGEBA has severe effects on living organisms due to the toxicity of BPA [7]. Since BPA has been involved in the manufacture of many products, especially in epoxy resin thermosets, concerns about exposure to high dosages of BPA seems harmful for human life. Given this, legislation in many countries has banned the use of BPA in infant-related products [8].
- (II) From an economic point of view, as DGEBA is derived from petroleum, it has experienced a rise in raw materials prices that have had a negative effect on the market.
- (III) CO₂ emission from fossil fuels is the major suspect for recent global



Bioprospecting of Three Rapid-Growing Freshwater Green Algae, Promising Biomass for Biodiesel Production

Prasanthkumar Santhakumaran¹ · Santhosh Kumar Kookal² · Linu Mathew³ · Joseph George Ray³ 

Published online: 6 June 2019

© Springer Science+Business Media, LLC, part of Springer Nature 2019

Abstract

Discovery of high-yielding microalgae rich in valuable lipids, proteins, pigments, or carbohydrates is essential to the growth of nutraceutical and biofuel industries. Therefore, bioprospecting of microalgae from diverse environmental conditions has become highly significant to meet the demand of such bioresources globally. In this context, bioprospecting of three species of microalgae isolated from bloomed freshwaters of Kerala, India, was carried out; morphological and molecular characterizations revealed two of the algae as new species to science and named accordingly. The industrial potentials of these algae (*Fasciculochloris boldii* (MH992105.1), *Sphaerocystis antoni-kadavilaii* Ray & Prasanth sp. nov. (MK005299.1), and *Chlorella zachariaii* Ray & Prasanth sp. nov. (MH930447.1)) were assessed in terms of biomass yield and biochemical profile. The alga *Sphaerocystis antoni-kadavilaii* with a biomass yield of $176.8 \pm 2.0\%$ increase $L^{-1} day^{-1}$, lipid productivity of $4.4 \pm 0.3 mg L^{-1} day^{-1}$, the protein content of 46.1%, is found promising, in comparison with the known species such as *Spirulina* sp. and *Chlorella* sp. It is high in chlorophyll *a*, and total carotenoid content as well. The alga *Fasciculochloris boldii* showed high lipid content of $26.8 \pm 1.1\%$ and the alga *Chlorella zachariaii* showed 30.1% of omega-3 fractions in its total fatty acids. The Fourier transform infrared spectroscopy confirmed biodiesel feasibility of lipids from all these algae. However, the alga *Fasciculochloris boldii* with high proportions of saturated fatty acids in its lipid (71.2%) can be considered as a potential species for biodiesel as the biodiesel from the same also shows the required cetane number (63.3) and low iodine value (38.9).

Keywords Microalgae · Bioprospecting · Proteins · Nutraceuticals · Lipids · Biofuel

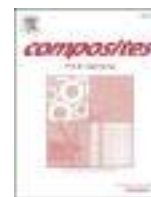
Introduction

Global warming is an unprecedented kind of developmental crisis in the history of human survival on the earth. There are three challenging measures for solving the crisis, which includes finding alternate better energy sources, taking measures for not increasing the existing atmospheric carbon level, and searching for means to reduce the same. All three measures are quite interlinked and difficult to achieve success. But

suitable technological and social interventions can properly manage the crisis. It is in this context, microalgae appear to be an efficient means of carbon sequestration and an important carbon-neutral renewable energy source [1].

Microalgae rich in saturated fatty acids, proteins, minerals, antioxidants, and vitamins are promising third-generation bioresources, highly valuable as nutritious food and feeds, medicine, nutraceuticals, and biofuels [2–4]. Certain microalgae can provide a huge amount of high-quality biomass in limited time. Such algae have the potential to meet the resource crunch for bioresources currently existing in the world. The biodiesel prepared from algal oil is carbon neutral as the burning of the same does not create an increase in the net carbon content of the atmosphere. Moreover, as a

Electronic supplementary material The online version of this article (<https://doi.org/10.1007/s12155-019-09990-9>) contains supplementary material, which is available to authorized users.



Super-hydrophobic graphene oxide-azobenzene hybrids for improved hydrophobicity of polyurethane



Karthika M^{a,b}, Hong Chi^{a,*}, Tianduo Li^a, Hongjuan Wang^a, Sabu Thomas^{b,**}

^a Shandong Provincial Key Laboratory of Molecular Engineering, School of Chemistry and Pharmaceutical Engineering, Qilu University of Technology (Shandong Academy of Sciences), Jinan, 250353, China

^b International and Inter University Centre for Nanoscience and Nanotechnology, Mahatma Gandhi University, Priyadarshini Hills P. O, Kottayam, Kerala, 686 560, India

ARTICLE INFO

Keywords:

Graphene
Polyurethane
Hybrids
Superhydrophobic
Enhanced stability

ABSTRACT

A super-hydrophobic graphene oxide (GO)-azobenzene (Azo) hybrid material was synthesized through a covalent grafting of amide linkage. Fourier transforms infrared spectra (FTIR) and UV-visible (UV-vis) spectra confirmed the successful formation of GO-Azo hybrid material. The GO-Azo exhibited high water repellence with water contact angle of $\sim 152^\circ$. As a new kind of filler material, the scope GO-Azo in improving the hydrophobicity of polyurethane was investigated through contact angle measurements of polyurethane films with varying amount of GO-Azo. Mechanical and thermal studies showed improved stability and rigidity of the composite film as well at doping ratio of only 3 wt% the of the filler.

1. Introduction

Super-hydrophobic materials, owing to their significance in fundamental research and industrial interest, have established an astonishing impact in the field of material research, in a variety of functional applications. The super-hydrophobic state of surface manifests fascinating water repellence, accompanied with a high-water contact angle (WCA), which is greater than 150° . Currently, the high water repellence have raised their demands in designing a variety of needful products to be employed in anti-biofouling [1–3], fluid transportation [4,5], sensors [6–8], self-cleanings [9–12], super-hydrophobic valves [13], battery and fuel cell applications etc. [14].

Polyurethane (PU) is a thermoplastic elastomeric polymer, consisting of both hard and soft segments, with high resistance to abrasion, flexibility, stretchability and high adhesiveness. These characteristics combined with their low cost and ease of processability made it a demanding choice in numerous applications such as in coatings [15], adhesives [16,17], footwear [18,19], furniture [20], automotive [21] and holds a unique importance in daily life. Despite the advantageous as mentioned above, there are certain factors that minimize its use in many

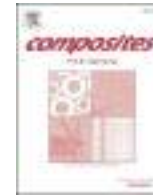
has hydropscopic tendencies, i.e. water absorption characteristics. Therefore, the poor hydrophobicity of polyurethane products is not guaranteed for their durability as they absorb water and gradually decomposed and lose their quality. As a solution to this problem, there is a growing interest in the research to improve the hydrophobicity of polyurethane by incorporating various fillers that helps to improve water repellence of polyurethane [22–27].

Graphene, a two dimensional carbon material with a honeycomb, hexagonal lattice structure, has evolved to be a multifunctional material by virtue of its exciting electronic [28,29] optical [30], thermal [28,31] and mechanical [28] properties. Apart from this, recent research have also focused on revealing its ability to create super-hydrophobic materials and surfaces, either by controlling their surface roughness or changing the chemical composition that offer reasonable change in their wetting properties [32–35]. Covalent functionalization with a hydrophobic moiety seems to be an effective method among all these. Manipulatable precursors like graphene oxide (GO) offers better solubility and processability than pristine graphene. Moreover, GO, an oxygenated form of graphene, can be easily functionalized through its oxygen functional groups in its basal plane and edges. For example,



Contents lists available at ScienceDirect

Composites Part B

journal homepage: www.elsevier.com/locate/compositesb

Excellent electromagnetic shield derived from MWCNT reinforced NR/PP blend nanocomposites with tailored microstructural properties



T. Sharika^{a,d}, Jiji Abraham^a, Mohammad Arif P^a, Soney C. George^{a,b}, Nandakumar Kalarikkal^a, Sabu Thomas^{a,c,*}

^a International and Interuniversity Centre for Nanoscience and Nanotechnology, Mahatma Gandhi University, Priyadarshini Hills P.O., Kottayam 686 560, Kerala, India

^b Centre for Nanoscience and Nanotechnology, Amal Jyothi College of Engineering, Koovapally P.O., Kottayam, Kerala 686518, India

^c School of Chemical Sciences, Mahatma Gandhi University, Priyadarshini Hills P.O., Kottayam 686 560, Kerala, India

^d Department of Chemistry, St.Xavier's College Vaikom, Kothavara P.O, Kottayam 686607, Kerala, India

ARTICLE INFO

Keywords:

Natural rubber
Polypropylene
Selective localization
Droplet morphology
Co-continuous morphology
EMI shielding

ABSTRACT

Blends of polypropylene (PP) and natural rubber (NR) with different loadings (1,3,5 & 7 wt%) of multiwalled carbon nanotubes (MWCNTs) were prepared by melt blending process to design a nanocomposite with tunable electromagnetic interference (EMI) shielding performance. Scanning electron microscopy (SEM) studies show that the addition of MWCNTs changes the droplet morphology into quasi co-continuous morphology for PP/NR 80/20 (wt/wt) blend system. However there is a refinement in the co-continuous morphology of PP/NR (50/50) by the addition of MWCNTs. The effects of the blend morphology and selective localization of MWCNTs on the dielectric, electrical properties and EMI shielding performance were systematically investigated. The largely enriched dielectric performance originates from the interfacial polarization of MWCNTs within the polymer. It is understood that the shielding performance significantly enhanced due to the selective localization of MWCNTs in the NR phase that provided high conductivity and heterogeneous dielectric media with multiple interfaces. The blend nanocomposites show a shielding effectiveness of ca.29 dB at 3 GHz for 7 wt% of MWCNT loading.

1. Introduction

Electromagnetic interference (EMI) is a major concern in the present era because of the radiation emitted from electrical equipment and devices are ubiquitous sources of severe pollution. Since these radiations are harmful to human beings and can damage precise electronic circuitry, developing a material that can block these EM radiations became an urgent necessity for the researchers [1]. Thus rapid growth in electronic equipment and telecommunication devices has led to the demand for high performance electromagnetic interference (EMI) shielding materials [2,3]. A good shielding material must be capable to shield both incoming and outgoing radiation [4] And their ability to block electromagnetic waves depends on materials electrical conductivity, permittivity and permeability. Use of metals as conventional shielding materials is very much restricted because they have disadvantages like

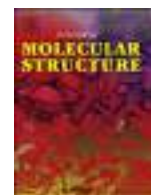
further interference. Recently, polymer composites have gained popularity because of their light weight, resistance to corrosion, structural flexibility, superior processability which can be further tuned based on user needs compared with traditional metal based structures [5].

Polymeric materials are transparent to electromagnetic radiations because of their electrically insulating and non-magnetic nature. The best strategy to overcome this problem consists of dispersing electrically conductive fillers or intrinsically conducting polymers within polymer matrices. Attenuation of EM wave by polymer composites is through combination of absorption, reflection, and multiple reflections rather than reflection which is dominant in the case of metals [6]. Even though addition of very high concentration of conducting reinforcements helps to attain very high electrical conductivity it deteriorates the overall mechanical performance of the composites. Moreover for better processing and cost saving the realization of a high shielding effectiveness



Contents lists available at ScienceDirect

Journal of Molecular Structure

journal homepage: <http://www.elsevier.com/locate/molstruc>

Tailor made biheterocyclic pyrazoline-thiazolidinones as effective inhibitors of *Escherichia coli* FabH: Design, synthesis and structural studies



Vinutha V. Salian^a, Badiadka Narayana^{a,*}, Balladka K. Sarojini^b, Madan S. Kumar^c, K. Sharath Chandra^d, Anupam G. Lobo^e

^a Department of Studies in Chemistry, Mangalore University, Mangalagangothri, 574 199, Karnataka, India

^b Department of Industrial Chemistry, Mangalore University, Mangalagangothri, 574 199, Karnataka, India

^c PURSE Lab, Mangalore University, Mangalagangothri, 574 199, Karnataka, India

^d Department of Botany, Canara First Grade College, Mangalore, 575 003, Karnataka, India

^e Department of Polymer Science and Technology, School of Chemical Sciences, Mahatma Gandhi University, Kottayam, Kerala, 686 560, India

ARTICLE INFO

Article history:

Received 9 January 2019

Received in revised form

8 April 2019

Accepted 24 April 2019

Available online 4 May 2019

Keywords:

Thiazolidinone

Crystal structure

Hirshfeld surface

MEP map

Molecular docking

ABSTRACT

In the present study, a new series of biheterocycles pyrazoline-thiazolidinones derivatized at fifth position with substituted arylidene groups were developed as potent inhibitors of *Escherichia coli* FabH (PDB: 5BNS) an antimicrobial target. These compounds are conveniently synthesized from 3,5-substituted pyrazolinyl carbothioamide precursor. The virtual inhibition assay and pharmacokinetic profiling were carried out based on *in vitro* antimicrobial assay on pathogenic microbes. Amongst, the compound with 4-methoxy benzylidene substituent emerged as effective against all tested bacterial strains. The compound binds very effectively to the active site of the target with minimum glide score = -8.400 kcal/mol. The structure of newly synthesized derivatives was confirmed by several spectroscopic techniques and some of the hybrids by single crystal XRD studies. The compounds **3**, **4a** and **4g** were crystallized in monoclinic crystal system with $P2_1/c$, $P2_1/n$ and Cc space group respectively. The intermolecular contacts in the crystal structure were elucidated by Hirshfeld computational methods and molecular electrostatic potential maps illustrated the charge distribution of the molecules.

© 2019 Elsevier B.V. All rights reserved.

1. Introduction

Drug design or tailor made compounds aim at developing highly effective lead molecules for a particular target with specific mode of action. The drug discovery process involves the identification of the candidates, synthesis, characterization by modern analytical techniques, screening for their potential therapeutic efficacy and computer assisted drug design by molecular modeling tools. To

In recent years significant strategy in developing pharmaceutically important molecules based on thiazolidinone derivatives has gained impetus due to its great affinity for various biotargets/enzymes [1]. The thiazolidinone scaffold attracts great attention as building block in the synthesis of widespread target molecules which displayed significant importance as simple methodology for its synthetic design, also found in various biologically active compounds like vitamin B (thiamine), appears in various natural



Contents lists available at ScienceDirect

Composites Science and Technology

journal homepage: www.elsevier.com/locate/compscitech

Tailoring of photo-responsive molecularly imprinted polymers on multiwalled carbon nanotube as an enantioselective sensor and sorbent for L-PABE

T. Sajini^{a,b}, Sam John^a, Beena Mathew^{b,*}^a Research & Post Graduate Department of Chemistry, St Berchmans College (Autonomous), Affiliated to Mahatma Gandhi University, Changanassery P O, Kottayam, 686101, Kerala, India^b School of Chemical Sciences, Mahatma Gandhi University, Priyadarshini Hills P O, Kottayam, 686560, Kerala, India

ARTICLE INFO

Keywords:

Photo-responsive functional monomer
L-PABE
Multiwalled carbon nanotube
Electrochemical measurements
Impedance spectroscopy
Photo-switching reversibility

ABSTRACT

The present work is aimed to the fabrication of enantioselective sorbent and sensor for the selective and specific recognition of L-phenylalanine benzyl ester (L-PABE) template molecule in photo-responsive molecularly imprinted polymer (PR-MIP). Here a photo-switchable azo-benzene derivative, 4-[(4-methacryloyloxy)phenylazo] benzoic acid (MPABA) is synthesised and used as the functional monomer. Composites of multiwalled carbon nanotubes (MWCNTs) and imprinted polymer were prepared using 1:4 mol imprinting ratio of L-PABE and MPABA and *N,N*-ethylene bismethacrylamide (EBMAA) as the crosslinking agent. Conventional bulk MIP and their respective non-imprinted polymers were also synthesised and characterized to investigate the influence of pre-organization of binding sites on the selectivity of L-PABE. The enantioselective sensor is fabricated on platinum working electrode using imprinted and non-imprinted polymers and their electrochemical measurements are investigated using cyclic voltammetry (CV), differential pulse voltammetry (DPV) and electrochemical impedance spectroscopy (EIS). The platinum modified sensors possess a limit of detection and limit of quantification as $0.2086 \mu\text{mol L}^{-1}$ and $0.6953 \mu\text{mol L}^{-1}$ respectively. MWCNT-MIPs and MIPs exhibit the largest adsorption capacity towards L-PABE. The synthesised polymers reveal characteristic adsorption features and selectivity towards L-PABE in comparison with its enantiomer analogues. Photo-regulated uptake and release studies of MWCNT-MIP and MIP on L-PABE were also done to determine the photoswitching reversibility of functional monomer.

1. Introduction

Stimuli-responsive molecularly imprinted polymers (MIPs) have recently got a significant consideration because they represent a new generation of intelligent and self-regulated artificial receptors and have shown pronounced potential in various applications [1]. Stimuli-responsive materials are able to alter volume and properties in response to environmental stimuli such as pH, temperature, ionic strength, electric field, and photo-irradiation [2]. Among these, photo-irradiation is one of the most frequently accepted external stimuli for stimuli-responsive polymers, since it is suitable to apply and easy to control using

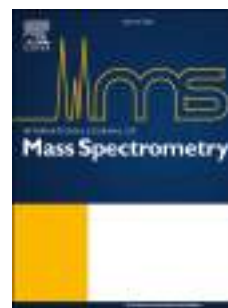
special characteristic features such as good stability, bright colours, low flammability and rapid reverse photo isomerization [8]. Azo-benzene is composed of two aromatic rings where an azo linkage ($-\text{N}=\text{N}-$) joins the two phenyl rings, when irradiated with UV light thermodynamically stable trans-isomer of azo-benzene derivative undergo photo-isomerization to form metastable cis configuration and upon visible light irradiation or thermally in dark, this cis-form get converted photo-chemically to trans form [9] which is schematically shown in Fig. 1.

Molecular imprinted polymers were fabricated for the selective and specific recognition of template molecule via simple polymerization method [10–12]. In a typical imprinting process, template and func-

Accepted Manuscript

ESI-CID spectral characterization and differentiation of the cross links of thymine formed by one electron oxidation with $\text{SO}_4^{\bullet-}$

Jisha Chandran, N.R. Vishnu, Usha K. Aravind, C.T. Aravindakumar



PII: S1387-3806(18)30492-5

DOI: <https://doi.org/10.1016/j.ijms.2019.05.001>

Reference: MASPEC 16147

To appear in: *International Journal of Mass Spectrometry*

Received Date: 5 December 2018

Revised Date: 17 April 2019

Accepted Date: 2 May 2019

Please cite this article as: J. Chandran, N.R. Vishnu, U.K. Aravind, C.T. Aravindakumar, ESI-CID spectral characterization and differentiation of the cross links of thymine formed by one electron oxidation with $\text{SO}_4^{\bullet-}$, *International Journal of Mass Spectrometry* (2019), doi: <https://doi.org/10.1016/j.ijms.2019.05.001>.

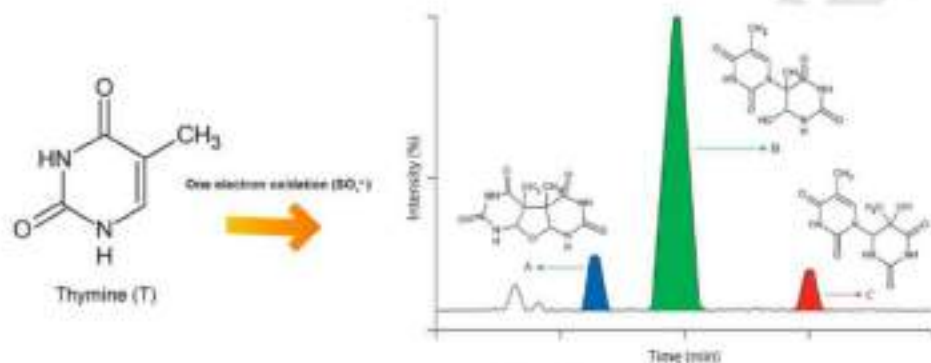
This is a PDF file of an unedited manuscript that has been accepted for publication. As a service to our customers we are providing this early version of the manuscript. The manuscript will undergo copyediting, typesetting, and review of the resulting proof before it is published in its final form. Please note that during the production process errors may be discovered which could affect the content, and all legal disclaimers that apply to the journal pertain.

ESI-CID spectral characterization and differentiation of the cross links of thymine formed by one electron oxidation with $\text{SO}_4^{\bullet-}$

Jisha Chandran^a, Vishnu N. R.^b, Usha K. Aravind^c and C. T. Aravindakumar^{a,b}

^aInter University Instrumentation Center, ^bSchool of Environmental Sciences, ^cAdvanced Centre of Environmental Studies and Sustainable Development, Mahatma Gandhi University, Kottayam, Kerala, India

Abstract



The analysis of urinary nucleosides is becoming a very good tool in the diagnosis of diseases like AIDS and cancer and consequently the identification of modified nucleosides using mass spectrometry is an area of utmost importance. In this context, there is a high relevance in the understanding of the mechanism of collisionally induced dissociation (CID) of these heterocyclics. The present work characterizes and differentiates the cross-linked products formed by one electron oxidation of thymine (T). Three dimers A, B and C, were analyzed, out of which the dimer A is a C5-C5' cross link of two T molecules containing a fused tetrahydrofuran ring,



Poly (ϵ -caprolactone) Microsphere Decorated with Nano-ZnO Based Phytoformulation: A Promising Antimicrobial Agent

S. Snigdha¹ · M. Rahul² · Nandakumar Kalarikkal^{1,3} · Sabu Thomas^{1,4} · E. K. Radhakrishnan²

Received: 8 January 2019 / Accepted: 21 February 2019

© Springer Science+Business Media, LLC, part of Springer Nature 2019

Abstract

In this study, an ethnonanocomposite was produced by using *Curcuma zedoaria* and ZnO nanoparticles. This was immobilised on poly (ϵ -caprolactone) (PCL) microspheres for effective delivery. The presence of curcuminoids in *C. zedoaria* extract was confirmed by GC–MS and LC–MS analyses. The ZnO/*C. zedoaria*. nanocomposite synthesised in this study was subjected to X-ray diffraction and field emission scanning electron microscopy, which revealed the crystalline nature of formed nanocomposite. The nanocomposite was then immobilised on PCL microspheres by emulsion solvent evaporation. Further, XRD and FE-SEM confirmed the presence of nanocomposites and the spherical nature of the polymeric microspheres with diameter ranging from 4 to 36 μm . The antimicrobial activity analysis revealed the remarkable effectiveness of the nanocomposite loaded microspheres. The ethnonanocomposite loaded PCL microspheres generated in the study can thus be an effective antimicrobial agent with diverse biomedical applications.

Keywords *Curcuma zedoaria* · Nano-phyto formulation · Antimicrobial · Polymer microsphere · PCL microsphere · Ethnic-nanomedicine

1 Introduction

The quest for antimicrobial agents has been going on for centuries and hence nanotechnological exploration of ethnomedicine offers great promise. *Curcuma zedoaria* has been well documented in ethnic pharmacotherapy [1]. It has been known for its antibacterial as well as fungicidal properties. Moreover, it has shown pronounced analgesic, anti-oxidant, anti-tumor, and anti-clastogenic properties [2]. The dark orange colored rhizome contains several active ingredients that are highly sought out among traditional medicine practitioners [3]. With the alarming increase in antibiotic

resistance among pathogens, an emerging interest to explore the efficiency of age-old herbal remedies through nanotechnological methods has evolved [4, 5]. Such combinatorial therapeutics are likely to possess multi-targeting capabilities against pathogenic microbes and could hold great potential in managing drug resistant pathogens.

Metal nanoparticles have been established as effective antimicrobial agents [6–10]. In this study, ZnO NPs with well known antimicrobial and anti-inflammatory properties were selected to develop nanoparticle-based phytomedicine [11, 12]. ZnO NPs have proved to be highly efficient in conjugation with materials of plant origin [13–15]. The ZnO NPs have superior effect to eradicate microbes at significantly low concentration. By using a carrier to house ZnO NPs, a small amount of material can be effectively delivered to the target site [16, 17]. PCL has proved its versatility in

✉ E. K. Radhakrishnan
radhakrishnanek@gmail.com; radhakrishnanek@mgu.ac.in

Contents lists available at [ScienceDirect](https://www.sciencedirect.com)

European Polymer Journal

journal homepage: www.elsevier.com/locate/europolj

Effect of MA-g-PP compatibilizer on morphology and electrical properties of MWCNT based blend nanocomposites: New strategy to enhance the dispersion of MWCNTs in immiscible poly (trimethylene terephthalate)/polypropylene blends

Ajitha Anthickamalil Ramachandran^{a,b}, Lovely P. Mathew^a, Sabu Thomas^{a,c,*}^a International and Inter University Centre for Nanoscience and Nanotechnology, Mahatma Gandhi University, Kottayam, Kerala 686 560, India^b Department of Chemistry, Nirmala College Muvattupuzha, Ernakulam, Kerala 686 661, India^c School of Chemical Sciences, Mahatma Gandhi University, Kottayam, Kerala 686 560, India

ARTICLE INFO

Keywords:

Polymer blend
 Compatibilization
 Morphology
 Electrical properties
 Interfacial adhesion

ABSTRACT

Present paper deals with the combined effect of multiwalled carbon nanotubes (MWCNTs) and maleic anhydride grafted polypropylene (MA-g-PP) on morphology and electrical properties of poly (trimethylene terephthalate)/polypropylene (PTT/PP) blends. The enhanced dispersion of MWCNTs which was observed in TEM images is due to the improved adhesion between PTT and PP by the compatibilization effect of MA-g-PP. Major portion of MWCNTs found in the PTT phase and also at the interface, minimal amount of MWCNTs extended their dispersion along the interface to PP phase. The observed morphology of the composites was correlated with the electrical properties. Due to the compatibilization by MA-g-PP of PTT/PP blend, the interaction between PTT and PP phase was improved, thereby interfacial adhesion between the components enhanced along with the extended dispersion of MWCNTs and it resulted in the minimization of effective double percolation phenomena and electrical properties. It was observed that combined action of MA-g-PP and MWCNTs promoted noticeable changes in morphology of the PTT/PP system and is directly related to the electrical properties of the system. Compatibilization by MA-g-PP is a new scheme to enhance the dispersion of MWCNTs in immiscible PTT/PP blends and to improve the mechanical properties of the PTT/PP blend.

1. Introduction

Blending of polymers has great significance since it can produce new material with desired properties. Polymer blending leads to the formation of new material in a simpler and cost effective manner rather than synthesizing a new one in lab. But thermodynamically most of the polymers are immiscible. The immiscibility of the blend causes poor interfacial adhesion between the polymeric components which leads to inferior properties than that of the individual components. Improvement in miscibility or morphology stabilization of an immiscible blend is necessary for its superior applications. To attain the desired properties and enhanced performance, stabilized morphology of

between the polymer components [1–4]. Polypropylene (PP) can be considered as one of the most adaptable commodity polymers with wide range of applications and is produced in large scale [5]. Their application has been enhanced by blending with high performance engineered poly (trimethylene terephthalate) (PTT) thermoplastic polymers. PTT is a biopolymer based engineering thermoplastic semi-crystalline polyester with high-quality properties. Among different engineering thermoplastics, PTT has attained great interest due to its versatile properties and good potential for several applications. But the brittle nature of PTT confines its applications [6–8]. So on blending PTT and PP, one can expect a high performance material with desired properties for engineering applications. But PTT/PP blends are het-



Starch-PVA composite films with zinc-oxide nanoparticles and phytochemicals as intelligent pH sensing wraps for food packaging application



Aswathy Jayakumar^a, Heera K.V.^a, Sumi T.S.^a, Meritta Joseph^a, Shiji Mathew^a, Praveen G.^b, Indu C. Nair^c, Radhakrishnan E.K.^{a,*}

^a School of Biosciences, Mahatma Gandhi University, P.D. Hills (P.O.), Kottayam, Kerala 686560, India

^b International and Inter University Centre for Nanoscience and Nanotechnology, Mahatma Gandhi University, P.D. Hills (P.O.), Kottayam, Kerala 686560, India

^c Department of Biotechnology, SAS SNDP YOGAM College, Konni, Pathanamthitta, India

ARTICLE INFO

Article history:

Received 17 March 2019

Received in revised form 18 May 2019

Accepted 3 June 2019

Available online 04 June 2019

Keywords:

Starch-PVA composite films

pH sensing

Anti-microbial

Food packaging

ABSTRACT

The increasing acceptance of ready to eat food generates demand on development of active and intelligent food packaging material. Even though many polymers have been used for the packaging, they have limitations for broad applications. Among the various polymers, Poly Vinyl Alcohol is a promising film forming polymer with highly flexible, emulsifying and adhesive properties. A variety of nano-fabrication techniques have already been reported to improve the mechanical and antimicrobial properties of PVA to exploit its wider applications. In the present study, starch-PVA based composite films incorporated with zinc oxide nanoparticles and phytochemicals were prepared by solvent casting technique. The films were characterized by XRD, FT-IR, UV-Vis spectrometry and SEM. The developed nanocomposite films were demonstrated to have enhanced water barrier, mechanical and antimicrobial properties. The unique features of the nanocomposite with its pH indication property demonstrated in the study indicate its potential usage in food packaging applications.

© 2019 Published by Elsevier B.V.

1. Introduction

Innovations in food packaging are rapidly triggered in response to the developments in nanotechnology, biological approach and the ever increasing consumer demands. Elevated environmental problems and human health concerns caused by the petroleum based non-biodegradable packaging materials have motivated the newer developments of biopolymer based nanocomposite films. The strategy used here involves augmentation of biodegradable polymers with nontoxic nanomaterials and other bioactive natural products to improve its desirable material properties. This makes it possible to explore the packaging material as vehicles of variety of additives such as antimicrobials, antioxidants and pH indicators for containment, convenience, protection, preservation, long term storage and marketing. By this, it can be made

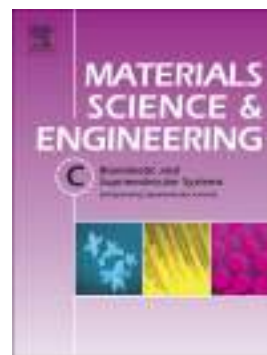
heterophyllus) is of great significance for packaging applications [1]. The functional role of starch in food products is enormous which include its use as an adhesive for binding, film forming, gelling, glazing, moisture retaining, stabilizing, and thickening material [2]. Even though starch is widely used in the development of food packaging films, it has poor mechanical and thermal properties. To overcome this crisis, starch is blended with other polymers such as PVA and PLA, lignin etc. [3] where PVA has been reported to have excellent compatibility with starch [4].

Polyvinyl alcohol (PVA) is a hydrophilic and nontoxic polymer having excellent film forming, emulsifying and adhesive properties along with higher tensile strength and flexibility [5]. But, the major drawback of PVA is the humidity induced mechanical property changes which greatly limits its application. However, fabrication of polymers with

Accepted Manuscript

Chemical modification of graphene with grape seed extract: Its structural, optical and antimicrobial properties

Srinivasarao Yaragalla, Rajakumari Rajendran, Mariam A. AlMaadeed, Nandakumar Kalarikkal, SabuThomas



PII: S0928-4931(18)33403-9
DOI: <https://doi.org/10.1016/j.msec.2019.04.061>
Reference: MSC 9682

To appear in: *Materials Science & Engineering C*

Received date: 6 November 2018
Revised date: 9 April 2019
Accepted date: 20 April 2019

Please cite this article as: S. Yaragalla, R. Rajendran, M.A. AlMaadeed, et al., Chemical modification of graphene with grape seed extract: Its structural, optical and antimicrobial properties, *Materials Science & Engineering C*, <https://doi.org/10.1016/j.msec.2019.04.061>

This is a PDF file of an unedited manuscript that has been accepted for publication. As a service to our customers we are providing this early version of the manuscript. The manuscript will undergo copyediting, typesetting, and review of the resulting proof before it is published in its final form. Please note that during the production process errors may be discovered which could affect the content, and all legal disclaimers that apply to the journal pertain.

Chemical modification of Graphene with Grape seed extract: Its Structural, Optical and Antimicrobial properties

Srinivasarao Yaragalla^{a,b,c}, Rajakumari Rajendran^a, Mariam A AlMaadeed^{*c}, Nandakumar Kalarikkal^{**a,d}, SabuThomas^{**a,e}**

^a*International and Inter-University Centre for Nanoscience and Nanotechnology, Mahatma Gandhi University, Kottayam-686560, Kerala, India*

^b*Istituto Italiano di Tecnologia, Smart Materials Group, Via Morego 30, Genova 16163, Italy*

^c*Centre for Advanced Materials, Qatar University, Doha, Qatar*

^d*School of Pure and Applied Physics, Mahatma Gandhi University, Kottayam-686560, Kerala, India*

^e*School of Chemical Sciences, Mahatma Gandhi University, Kottayam-686560, Kerala, India*

*Corresponding Author: Srinivasarao Yaragalla, email address: yaragallasrinu@gmail.com

^{a,b} Both authors have equal contribution

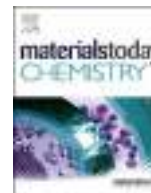
Abstract

Herein, we modified for the first time thermally reduced graphene oxide (TRG) using grape seed extract (GSE), by simple probe sonication method. The effect of GSE on the structural changes of TRG has been carefully analyzed through Fourier Transform Infrared (FT-IR), X-ray photoelectron spectroscopy (XPS) and Raman spectroscopy and these spectral data proved that the TRG has been modified successfully. Furthermore, X-ray investigations proved the change in crystallinity and coherence length of TRG, which could be further, authenticated by



Contents lists available at ScienceDirect

Materials Today Chemistry

journal homepage: www.journals.elsevier.com/materials-today-chemistry/

General scenarios of cellulose and its use in the biomedical field

S. Gopi^{a, b, c, *}, P. Balakrishnan^c, D. Chandradhara^{a, b}, D. Poovathankandy^{a, b}, S. Thomas^c^a Department of Research and Development, ADSO Naturals Pvt. Ltd., # 2/5, 80 Feet Road, Dhalia 3rd Floor Building, RMV 2nd Stage, Bangalore 560094, Karnataka, India^b Zuthpensweg 55, 7418, AH, Deventer, the Netherlands^c School of Chemical Sciences, International and Inter University Centre for Nanoscience and Nanotechnology, Mahatma Gandhi University, Kottayam, Kerala 686560, India

ARTICLE INFO

Article history:

Received 7 January 2019

Received in revised form

19 March 2019

Accepted 27 April 2019

Keywords:

Cellulose

Nanofibers

Nanocrystals

Polysaccharides

Carbohydrates

ABSTRACT

Cellulose is a naturally abundant organic polymer used by many researchers in establishing various biomedical applications due to its biocompatibility, biodegradability, low toxicity, and excellent physical, chemical and mechanical properties. In this review, we focused on general aspects such as sources, structure, and properties of cellulose, nanocellulose, types of cellulose nanocomposites, etc. The incorporation of nanoobjects of cellulose in biomedical applications, viz., drug delivery, targeted drug delivery, and wound healing, was reviewed extensively. The microencapsulation and three-dimensional (3D) printing using cellulose nanomaterials also have been reviewed. As a final note, we discussed and reviewed the future aspects of cellulose nanomaterials or nanocellulose in biomedical engineering applications.

© 2019 Elsevier Ltd. All rights reserved.

1. Introduction

1.1. Biopolymers

Polymers or so-called macromolecules are large molecules made by linkage of small repeating units called monomers, and they may have unique properties depending on the type of molecules being bonded and how they are bonded. Polymers are everywhere and play a vital role in our daily lives. Generally, they fall into two broad categories: synthetic and natural polymers. Synthetic polymers are human-made polymers, whereas natural polymers or biopolymers are polymers synthesized under natural conditions during the growth cycles of all organisms. Biopolymers can be derived from microbial systems, extracted from higher organisms such as plants, or synthesized chemically

biological building blocks so that they can be used as medical materials, renewable packaging materials, cosmetics, food additives, clothing fabrics, water treatment materials, industrial bioplastics, absorbents, biosensors, and even data storage elements [1–3].

Biopolymers can be categorized into two principal classes, viz., natural biopolymers and synthetic biopolymers, the division and the subdivision of which are represented in Fig. 2. Natural polymers are produced by the biological systems such as animals and microorganisms, whereas synthetic biopolymers are derived from biological precursor materials [3]. Synthetic biodegradable polymers include polyesters, polycarbonates, and polyanhydrides, whereas polyethylene, polypropylene, and polyvinyl carbonate are some of the common synthetic non-biodegradable polymers.

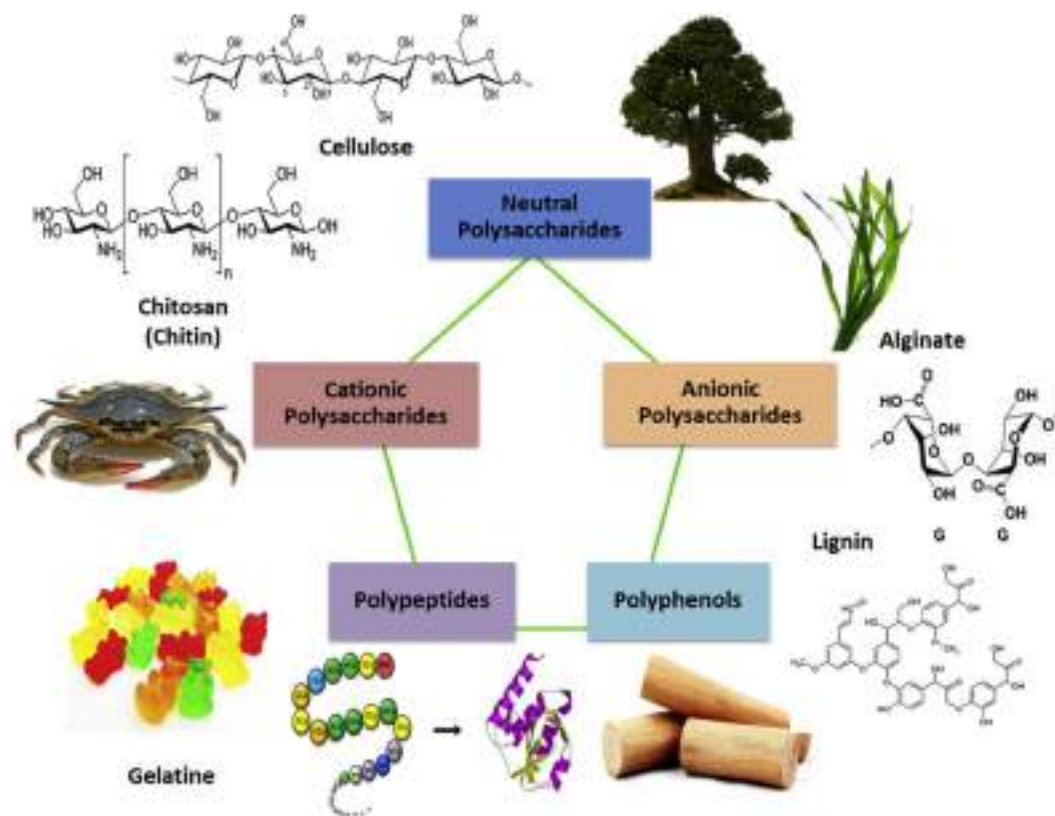
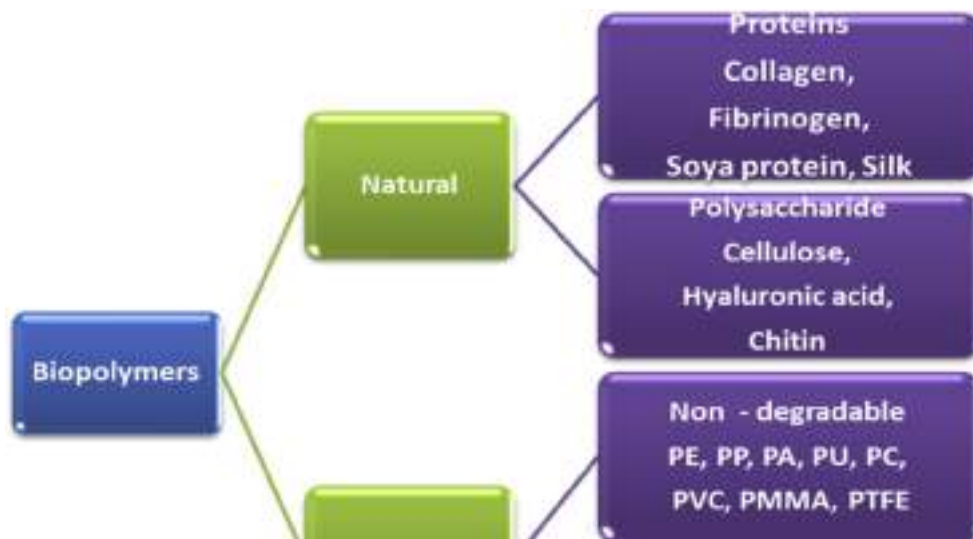


Fig. 1. Different sources of biopolymers.



famous for its high tensile strength and mechanical properties. Similarly, another protein polymer called collagen can be used as a carrier for drug delivery and in reconstruction surgeries [6]. Polysaccharides consist of monosaccharides (sugars) linked together by O-glycosidic linkages, in which cellulose, the first abundant natural polysaccharide carbohydrate molecule, is available on the earth with a global production of $\sim 1.5 \times 10^{12}$ tons per year [3,5].

1.2. Cellulose

Cellulose is a renewable biopolymer resource, extensively available in several forms of biomasses, such as trees, tunicates, and bacteria. They are non-toxic, biodegradable, solid homopolymers, white at its pure state, with a molecular mass around 1.44×10^6 to 1.8×10^6 g. They are extensively stable in the thermal conduction and exhibit thermal softening at a temperature of 231–253 °C [5]. The resistivity of pure cellulose is maximum with minimum conductivity. Many natural fibers such as cotton and higher plants have cellulose as their main constituent having linear, stereoregular polysaccharide, and the basic units are β -1, 4-D-linked glucose chains (molecular formula of $(C_6H_{10}O_5)_n$, n ranging from 10,000 to 15,000) connected via an acetal oxygen covalently bond, i.e., the C₁ of one glucose ring and C₄ of the adjoining ring will be covalently bonded. Common examples of cellulose include wood (40–50 wt %), cotton (87–90 wt %), jute (60–65 wt %), flax (70–80 wt %), and ramie (70–75 wt %). Cellulose materials are used widely in manufacturing industries of textiles, pharmaceuticals, energy drinks, and industrial sugar. They can be used as wood for building; paper products; cotton, linen, and rayon for clothes; and cellulose acetate for packaging films. Cellulose is used as an excipient in formulating solid oral dosages because it is stable, non-toxic, reliable, and renewable. Cellulose and its derivatives are in general strong, reproducible, recyclable, and biocompatible, being used in various biomedical applications such as blood purification membranes [7,8].

1.3. Sources of cellulose

Cellulose can be produced with the help of major sources including plant fibers. Cellulose occurs in an authentic form in plants, but it is usually shadowed by several other components such as hemicelluloses, lignin, and comparatively limited amounts of extractives. 'Extractives are the compounds with low molecular weight that are present in porous wood' [9]. The primary natural source of the cellulose is lignocellulosic material in wood; vegetable fibers can also be a part of natural source, which includes cotton, jute, flax, ramie, sisal, and hemp (Osullivan et al. [11]). These fibers are further categorized into seed, leaf, skin, fruit, and stalk fibers where the cellulose fibers will be collected from the respective plant part [5]. As discussed previously, raw cotton is a naturally highly pure source of cellulose, and its fiber cells are found on the

tree), bamboo fiber (made from bamboo), and sea cell (made from seaweed) [7–13].

Synthetic cellulose fibers are extracted from natural cellulose, and examples include rayon, viscose, and lyocell. They are originated from plants that are processed into a pulp followed by extrusion in the same way the synthetic man-made fibers are made. Chemosynthesis of functionalized cellulose by ring-opening polymerization of 6-di-O-benzyl- α -D-glucopyranose 1,2,4-orthopivalate or by stepwise reactions of selectively protected β -D-glucose as, e.g., 1-allyl-2,6-di-O-acetyl-3-benzyl-4-O-(p-methoxybenzyl)- β -D-glucopyranoside is a well-established and widely used method for manufacturing synthetic cellulose fibers in bulk [14]. Fig. 3 shows the different sources of cellulose available in nature.

1.4. Structure and chemical properties of cellulose

As mentioned in section 2, cellulose is made up by the fundamental D-glucopyranose ring units that occur in ⁴C₁ chair configuration, and therefore, it exhibits the lowest energy conformation. These basic ring components are connected to each other by β -1, 4-glycosidic bonds. Therefore, owing to these chemical bonds, there is an alternate turning of the cellulose chain axis by 180°. The hydroxyl groups are positioned in the ring plane (equatorial), while the hydrogen atoms are in the vertical position (axial). The polymer contains free hydroxyl groups at the C-2, C-3, and C-6 atoms, and the hydrogen bonds associated with these groups will result in the formation of various types of supramolecular semicrystalline structures. Another factor of characterization was degree of polymerization (DP) of the native cellulose or otherwise cellulose I from different sources, with a chain length of 500 to 15,000 nm lies in the range between 1000 and 3000. In general, cellulose exhibits two types of polymorphs – cellulose I (native cellulose) and cellulose II [8,11]. Fig. 4 represents a cellulose molecule.

In native cellulose molecule or cellulose I molecule, the presence of both intramolecular and intermolecular hydrogen bonding has been noticed [8,15]. From the C-nuclear magnetic resonance and infrared examinations, it was understood that there exists an intramolecular hydrogen bonding between the hydroxyl group at C3 position and the nearby ether oxygen in anhydroglucose units and between the oxygen atoms in the –OH group at C6 position and adjacent –OHs linked to C2 position. These bonds are responsible for the rigidity or stiffness of the cellulose polymer [1,8,15]. Hydrogen bonds present between the molecules of cellulose results in a strong interaction of cellulose chains. Intermolecular hydrogen bonding is responsible for the strong interaction between cellulose chains. All these hydrogen bonds and weak –CHO bonds result in a cellulose assembly in layer format. The neutron diffraction and synchrotron X-ray experiments are proof for the existence of cellulose layer assembly [15]. In the case of cellulose II molecule, hydrogen bonds are different. Intrahydrogen bonds are avoided in the structure because there already exists a hydrogen bond between the hydroxyl groups at the C6 and C2 position of the adjacent

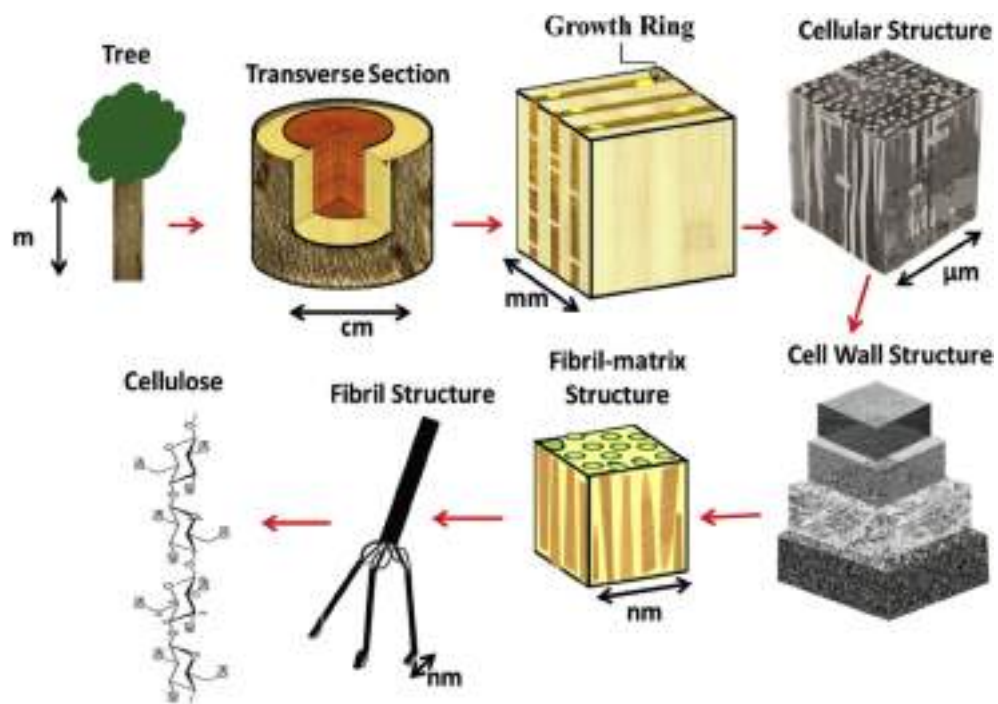


Fig. 3. Sources of cellulose.

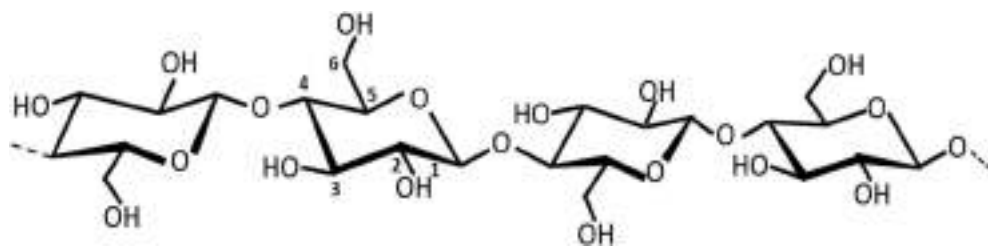
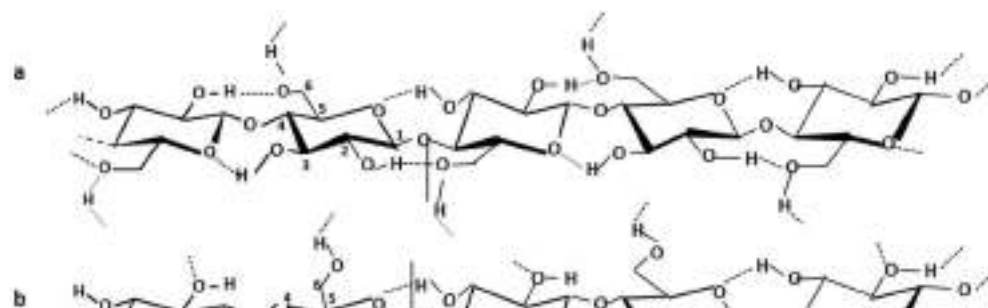


Fig. 4. Chemical structure of a cellulose molecule.



2. Cellulose nanomaterials

In the modern world, different industries, namely food, consumer goods, military, construction, and so on, demand for renewable materials that possess the properties of biodegradability, are non-petroleum-based, carbon neutral; and have low environmental, animal/human health, and safety risks. Traditional cellulose materials are well-renowned biodegradable material produced from sustainable environment. They have been incorporated in the daily life for thousands of years, and applications involve various industries such as forest products, paper, textiles, food, and pharmaceuticals. The next level of engineering applications requires materials with high specific strength and modulus, hydrophilicity, and extensive ability for chemical modification. Therefore, cellulose extracting at the nanoscale can achieve these properties and can reduce the hierarchical defects in the traditional cellulose materials [17–20].

The term ‘nanoscale’ refers to the values of order 10^{-9} m. Nanomaterials have at least one linear dimension in the range from approximately 1 nm to 100 nm. As the size of a particle decreases down to the nanometer scale, important changes occur in the physical, chemical, and mechanical properties. Engineered nanomaterials are resources designed at the molecular (nanometer) level to take advantage of their small size and novel properties which are generally not seen in their conventional, bulk counterparts. Because of these reasons, nanomaterials choose to have an increased relative surface area and new quantum effects. Nanocellulose refers to cellulose particles with at least one dimension in the range of 1–100 nm. Thus, they get a high reactive area for hydroxyl groups. The presence of a large number of hydroxyl groups results in a unique substrate that is amenable to various types of surface modifications, extending its use to sophisticated applications [21–23]).

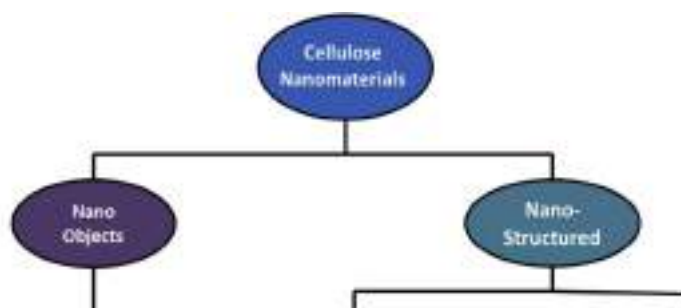
For defining various classes of nanocellulose, the Technical Association of the Pulp and Paper Industry (TAPPI) proposed standard terms and their definitions [24]. Fig. 6 shows the nomenclature, abbreviation, and dimensions applicable to each subgroup.

On the basis of structure and extraction methods, nanocellulose can be classified into two major categories such as cellulose

nanocrystals (CNCs) and cellulose nanofibrils (CNFs). CNCs are needle-shaped structures with a diameter in the nanoscale order and length in the range of 100–500 nm, whereas CNFs are flexible nanofibers with a diameter in the nanoscale order and length in terms of micrometers. Fig. 7 shows a detailed representation of cellulose nanocrystals and nanofibrils along with their scanning electron microscopy (SEM) and transmission electron microscopy (TEM) images. Preparation methods affect the properties of these structures, and the major difference between CNCs and CNFs lies in the proportion of the amorphous phase and dimensions of the material [25] (Fig. 8).

2.1. Cellulose nanocrystals

CNCs are rod-shaped structures formed by acid hydrolysis. In the previous literature, different terms such as nanocrystalline cellulose, cellulose whiskers, cellulose nanowhiskers, and cellulose microcrystals have been used [26]. By appearance, they resemble whiskers because of their extraction process. CNCs are widely incorporated in major chemical and even electronic applications such as gas sensors and temperature sensors because of their properties such as flexibility and stretchability, easy integration with variety of substrates, and availability [27–29]. Coming to the production method, i.e., the acid hydrolysis process, the acid used (mostly sulfuric acid), hydrolyzes the amorphous regions within the cellulose microfibrils [30–32]. The starting material will be fibers from plants or wood, microcrystalline, microfibrillated or nanofibrillated cellulose. Based on the conditions in the extraction process, as discussed earlier, the geometrical properties of CNCs can be varied. Typically, CNCs have high aspect ratio ranging from 3 to 5 nm in width, 50–500 nm in length, and higher percentage of cellulose (~100%). In addition, they constitute high fraction of β in the range of 68–94% and are highly crystalline. But if the hydrolysis is inadequate, incomplete removal of the amorphous regions can occur, which results in the decreased rate of crystallinity and morphological changes. Similarly, if the hydrolysis rate is more, DP of the microcrystalline cellulose (MCC) and reduction in the particle length can be caused. These factors affect the aspect ratio of the



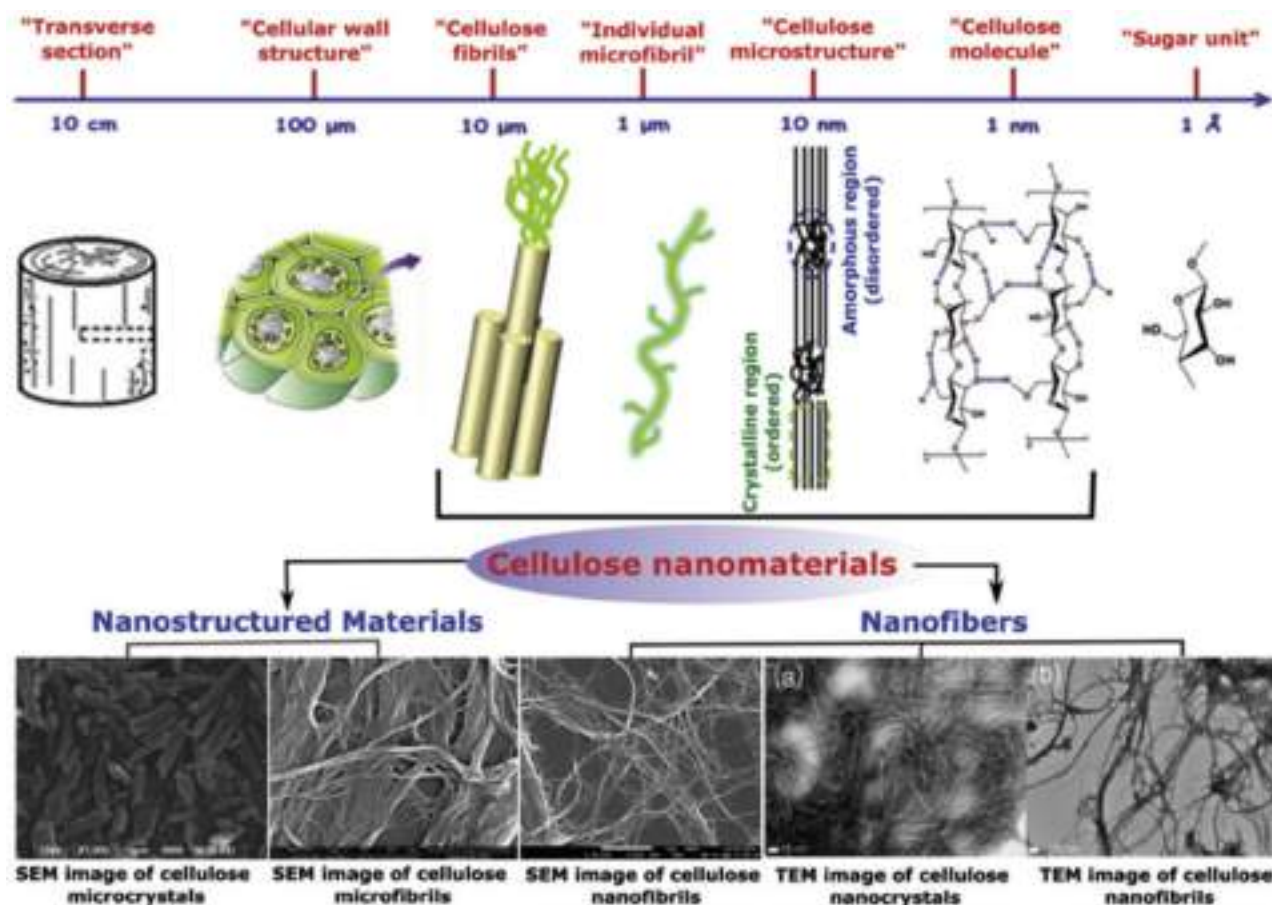


Fig. 7. Cellulose nanomaterials – major divisions and their SEM and TEM images (Source: Trache et al., [24] 2017, Reproduced with permission from RSC. Copyright 2018). SEM, scanning electron microscopy; TEM, transmission electron microscopy.

nanoparticle and, sometimes, result in the formation of spherical structures [31–33].

Production of CNCs

In 1949, CNCs were first produced by Ranby et al. [34] by acid hydrolysis technique. The whole extraction process can be divided into four steps, namely, (1) mechanical size reduction, (2) alkali purification and bleaching treatments, (3) controlled chemical treatment, and (4) mechanical or ultrasound treatment [35]. Initially, the raw materials will be washed and dried and milled into particles of uniform millimeter or macrometer size. It enhances the performances of further chemical treatments. The next step involves the use of alkali such as aqueous KOH or NaOH solutions to remove the alkali-soluble materials such as hemicellulose and lignin. This is followed by the treatment of the cellulose with

Cellulose nanowhiskers are a fibrous form of cellulose or rod-like structures produced by the acid hydrolysis of plant-based cellulose with its sides ranging from 3 to 30 nm in length and 2 nm to 20 nm in diameter. The name ‘nanowhiskers’ is due to their characteristics such as high crystallinity, rigidity, length, strong hydrophilicity, and high strength. They are used as reinforcements in nanocomposite materials, adhesives, electronic components, biological materials, aerogel, and textiles [37–39]. Fig. 10 shows the pictorial representation of hierarchical structure from wood to nanowhiskers. The fact that nanowhiskers have a large specific surface area, higher modulus about 150 GPa, and high ratio appearance (length/diameter) has favored its use as a reinforcing agent. They have high ability to act as reinforcements under very low application percentages and possess low density, non-abrasive nature, providing less wear to the equipment at the time of processing, non-toxic character, biocompatibility, and biodegrad-

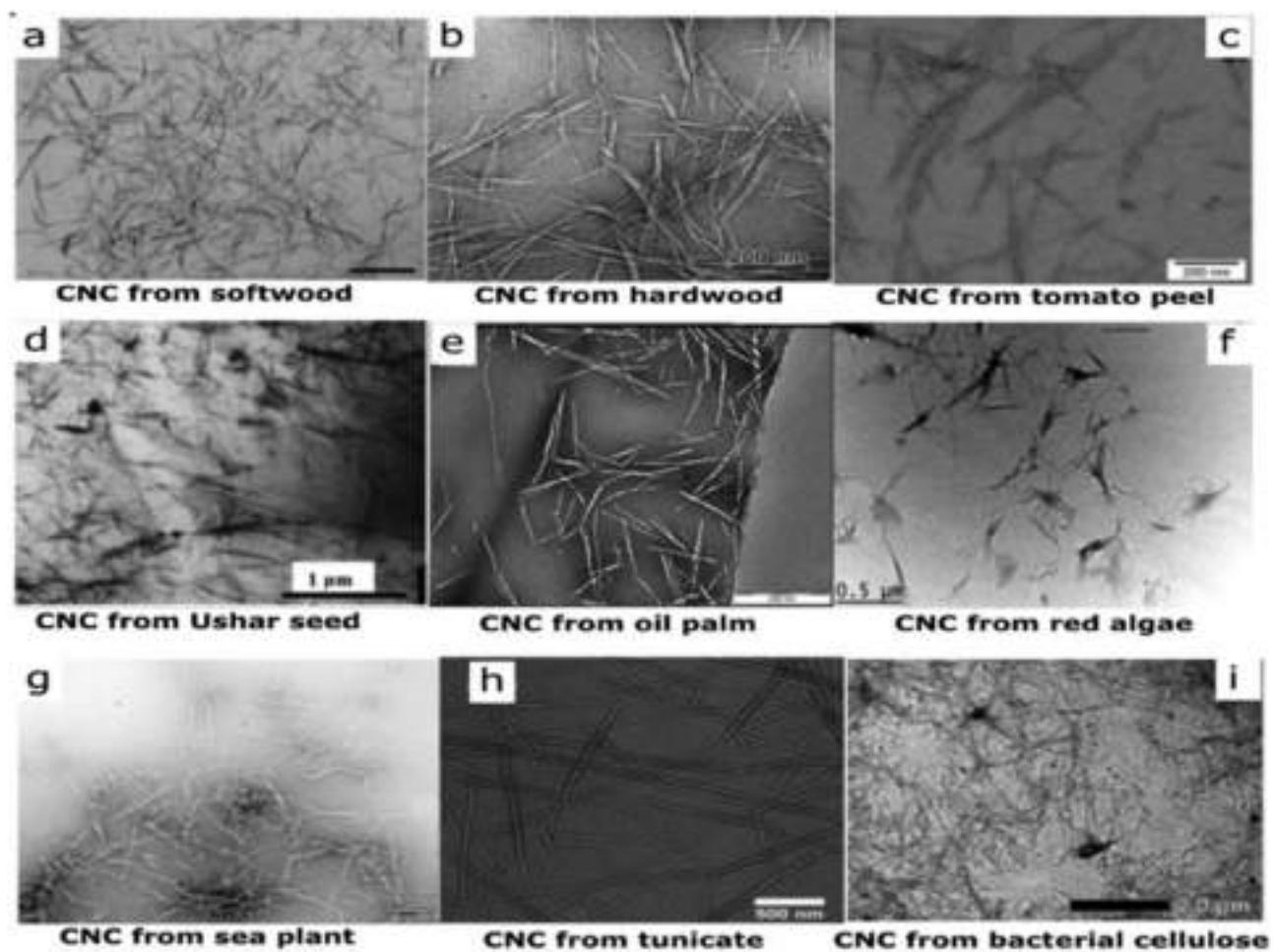


Fig. 8. TEM images of CNCs derived from various sources (Source: Trache et al., [24] 2017, Reproduced with permission from RSC. Copyright 2018). CNCs, cellulose nanocrystals; TEM, transmission electron microscopy.

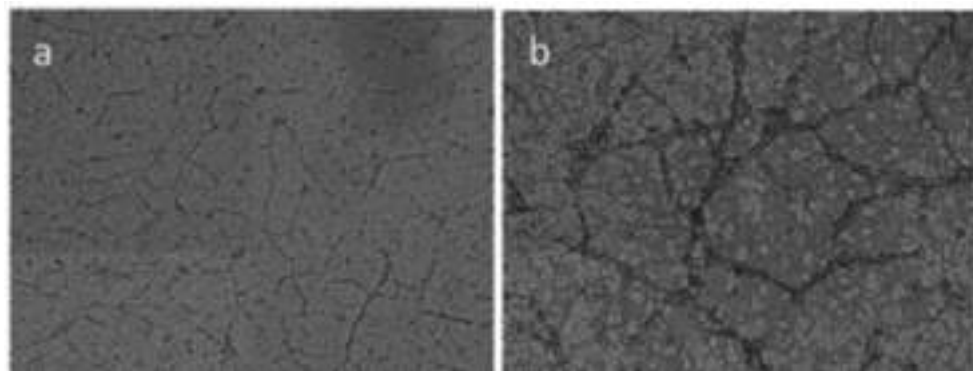




Fig. 10. Hierarchical structure of nanowhiskers from tree to wood, trunk, cell walls, fibrils, and cellulose molecules (Source: Stephen et al., 2011 [177], Reproduced with permission from RSC. Copyright 2018).

starter materials, such as tunicate cellulose, straw or kraft pulp, sisal, bacterial cellulose, MCC, sugar beet (primary cell wall), softwood pulp, ramie, and cotton [41]. Considering the starters and the extraction process, dimensions of the nanowhiskers will vary because of the cellulosic structural differences such as crystallinity and amorphous area. If sulfuric acid (H_2SO_4) is used to hydrolyze the native cellulose, negative sulfate groups will be introduced on the outer crystals surface, which is responsible for the stabilization of crystals which results in a colloidal solution. But the presence of sulfate groups can cause reduction in thermal stability of nanowhiskers because a large amount of sulfate groups on the cellulose leads to increased thermal degradation of the cellulose. If hydrochloric acid is used instead of sulfuric acid during the acid hydrolysis process, the thermal stability of the prepared nanocrystals is improved. But owing to a lack of electrostatic repulsion force between the particle crystals, the nanowhiskers are likely to agglomerate, which results in the formation of an unstable solution [42].

Nanowhiskers may be engineered for accommodating various applications ranging from textile to automotive industry which

2.2. Cellulose nanofibrils

As discussed previously, bio-based nanomaterials such as CNCs and cellulose nanofibrils have a great research interest in the area of high-value product manufacturing where these materials have less impact in the environment. CNFs are incorporated in several applications including biomedical, bioimaging, nanocomposite, gas barrier films, and optically transparent functional materials [45]. CNF are long fiber-like structures with a diameter similar or larger than that of CNCs. CNCs and CNFs differ from each other by the proportion of the amorphous phase and dimensions of the material, and these factors are affected by the production conditions involved. Fig. 9 shows the TEM images of CNFs in different dimensional views. CNFs are less crystalline and therefore more flexible than CNCs. CNFs can be extracted by various processes, such as mechanical delamination of cellulosic pulp aqueous suspensions in a high-pressure homogenizer (HPH), TEMPO-mediated oxidation, multipass high-pressure homogenization, and enzymatic hydrolysis [46–48].

Production of CNFs

As a new cellulosic material, nanofibrils or CNFs were introduced by Turbak et al. [49] and Herrick et al. in 1983 [179]. They used the technique high-pressure homogenization (HPH) where the softwood pulp suspension was allowed to pass through a homogenizer. CNFs can be extracted by mechanical or chemical routes, and it includes techniques such as HPH, mechanical smearing of plant cell walls, grinding, cryocrushing, and high-intensity ultrasonic treatment [50]. Among these methods, HPH is widely used for large-scale or industrial-scale production and involved in food, cosmetic, pharmacy, and biotechnology industries [33,50,51]. In this technique, cellulose slurry is pumped at a high pressure and fed through a spring-loaded valve assembly or homogenizer. When the valve opens and closes rapidly, the fibers are exposed to a large pressure drop and subjected to shearing and impact forces. These forces lead to a high degree of microfibrillation of the cellulose fibers. The degree of cellulose fibrillation depends on the number of homogenization cycles and pressure used. The disruption efficiency per pass through the equipment increases when the pressure rises [52]. Instead of a homogenizer, microfluidizers can also be used for the extraction process. It was first reported by Zimmermann et al. [53] in 2004. Compared with a homogenizer, a microfluidizer uses constant shear rate instead of constant pressure rate. During this process, sulfate suspension is passed through a thin chamber of a specific geometry (can be in Z or Y shape) with an orifice 100–400 μm in width. The suspension is treated using an Ultra-turrax (FA IKA) at 24,000 rpm for 8 h and further passed through an M-100Y Microfluidizer processor at a pressure of 1000 bar for 60 min. When high pressure is applied, corresponding shear forces tend to be generated, which results in the formation of cellulose fibers. To improve the extent of fibrillation, various methods such as

modified grooved discs or stones. The gaps between the discs can be adjusted and can reduce the problem of clogging in the system. In 1998, Taniguchi and Okamura [57] reported the first grinding technique for the production of CNFs. One of the discs will be in static state and the other will be revolving at a speed of 1500 rpm. During the process, the high shear forces break the cell wall, resulting in the production of individual nanosized fibers. The degree of fibrillation depends on the gap between the discs, morphology of the grooved disc channels, and number of cycles of pass through the grinder [58,59]. To increase the fibrillation efficiency, Wang et al. [60] reported the use of reducing the gap between the grinding stones to $-100\ \mu\text{m}$ from the zero position of motion.

In the cryocrushing technique, the fibers are frozen using liquid nitrogen and then subjected to high shear forces. These high-impact forces act on the frozen fibers which forces the ice crystals to exert pressure on the cell walls. Finally, it causes rupturing of fibers leading to formation of microfibrils [61].

High-intensity ultrasonic treatment is a process in which both chemical and mechanical treatments are incorporated. Initially, mild acid hydrolysis and bleaching techniques are used to purify plant fibers, which removes lignin and hemicelluloses. After this chemical pretreatment, the purified cellulose fibers are soaked in distilled water, and about 110 mL of this solution is placed in an ultrasonic generator operating at a frequency of 20–25 kHz. To isolate the nanofibers, ultrasonication is conducted for 30 min [50,52,60,62].

3. Cellulose-reinforced thermoplastic composites

Composite is a heterogeneous mixture which constitutes two or more distinct microscopic components with significantly different physical and/or chemical properties. They are defined to be a material in which a homogeneous matrix component is reinforced by a stronger and stiffer constituent that is usually fibrous but may have a particulate shape or other shapes. Compared with matrices, they have an improved mechanical performance with or without new functionalities, for example, barrier performances [63,64]. Typically, a composite is formed by embedding a strong and stiff reinforcement, usually in fibrous phase, in a soft matrix; thus, its strength properties lie in between the matrix and reinforcements. Based on the physical size, the reinforcements used in composite formation can be classified into macroscopic, microscopic, or nanoscopic structures. Nanoscopic reinforcement has at least one dimension less than 100 nm. It will enhance the properties of the composite because they can provide high specific surface area [64,65]. Other than the reinforcement's properties, the main factors that affect the strength of a composite are the properties of the matrix, the reinforcement-matrix compatibility, and also the interaction and the dispersion of the reinforcement in the matrix. The composite having fibers/fabrics as the reinforcement constituent is named as fiber-reinforced composite (FRC), and it can be

when heated. Thermoplastic polymers are polymers that can be molded, melted, and remolded without any alteration in their physical properties. They can be recycled more broadly than thermosets. Thermoplastics have three main advantages compared with traditional materials: low specific gravities, low energy requirements for manufacture, and low costs of fabrication. They have high strength-to-weight ratios with low stiffness-to-weight ratios when compared with industrial materials such as aluminum and steel [66,68]. Therefore, for low-melting thermoplastics manufactured by the conventional plastic processes extrusion and injection molding process, the use of natural fibers is being increased [69–71].

Fibers used as reinforcements can be widely classified into two major sectors such as natural and synthetic fibers. Natural fibers are plant-, animal-, or mineral-based ones, whereas synthetic fibers include nylon, acrylic, aromatic polyester, polyethylene, aramid, glass, carbon, boron, silicon carbide, stainless steel, etc. [72]. Because composites continue to be adopted in several industries, over the past few decades, there has been a growing interest in the use of natural fibers in various applications. Compared with synthetic FRCs, they have a low rate of tool wear and low density; cost less; and are easily available and biodegradable. Natural fibers are broadly classified into 3 groups – fibers derived from plants, animals, and minerals [72,73]. Plant fibers are commonly used as reinforcements in FRCs include bast (or stem, soft, or sclerenchyma) fibers, leaf or hard fibers, seed, fruit, wood, cereal straw, and other grass fibers. By nature, plant fibers are basically comprised of a rigid, crystalline cellulose microfibril-reinforced amorphous lignin, and/or hemicelluloses matrix, and the main constituent of any plant fiber is cellulose [72]. Cellulose is well known for its high specific strength and modulus, high sound-damping performance, low density, and a relatively reactive surface. Nonetheless, natural fiber-reinforced composites are not deployed in applications related to industries because they contain large amounts of the hydroxyl group, which makes them polar and hydrophilic in nature and non-compatible with non-polar and hydrophobic thermoplastics. In addition, the processing temperature limits the compounding of cellulose fibers with major engineering plastics such as polyethylene, polypropylene, etc., and the composites are hygroscopic and swell, which affects the mechanical properties. Therefore, to accept natural (plant) fibers as a quality alternative to conventional reinforcing fibers, there exists a need of high-performance natural fiber-reinforced composites [72–74].

The mechanical properties of cellulose-reinforced thermoplastic composites strongly depend on the interfacial adhesion between components and can be improved by making certain modifications in the polymeric matrix and lignocellulose fibers. Coupling agents are used to modify the polymeric matrix, thereby enhancing the mechanical properties. In the second approach, fibers used as reinforcements will be treated with physical (plasma and corona treatments) and chemical methods to change their properties. Owing to the presence of hydroxyl groups in the cellulose fibers, the

form short fiber–reinforced composites which can be manufactured in bulk by techniques such as injection molding or extrusion [91].

4. Cellulose-reinforced thermoset composites

Thermoset materials are formed by joining different polymer groups together by chemical bonds, acquiring a highly cross-linked polymer structure. The highly cross-linked structure in thermoset materials is directly responsible for the high mechanical and physical strength compared with thermoplastics or elastomers. At the same time, these highly cross-linked structures provide poor elasticity or elongation of thermoset materials. Therefore, they are stiff in nature and do not stretch the way elastomers and thermoplastics do [91]. Thermoset composites are a subclassification of PMCs. In PMCs, a polymer thermoplastic or thermosetting matrix or resin will be reinforced by fibers. These materials can be tailored into a variety of shapes and sizes. They provide great strength and stiffness along with resistance to corrosion. The reason for these being most common is their low cost, high strength, and simple manufacturing principles [92–94]. Unsaturated polyesters are the most common thermoset polymer matrix for reinforcing natural cellulosic fibers because they possess many advantages such as room temperature cure capability, good mechanical properties, and transparency, when compared with other thermosetting resins [95–97]. Several research groups employed in the academic and industrial sector have shown great interest in the use of natural fiber for the reinforcement of the composites because of their eco-friendly advantages, economical production, and higher specific strength/stiffness compared with the traditional synthetic fibers [98–102].

Thermoset polymer matrices possess certain advantages while preparing the cellulose fiber–reinforced composites, which make it an ideal one compared with other matrices. Easy processing of natural fiber–reinforced composites helps in obtaining a liquid form, thereby enhancing the mixing of the fiber with the resin. Compared with the thermoplastic composites, they require only lower rates of temperature and pressure for the preparation of composites. For many industrial applications, thermosetting resins are preferred because the viscosity is low; thus, various impregnation techniques for fibers are allowed. The overall cost involved in the preparation of these composite systems can be reduced by using self-made or simple systems. Moreover, it is easy to obtain a higher loading of fibers in the thermoset composite materials [99–102]. Even though they offer these advantages, several demerits are also present because they are not recyclable and have high curing time compared with thermoplastic composites [103–105].

5. Cellulose nanomaterials for biomedical applications

Many researchers are now focusing on the extensive incorpora-

tion of cellulose nanomaterials in biomedical applications because of their barrier properties, surface chemical reactivity, biocompatibility, low cytotoxicity, outstanding mechanical properties, biodegradability, and biosafety compared with others [109,110]. For example, as discussed in the previous section, there are different varieties of nanocellulose, and among these, bacterial nanocellulose or microbial cellulose is a well-established material for manufacturing wound dressings and used widely in tissue engineering applications. Most of the products have been realized and commercialized, so they were considered as revolutionary products in the medicine field [111,112]. Fig. 11 shows the overall summary of various cellulose-based nanomaterials used in biomedical applications.

5.1. Drug delivery

The term ‘drug delivery’ can be defined as a method or process of administering a pharmaceutical compound to achieve a therapeutic effect in humans or animals. For any pharmacological treatments, the therapeutic effectiveness mainly depends on the availability of the active drug with a specific concentration at the site of action [113]. With the advancements in the nanotechnology engineering, various nanomaterials such as gold nanoparticles, quantum dots, carbon nanotubes, fullerenes, etc., have been designed and developed for drug delivery processes [114,115]. Even though each of these nanomaterials possesses its own merits and demerits, it remains as a challenge for the scientific world in identifying an ideal material for drug delivery. An ideal drug delivery material should have high payload, biocompatibility, and non-toxic and non-immunogenic properties [113,114,116]. Considering these factors, nanocellulose materials can be an ideal choice for drug delivery applications. Cellulose is a well-established material used as a pharmaceutical excipient in various types of formulations for many years. They can condense the drug-loaded matrices and form suitable tablets for oral administration. According to the European Pharmacopoeia, excipient is an auxiliary substance which is a constituent of a medicine but not its active part. It plays a pivotal role in the dosage formulations and dosage forms. It is a fact that biological drugs such as proteins, peptides, and monoclonal antibodies require a special type of excipient because they are known for their poor membrane permeability, enzymatic instability, large molecular size, and hydrophilic properties. Moreover, the pharmaceutical industry faces the problem of high production costs, and choosing a correct excipient can significantly reduce it [115]. As described previously, cellulose and its acidic and basic derivatives can be an excellent replacement for chemical excipients used because they provide excellent compactibility at low pressures, have an increased dilution potential, improve the flowability of powder blend, and, at the same time, have low production cost [113–115].

One of the prominent works considered using pure CNCs to bind with water-soluble antibiotics and compared the capability of cationic CNCs to bind with non-ionized hydrophobic anticancer agents [117]. Similarly, another study investigated the efficiency of CNCs in stabilizing protein formulations. The study showed that

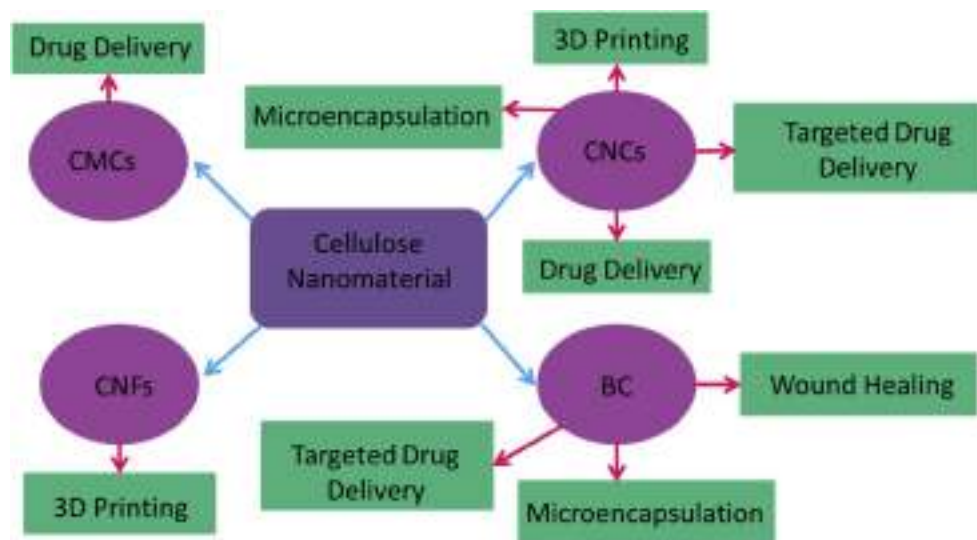
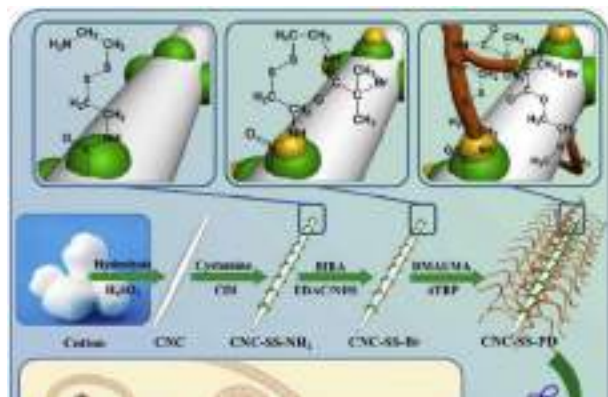


Fig. 11. Different cellulose-based nanomaterials used in biomedical applications. 3D, three-dimensional; BC, bacterial cellulose; CNCs, cellulose nanocrystals; CNFs, cellulose nanofibrils.

establishing a drug release time of 5–10 min. The CNCs from cotton wool functionalized with disulfide bond-linked poly(2-dimethylamino)ethyl methacrylate (PDMAEMA) and CNC-graft-PDMAEMA (CNC-SS-PDs), with different molecular weights of PDMAEMA, were synthesized for another type of drug delivery system – gene delivery system [119]. The CNC-SS-PDs presented good transfection efficacy and low cytotoxicity. The antitumor effect of CNC-SS-PDs was assessed *in vitro* and *in vivo* by a suicide gene/prodrug system (e.g., cytosine deaminase/5-fluorocytosine [CD/5-FC]). The authors stated that the modification of CNCs with redox-responsive polycations was an effective method for new gene delivery system development. Fig. 12 shows the schematic diagram of the same (Fig. 13).



Another variety of cellulose material which attracts the interest of many researchers in the field of drug delivery is carboxymethylcellulose (CMC). In 2013, a study was published based on the development of CMC microspheres with adjustable anticancer drug-release properties for the applications in arterial embolization. Anticancer drug – doxorubicin – was loaded in the CMC-based microsphere, and results showed that under physiological conditions, the burst release profile occurred in the first 8 h of drug administration, followed by a plateau release over a 24-h period. *In vivo* or preclinical studies conducted on laboratory animal kidneys, analyzed in the interval of 6, 7, and 73 days of embolization, proved that the CMC microspheres are biodegradable with a mild tissue response issue [120]. Recently, another study was reported based on the fabrication of dual stimuli-responsive CMC-based nanogels which can be incorporated in the intracellular anticancer drug-delivery systems. Here, two nanocarriers were developed by the polymerization technique: (1) Oligo (ethylene oxide)-containing methacrylate (OEOMA) was polymerized in the presence of CMC and (2) disulfide-labeled dimethacrylate with free-radical cross-linking polymerization. The drug was released only when there was an acidic pH and thiol-reducing agents. *In vitro* studies confirmed the drug release with the help of HeLa cancer cells, and the model anticancer drug loaded was doxorubicin [121].

5.2. Wound healing

Wound healing is a process that involves various pathophysiological and biochemical events. It is a complex process that involves

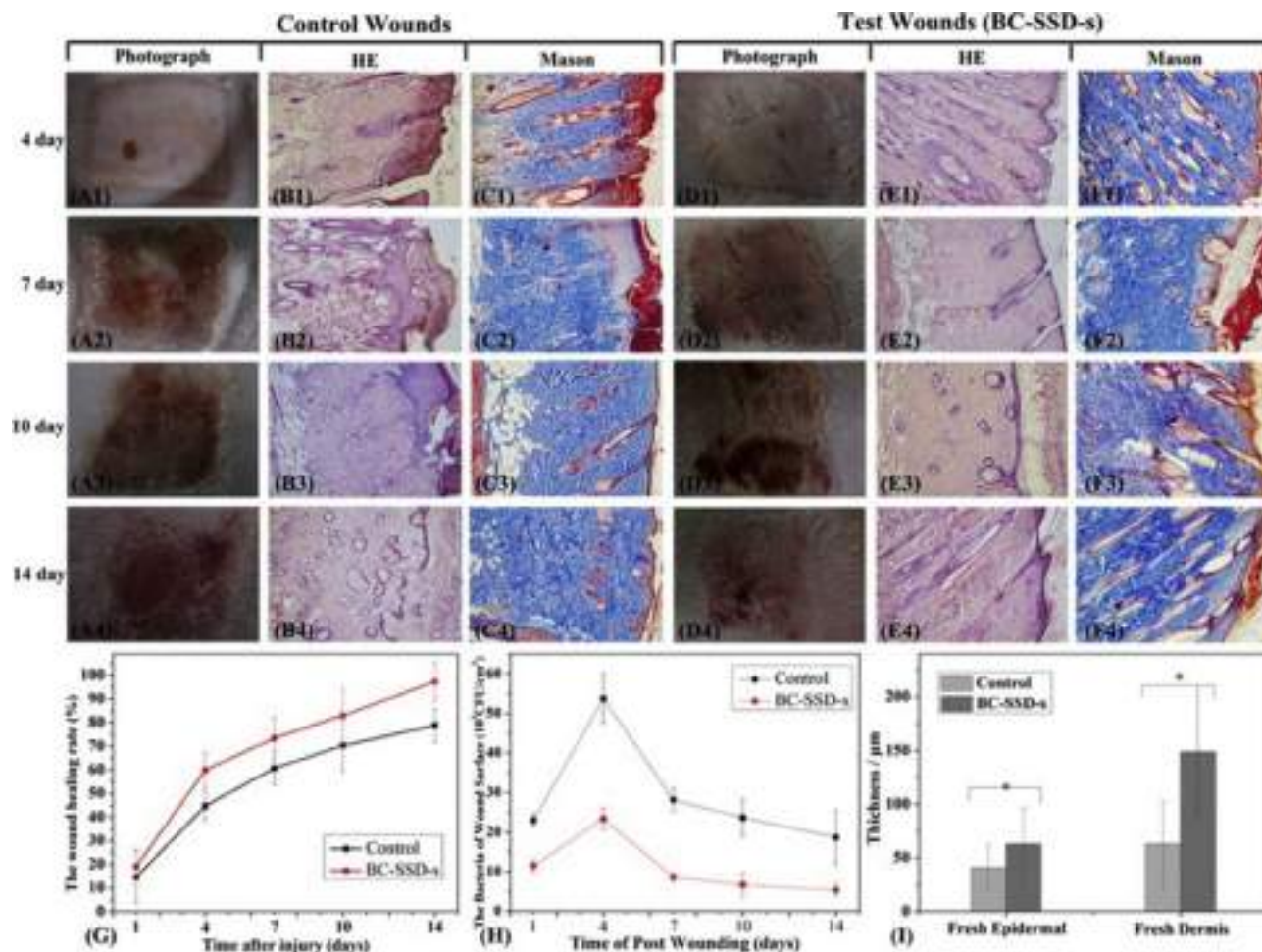


Fig. 13. Representative photographs of macroscopic appearance of 20 mm × 20 mm partial-thickness wound excised on the rat: control wounds (covered with gauze) at the 4th (A1), 7th (A2), 10th (A3), and 14th (A4) day and test wounds (covered with Bacterial cellulose–Silver sulfadiazine composite membrane) at the 4th (D1), 7th (D2), 10th (D3), and 14th (D4) day. Histology of partial-thickness wound: hematoxylin and eosin staining of control wound sections at 4th (B1), 7th (B2), 10th (B3), and 14th (B4) day and test wound sections at 4th (E1), 7th (E2), 10th (E3), and 14th (E4) day; Masson's trichrome staining of control wound sections at 4th (C1), 7th (C2), 10th (C3), and 14th (C4) day and test wound sections at 4th (F1), 7th (F2), 10th (F3), and 14th (F4) day. Wound healing rate (G), bacteria of wound surface (H), and epidermal and dermal thickness (I) after wounding. HE, hematoxylin and eosin.

formation of scars which can be a permanent mark. For large skin defects (in case of burns), clinicians follow the conventional treatment of skin transplantation. But only a limited amount of skin, with matching properties and biocompatibility, can be transplanted. Because of all these reasons, there arises a need of promising skin substitutes, modern wound dressings, and skin scaffolds [122–125].

For developing optimal wound dressings, the main properties that should be analyzed are (1) their ability to absorb exudate during the dressing process, (2) how it is removed from a wound surface after recovery, (3) and its aftereffect. There are many criteria for developing a skin substitute, which include the ability

Several studies had been conducted to confirm the benefits of BC wound dressings compared with the conventional dressings. Animal and histopathological experiments conducted by Fu et al. [128,129] had proven this fact, and they showed the comparative data with the commercial dressings. In 2014, Park et al. [130] synthesized BC through fermentation process and achieved a low-cytotoxic-profile material with a high rate of skin proliferation. Various matrices such as collagen [131], alginate [132], chitosan [133], cotton gauze [134], and poly (ethylene glycol) [135] have been incorporated to form biocomposites of enhanced wound healing or skin tissue repair dressings. Clinical studies were also

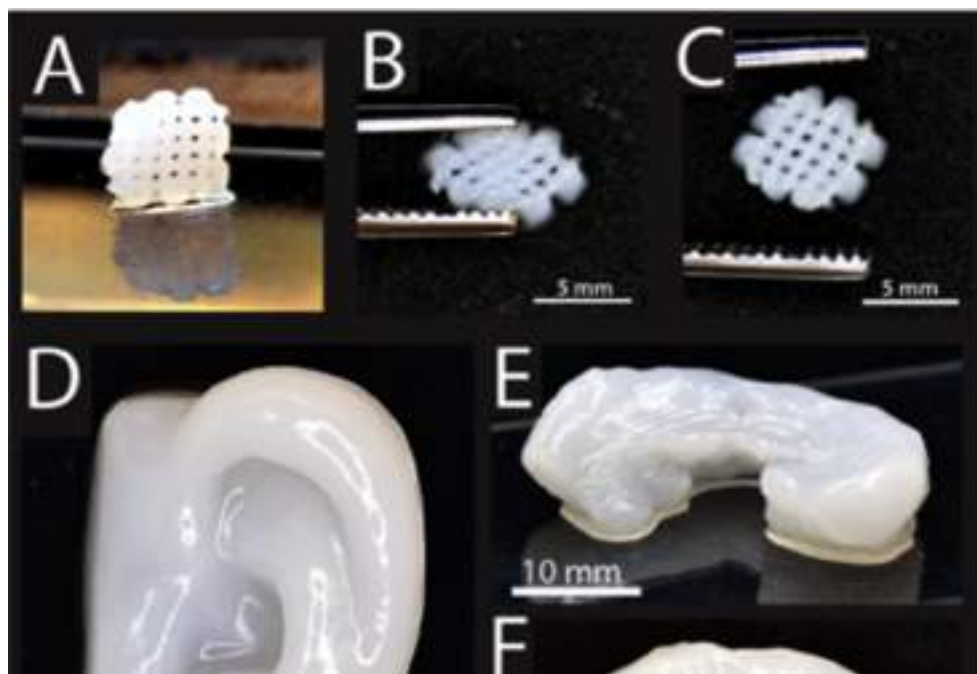
Brazil) and Xylos Corporation had realized and commercialized products based on the basic research studies conducted. Biofill[®] and Bioprocess[®] (used in the therapy of burns and ulcers as temporary artificial skin), Gengiflex[®], and XCell[®] family are some of those products available in market [138]. Wang et al. [139] had created another type of BC burn wound healing dressing impregnated with silver sulfadiazine nanoparticles to enhance its antimicrobial activity against microbes such as *Staphylococcus aureus*, *Pseudomonas aeruginosa*, and *Escherichia coli*. They proved the results using rat models, and Fig. 15 shows the detailed results of the same.

5.3. Targeted drug delivery

As mentioned in section 5.1, effectiveness of any pharmacology treatments in humans depends on the amount of active drug at the target site of action in a concentration more than the minimum effective level. Owing to several pharmaceutical and pharmacological properties of the drug, it is very difficult to achieve a high rate of therapeutic effectiveness. Some of the general reasons why the bioavailability of drugs is less are as follows: (1) lower rate of water solubility, (2) lower rate of permeability, that is, the drug cannot pass through the biological membrane, and (3) faster metabolism and elimination from the body. Therefore, to overcome these demerits, targeted drug delivery or controlled drug delivery systems are realized in which the drug will be released at the specific site in a controlled manner with a constant rate [140].

These are more advantageous than the conventional methods because of less toxicity; requirement of comparatively a small amount of drug; faster and rapid recovery; more convenient dosing; and high patient compliance [141]. Owing to the major advancements in nanotechnology techniques, they have been incorporated in applications such as treatment, diagnosis, monitoring, and control of biological systems, and scientists have coined a term called ‘nanomedicine’ [142]. It is a challenging factor for scientists to choose a natural polymer in accordance with the different types of drug administration routes [141,142].

Cellulose-based nanomaterials are considered to be an ideal option for the vehicle drug molecule because cellulose materials are biocompatible, which does not elicit any immunological response in the body, and the rate of clearance from the renal system is less because the size of cellulose nanomaterials makes it difficult for the renal system to filter them from the body (Sunasee et al. [143]). Moreover, owing to high hydrophilicity of cellulose, the adsorption of opsonin proteins is hindered, and it is a crucial step before phagocytosis during removal of nanoparticles from the bloodstream. This will lead to an inherently prolonged blood circulation half-life compared with hydrophobic nanomaterials. Hydroxyl groups present in the surface of the cellulose molecule can be attached to any biomolecules with the help of covalent and non-covalent binding [144]. Several research groups investigated the effectiveness of different types of nanocellulose-based delivery systems to analyze the major factors such as biodegradability, cytotoxicity to a range of human cell types, and the mechanism of



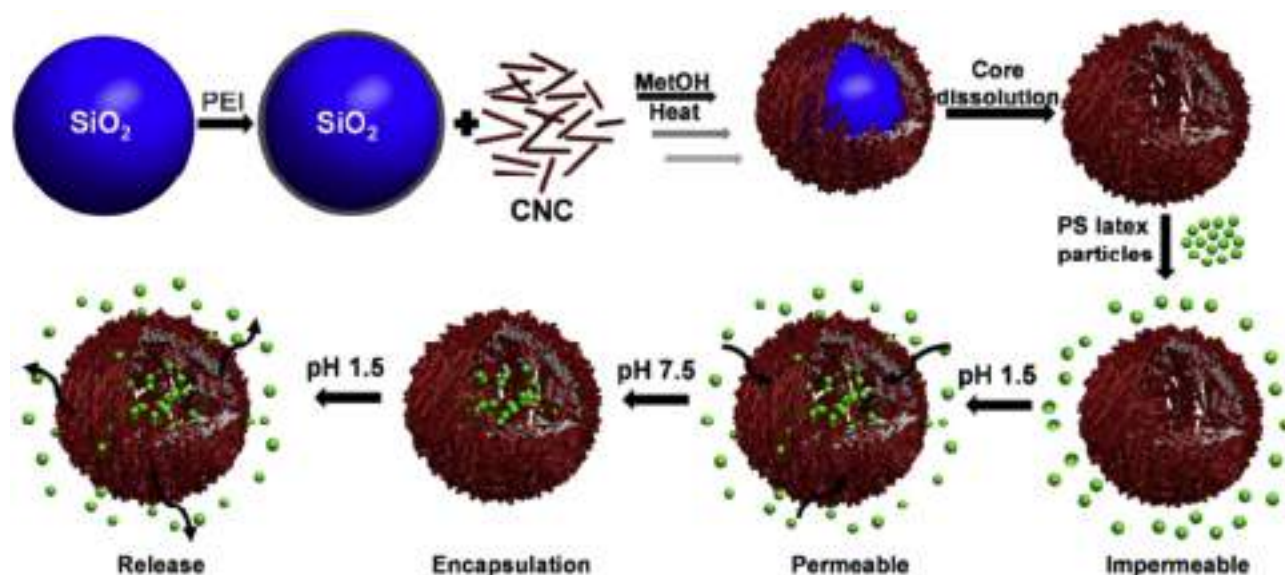


Fig. 15. Schematic representation of cellulose on cellulose microparticles and their working on different pH levels. CNC, cellulose nanocrystal.

cellular uptake. They have studied formulation types such as nanocrystals, negatively charged fluorescein isothiocyanate-labeled CNCs, positively charged rhodamine B isothiocyanate-labeled CNCs [145], folic acid-conjugated CNCs [146], acid-hydrolyzed CNCs [147], curcumin-cyclodextrin/CNC nanocomplex [148], and polyphosphoester-grafted CNCs [149] against nine different cell lines such as HBMEC, bEnd.3, RAW 264.7, MCF-10A, MDA-MB-231, MDA-MB-468, KB, PC-3, and C6 following the methyl tetrazolium (MTT) assay and lactate dehydrogenase leakage assay (LDH) assay methods. It was found that the filamentous CNCs showed no cytotoxic effects against any of those cell lines in the concentration range of 0–50 $\mu\text{g ml}^{-1}$ during the exposure time (48 h). Similarly, BC has also been studied for establishing controlled drug delivery systems. Various production techniques of BC-based nanocomposites have developed to optimize a controlled drug delivery system. BC has been blended with poly acrylic acid (PAA) by polymerization initiated through electron beam irradiation using various doses of radiation [150]. Moreover, these composites were sensitive to pH, and at neutral pH, their swelling reached maximum values. Therefore, they are considered to be pH-responsive substances for controlled in vitro drug delivery using different contents of bovine serum albumin (BSA) as a model compound. BC composites have also been used as a substitute carrier for transdermal drug delivery. By the diffusion cell technique, the diffusion rate of drugs through BC membranes was investigated. Compared with irradiated BC membranes, non-irradiated BC membranes showed faster drug diffusion. The therapeutic possibility of BC membranes was evaluated, and in vitro

manufacturing technique where any customized object with complex geometric structures can be fabricated within a very short time. This helps in meeting the increasing demand of customized products, especially in the area of biomedical engineering [152]. Scientists have coined a new term for rapid prototyping of biomedical products called 3D bioprinting, and the ink used for printing the products is known as bioink. Bioinks can be any biocompatible substances mixed with living cells [153]. Three-dimensional printing is a bottom-to-top-layer additive process, i.e., the products will be fabricated by depositing the ink layer by layer. Customized products will be initially modeled using any 3D modeling software which will be fed into the 3D printer. In other words, the accurate data of the tissues and organs that need to be printed will be collected and converted into electrical signals which will control the 3D printer [152]. It also involves the selection of a suitable fabrication method which helps in preserving the viability of cells during the entire prototyping process. Three-dimensional printing enhances the accuracy of the dimensions of the product which cannot be achieved through any conventional fabrication methods [152–154]. In addition to this, the speed of the addition process will be more, thus dramatically reducing the production cycle time. In this technique, there is no need of any molds, dies, and tools as in the conventional manufacturing methods, and this is a main factor in decreasing the cost per product involved in 3D printing [155]. In the medical field, this technique has been incorporated in tissue engineering, implants, and reconstructive surgery fields where there exists a high demand for customized products. Some of the common materials used in realizing 3D models include polyamide (PA), polyethylene terephthalate (PET), polyethylene glycol (PEG), polydimethylsiloxane (PDMS), and polylactide (PLA).

filamentous-shaped structure because it exhibits enough elastic modulus (G'), typically higher than few kPa, and yield stress in the order of few 10^2 Pa when the shear stress ceases. It ceases when the ink is allowed to flow through the micronozzle of the printer [156].

Common techniques involved in rapid prototyping in biomedical applications are direct ink writing (DIW), standard lithography, laser-based polymerization, and epitaxial assembly techniques. Compared with all these, DIW is found to be more advantageous because it enables programmable assembly of 3D periodic geometrical structures. It can be performed better than others by printing on various types of materials in a micrometer range. DIW uses ink that should have an optimum range of rheological properties. For maintaining the rheological properties of the ink used in DIW, nanocellulosic materials will be the best option. They enable the proper viscoelastic response of the ink, and as discussed, they can conserve the viability of the cells and support the prototyping of porous structures such as biological scaffolds [154,155].

Till date, only a few studies have been reported on the nanocellulose 3D printing for biomedical products. In 2015, Markstedt et al. developed a bioink using CNFs and alginate to print human chondrocytes and proved it to be a suitable hydrogel to be incorporated in cartilage tissue engineering applications. CNF itself showed a shear thinning with a good printing resolution, which assured the high structural fidelity. When cross-linked with alginate (using CaCl_2 in the matrix), even though alginate showed a dominance in showing properties, the *in vitro* and *ex vitro* cytotoxicity studies proved that the ink encourages the growth of cell culture. In addition to that, they maintained the cell viability in the printed constructs after 7 days of 3D culture ($85.7 \pm 1.9\%$) compared with day 1 ($72.8 \pm 6.0\%$) [157]. Fig. 14 shows the results of the study performed.

Trademarked bioink CELLINK[®] (from Sweden) is proven to be a good bioink in the auricular cartilage tissue engineering, where the serious or congenital auricular defects can be treated permanently [158]. They are said to contain 2% (w/w) of plant-derived CNFs and 0.5% (w/w) of sterile sodium alginate. In another study, Muller et al. [159] used alginate sulfate along with CNFs to develop a bioink for the printing of chondrocytes. CNFs enhanced the printing properties of the alginate sulfate. Alginate sulfate is generally mitogenic in nature, and even though it is mixed with CNFs, this dominant character has been preserved well and it shows superior cell proliferation compared to alginate and nanocellulose. Cell viability is also shown to be good because of the lower extrusion pressure and shear stresses, given by conical needles with a wide diameter [159]. In a study reported by Schütz et al. [160], functionalized cellulose has been used to fabricate centimeter-sized tissue engineering constructs with tailored architecture of an optimized alginate/methylcellulose hydrogel. The printability of the hydrogel obtained was enhanced by the addition of methyl cellulose in the alginate matrix. It was also helpful in maintaining the structural accuracy of the tissue engineering constructs. Cytotoxic studies conducted on methyl cellulose showed no results of toxicity and

widths <20 nm and lengths <200 nm. Short nanofibrillar geometry enhanced the reduction of viscoelastic properties of the bioink, which in turn resulted in good rheological properties.

5.5. Microencapsulation

Microencapsulation is a rapidly expanding technique in which very tiny droplets of any active substance (liquid form probably) will be covered or encapsulated with a continuous film of polymer [162]. The active ingredients or particle components, which are encapsulated, are termed as core materials, and the outer polymer covering is called wall material, carrier, or encapsulate. The main benefits are as follows: (1) It can convert the liquid core ingredient into solid form which modifies colloidal and surface properties for easy transportation and storage and (2) it can provide environment protection and control the releasing properties of the covering materials [162,163]. In 1931, it was first introduced by Bungenburg de Jon and Kan [162,181]. A microencapsulated model typically has a diameter in the range of 1–1000 μm , and it is incorporated in encapsulating core materials such as proteins, flavanoids, enzymes, pharmaceuticals, and even live cells [164]. Owing to several advancements in biomedical and tissue engineering arena, there exists the need of microcapsules which can carry and release any form of active materials. For example, microcapsules can act as a supporting aid in the controlled drug delivery because they are found to have prolonged sustainability or prolonged drug release compared with conventional drugs. Microencapsulation is also helpful in masking odor and taste of any oral drug and can convert any liquid drug into freely flowing powder [162,165]. It assists in overcoming drugs and can control the volatile property of a vaporizing drug. In addition to this, it can significantly reduce toxicity and gastrointestinal irritation which occurs after the drug administration. Cellulose polymers play an important role in developing the wall material because they are biocompatible, possess high yield and load-bearing capability, are mechanically stable, and highly encourage chemical modification [166]. In most of the studies, cellulose nanomaterials are used to enhance the property of alginate biopolymer, which is a linear one, compatible with encapsulation processes.

Cell microencapsulation is a recent technique in the biomedical field, which enables the treatment of multiple diseases in the absence of immunosuppression [167]. Over the past decades, studies had been conducted across the globe for developing immunoisolation technologies which will be useful in preventing the immune rejection of foreign bodies – grafts or transplants inside the human body. Encapsulate provides a semipermeable membrane that allows nutrients and secreted proteins to permeate, simultaneously isolating the cells from hostile immune reactions. For many years, alginate hydrogels have been used as an option for forming the wall material. It is the biopolymer that forms hydrogels when exposed to cations. Even though they are biocompatible, their mechanical and chemical stability do not allow them to be

strength of alginate microbeads. CNCs can be used as fillers in establishing various composites with matrices such as siloxanes, poly(caprolactone), glycerol-plasticized starch, styrene-butyl acrylate latex, and epoxies. The surface chemistry of CNCs allows them to bind with drug molecules and be used as drug excipients in common. It was proved that CNCs can easily create bonds with water-soluble and ionizable drugs such as tetracycline and doxorubicin. In 2015, Ye et al. [170] were successful in developing CNC microcapsules as tunable cages for holding microparticles and nanoparticles. It was an open-network morphology model facilitating the permeability of large solid particles with a diameter from 30 nm to 100 nm across the shell [170]. Fig. 15 shows the preparation and workflow of the cellulose on cellulose microcapsules under the influence of various pH levels.

6. Future ascents on cellulose nanomaterials

As discussed in the previous sections, the use of cellulose nanomaterials, in diverse range of biomedical applications, has been increased to a great extent. In a future scope of view, it can undoubtedly be said that functional modification of nanocellulose before the actual development of real materials is important because it leads to identification of the potential biomedical applications. For example, surface modification of cellulose nanomaterials with fluorescent molecules can enhance the fluorescent labeling ability, and thus, it can be incorporated in applications such as optical bioimaging, biosensors, and photodynamic therapy. Because these molecules can be traced easily by fluorescent analytical methods, the toxicity and biological activity of materials can be evaluated with less effort. Several prominent works have been reported on this exciting topic, starting from 2007 [166]. To date, molecules such as fluorescein-5-isothiocyanate (FITC) [171], rhodamine B isothiocyanate [145], pyrene dyes [172], terpyridine and its derivatives [111], 5-(and-6)-carboxyfluorescein succinimidyl ester, 5-(and-6)-carboxytetramethylrhodamine succinimidyl ester, 7-amino-4-methylcoumarin [173], etc were used for therapeutic applications. In gene therapeutic applications, a proper nanocarrier is essential to carry the DNA or genetic material to the targeted site. Surface modification of nanocellulose with amino acids can accommodate these biologically active building blocks. Different strategies are developed for establishing chemical conjunction between an amino acid and a CNC or CNF. A while back, a work was reported in which complementary DNA oligonucleotides have been grafted onto CNCs to produce DNA-based biocompatible nanomaterials by the principle of molecular recognition ability of DNA oligomeric base pairs. The resultant material is used successfully in enzyme/protein immobilization applications [174]. Another chemically modified molecule called ferrocene-decorated CNC was reported, which was fabricated by grafting ethynylferrocene onto azide-functionalized CNC using azide-

7. Conclusions

Cellulose is a fascinating biopolymer, and so far, it is the most abundant renewable compound present in the earth. It is proved to be an excellent replacement for petroleum-based non-renewable polymers and is considered to be an inexhaustible raw material. The main agenda of this article is to review nanocellulose, different types and properties, cellulose-reinforced composites, their classifications and properties, and how they are used in various biomedical applications. Cellulose nanomaterials or nanocellulose are generally classified into CNCs and CNFs. Acid hydrolysis technique is commonly used in preparing CNCs, whereas high-pressure homogenization of plant fibers is used in the commercial manufacturing of CNFs. Major works related to the production of CNCs, CNFs, and nanowhiskers are briefly introduced in this article. Comparatively, cellulose polymers are widely used to establish thermoplastic and thermoset composites compared with the traditional synthetic reinforcements such as aromatic polyester, polyethylene, aramid, glass, carbon, boron, and silicon carbide. These composites offer different varieties of features including their eco-friendly advantages, economical production, and higher specific strength/stiffness, which cannot be offered by synthetic reinforcement composites.

Cellulose nanomaterials are demonstrated to be a promising biomedical material owing to their properties such as biocompatibility; biodegradability; low cytotoxicity; high sorption and absorption ability; porosity; small dimensions; a variety of shapes; and enhanced specific surface, surface chemistry, rheology, crystallinity, self-assembly, high thermal stability, and other desirable mechanical properties. Moreover, they act as an insulator to various dilute solutions, namely, acids and alkalis, organic solvents, proteolytic enzymes, and antioxidants. A brief discussion on the applications of cellulose nanomaterials in the biomedical arenas – drug delivery, targeted drug delivery, wound healing, and new emerging fields such as 3D printing and microencapsulation, is made in this article. In drug delivery, nanocellulose is built in three forms – microspheres (beads) or microparticles, hydrogels or merely gels, and membranes or films. CNCs and nanowhiskers are extensively used in drug delivery and pharmaceutical applications. Critical drugs including anticancer agents were successfully bound with cationic CNCs. In targeted drug delivery, CNCs and BC-based nanocomposite systems are incorporated for delivering the drugs to the targeted site. Several works compared the efficiency of BC nanocomposite drug delivery systems with traditional therapeutic techniques such as gel and ointments in dermal applications, and results were hopeful enough in building a targeted drug delivery platform with nanocellulose materials. For proper wound healing, the dressings used should be porous in nature, able to keep moisture around the wound, and biocompatible in nature. BC or microbial cellulose can be an excellent option that satisfies all these properties, and many companies realized wound dressings using BC. Biofill[®] and Bioprocess[®] (used in the therapy of burns and ulcers

applications. As discussed, there is still a great way to go in achieving nanocellulose-based biomaterials by overcoming insurmountable challenges and concerns.

Acknowledgment

The authors would like to express their gratitude to the management of ADSO Naturals Pvt Ltd, for their support and encouragement.

Appendix A. Supplementary data

Supplementary data to this article can be found online at <https://doi.org/10.1016/j.mtchem.2019.04.012>.

References

- [1] P.A.L. Robert J.Y., Introduction to Polymers, third ed., 2011. New York.
- [2] W.H. Frank, Introduction to polymer chemistry, J. Chem. Educ. 58 (1981).
- [3] O. of T.A. U.S.Congress, Biopolymers: Making Materials Nature's Way Septzember 1993, 1993.
- [4] David L. Kaplan, Introduction to biopolymers from renewable resources. Biopolymers from renewable resources, Springer, Berlin, Heidelberg, 1998, pp. 1–29.
- [5] R. Chandra, R. Rustgi, Biodegradable polymers, Prog. Polym. Sci. 23 (1998) 1273–1335.
- [6] FriessW, Collagen – biomaterial for drug delivery, Eur. J. Pharm. Biopharm. 45 (1998) 113–136.
- [7] D. Klemm, B. Heublein, H.-P. Fink, A. Bohn, Cellulose: fascinating biopolymer and sustainable raw material, Angew. Chem. Int. Ed. 44 (2005) 3358–3393, <https://doi.org/10.1002/anie.200460587>.
- [8] T. Heinze, Cellulose: structure and properties, in: O. Rojas (Ed.), Cellulose Chemistry and Properties: Fibers, Nanocelluloses and Advanced Materials, vol. 271, Adv. Polym. Sci., 2015.
- [9] O. Theander, Cellulose, hemicellulose and extractives, Fundam. Thermochem. Biomass Convers. (1985) 35–60, https://doi.org/10.1007/978-94-009-4932-4_2.
- [10] P.D.D. Klemm, P.D.T. Schmauder, Hans-Peter Heinze, Cellulose, biopolym, in: Polysaccharides II Polysaccharides from Eukaryotes, vol. 6, 2002, pp. 275–287, <https://doi.org/10.1002/3527600035.bpol6010>.
- [11] A.C. O'Sullivan, Cellulose: the structure slowly unravels, Cellulose 4 (No.3) (1997) 173–207.
- [12] K.A. Heinze T. O.A. El Seoud, Production and characteristics of cellulose from different sources, in: Cellulose Derivatives, Springer Ser. Polym. Compos. Mater., 2018.
- [13] J.C. Courtenay, R.I. Sharma, J.L. Scott, Recent advances in modified cellulose for tissue culture applications, Molecules 23 (2018), <https://doi.org/10.3390/molecules23030654>.
- [14] A.L. Harold, Cellulose sources as raw materials for chemical manufacture, Ind. Eng. Chem. 14 (4) (1936) 70.
- [15] H.L. Jong, R.B. Malcolm, et al., Assembly of synthetic cellulose I, Proc. Natl. Acad. Sci. USA 91 (1994) 7425–7429.
- [16] A.M. Bocek, Effect of hydrogen bonding on cellulose solubility in aqueous and nonaqueous solvents, Russ. J. Appl. Chem. 76 (11) (2003) 1711–1719.
- [17] K. Oksman, M. Sain (Eds.), Cellulose Nanocomposites: Processing, Characterization and Properties, 2006.
- [18] M. Roman (Ed.), Model Cellulosic Surfaces, 2009.
- [19] Lucian A. Lucia, Orlando Rojas (Eds.), The nanoscience and technology of renewable biomaterials, John Wiley & Sons, 2009.
- [20] A.C. O'Sullivan, The structure slowly unravels, Cellulose 4 (1997) 173–207.
- [21] Stephen J. Eichhorn, A. Dufresne, M. Aranguren, N.E. Marcovich, J.R. Capadona, S.J. Rowan, Christoph Weder, et al., Current international research into cellulose nanofibres and nanocomposites, J Mater. Sci. 45 (1) (2010) 1–33.
- [22] Y. Habbibi, L. A. Lucia, O.L. Rojas, Cellulose Nanocrystals: Chemistry, Self-iron oxide composites, Sensor. Actuator. B Chem. 233 (2016) 633–638, <https://doi.org/10.1016/j.snb.2016.04.134>.
- [28] K.K. Sadasivuni, A. Kafy, H. Kim, H. Ko, S. Mun, J. Kim, Reduced Graphene Oxide Filled Cellulose Films for Flexible Temperature Sensor Application, vol. 2006, 2015, pp. 154–161, <https://doi.org/10.1016/j.synthmet.2015.05.018>.
- [29] K.K. Sadasivuni, A. Kafy, L. Zhai, H. Ko, Transparent and Flexible Cellulose Nanocrystal/Reduced Graphene Oxide Film for Proximity Sensing, 2014, pp. 1–9, <https://doi.org/10.1002/sml.201402109>.
- [30] N.L. Garcia de Rodriguez, W. Thielemans, A. Dufresne, Sisal cellulose whiskers reinforced polyvinyl acetate nanocomposites, Cellulose 13 (2006) 261–270, <https://doi.org/10.1007/s10570-005-9039-7>.
- [31] S. Beck-Candanedo, M. Roman, D.G. Gray, Effect of reaction conditions on the properties and behavior of wood cellulose nanocrystal suspensions, Biomacromolecules 6 (2005) 1048–1054, <https://doi.org/10.1021/bm049300p>.
- [32] W. Bai, J. Holbery, K. Li, A technique for production of nanocrystalline cellulose with a narrow size distribution, Cellulose 16 (2009) 455–465.
- [33] R.J. Moon, A. Martini, J. Nairn, J. Simonsen, J. Youngblood, Cellulose nanomaterials review: structure, properties and nanocomposites, Chem. Soc. Rev. 40 (2011) 3941, <https://doi.org/10.1039/c0cs00108b>.
- [34] B.G. Rånby, A. Banderet, L.G. Sillén, Aqueous colloidal solutions of cellulose micelles, Acta Chem. Scand. 3 (1949) 649–650, <https://doi.org/10.3891/acta.chem.scand.03-0649>.
- [35] N.R. Savadekar, S.T. Mhaske, Synthesis of nano cellulose fibers and effect on thermoplastics starch based films, Carbohydr. Polym. 89 (2012) 146–151, <https://doi.org/10.1016/j.carbpol.2012.02.063>.
- [36] S.Y.Z. Zainuddin, I. Ahmad, H. Kargazadeh, I. Abdullah, A. Dufresne, Potential of using multiscale kenaf fibers as reinforcing filler in cassava starch-kenaf biocomposites, Carbohydr. Polym. 92 (2013) 2299–2305, <https://doi.org/10.1016/j.carbpol.2012.11.106>.
- [37] R.M.D.F. Nascimento D M, J.S. Almeida, A.F. Dias, M.C.B. Figueiredo, J.P.S. Morais, J.P.A. Feitosa, A Novel Green Approach for the Preparation of Cellulose Nanowhiskers from White Coir, Carbohydr Polym [Internet], vol. 110, Elsevier Ltd, 2014, pp. 456–463.
- [38] D. De Jesus Silva, M.L.O. D'Almeida, Nanocrystals de celulose, Pap. 70 (2009) 34–52, <https://doi.org/10.1002/marc.200300268>.
- [39] A. Dufresne, Interfacial phenomena in nanocomposites based on polysaccharide nanocrystals, Compos. Interfac. 10 (2003) 369–387, <https://doi.org/10.1163/156855403771953641>.
- [40] B.G. Rånby, The cellulose micelles, TAPPI (Tech. Assoc. Pulp Pap. Ind.) 35 (1952) 53–58.
- [41] O. Nechyporchuk, M.N. Belgacem, J. Bras, Production of cellulose nanofibrils: a review of recent advances, Ind. Crops Prod. 93 (2016) 2–25, <https://doi.org/10.1016/j.indcrop.2016.02.016>.
- [42] P.D. Martins D F, A.B. de Souza, M.A. Henrique, H.A. Silverio, W.P. Flauzino Neto, The Influence of the Cellulose Hydrolysis Process on the Structure of Cellulose Nanocrystals Extracted from Capim Mombaça (Panicum Maximum), Ind Crop. Prod [Internet], Elsevier B.V., 2014, p. 65.
- [43] J.C.O. Villanova, E. Ayres, S.M. Carvalho, P.S. Patrício, F.V. Pereira, R.L. Orefice, Pharmaceutical acrylic beads obtained by suspension polymerization containing cellulose nanowhiskers as excipient for drug delivery, Eur. J. Pharm. Sci. 42 (2011) 406–415, <https://doi.org/10.1016/j.ejps.2011.01.005>.
- [44] M. Rajan, M. Murugan, D. Ponnamma, K. Kumar, M.A. Munusamy, ScienceDirect Poly-carboxylic acids functionalized chitosan nanocarriers for controlled and targeted anti-cancer drug delivery, Biomed. Pharmacother. 83 (2016) 201–211, <https://doi.org/10.1016/j.biopha.2016.06.026>.
- [45] H. Charreau, M.L. Foresti, A. Vazquez, Nanocellulose patents trends: a comprehensive review on patents on cellulose nanocrystals, microfibrillated and bacterial cellulose, Recent Pat. Nanotechnol. 7 (2012) 56–80, <https://doi.org/10.2174/1872210511307010056>.
- [46] Y.H. Abe K, S. Iwamoto, Obtaining cellulose nanofibers with a uniform width of 15 nm from wood, Biomacromolecules 8 (2007) 3276–3278.
- [47] T.S. Chirayil C, J. Joy, L. Mathew, M. Mozetic, J. Koetz, Isolation and characterization of cellulose nanofibrils from helicteres isora plant, Ind. Crops Prod. 59 (2014) 27–34.
- [48] B. Deepa, E. Abraham, B.M. Cherian, A. Bismarck, J.J. Blaker, L.A. Pothen, A.L. Leao, S.F. de Souza, M. Kottaisamy, Structure, morphology and thermal characteristics of banana nano fibers obtained by steam explosion, Bioresour. Technol. 102

- [54] G. Eriksen Ø, K. Syverud, The use of microfibrillated cellulose produced from kraft pulp as strength enhancer in TMP paper, *Nord. Pulp Pap. Res. J.* 23 (2008) 299–304.
- [55] T. Lindström, C. Aulin, Market and technical challenges and opportunities in the area of innovative new materials and composites based on nanocellulosics, *Scand. J. For. Res.* 29 (2014) 345–351, <https://doi.org/10.1080/02827581.2014.928365>.
- [56] K.L. Spence, R.A. Venditti, O.J. Rojas, Y. Habibi, J.J. Pawlak, A comparative study of energy consumption and physical properties of microfibrillated cellulose produced by different processing methods, *Cellulose* 18 (2011) 1097–1111, <https://doi.org/10.1007/s10570-011-9533-z>.
- [57] T. Taniguchi, K. Okamura, New films produced from microfibrillated natural fibres, *Polym. Int.* 47 (1998) 291–294, [https://doi.org/10.1002/\(SICI\)1097-0126\(199811\)47:3<291::AID-PI11>3.0.CO;2-1](https://doi.org/10.1002/(SICI)1097-0126(199811)47:3<291::AID-PI11>3.0.CO;2-1).
- [58] O. Nechyporchuk, F. Pignon, M.N. Belgacem, Morphological properties of nanofibrillated cellulose produced using wet grinding as an ultimate fibrillation process, *J. Mater. Sci.* 50 (2014) 531–541, <https://doi.org/10.1007/s10853-014-8609-1>.
- [59] O. Nechyporchuk, M.N. Belgacem, F. Pignon, Concentration effect of TEMPO-oxidized nanofibrillated cellulose aqueous suspensions on the flow instabilities and small-angle X-ray scattering structural characterization, *Cellulose* 22 (2015) 2197–2210, <https://doi.org/10.1007/s10570-015-0640-0>.
- [60] Q.Q. Wang, J.Y. Zhu, R. Gleisner, T.A. Kuster, U. Baxa, S.E. McNeil, Morphological development of cellulose fibrils of a bleached eucalyptus pulp by mechanical fibrillation, *Cellulose* 19 (2012) 1631–1643, <https://doi.org/10.1007/s10570-012-9745-x>.
- [61] A. Dufresne, J.-Y. Cavaille, M.R. Vignon, Mechanical behavior of sheets prepared from sugar beet cellulose microfibrils, *J. Appl. Polym. Sci.* 64 (1997) 1185–1194, [https://doi.org/10.1002/\(SICI\)1097-4628\(19970509\)64:6<1185::AID-APP19>3.0.CO;2-V](https://doi.org/10.1002/(SICI)1097-4628(19970509)64:6<1185::AID-APP19>3.0.CO;2-V).
- [62] K. Kekäläinen, H. Liimatainen, F. Biale, J. Niinimäki, Nanofibrillation of TEMPO-oxidized bleached hardwood kraft cellulose at high solids content, *Holzforchung* 69 (2015) 1077–1088, <https://doi.org/10.1515/hf-2014-0269>.
- [63] G. Lubin, *Handbook of Fiberglass and Advanced Plastics Composites*, 1969.
- [64] M.P. Groover, *Fundamental of Modern Manufacturing*, second ed., 2004. River Street, Hoboken, NJ.
- [65] T.M. Maloney, In *International Encyclopedia of Composites*, VCH Publ., New York, 1995.
- [66] R.M. Tennant, *Science Data Book*, 1971.
- [67] J.A. Youngquist, in: L. Vigo (Ed.), *The Role of Matrix, Fiber, and Znterjace*, *Compos. Appl.*, 1992, pp. 383–401.
- [68] J.A. Brydson, *Plastics Materials*, Butterworth-Heinemann, 1982.
- [69] D. Nabi Saheb, J.P. Jog, Natural fiber polymer composites: a review, *Adv. Polym. Technol.* 18 (1999) 351–363, [https://doi.org/10.1002/\(SICI\)1098-2329\(199924\)18:4<351::AID-ADV6>3.0.CO;2-X](https://doi.org/10.1002/(SICI)1098-2329(199924)18:4<351::AID-ADV6>3.0.CO;2-X).
- [70] A.G. Facca, M.T. Kortschot, N. Yan, Predicting the tensile strength of natural fibre reinforced thermoplastics, *Compos. Sci. Technol.* 67 (2007) 2454–2466, <https://doi.org/10.1016/j.compscitech.2006.12.018>.
- [71] Carl Eckert, Opportunities for natural fibers in plastic composites, in: *Proceedings of progress in wood Fiber-plastic composites Conference*, Toronto, Canada, p. 14, 2000.
- [72] M. Jawaid, H.P.S. Abdul Khalil, Cellulosic/synthetic fibre reinforced polymer hybrid composites: a review, *Carbohydr. Polym.* 86 (2011) 1–18, <https://doi.org/10.1016/j.carbpol.2011.04.043>.
- [73] A. Amash, P. Zugenmaier, Morphology and properties of isotropic and oriented samples of cellulose fibre-polypropylene composites, *Polymer* 41 (2000) 1589–1596, [https://doi.org/10.1016/S0032-3861\(99\)00273-6](https://doi.org/10.1016/S0032-3861(99)00273-6).
- [74] L.T. Bismarck A, S. Mishra, Plant fibers as reinforcement for green composites, in: D.L.T. Mohanty A K, M. Misra (Eds.), *Nat. Fibers, Biopolym. Bio-composites*, CRC Press, 2005.
- [75] X. Li, L.G. Tabil, S. Panigrahi, Chemical treatments of natural fiber for use in natural fiber-reinforced composites: a review, *J. Polym. Environ.* 15 (2007) 25–33, <https://doi.org/10.1007/s10924-006-0042-3>.
- [76] D. Ray, B.K. Sarkar, A.K. Rana, N.R. Bose, Effect of alkali treated jute fibres on composite properties, *Bull. Mater. Sci.* 24 (2001) 129–135, <https://doi.org/10.1007/BF02710089>.
- [77] L.Y. Mwaikambo, N. Tucker, A.J. Clark, Mechanical properties of hemp-fibre-reinforced euphorbia composites, *Macromol. Mater. Eng.* 292 (2007) 993–1000, <https://doi.org/10.1002/mame.200700092>.
- [78] J. George, Jan Ivens, Ignace Verpoest, Surface modification to improve the impact performance of natural fibre composites, in: *Proceedings of ICCM 12*, France, 1999.
- [79] K.M. Rahman MM, A.K. Mallik, Influences of various surface pretreatments on the mechanical and degradable properties of photografted oil palm fibers, *Polym. Polym. Compos.* 21 (2007) 449–456, <https://doi.org/10.1002/app>.
- [80] V. Tserki, N.E. Zafeiropoulos, F. Simon, C. Panayiotou, A study of the effect of acetylation and propionylation surface treatments on natural fibres, *Compos Part A Appl. Sci. Manuf.* 36 (2005) 1110–1118, <https://doi.org/10.1016/j.compositesa.2005.01.004>.
- [81] M.S. Sreekala, M.G. Kumaran, S. Joseph, M. Jacob, Oil Palm Fibre Reinforced Phenol Formaldehyde Composites: Influence of Fibre Surface Modifications on the Mechanical Performance, 2000, pp. 295–329.
- [82] B. Wang, S. Panigrahi, L. Tabil, W. Crerar, Pre-treatment of flax fibers for use in rotationally molded biocomposites, *J. Reinf. Plast. Compos.* 26 (2007) 447–463, <https://doi.org/10.1177/0731684406072526>.
- [83] G. Groeninckx, G. Kalaprasad, S. Thomas, S. Thomas, C.R. Kumar, C. Pavithran, B. Francis, Effect of fibre length and chemical modifications on the tensile properties of intimately mixed short sisal/glass hybrid fibre reinforced low density polyethylene composites, *Polym. Int.* 53 (2004) 1624–1638, <https://doi.org/10.1002/pi.1453>.
- [84] D.H. Page, F. El Hosseiny, K. Winkler, A.P.S. Lancaster, Elastic modulus of single wood pulp fibers, *TAPPI (Tech. Assoc. Pulp Pap. Ind.)* 60 (1977) 114.
- [85] M.M. Kabir, H. Wang, K.T. Lau, F. Cardona, Chemical treatments on plant-based natural fibre reinforced polymer composites: an overview, *Compos. B Eng.* 43 (2012) 2883–2892, <https://doi.org/10.1016/j.compositesb.2012.04.053>.
- [86] M.V.M. De S K, Short fiber-rubber composites, *Polym. Eng. Revis.* 4 (4) (1984) 313–343.
- [87] T.W. Hull, D. Clyne, *An Introduction to Composite Materials*, Cambridge University Press, Cambridge, 1996.
- [88] J. Bledzki, A.K. Reinhmane, S. Gassan, Thermoplastics reinforced with wood fillers, *Polym. Plast. Technol. Eng.* 37 (1998) 451–468.
- [89] K. Chawla, *Composite Materials. Science and Engineering*, Springer-Verlag, New York, 1987.
- [90] M. Roe, P. Ansell, Jute reinforced polyester composites, *J. Mater. Sci.* 20 (1985) 4015–4020.
- [91] J. De Albuquerque, K. A. Joseph, Hecker de Carvalho, L. Carvalho, Morais d'Almedia, Effect of wettability and ageing conditions on the physical and mechanical properties of uniaxially oriented jute-roving-reinforced polyester composites, *Compos. Sci. Technol.* 60 (1999) 833–844.
- [92] I. Owolabi, O. Czvikovszky, T. Kovacs, Coconut fiber reinforced thermosetting plastics, *J. Appl. Polym.* 30 (1985) 1827–1836.
- [93] A. Shalwan, B.F. Yousif, In state of art: mechanical and tribological behaviour of polymeric composites based on natural fibres, *Mater. Des.* 48 (2013) 14–24, <https://doi.org/10.1016/j.matdes.2012.07.014>.
- [94] V.K. Singha, A.S. Thakur, Chemical resistance, mechanical and physical properties of biofibers -based polymer composites, *Polym. Plast. Technol. Eng.* 48 (7) (2009) 736–744.
- [95] D.E. El-Saied, H. El-Diwany, A.I. Basta, A.H. Atwa, N.A. El-Ghwas, Production and characterization of economical bacterial cellulose, *BioResources* 3 (4) (2008) 1196–1217.
- [96] A.S. Singha, V.K. Thakur, Mechanical, morphological, and thermal characterization of compression-molded polymer biocomposites, *Int. J. Polym. Anal. Charact.* 15 (2010) 87–97, <https://doi.org/10.1080/10236660903474506>.
- [97] A.D. La Rosa, G. Cozzo, A. Latteri, A. Recca, A. Björklund, E. Parrinello, G. Cicala, Life cycle assessment of a novel hybrid glass-hemp/thermoset composite, *J. Clean. Prod.* 44 (2013) 69–76, <https://doi.org/10.1016/j.jclepro.2012.11.038>.
- [98] D. Liu, J. Song, D.P. Anderson, P.R. Chang, Y. Hua, Bamboo fiber and its reinforced composites: structure and properties, *Cellulose* 19 (2012) 1449–1480, <https://doi.org/10.1007/s10570-012-9741-1>.
- [99] H.M. Akil, M.F. Omar, A.A.M. Mazuki, S. Safiee, Z.A.M. Ishak, A. Abu Bakar, Kenaf fiber reinforced composites: a review, *Mater. Des.* 32 (2011) 4107–4121, <https://doi.org/10.1016/j.matdes.2011.04.008>.
- [100] M.E.E.G. Bogoeva-Gaceva, M. Avella, M. Malinconico, A. Buzarovska, A. Grozdanov, G. Gentile, Natural fiber eco-composites, *Polym. Polym. Compos.* 16 (2008) 101–113, <https://doi.org/10.1002/pc>.
- [101] Rui I. Reis, Nuno M. Neves, João F. Mano, Manuela E. Gomes, Alexandra

- [112] N. Shah, M. Ul-Islam, W.A. Khattak, J.K. Park, Overview of bacterial cellulose composites: a multipurpose advanced material, *Carbohydr. Polym.* 98 (2013) 1585–1598, <https://doi.org/10.1016/j.carbpol.2013.08.018>.
- [113] G. Tiwari, R. Tiwari, S. Bannerjee, L. Bhati, S. Pandey, P. Pandey, B. Sriwastawa, Drug delivery systems: an updated review, *Int. J. Pharm. Investig.* 2 (2012) 2, <https://doi.org/10.4103/2230-973X.96920>.
- [114] K. Kataoka, A. Harada, Y. Nagasaki, Block copolymer micelles for drug delivery: design, characterization and biological significance, *Adv. Drug Deliv. Rev.* 64 (2012) 37–48, <https://doi.org/10.1016/j.addr.2012.09.013>.
- [115] M. Thompson, A review of: “making medicines – a brief history of pharmacy and pharmaceuticals”, *Drug Dev. Ind. Pharm.* 32 (2006) 909, <https://doi.org/10.1080/03639040600559008>.
- [116] J. Shi, A.R. Votruba, O.C. Farokhzad, R. Langer, Nanotechnology in drug delivery and tissue engineering: from discovery to applications, *Nano Lett.* 10 (2010) 3223–3230, <https://doi.org/10.1021/nl102184c>.
- [117] J.K. Jackson, K. Letchford, B.Z. Wasserman, L. Ye, W.Y. Hamad, H.M. Burt, The use of nanocrystalline cellulose for the binding and controlled release of drugs, *Int. J. Nanomed.* 6 (2011) 321–330, <https://doi.org/10.2147/IJN.S16749>.
- [118] H.J. Kolakovics, R. L. Peltonen, T. Laaksonen, K. Putkisto, A. Laukkanen, Spray-dried cellulose nanofibers as novel tablet excipient, *AAPS PharmSciTech* 48 (12) (2011) 1366–1373.
- [119] A.J. Paula, J.S. Bernardes, A.B. Seabra, N. Durán, W.J. Fávaro, Cellulose nanocrystals as carriers in medicine and their toxicities: a review, *Carbohydr. Polym.* 181 (2017) 514–527, <https://doi.org/10.1016/j.carbpol.2017.12.014>.
- [120] L. Weng, P. Rostamzadeh, N. Nooryshokry, H.C. Le, J. Golzarian, In vitro and in vivo evaluation of biodegradable embolic microspheres with tunable anticancer drug release, *Acta Biomater.* 9 (2013) 6823–6833, <https://doi.org/10.1016/j.actbio.2013.02.017>.
- [121] Y. Wen, J.K. Oh, Dual-stimuli reduction and acidic pH-responsive bio-nanogels: intracellular delivery nanocarriers with enhanced release, *RSC Adv.* 4 (2014) 229–237, <https://doi.org/10.1039/c3ra46072j>.
- [122] Y. Liu, H. Ye, K. Satkunendrarajah, G.S. Yao, Y. Bayon, M.G. Fehlings, A self-assembling peptide reduces glial scarring, attenuates post-traumatic inflammation and promotes neurological recovery following spinal cord injury, *Acta Biomater.* 9 (2013) 8075–8088, <https://doi.org/10.1016/j.actbio.2013.06.001>.
- [123] S. Liekens, E. De Clercq, J. Neyts, Angiogenesis: regulators and clinical applications, *Biochem. Pharmacol.* 61 (2001) 253–270, [https://doi.org/10.1016/S0006-2952\(00\)00529-3](https://doi.org/10.1016/S0006-2952(00)00529-3).
- [124] J.R. Sharpe, Y. Martin, Strategies demonstrating efficacy in reducing wound contraction, *in vivo*, *Adv. Wound Care* 2 (2013) 167–175.
- [125] D.N. Heo, D.H. Yang, J.B. Lee, M.S. Bae, J.H. Kim, S.H. Moon, H.J. Chun, C.H. Kim, H.N. Lim, I.K. Kwon, Burn-wound healing effect of gelatin/polyurethane nanofiber scaffold containing silver-sulfadiazine, *J. Biomed. Nanotechnol.* 9 (2013) 511–515, <https://doi.org/10.1166/jbnn.2013.1509>.
- [126] L. Fu, J. Zhang, G. Yang, Present status and applications of bacterial cellulose-based materials for skin tissue repair, *Carbohydr. Polym.* 92 (2013) 1432–1442, <https://doi.org/10.1016/j.carbpol.2012.10.071>.
- [127] S. Mondal, Preparation, properties and applications of nanocellulosic materials, *Carbohydr. Polym.* 163 (2017) 301–316, <https://doi.org/10.1016/j.carbpol.2016.12.050>.
- [128] L. Fu, Y. Zhang, C. Li, Z. Wu, Q. Zhuo, X. Huang, G. Qiu, P. Zhou, G. Yang, Skin tissue repair materials from bacterial cellulose by a multilayer fermentation method, *J. Mater. Chem.* 22 (2012) 12349–12357, <https://doi.org/10.1039/c2jm00134a>.
- [129] L. Fu, P. Zhou, S. Zhang, G. Yang, Evaluation of bacterial nanocellulose-based uniform wound dressing for large area skin transplantation, *Mater. Sci. Eng. C* 33 (2013) 2995–3000, <https://doi.org/10.1016/j.msec.2013.03.026>.
- [130] S.U. Park, B.K. Lee, M.S. Kim, K.K. Park, W.J. Sung, H.Y. Kim, D.G. Han, J.S. Shim, Y.J. Lee, S.H. Kim, I.H. Kim, D.H. Park, The possibility of microbial cellulose for dressing and scaffold materials, *Int. Wound J.* 11 (2014) 35–43, <https://doi.org/10.1111/j.1742-481X.2012.01035.x>.
- [131] Y.G. Cai Zhijiang, Bacterial cellulose/collagen composites: characterization and first evaluation of cytocompatibility, *J. Appl. Polym. Sci.* 120 (2011) 2938–2944, <https://doi.org/10.1002/app>.
- [132] A. Nakayama, A. Kakugo, J.P. Gong, Y. Osada, M. Takai, T. Erata, S. Kawano, High mechanical strength double-network hydrogel with bacterial cellulose, *Adv. Funct. Mater.* 14 (2004) 1124–1128, <https://doi.org/10.1002/advf.10002>.
- [133] Y. Huang, C. Zhu, J. Yang, Y. Nie, C. Chen, D. Sun, Recent advances in bacterial cellulose, *Cellulose* 21 (2014) 1–30, <https://doi.org/10.1007/s10570-013-0088-z>.
- [134] C. Wang, Y. Zheng, K. Wang, J. Wu, J. Luan, X. Wen, Z. Wu, L. Yue, In vitro and in vivo investigation of bacterial cellulose dressing containing uniform silver sulfadiazine nanoparticles for burn wound healing, *Prog. Nat. Sci. Mater. Int.* 25 (2015) 197–203, <https://doi.org/10.1016/j.pnsc.2015.05.004>.
- [135] A.M. Hillery, A.H. Lloyd, *Drug Delivery and Targeting*, Taylor & Francis e-Library, London, 2005.
- [136] R. Paper, G. Manish, S. Vimukta, Targeted drug delivery system, *Review* 1 (2011) 1–24, <https://doi.org/10.20959/wjpps20166-6679>.
- [137] V. Rajendran, S. Jagannathan, R.G. Pachamuthu, Application of Nanotechnology in Medicine: A View Applications of Nanotechnology in Medicine: A View, 2013.
- [138] U.D.H. K.C. Rajesh Sunasee, Cellulose nanocrystals: a versatile nanopatform for emerging biomedical applications, *Expert Opin. Drug Deliv.* 13 (9) (2016) 1243–1256.
- [139] Vibhuti Agrahari, Vivek Agrahari, Ashim K. Mitra, Nanocarrier fabrication and macromolecule drug delivery: challenges and opportunities, *Ther. Deliv.* 7 (4) (2016) 257–278.
- [140] K.A. Mahmoud, J.A. Mena, K.B. Male, S. Hrapovic, A. Kamen, J.H.T. Luong, Effect of surface charge on the cellular uptake and cytotoxicity of fluorescently labeled cellulose nanocrystals, *ACS Appl. Mater. Interfaces* 2 (2010) 2924–2932, <https://doi.org/10.1021/am1006222>.
- [141] S. Dong, H.J. Cho, Y.W. Lee, M. Roman, Synthesis and cellular uptake of folic acid-conjugated cellulose nanocrystals for cancer targeting, *Biomacromolecules* 15 (2014) 1560–1567, <https://doi.org/10.1021/bm401593n>.
- [142] Laldhupanga Pachuau, Pranab Jyoti Das, Bhaskar Mazumder, Therapeutic nanostructures for improved wound healing, *Nanotechnol. Ther. Nutraceutical Cosmet. Adv.* (2019) 75.
- [143] L. Zhang, S. Man, H. Qiu, Z. Liu, M. Zhang, L. Ma, W. Gao, Curcumin-cyclodextrin complexes enhanced the anti-cancer effects of curcumin, *Environ. Toxicol. Pharmacol.* 48 (2016) 31–38, <https://doi.org/10.1016/j.etap.2016.09.021>.
- [144] Kam Chiu Tam, Peihong Ni, H. Wang, J. He, M. Zhang, A New pathway towards polymer modified cellulose nanocrystals via a “grafting onto” process for drug delivery, *Polym. Chem.* 00 (2015) 1–3, <https://doi.org/10.1039/x0xx00000x>.
- [145] M. Moniri, A. Boroumand Moghaddam, S. Azizi, R. Abdul Rahim, A. Bin Ariff, W. Zuhainis Saad, M. Navaderi, R. Mohamad, Production and status of bacterial cellulose in biomedical engineering, *Nanomaterials* 7 (2017) 257, <https://doi.org/10.3390/nano7090257>.
- [146] D.K. Astrid Muller, N.I. Zhixu, Hessler Nadine, Wesarg Falko, Frank A. Muller, The biopolymer bacterial nanocellulose as drug delivery system: investigation of drug loading and release using the model protein albumin, *J. Pharm. Sci.* 102 (2012) 579–592, <https://doi.org/10.1002/jps>.
- [147] T.A. Campbell, O.S. Ivanova, 3D printing of multifunctional nanocomposites, *Nano Today* 8 (2013) 119–120, <https://doi.org/10.1016/j.nantod.2012.12.002>.
- [148] J.S. Kim, S. Hong, C. Hwang, Bio-ink Materials for 3D Bio-Printing, 2016, <https://doi.org/10.18204/JISSIS.2016.3.2.049>.
- [149] A.R. Studart, Additive manufacturing of biologically-inspired materials, *Chem. Soc. Rev.* 45 (2016) 359–376, <https://doi.org/10.1039/c5cs00836k>.
- [150] S.V. Murphy, A. Atala, 3D bioprinting of tissues and organs, *Nat. Biotechnol.* 32 (2014) 773–785, <https://doi.org/10.1038/nbt.2958>.
- [151] G. Siqueira, D. Kokkinis, R. Libanori, M.K. Hausmann, A.S. Gladman, A. Neels, P. Tingaut, T. Zimmermann, J.A. Lewis, A.R. Studart, Cellulose nanocrystal inks for 3D printing of textured cellular architectures, *Adv. Funct. Mater.* 27 (2017), <https://doi.org/10.1002/adfm.201604619>.
- [152] K. Markstedt, A. Mantas, I. Tournier, H. Martínez Ávila, D. Hägg, P. Gatenholm, 3D bioprinting human chondrocytes with nanocellulose-alginate bioink for cartilage tissue engineering applications, *Biomacromolecules* 16 (2015) 1489–1496, <https://doi.org/10.1021/acs.biomac.5b00188>.
- [153] H. Martínez Ávila, S. Schwarz, N. Rotter, P. Gatenholm, 3D bioprinting of human chondrocyte-laden nanocellulose hydrogels for patient-specific articular cartilage regeneration, *Bioprinting* 1–2 (2016) 22–35, <https://doi.org/10.1016/j.bprint.2016.08.003>.
- [154] M. Müller, E. Öztürk, Ø. Arlov, P. Gatenholm, M. Zepobi-Wong, Alginate

- [163] M. Peanparkdee, S. Iwamoto, R. Yamauchi, Microencapsulation: a review of applications in the food and pharmaceutical industries, *Rev. Agric. Sci.* 4 (2016), <https://doi.org/10.7831/ras.4.56>.
- [164] V. Nedovic, A. Kalusevic, V. Manojlovic, S. Levic, B. Bugarski, An overview of encapsulation technologies for food applications, *Procedia Food Sci* 1 (2011) 1806–1815, <https://doi.org/10.1016/j.profoo.2011.09.265>.
- [165] A. Gupta, B. Dey, Microencapsulation for controlled drug delivery: a comprehensive review, *Sunsari Tech. Coll. J.* 1 (2013) 48–54, <https://doi.org/10.3126/stcj.v1i1.8660>.
- [166] N. Lin, A. Dufresne, Nanocellulose in biomedicine: current status and future prospect, *Eur. Polym. J.* 59 (2014) 302–325, <https://doi.org/10.1016/j.eurpolymj.2014.07.025>.
- [167] I. Kahouli, S.P. Catherine Tomaro-Duchesneau, Shyamalia Saha, Meenakshi Malhotra, Microencapsulation for the therapeutics delivery of drugs, live mammalian and bacterial cells, and other biopharmaceutics: current status and future directions, *J. Pharm. (Lahore)* (2013) 19.
- [168] M. Park, D. Lee, J. Hyun, Nanocellulose-alginate hydrogel for cell encapsulation, *Carbohydr. Polym.* 116 (2015) 223–228, <https://doi.org/10.1016/j.carbpol.2014.07.059>.
- [169] T. Huq, B. Riedl, J. Bouchard, S. Salmieri, M. Lacroix, Microencapsulation of nisin in alginate-cellulose nanocrystal (CNC) microbeads for prolonged efficacy against *Listeria monocytogenes*, *Cellulose* 21 (2014) 4309–4321, <https://doi.org/10.1007/s10570-014-0432-y>.
- [170] C. Ye, S.T. Malak, K. Hu, W. Wu, V.V. Tsukruk, Cellulose nanocrystal microcapsules as tunable Cages for nano- and microparticles, *ACS Nano* 9 (2015) 10887–10895, <https://doi.org/10.1021/acs.nano.5b03905>.
- [171] S. Dong, M. Roman, Fluorescently labeled cellulose nanocrystals for bioimaging applications, *J. Am. Chem. Soc.* 129 (2007) 13810–13811, <https://doi.org/10.1021/ja076196i>.
- [172] L. Zhang, Q. Li, J. Zhou, L. Zhang, Synthesis and photophysical behavior of pyrene-bearing cellulose nanocrystals for Fe³⁺ sensing, *Macromol. Chem. Phys.* 213 (2012) 1612–1617, <https://doi.org/10.1002/macp.201200233>.
- [173] L.J. Nielsen, S. Eyley, W. Thielemans, J.W. Aylott, Dual fluorescent labelling of cellulose nanocrystals for pH sensing, *Chem. Commun.* 46 (2010) 8929–8931, <https://doi.org/10.1039/c0cc03470c>.
- [174] C.A. Cateto, A. Ragauskas, Amino acid modified cellulose whiskers, *RSC Adv.* 1 (2011) 1695–1697, <https://doi.org/10.1039/c1ra00647a>.
- [175] S. Eyley, S. Shariki, S.E.C. Dale, S. Bending, F. Marken, W. Thielemans, Ferrocene-decorated nanocrystalline cellulose with charge carrier mobility, *Langmuir* 28 (2012) 6514–6519, <https://doi.org/10.1021/la3001224>.
- [176] M. Jorfi, E.J. Foster, Recent advances in nanocellulose for biomedical applications, *J. Appl. Polym. Sci.* 132 (2015) 1–19, <https://doi.org/10.1002/app.41719>.
- [177] Stephen J. Eichhorn, Cellulose nanowhiskers: promising materials for advanced applications, *Soft Matter* 7 (2) (2011) 303–315.
- [178] Leila Jowkarderis, Theo G.M. van de Ven, Mesh size analysis of cellulose nanofibril hydrogels using solute exclusion and PFG-NMR spectroscopy, *Soft Matter* 11 (47) (2015) 9201–9210.
- [179] F.W. Herrick, R.L. Casebier, J.K. Hamilton, K.R. Sandberg, Microfibrillated cellulose: morphology and accessibility, *J. Appl. Polym. Sci. Appl. Polym. Symp.* (1983, January) (United States) (Vol. 37, No. CONF-8205234-Vol. 2), ITT Rayonier Inc., Shelton, WA.
- [180] Hao Hu, Wei Yuan, Fu-Sheng Liu, Gang Cheng, Fu-Jian Xu, Jie Ma, Redox-responsive polycation-functionalized cotton cellulose nanocrystals for effective cancer treatment, *ACS Appl. Mater. Interfaces* 7 (16) (2015) 8942–8951.
- [181] S.P. Vyas, R.K. Khar, Targeted and controlled drug delivery, CBS Publisher and Distributer, New Delhi, India, 2002.

Mechanical performance of hybrid woven jute–roselle-reinforced polyester composites

Mohammad Hazim Mohamad Hamdan¹ ,
Januar Parlaungan Siregar², Sabu Thomas^{3,4}, Maya John Jacob⁵,
Jamiluddin Jaafar² and Cionita Tezara⁶

Polymers and Polymer Composites
2019, Vol. 27(7) 407–418
© The Author(s) 2019
Article reuse guidelines:
sagepub.com/journals-permissions
DOI: 10.1177/0967391119847552
journals.sagepub.com/home/ppc



Abstract

Natural fibre acts as a significant replacement for the known synthetic fibre that tends to cause critical environmental issues. Hence, the hybridization of natural fibre reinforcement has been considered as one of the strategies in reducing synthetic fibre applications. The current research was conducted to determine the effect of layering sequence on the mechanical performance of hybrid woven jute–roselle. In addition, eight different types of composite plate that consisted of single and hybrid were fabricated through the implementation of hand lay-up method. In this case, each composite plate had to undergo the tensile, flexural and impact testing in order to acquire the effect of varying layering sequences. The results of the present study showed that the hybridization of jute–roselle provided was significant, especially on the flexural and impact performance. Furthermore, the tensile strength and modulus were higher on the JRRJ sample and maximum flexural strength also managed to be recorded by the same sample. However, the maximum flexural modulus only managed to be recorded in sample RRJJ. Meanwhile, the impact testing revealed that the composite plate of sample JJRR had the highest impact strength. The void content for all the samples was acceptable because all of them were less than 7%. Finally, scanning electron microscopic image illustrated that the fractured surfaced of composite sample was typically smooth with less formation of void and fibre pull-out.

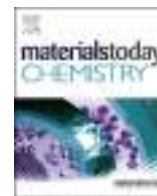
Keywords

Natural fibre, hybridization, mechanical properties, layering sequence, woven

Received 27 August 2018; accepted 2 April 2019

Introduction

Fibres are classified into synthetic or natural types, depending on their origin. In the past decade, synthetic fibres have been widely applied due to its excellent mechanical performance as well as its ability to be easily produced in a significant quantity. However, the most significant disadvantage of synthetic fibres is closely related to environmental problems and health risks. For example, glass fibres contribute to several health hazards which include skin irritations¹ and respiration problems.² At the same time, the wastes from synthetic fibres can hardly be disposed when they are discarded to the



Green synthesized metal nanoparticles as a selective inhibitor of human osteosarcoma and pathogenic microorganisms

S. Francis ^a, K.M. Nair ^b, N. Paul ^c, E.P. Koshy ^a, B. Mathew ^{d,*}

^a Department of Chemistry, St. Joseph's College, Moolamattom, Idukki, 685591, Kerala, India

^b School of Chemistry, Indian Institute of Science Education and Research, Thiruvananthapuram, 695551, Kerala, India

^c Department of Chemistry, Stella Maris College (Autonomous), Chennai, 600 086, India

^d School of Chemical Sciences, Mahatma Gandhi University, Kottayam, 686560, Kerala, India

ARTICLE INFO

Article history:

Received 29 November 2018

Received in revised form

28 April 2019

Accepted 29 April 2019

Keywords:

Nanoparticles

Green

U2OS

L929

H₂O₂

Antimicrobial

ABSTRACT

Nanobiotechnology gained at most importance in the current health-care systems. The present study reports the synthesis and characterization of silver and gold nanoparticles which in turn act as a selective inhibitor of human osteosarcoma. The *in vitro* anticancer studies on U2OS produced IC₅₀ values in the therapeutic range of 29.22 ± 0.42 and 32.83 ± 0.81 µg/mL for silver and gold nanoparticles, while the fibroblast cells (L929) produced IC₅₀ values of 141.26 ± 2.5 and 157.23 ± 2.11 µg/mL for silver and gold nanoparticles, respectively. The growth and action of infectious pathogens can be inhibited by the synthesized nanoparticles. The silver nanoparticles is used to scavenge the hydrogen peroxide and served as a sensor. The time-conserving microwave-assisted nanoparticle fabrication procedure is used here at the natural pH. Silver and gold nanoparticles have surface plasmon resonance peaks at 437 and 553 nm, respectively. The Fourier Transform Infrared spectroscopy fingerprints the role of amide groups of proteins in the synthesis and stabilization process. Transmission electron microscopic analysis proved the spherical geometry of silver and gold nanoparticles with an average size of 20.49 ± 6.68 nm and 25.05 ± 7.31 nm, respectively.

© 2019 Elsevier Ltd. All rights reserved.

1. Introduction

Nanoscience and technology provided the development activity that has been growing explosively worldwide in the past few years. Nanomaterials gained much importance in various fields of life, including health care, cosmetics, drug and gene delivery systems and cancer therapy, and food and paint industry. The properties of nanometer-sized materials differ from those of the individual molecules [1]. Among these, silver nanoparticles (AgNPs) and gold nanoparticles (AuNPs) are of much importance owing to their enormous applicability in the fields of catalysis [2], therapeutics [3], and sensor technology [4].

Various methods for the synthesis of AgNPs and AuNPs are known. Few of them are the chemical [5], photochemical [6], and electrochemical [7] reduction pathways. Because these methods included expensive techniques and hazardous chemicals, a novel alternate approach using biological entities such as bacteria [8,9],

fungi [10], yeast [11], and plant extracts [12] was practiced. The use of plant extracts is considered as the simple, efficient, inexpensive, and safe approach [13]. Many successful works have been reported on the synthesis of nanoparticles using plant extract as both reducing and stabilizing agents [14,15]. The benefit of purity of the product in the biological synthesis was overruled by its large time consumption [16]. Microwave initiates the selective and rapid heating of polar molecules [17], providing uniform nucleation and growth conditions, ensuing evenly dispersed nanoparticles [18].

Morinda citrifolia (noni) has been well known for its high traditional medicinal values [19]. It is a small evergreen plant, belonging to the Rubiaceae family. Noni has traditionally been used for colds, flu, diabetes, and high blood pressure, as well as for depression and anxiety. Its bark extract has been used for the treatment of bacterial infections, cough, diarrhea in infants, and stomach ailments. Its fruit is an effective famine food because it is the remedy to many health challenges in women. Its bark and root were used for the preparation of herbal and textile dyes. The constituents such as flavonoids, anthraquinones, triterpenoids, proteins, and so on, present in the various parts of the plant *M. citrifolia*, were proved to be responsible for their high antioxidant,

* Corresponding author.

E-mail address: beenamscs@gmail.com (B. Mathew).

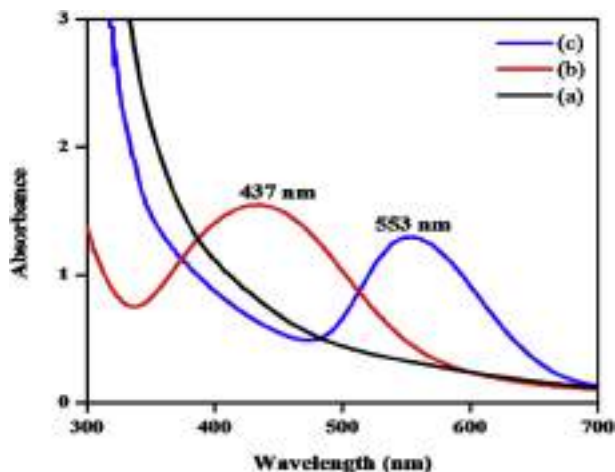


Fig. 1. UV–vis. spectra of (a) aqueous bark extract of *M. citrifolia*, (b) AgNP-*M. citrifolia*, and (c) AuNP-*M. citrifolia*. AgNP, silver nanoparticle; AuNP, gold nanoparticle.

antimicrobial, and anticarcinogenic activities [20]. Using root extract of *M. citrifolia*, AgNPs [21] and AuNPs [22] were prepared by overnight incubation at ambient temperature.

In this current article, we report the synthesis and characterizations of AgNPs and AuNPs were conducted using green routes using a microwave-assisted synthetic pathway. The anticancer properties of the synthesized metal nanoparticles are tested here by using the anticancer assay called MTT. MTT is colorimetric assay and is chemically 3-(4,5-dimethylthiazol-2-yl)-2,5-diphenyltetrazolium bromide. The cancer cells employed are the human bone osteosarcoma epithelial cells (U2OS) and the normal cells, namely fibroblast cells (L929). The colorimetric sensing properties of nanoparticles along with their antimicrobial, and antioxidant potentials enhance the biological relevance of the present study. All the analysis was conducted using standard procedures.

2. Materials and methods

Silver nitrate (AgNO_3) and chloroauric acid ($\text{HAuCl}_4 \cdot 3\text{H}_2\text{O}$) from Sigma-Aldrich were functional as the sources of silver and gold ions. Aqueous solutions were prepared using double distilled water.

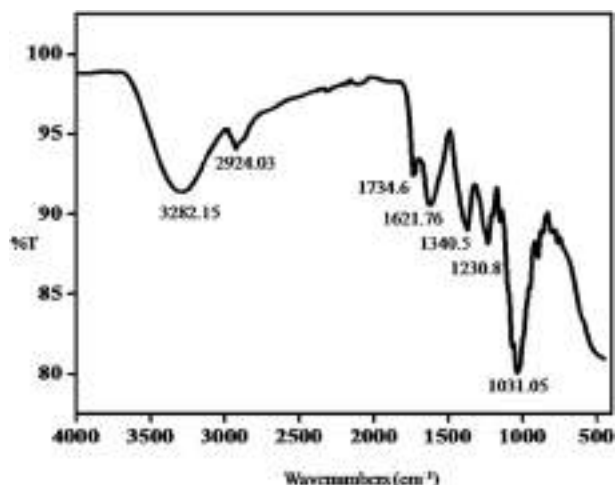


Fig. 2. FT-IR spectrum of aqueous bark extract of *M. citrifolia*.

2.1. Preparation of *M. citrifolia* bark extract

The bark of *M. citrifolia* was collected from mature trees and washed thoroughly using double distilled water to remove the impurities adhering to it. They were then sliced into small pieces and air-dried for five days. Five grams of the sample was taken in a round bottom flask fitted with a water condenser and refluxed for 1 h with 100 mL of double distilled water. The cooled extract was filtered through Whatman No.1 filter paper and then stored at 4 °C for further use.

2.2. Microwave synthesis of nanoparticles

The present microwave-assisted synthesis, 80 mL of 1 mM silver nitrate/chloroauric acid solution was taken and 20 mL of *M. citrifolia* bark extract were added and shaken well. The solution was then placed in a domestic microwave oven (Sharp R-219T (W)), operating at a power of 800 W and frequency 2450 MHz, and subjected to microwave irradiation for 3 min. The development of silver/gold nanoparticles (AgNP-*M. citrifolia*/AuNP-*M. citrifolia*) in the vessel was identified by a sudden color change from colorless to brown/pale yellow to wine red and confirmed using a UV–vis. spectrometer in the range of 200–800 nm. The purification and separation of nanoparticles were conducted using a refrigerated centrifuge (12000 rpm). After each step of centrifugation, the sample is redissolved in double distilled water and the components of plant extract adhered on the nanoparticles were removed. The samples were air-dried, and pure samples were used for analysis.

2.3. Characterization

UV–vis. spectral analysis was carried out using a Shimadzu UV-2450 spectrophotometer. FT-IR spectrum was recorded on a PerkinElmer-400 spectrometer with ATR attachment. X-ray diffraction (XRD) measurement was made on a PANalytic X'PERT-PRO X-ray spectrometer. High-resolution transmission electron microscopic (TEM) images were taken using a JEOL JEM-2100 microscope.

2.4. Optical sensing of H_2O_2

Sensing of H_2O_2 is performed colorimetrically using the synthesized metal nanoparticles. H_2O_2 (1 mL, 20 mM) is added to the nanoparticle solution (2 mL, 200 $\mu\text{g}/\text{mL}$) to get a final volume of

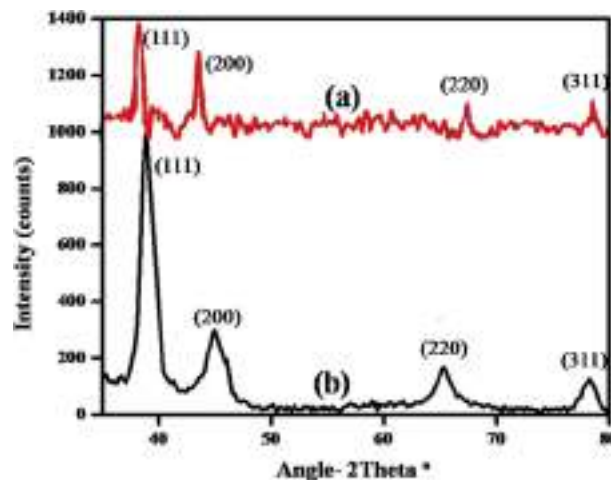


Fig. 3. XRD pattern of (a) AgNP-*Morinda citrifolia* and (b) AuNP-*Morinda citrifolia*. XRD, X-ray diffraction; AgNP, silver nanoparticle; AuNP, gold nanoparticle.

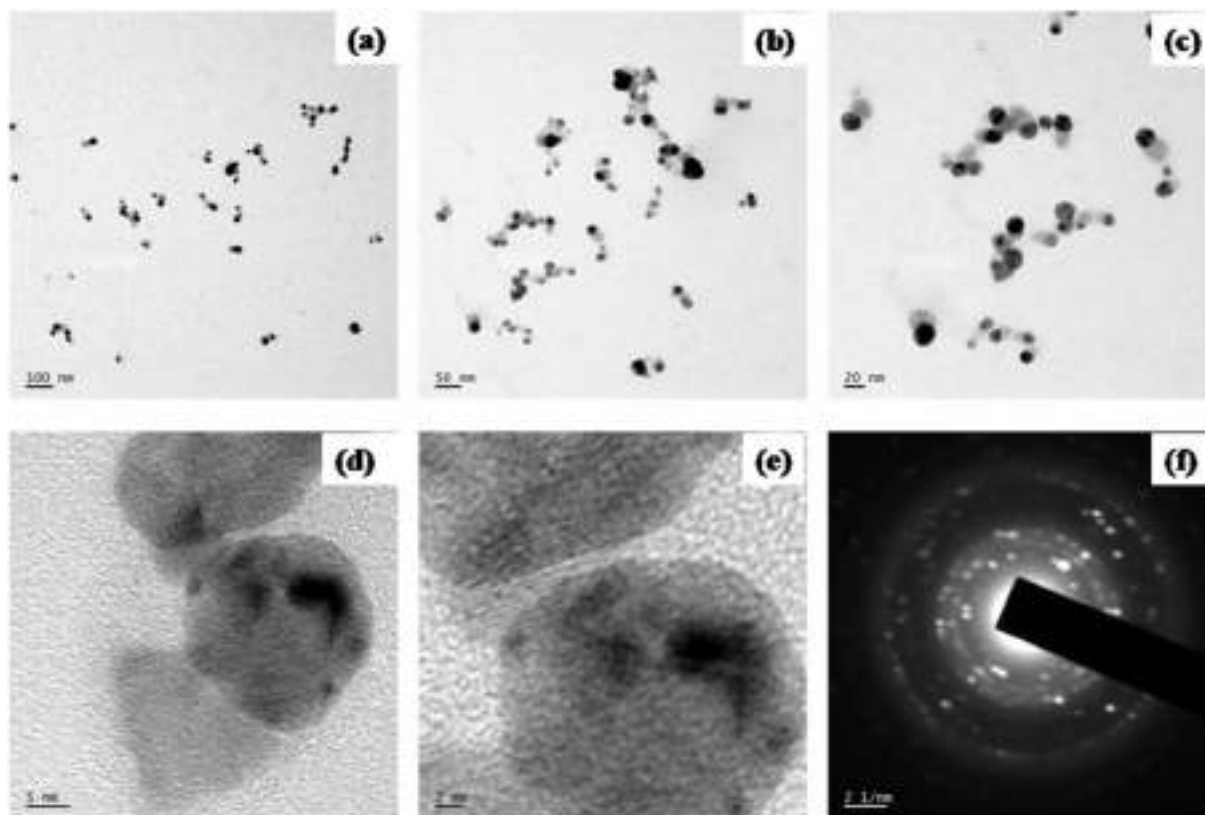


Fig. 4. TEM images (a–e) of AgNP-*M. citrifolia* at various amplifications and (f) selected area electron diffraction (SAED) pattern of AgNP-*M. citrifolia*. TEM, transmission electron microscopic; AgNP, silver nanoparticle.

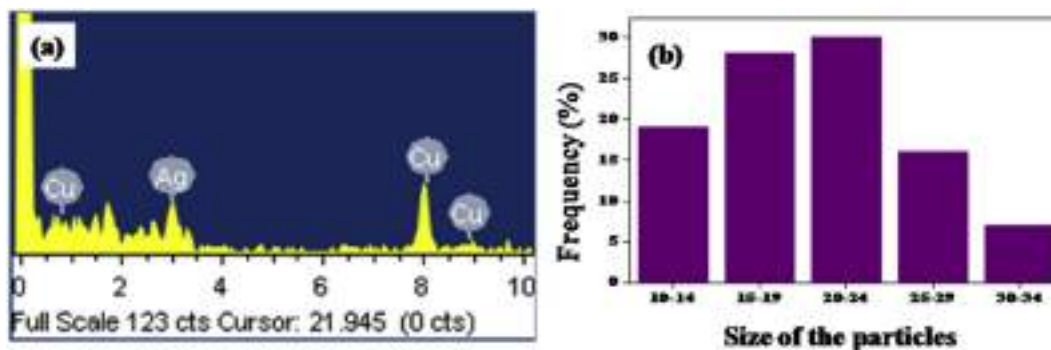


Fig. 5. EDAX spectrum (a) and particle size histogram (b) of AgNP-*M. citrifolia*. AgNP, silver nanoparticle.

3 mL. UV–vis. spectral measurements at regular intervals were conducted to detect the extinction of H_2O_2 from the system. Kinetics of the reaction was also followed by noting the absorbance at 437 nm. The effects of the concentrations of H_2O_2 and the nanoparticles on the sensing action were also experimented.

2.5. Antioxidant activity-DPPH assay

The antioxidant properties of bark extract and the AgNP-*M. citrifolia* and AuNP-*M. citrifolia* were analyzed using the 2,2-diphenyl-1-picrylhydrazyl (DPPH) assay [23]. DPPH possessed a single electron, and its methanolic solution has λ_{max} at 517 nm. When scavenged, the color of the DPPH radical changed to yellow from pink. Different concentrations of samples (12.5–200 $\mu\text{g}/\text{mL}$) were used for the scavenging analysis. Ascorbic acid was used as

the reference standard. Using UV–vis. spectrophotometer, the decrease in absorbance of the samples at 517 nm after 30 min of the reaction was measured. DPPH of 3 mL was used as the experimental control. Scavenging activity was expressed as Inhibition (%) = $[(\text{Abs}_{\text{control}} - \text{Abs}_{\text{sample}})/(\text{Abs}_{\text{control}})] \times 100$. All the experiments were conducted thrice, and the mean values along with standard deviation were found out.

2.6. Antimicrobial activity

Considering the possible application of AgNPs/AuNPs in various biomedical fields, the antibacterial activity of the synthesized AgNPs and AuNPs was tested by the agar well diffusion method against six selected microorganisms. Microorganisms were procured originally from Microbial Type Culture Collection, Institute of

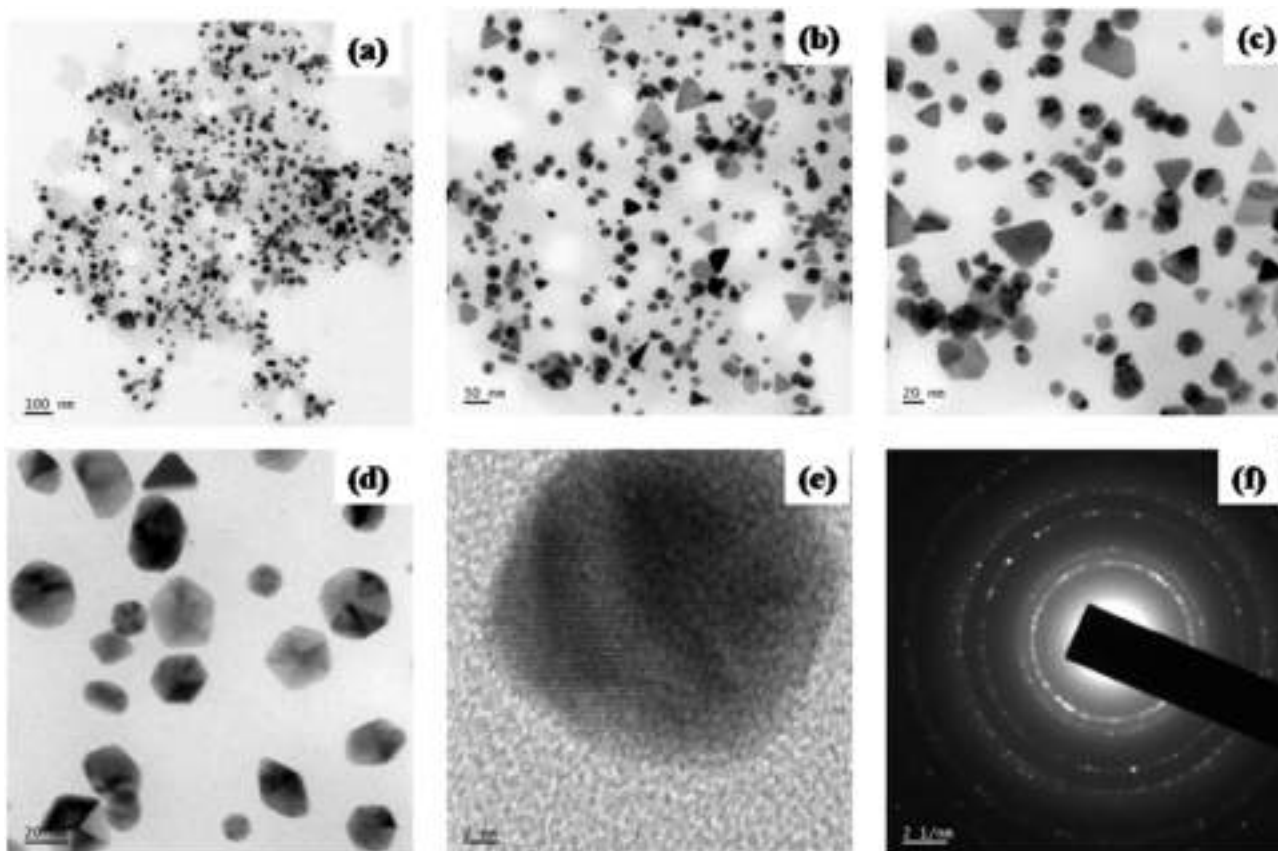


Fig. 6. TEM images (a–e) of AuNP-*M. citrifolia* at various amplifications and (f) selected area electron diffraction (SAED) pattern of AuNP-*M. citrifolia*. TEM, transmission electron microscopic; AuNP, gold nanoparticle.

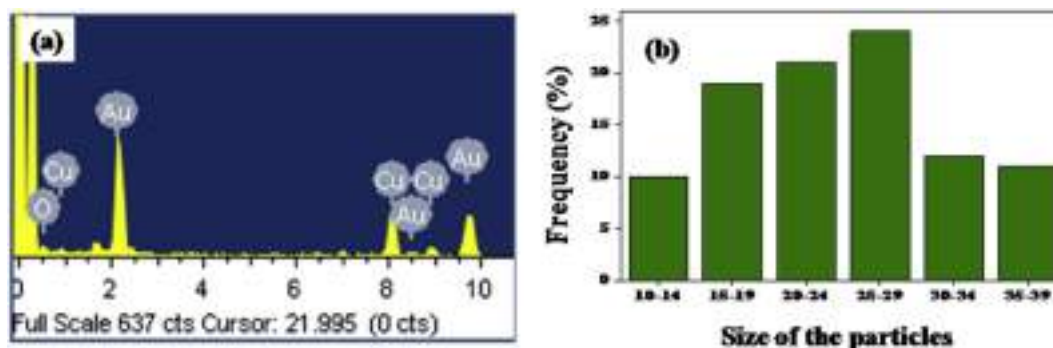


Fig. 7. EDAX spectrum (a) and particle size histogram (b) of AuNP-*M. citrifolia*. AuNP, gold nanoparticle.

Microbial Technology, Chandigarh, India. Muller Hinton agar plates (20 mL) were swabbed with two of the gram-positive strains *Bacillus subtilis* (MTCC 441) and *Lactococcus lactis* (MTCC 3041) and two of the gram-negative strains *Pseudomonas aeruginosa* (MTCC 424) and *Enterobacter aerogenes* (MTCC 6804). The fungi *Aspergillus terreus* (MTCC) and *Penicillium citrinum* (MTCC 1256) were swabbed on the Potato Dextrose agar plates that were overnight incubated. Wells of approximately 6 mm were bored on the confluent lawn using a well cutter that is sterile. Wells were named as A, B, C, and D and were loaded with double distilled water (50 μ L) and aqueous bark extract of *M. citrifolia* (0.05 mg/mL, 50 μ L), AgNP-*M. citrifolia* (0.02 mg/mL, 50 μ L), and AuNP-*M. citrifolia* (0.02 mg/mL, 50 μ L), respectively. The positive control streptomycin/griseofulvin (50 μ L, 10 mg/mL), respectively, was used against bacterial and fungal

strains, and double distilled water constitutes the negative control. After 24 h and 1 week of incubation span for bacterial and fungal plates, the zone of inhibition was measured in millimeter, respectively, for bacterial and fungal strains. All the experiments were replicated, and the mean and standard deviation of the zone of inhibition was found out. Data were statically analyzed.

2.7. In vitro cytotoxicity assay (MTT)

In vitro cytotoxicity of the synthesized nanoparticles, AgNP-*M. citrifolia* and AuNP-*M. citrifolia*, was investigated along with the plant extract using bone osteosarcoma cell lines U2OS and fibroblast cell lines L929 that were used for anticancer analysis using the dye MTT [24]. MTT is 3-(4,5-dimethylthiazol-2-yl)-2,5-

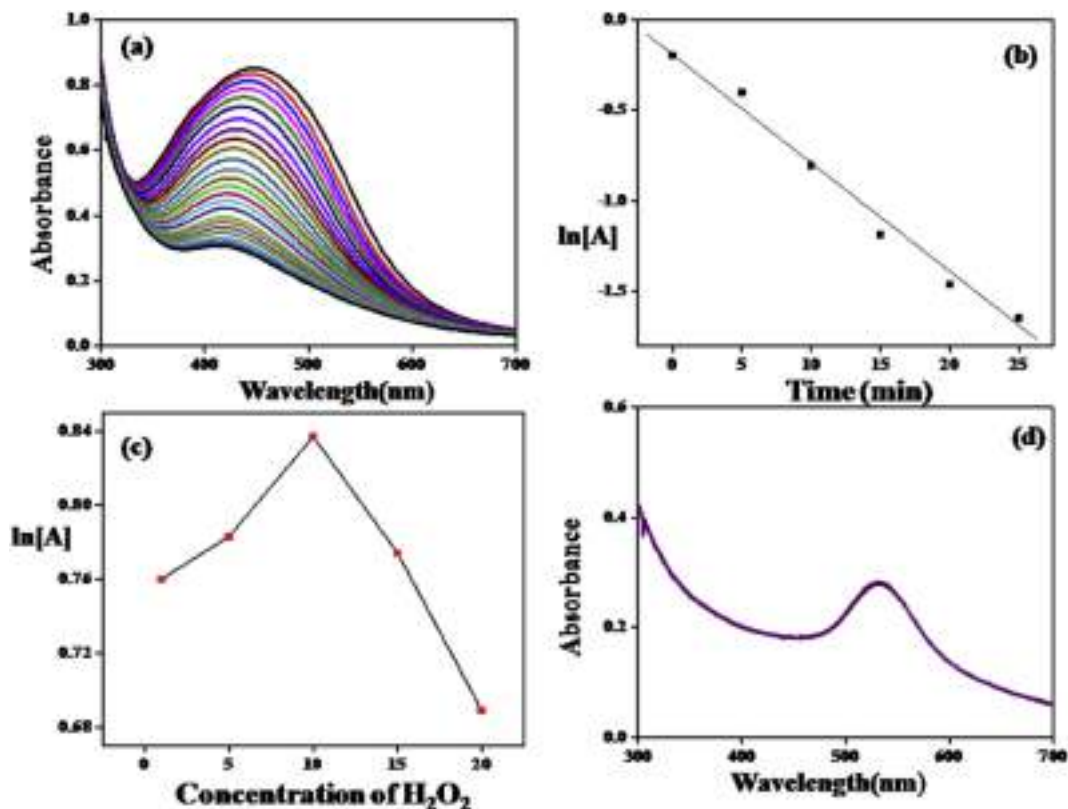


Fig. 8. Sensing of H₂O₂ (20 mM) using (a) AgNP-M. citrifolia (200 µg/mL), (b) plot of ln[A] versus time (A = 439 nm), (c) effect of concentration of H₂O₂ (1–20 mM) on and (d) ineffectiveness of AuNP-M. citrifolia (200 µg/mL) in sensing H₂O₂ (20 mM). AgNP, silver nanoparticle; AuNP, gold nanoparticle.

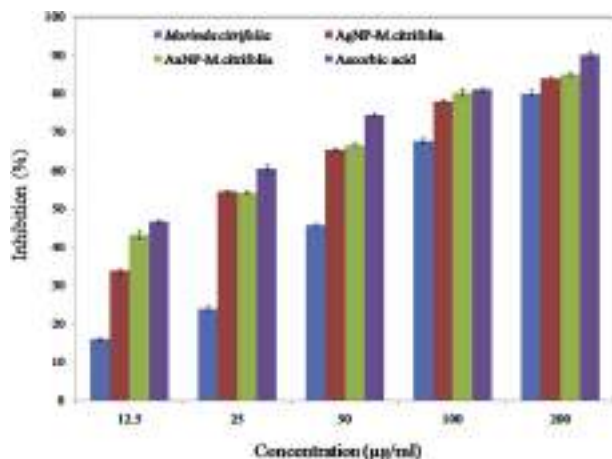


Fig. 9. Free radical scavenging (DPPH) activity of *M. citrifolia*, AgNP-M. citrifolia, and AuNP-M. citrifolia compared to standard ascorbic acid (12.5–200 µg/mL). Values are mean ± SD (n = 3). DPPH, 2,2-diphenyl-1-picrylhydrazyl; SD, standard deviation; AgNP, silver nanoparticle; AuNP, gold nanoparticle.

diphenyltetrazolium bromide. The cells were procured from National Centre for Cell Sciences, Pune, India, and were maintained in Dulbecco's Modified Eagle's Medium (Gibco, Invitrogen).

A monolayer of two-day-old confluent cells was trypsinized; 100 µL of cultured cell suspension (5×10^4 cells/wells) was seeded in 96 well plates and was kept at 37 °C in a humidified 5% CO₂ incubator (NBS Eppendorf, Germany). When the cells are sufficiently grown, the culture medium was removed and different concentrations of freshly prepared samples (6.25, 12.5, 25, 50, and

100 µg/mL in 100 µL of 5% MEM, modified eagles medium) were added in triplicates and then five times serially diluted by the twofold dilution method. The system was again incubated at 37 °C in a CO₂ (5%) humidified incubator. The control of the experiment was constituted by the untreated cells.

To the test and control wells, the reconstituted MTT solution (30 µL, 5 mg/mL in PBS, phosphate-buffered saline medium) was added after 24 h of the incubation period. The plates were gently shaken well and incubated again for 4 h (5% CO₂, at 37 °C). In order to solubilize the formazan crystals formed in each well, 100 µL of DMSO (dimethyl sulphoxide) was added after detaching the supernatant and the contents were well mixed. The absorbance at 570 nm for each set of test and the control solutions were measured by using a plate-reading spectrophotometer. The viability (%) of cells is directly proportional to the percentage conversion of the tetrazolium salt (MTT) to the colored formazan crystals [25]. The percentage of growth inhibition was calculated by Eq. (1).

$$\text{Viability}(\%) = \frac{\text{Mean OD Samples}}{\text{Mean OD of Control}} \times 100 \quad (1)$$

The IC₅₀ values were calculated for each set of data using GraphPad Prism software, and the mean ± standard deviation was identified.

2.8. Statistical analysis

Experimental data were expressed as the mean ± standard deviation and were analyzed by one way analysis of variance followed by post hoc (Tukey's) analysis using Graphpad Prism software. A value of P < 0.05 was considered as statistically important.

Table 1
ANOVA and Tukey's post-hoc analysis results for Antioxidant studies (DPPH assay).

ANOVA result	Concentration (12.5µg/mL)	Concentration (25µg/mL)	Concentration (50µg/mL)	Concentration (100µg/mL)	Concentration (200µg/mL)	
F value	(F=936.2***)	(F=1771 ***)	(F=1796***)	(F=242.3***)	(F=73.65**)	
Tukey's post-hoc analysis						
(I)type	(J) type	Mean difference (I-J)				
<i>M. citrifolia</i> bark extract	AgNP- <i>M.citrifolia</i>	-17.73***	-30.64***	-19.78***	-10.22***	1.773***
<i>M. citrifolia</i> bark extract	AuNP- <i>M.citrifolia</i>	-27.20***	-30.38***	-21.00***	-12.55***	4.437**
<i>M. citrifolia</i> bark extract	Ascorbic acid	-30.57***	-36.72***	-28.78***	-13.42***	-4.247***
AgNP- <i>M.citrifolia</i>	AuNP- <i>M.citrifolia</i>	-9.470***	0.2633	-1.220	-2.330*	2.663
AgNP- <i>M.citrifolia</i>	Ascorbic acid	-12.85***	-6.083***	-8.997***	-3.197***	-6.020***
AuNP- <i>M.citrifolia</i>	Ascorbic acid	-3.377**	-6.347***	-7.777***	-0.8667	-8.683***

Note: ***, ** and * indicate significance at the level of 1%, 5% and 10% respectively.

3. Results and discussion

3.1. UV–vis. spectroscopic analysis

UV–vis. spectroscopic analysis is used to ascertain the formation and stability of AgNPs and AuNPs. The reduction of Ag^+ ions into Ag^0 and Au^{3+} to Au^0 nanoparticles was confirmed by measuring the absorption spectrum of the reaction mixtures in the range of 200–800 nm [26]. The UV vis. spectrum of the bark extract

of *M. citrifolia* does not show any peak in the given range (Fig. 1a). Upon continuous microwave irradiation for 3 min, the color of the reaction mixture changes from yellow to brown in the case of AgNPs. AuNPs formed in a span of irradiation of 2 min because of the reduction potential possessed by gold [16]. The change in color of the reaction mixture, i.e., yellow to wine red, is a clear evidence for the formation of AuNPs. The UV–vis. spectrum recorded for the silver and gold reaction mixtures is shown in Fig. 1b and Fig. 1c. The peak was observed around 437 nm, which is due to the surface

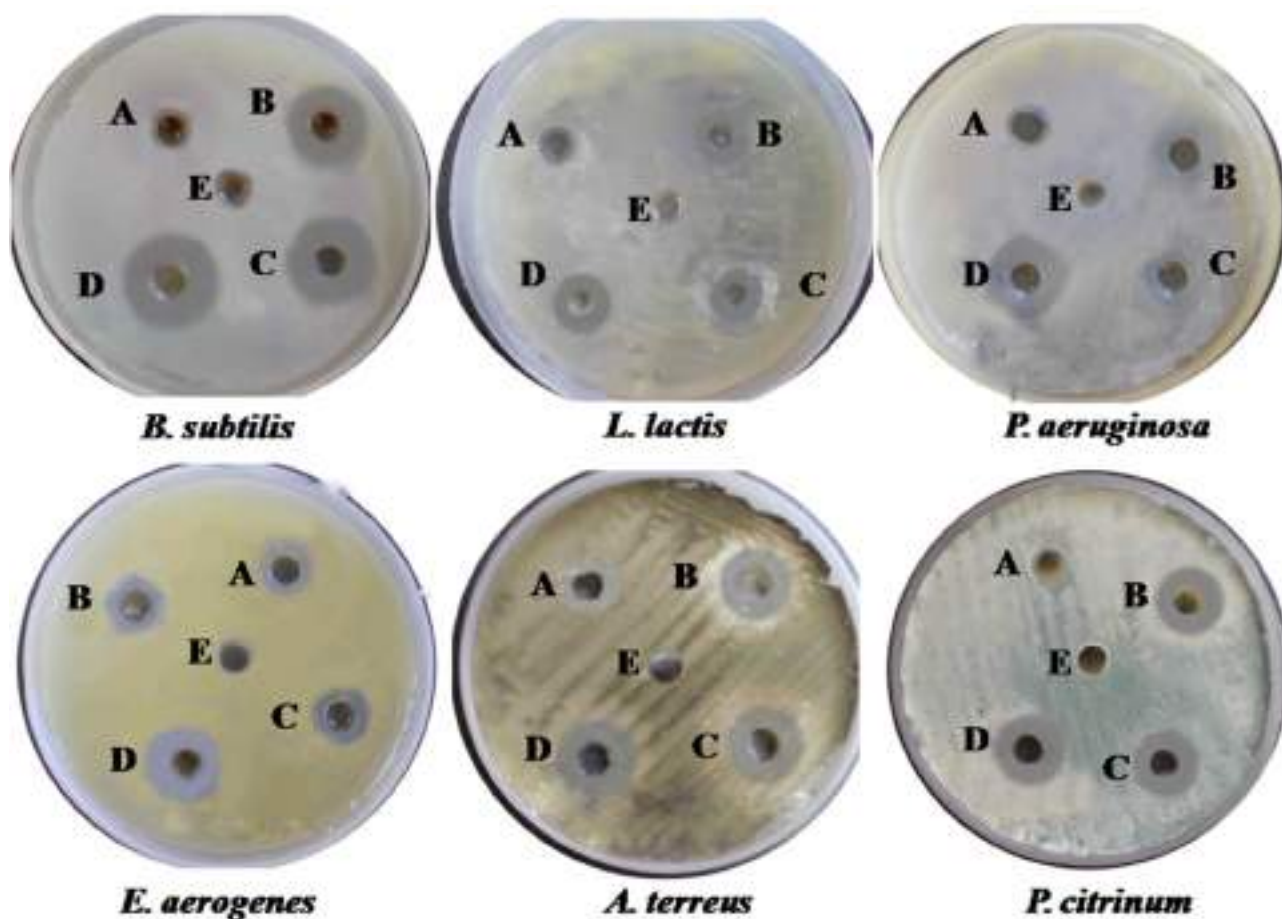


Fig. 10. Photographs shows the treated Petri plates of different microorganisms after their treatment with samples (A) *M. citrifolia*, (B) AgNP-*M. citrifolia*, (C) AuNP-*M. citrifolia*, (D) positive control (streptomycin/griseofulvin, 50 µL, 10 mg/mL), and (E) negative control (double distilled water) in the agar well diffusion method. AgNP, silver nanoparticle; AuNP, gold nanoparticle.

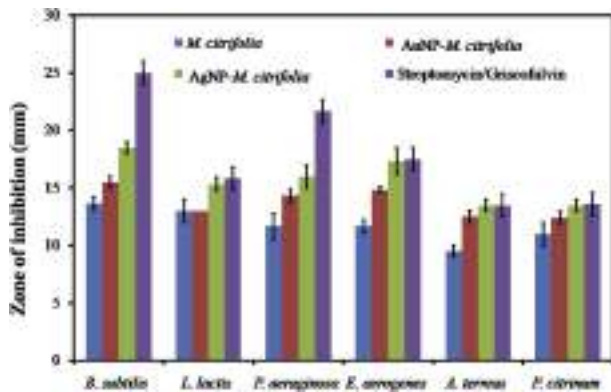


Fig. 11. Antimicrobial activities of *M. citrifolia*, AgNP-*M. citrifolia*, and AuNP-*M. citrifolia* expressed as zone of inhibition (mm) against various microorganisms using the agar well diffusion method. Error bars show standard deviation ($n = 3$). AgNP, silver nanoparticle; AuNP, gold nanoparticle.

plasmon resonance (SPR) of AgNPs, and the peak at 553 nm corresponds to nanogold. The SPR band arises due to the collective oscillations of electrons of nanoparticles in presence of visible light, which is highly influenced by the shape and size of nanoparticles [27]. They effectively reduce $\text{Ag}^+/\text{Au}^{3+}$ ions, which then join to form respective nanoparticles (AgNP-*M. citrifolia*/AuNP-*M. citrifolia*, respectively).

The UV–vis. spectral studies propose that both the nanoparticles are uniformly distributed and are more or less spherical in shape. As stated earlier, the extract of *M. citrifolia* is highly rich in phytochemicals and flavonoids. Almost 200 phytochemicals were identified and isolated from different parts of the plant. When *M. citrifolia* bark extract is added to the $\text{AgNO}_3/\text{HAuCl}_4$ solution, these phytochemicals play a dual role as both reducing and stabilizing agents. They effectively reduce $\text{Ag}^+/\text{Au}^{3+}$ ions, which then join to form AgNPs/AuNPs. The phytochemicals acted as capping agents and hence covering the nanoparticles to protect them from agglomeration.

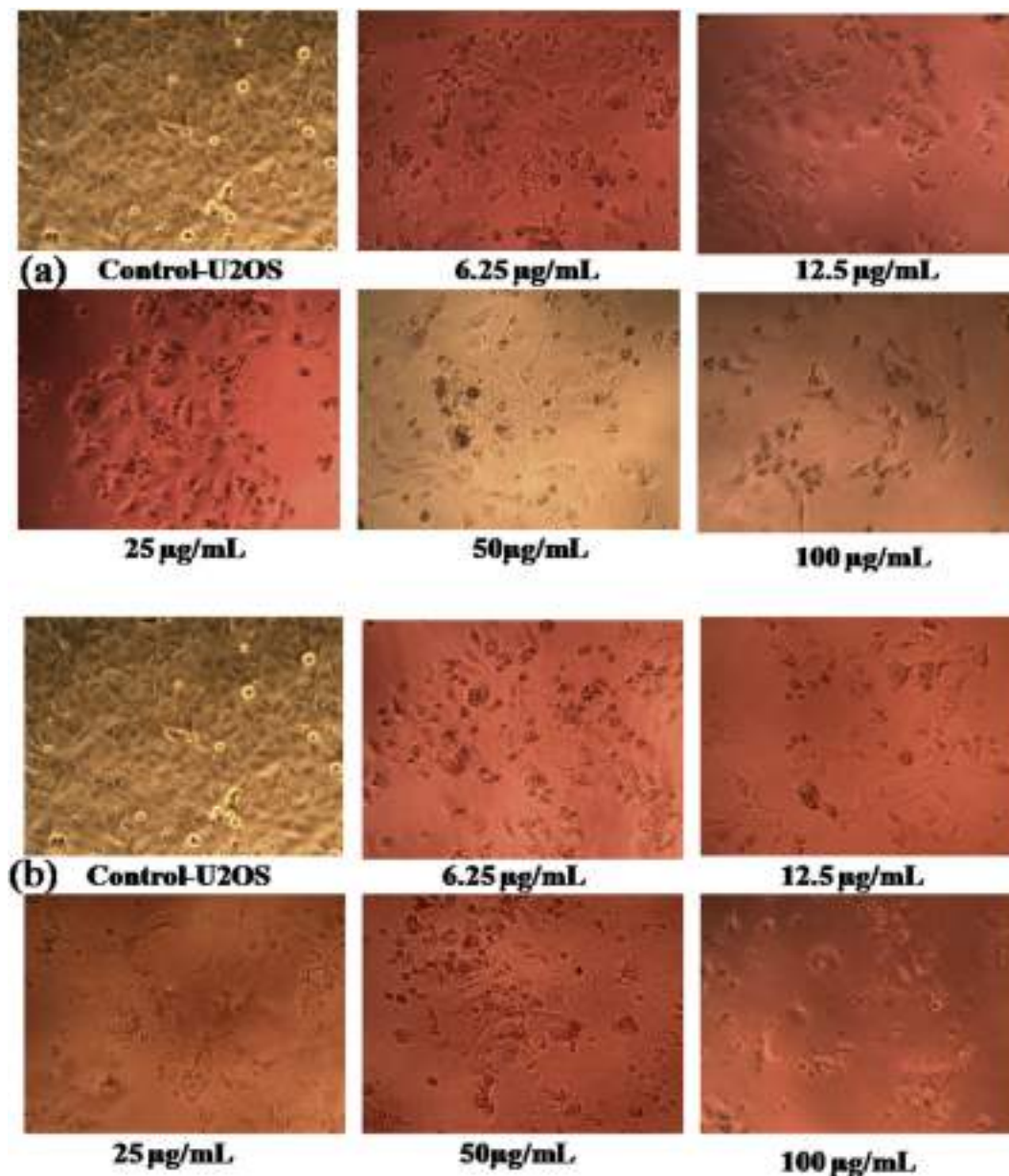


Fig. 12. Microscopic photographs of cancer cells showing the morphological changes after their treatment. (a) U2OS cells towards *M. citrifolia*, (b) U2OS cells towards AgNP-*M. citrifolia*, (c) U2OS cells towards AuNP-*M. citrifolia*, (d) L929 cells towards AgNP-*M. citrifolia* and (e) L929 cells towards AuNP-*M. citrifolia*. Images of the control cancerous cells (U2OS and L929) are also seen. AgNP, silver nanoparticle; AuNP, gold nanoparticle.

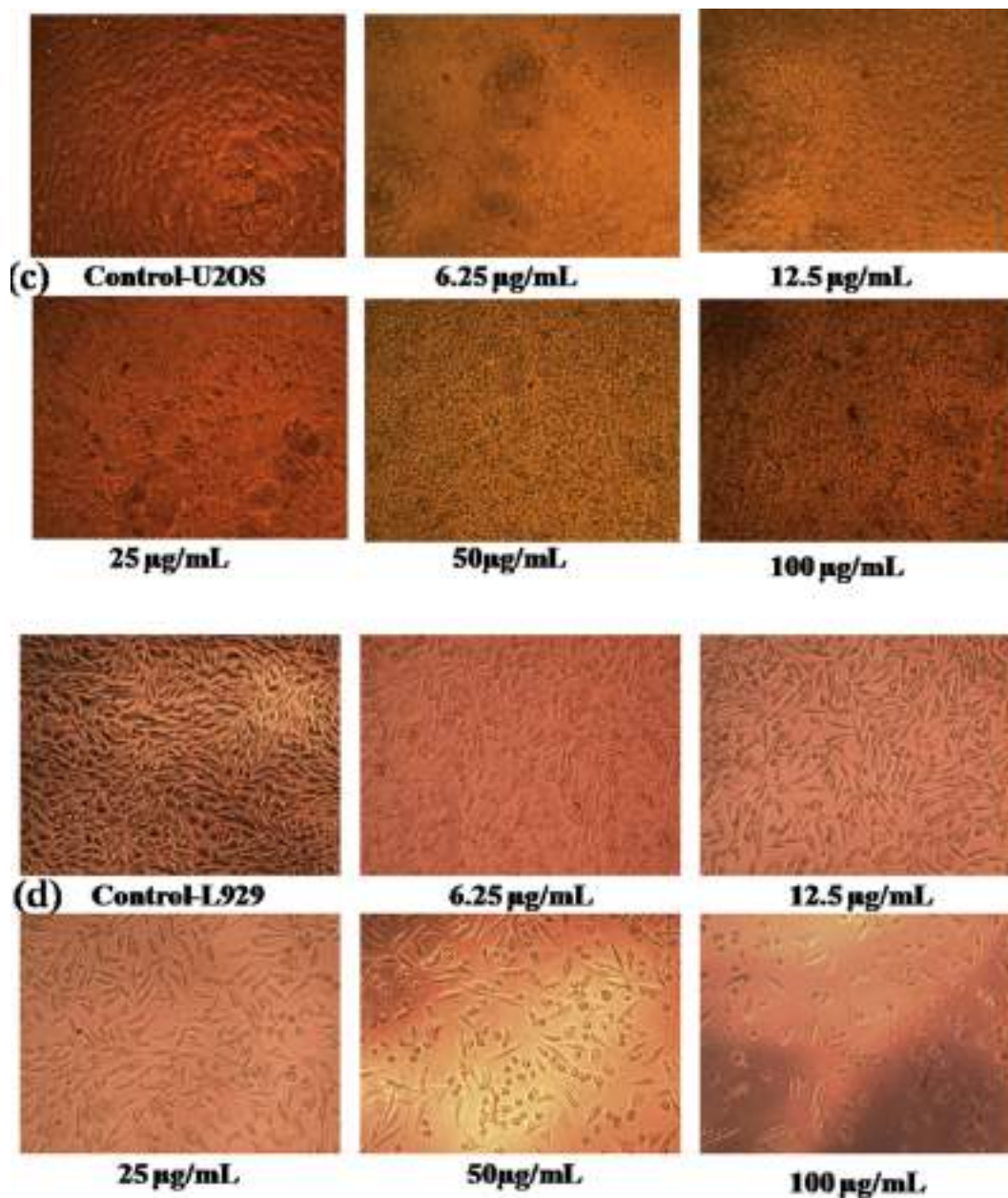


Fig. 12. (continued).

3.2. FT-IR spectral study

FT-IR identified the functional groups present in the bark extract of *M. citrifolia* which caused the reduction of silver/gold ions to zero-valent metal nanoparticles. Fig. 2 showed the FT-IR spectrum of the pure bark extract. The broad peak appearing in the range of $3400\text{--}2400\text{ cm}^{-1}$ resulted from the stretching vibrations of the hydroxyl ($-\text{OH}$) groups of plant chemicals. Carbonyl stretching was responsible for 1734.6 cm^{-1} . The amide $\text{C}=\text{O}$ stretch was the reason for the band at 1634.59 cm^{-1} [22]. The primary amine $-\text{NH}$ group that was also present gave peaks at 2924.03 cm^{-1} and 1230.81 cm^{-1} [28]. The $\text{C}-\text{N}$ vibrational peaks at 1340 and 1031 cm^{-1} again supported the attendance of aromatic and aliphatic amines [29]. The peaks suggested the amide linkages of

proteins and hydroxyl groups of polyphenols and flavonoids may be responsible for the reduction and capping.

3.3. XRD analysis

X-ray diffraction (XRD) studies were performed to confirm the crystalline nature of AgNPs and AuNPs. In Fig. 3(a), different peaks observed at 2θ values 38.89° , 43.83° , 64.14° , and 77.13° correspond to (111), (200), (222), and (311) atomic planes of the face-centered cubic (fcc) crystal lattice of silver, respectively. In Fig. 3(b), peaks at 38.80° , 44.87° , 65.30° , and 78.38° correspond to the aforementioned four planes of fcc structure of atomic nanogold. XRD patterns showed sharp peaks with small area, confirming the statement that the nanocrystalline phase is predominant. The XRD

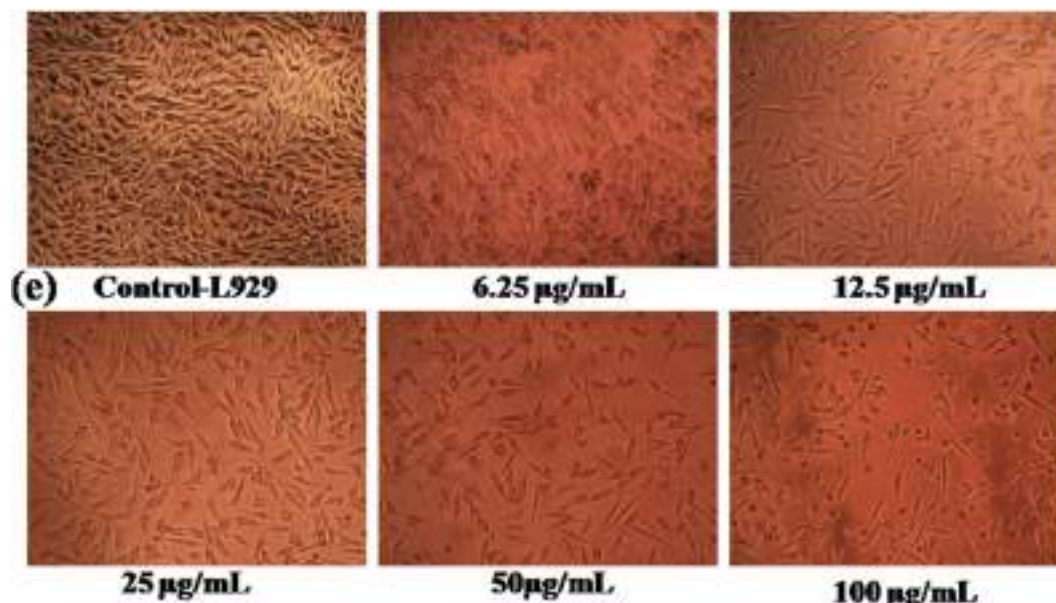


Fig. 12. (continued).

analysis undeniably indicated that the synthesized AgNPs and AuNPs are crystalline in nature.

3.4. TEM-EDAX analyses

The TEM images provided valuable information about the size and shape of the AgNPs and AuNPs. The representative TEM images of the synthesized AgNPs were given in Fig. 4. The TEM micrographs suggested that the AgNPs were nearly spherical and the individual silver particles were prevented from agglomeration by the plant phytochemicals. The average size of the AgNPs was estimated as 20.49 ± 6.68 nm. Fig. 5 represented the elemental analysis (a) along with particle size distribution plot (b).

The TEM images (Fig. 6) represented the AuNPs in different magnifications. The triangular and spherical shape of the AuNPs was clearly seen from the images. Fivefold symmetry of the microwave-synthesized AuNPs was interestingly seen from the

images Fig. 6 (d) [30]. The elemental presence of gold is verified by energy-dispersive X-ray spectroscopy (EDAX) spectrum (a), and the particles have a mean size of 25.05 ± 7.31 nm determined by particle size distribution analysis (b) using TEM measurements (Fig. 7). The reducing and protecting action of *M. citrifolia* bark extract in the case of AgNP-*M. citrifolia* and AuNP-*M. citrifolia* was best illustrated from the TEM micrographs.

3.5. Sensing and quantification of H_2O_2

H_2O_2 is toxic to cells and tissues [31]. Colorimetric sensing of the biologically important compound H_2O_2 was performed by noble metal nanoparticles. The peak corresponding to AgNPs (437 nm) was decreased in intensity with time, and after 48 min of reaction, it was completely disappeared [32] (Fig. 8a). The brown color of the medium changed to colorless. The kinetics of the reaction is shown in Fig. 8b. The concentration of H_2O_2 also influenced the detection limit. In the range of 1–20 mM, the experiment worked well (Fig. 8c). The AuNPs, AuNP-*M. citrifolia*, were not able to sense the H_2O_2 molecules (Fig. 8d). The optical sensing using AgNP-*M. citrifolia* produced good results that can be exploited in analytical or clinical territories.

3.6. Antioxidant assay

Oxidative stress caused by the imbalance between the formation and elimination of free radicals in the body must be defended [33]. Plant-based AgNPs and AuNPs were known for their high antioxidant power because of their low reduction potential and polyphenolic and flavonoid contents [34]. The antioxidants provided protection against conditions such as aging, asthma, arthritis, allergies, and cancer [35]. Free radical scavenging potential of *M. citrifolia*, AgNP-*M. citrifolia*, and AuNP-*M. citrifolia* was expressed as the inhibition (%) in Fig. 9, and the values increased in a dose-increasing manner [36]. The IC_{50} values are 55.83 ± 0.77 , 23.69 ± 0.39 , and 18.81 ± 0.92 $\mu\text{g/mL}$. The IC_{50} value corresponding to the standard ascorbic acid is 14.64 ± 0.14 $\mu\text{g/mL}$. DPPH radical scavenging activity showed by methanolic extract of *M. citrifolia* fruit is known to be depended intimately on the total phenolic

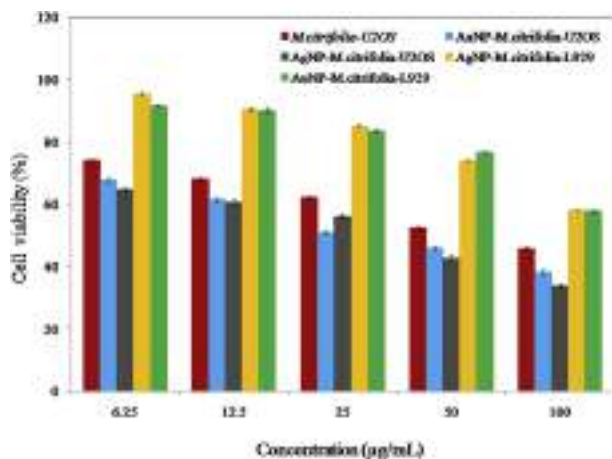


Fig. 13. Cytotoxicity studies for *M. citrifolia*, AgNP-*M. citrifolia*, and AuNP-*M. citrifolia* (6.25–100 $\mu\text{g/mL}$) towards U2OS and L929 cancer cells. Values are mean \pm SD and errors bars represent standard deviation ($n = 3$). AgNP, silver nanoparticle; AuNP, gold nanoparticle; SD, standard deviation.

Table 2
ANOVA and Tukey's post-hoc analysis results for cytotoxicity studies.

ANOVA result	Concentration (6.25µg/mL)	Concentration (12.5µg/mL)	Concentration (25µg/mL)	Concentration (50µg/mL)	Concentration (100µg/mL)	
F value	(F=2003 ^{***})	(F=1643 ^{***})	(F=3925 ^{***})	(F=2546 ^{***})	(F=1419 ^{***})	
Tukey's post-hoc analysis						
(I) type	(J) type	Mean difference (I-J)				
<i>M. citrifolia</i> bark extract	AgNP- <i>M.citrifolia</i> U2OS	9.243 ^{***}	7.476 ^{***}	6.092 ^{***}	9.581 ^{***}	12.09 ^{***}
<i>M. citrifolia</i> bark extract	AuNP- <i>M.citrifolia</i> U2OS	6.343 ^{***}	6.648 ^{***}	11.39 ^{**}	6.565 ^{***}	7.433 ^{***}
<i>M.citrifolia</i> bark extract	AgNP- <i>M.citrifolia</i> L929	-21.50 ^{***}	-22.35 ^{***}	-23.04 ^{***}	-21.59 ^{***}	-12.32 ^{***}
<i>M.citrifolia</i> bark extract	AuNP- <i>M.citrifolia</i> L929	-17.68 ^{***}	-22.05 ^{***}	-21.43 ^{***}	-24.40 ^{***}	-12.16 ^{***}
AgNP- <i>M.citrifolia</i> U2OS	AuNP- <i>M.citrifolia</i> U2OS	-2.901 ^{***}	-0.8280	5.303 ^{***}	-3.016 ^{***}	-4.660 ^{***}
AgNP- <i>M.citrifolia</i> U2OS	AgNP- <i>M.citrifolia</i> L929	-30.74 ^{***}	-29.83 ^{***}	-29.13 ^{***}	-31.17 ^{***}	-24.41 ^{***}
AgNP- <i>M.citrifolia</i> U2OS	AuNP- <i>M.citrifolia</i> L929	-26.92 ^{***}	-29.53 ^{***}	-27.52 ^{***}	-33.98 ^{***}	-24.25 ^{***}
AuNP- <i>M.citrifolia</i> U2OS	AgNP- <i>M.citrifolia</i> L929	-27.84 ^{***}	-29.00 ^{***}	-34.43 ^{***}	-28.16 ^{***}	-19.75 ^{***}
AuNP- <i>M.citrifolia</i> U2OS	AuNP- <i>M.citrifolia</i> L929	-24.02 ^{***}	-28.70 ^{***}	-32.82 ^{***}	-30.96 ^{***}	-19.59 ^{***}
AgNP- <i>M.citrifolia</i> L929	AuNP- <i>M.citrifolia</i> L929	3.817 ^{***}	0.3012	1.608 ^{**}	-2.805 ^{***}	0.1586

Note: ^{***}, ^{**} and ^{*} indicated significance at the level of 1%, 5% and 10% respectively [56].

content [19]. The adsorption of bioactive compounds, flavonoids, terpenoids, and proteins, present in the leaf extract on the surface of AgNP-*M. citrifolia* and AuNP-*M. citrifolia* contributed to the scavenging power [37]. The statistical analysis showed that the AgNPs and AuNPs have antioxidant power than the bark extract (Table 1).

3.7. Inhibitory effects on microbial agents

The invention of antibiotics conquered infectious diseases [38]. Plant and microbial originated AgNPs and AuNPs exhibited potent antimicrobial activity [39,40]. The photographs of bacterial and fungal agar plates after their treatment with the nanoparticles are shown in Fig. 10. The inhibition zone in millimeter for each microorganism in a replica (n = 3) is shown in Fig. 11. AgNPs and AuNPs showed significant antimicrobial activity against gram-positive and gram-negative microorganisms [41–46]. The disturbance caused by the adhesion of nanoparticles on the surface of the cell wall and the inhibition of the respiratory cycle by penetrating to the bacterial cell through the membrane may lead to cell death [47,48]. Antimicrobial property of nanoparticles will improve the bactericidal effect of standard antibiotics in future [49].

3.8. Anticancer properties

In vitro cytotoxic effects of AgNP-*M. citrifolia* and AuNP-*M. citrifolia* were studied by MTT assay towards osteosarcoma cell lines (U2OS) and normal cell lines (L929). Osteosarcoma represented the oldest, the most common, malignant bone tumor that affected human beings between the age of 10 and 20 years [50,51]. In the MTT assay, breaking of the tetrazolium ring is important and the cells that are alive only can reduce this quaternary amine to tertiary amine [52]. The microscopic images of the cells taken after 48 h of treatment with and without the samples (6.25–100 µg/mL) are displayed in Fig. 12. (a), (b), and (c) denoted the effects of *M. citrifolia*, AgNP-*M. citrifolia*, and AuNP-*M. citrifolia* on U2OS cells, respectively. (d) and (e) are images corresponding to L929 cells after treatment with AgNP-*M. citrifolia* and AuNP-*M. citrifolia*, respectively. The viability of cells (%) investigated at various concentrations of the treated samples was plotted in Fig. 13.

Their respective IC₅₀ values were 67.82 ± 2.35, 29.22 ± 0.42, 32.83 ± 0.81, 141.26 ± 2.5, and 157.23 ± 2.11 µg/mL. The statistical analysis of the data is included in Table 2. The capacity of samples to cause cell death of the cancerous cells follows the order AgNP-*M. citrifolia* > AuNP-*M. citrifolia* > *M. citrifolia*. Significant

cytotoxicity shown by the AgNPs and AuNPs selectively towards cancerous cells than normal cells paved the way for new therapeutics [53] against human bone cancer. Cell components such as proteins, nitrogen-containing bases, and phosphate groups undergoing bonded and non-bonded interactions with the AgNPs and AuNPs resulted in cytotoxicity [54]. Biocompatible green AgNPs and AuNPs can be exploited in drug delivery applications towards cancer [55].

4. Conclusions

Green production of AgNPs and AuNPs is cost-effective, reliable, and renewable. The medicinal plant *M. citrifolia* which has been admired through centuries proved its power as the best reducing and protecting agent in the case of AgNPs and AuNPs. Infectious pathogens and reactive oxygen species like free radicals can be inhibited using the prepared nanoparticles. Significant and concentration-dependent cytotoxicity shown by the synthesized nanoparticles towards human osteosarcoma cell lines is established.

Acknowledgements

Authors gratefully acknowledge the financial assistance to Sijo Francis from University Grants Commission (under FDP Scheme of UGC), Government of India.

References

- [1] C. Pfeiffer, C. Rehbock, D. Huhn, C. Carrillo-Carrion, D.J. de Aberasturi, V. Merk, S. Barcikowski, W.J. Parak, Interaction of colloidal nanoparticles with their local environment: the (ionic) nanoenvironment around nanoparticles is different from bulk and determines the physico-chemical properties of the nanoparticles, *J. R. Soc. Interface* 11 (2014), 20130931–20130931.
- [2] G. Manjari, S. Saran, T. Arun, S.P. Devipriya, A. Vijaya Bhaskara Rao, Facile aglaia elaeagnoida mediated synthesis of silver and gold nanoparticles: antioxidant and catalysis properties, *J. Clust. Sci.* 28 (2017) 2041–2056.
- [3] R. Vijayan, S. Joseph, B. Mathew, Indigofera tinctoria leaf extract mediated green synthesis of silver and gold nanoparticles and assessment of their anticancer, antimicrobial, antioxidant and catalytic properties, *Artif. Cells, Nanomedicine, Biotechnol.* 46 (4) (2018) 861–871.
- [4] F. Zarlaida, M. Adlim, Gold and silver nanoparticles and indicator dyes as active agents in colorimetric spot and strip tests for mercury(II) ions: a review, *Microchim. Acta* 184 (1) (2016) 45–58.
- [5] Z. Khan, S.A. Al-Thabaiti, A.Y. Obaid, A.O. Al-Youbi, Preparation and characterization of silver nanoparticles by chemical reduction method, *Colloids Surfaces B Biointerfaces* 82 (2) (2011) 513–517.
- [6] A. Haider, I.-K. Kang, Preparation of silver nanoparticles and their industrial and biomedical applications: a comprehensive review, *Ann. Mater. Sci. Eng.* 2015 (2015) 1–16.

- [7] B. Yin, H. Ma, S. Wang, S. Chen, Electrochemical synthesis of silver nanoparticles under protection of poly(*N*-vinylpyrrolidone), *J. Phys. Chem. B* 107 (34) (2003) 8898–8904.
- [8] M.M. Ganesh Babu, P. Gunasekaran, Extracellular synthesis of crystalline silver nanoparticles and its characterization, *Mater. Lett.* 90 (2013) 162–164.
- [9] C.G. Kumar, S.K. Mamidyalu, Extracellular synthesis of silver nanoparticles using culture supernatant of *Pseudomonas aeruginosa*, *Colloids Surfaces B Biointerfaces* 84 (2) (2011) 462–466.
- [10] A.G. Rodrigues, L.Y. Ping, P.D. Marcato, O.L. Alves, M.C.P. Silva, R.C. Ruiz, I.S. Melo, L. Tasic, A.O. De Souza, Biogenic antimicrobial silver nanoparticles produced by fungi, *Appl. Microbiol. Biotechnol.* 97 (2) (2012) 775–782.
- [11] X. Zhang, Y. Qu, W. Shen, J. Wang, H. Li, Z. Zhang, S. Li, J. Zhou, Biogenic synthesis of gold nanoparticles by yeast *Magnusiomyces ingens* LH-F1 for catalytic reduction of nitrophenols, *Colloids Surfaces A Physicochem. Eng. Asp.* 497 (2016) 280–285.
- [12] S. Ahmed, M. Ahmad, B.L. Swami, S. Ikram, A review on plants extract mediated synthesis of silver nanoparticles for antimicrobial applications: a green expertise, *J. Adv. Res.* 7 (1) (2016) 17–28.
- [13] S. Francis, S. Joseph, E.P. Koshy, B. Mathew, Synthesis and characterization of multifunctional gold and silver nanoparticles using leaf extract of: *naregamia alata* and their applications in the catalysis and control of mastitis, *New J. Chem.* 41 (23) (2017) 14288–14298.
- [14] P. Kuppusamy, M.M. Yusoff, G.P. Maniam, N. Govindan, Biosynthesis of metallic nanoparticles using plant derivatives and their new avenues in pharmacological applications - an updated report, *Saudi Pharmaceut. J.* 24 (2014) 473–484.
- [15] D. Raghunandan, B. Ravishankar, G. Sharanbasava, D.B. Mahesh, V. Harsoor, M.S. Yalagatti, M. Bhagawanraju, A. Venkataraman, Anti-cancer studies of noble metal nanoparticles synthesized using different plant extracts, *Cancer Nanotechnol.* 2 (1–6) (2011) 57–65.
- [16] S. Joseph, B. Mathew, Microwave assisted facile green synthesis of silver and gold nanocatalysts using the leaf extract of *Aerva lanata*, *Spectrochim. Acta Part A Mol. Biomol. Spectrosc.* 136 (PC) (2015) 1371–1379.
- [17] B. Baruwati, V. Polshettiwar, R.S. Varma, Glutathione promoted expeditious green synthesis of silver nanoparticles in water using microwaves, *Green Chem.* 11 (7) (2009) 926–930.
- [18] M.N. Nadagouda, T.F. Speth, R.S. Varma, Microwave-assisted green synthesis of silver nanostructures, *Acc. Chem. Res.* 44 (7) (2011) 469–478.
- [19] D. Krishnaiah, A. Bono, R. Sarbatly, S.M. Anisuzzaman, Antioxidant activity and total phenolic content of an isolated *Morinda citrifolia* L. methanolic extract from Poly-ethersulphone (PES) membrane separator, *J. King Saud Univ. - Eng. Sci.* 27 (1) (2015) 63–67.
- [20] R. Abou Assi, Y. Darwis, I.M. Abdulbaqi, A.A. Khan, L. Vuanghao, M.H. Laghari, *Morinda citrifolia* (Noni): a comprehensive review on its industrial uses, pharmacological activities, and clinical trials, *Arab. J. Chem.* 10 (5) (2017) 691–707.
- [21] T.Y. Suman, S.R. Radhika Rajasree, A. Kanchana, S.B. Elizabeth, Biosynthesis, characterization and cytotoxic effect of plant mediated silver nanoparticles using *Morinda citrifolia* root extract, *Colloids Surfaces B Biointerfaces* 106 (2013) 74–78.
- [22] T.Y. Suman, S.R. Radhika Rajasree, R. Ramkumar, C. Rajthilak, P. Perumal, “The Green synthesis of gold nanoparticles using an aqueous root extract of *Morinda citrifolia* L.” *Spectrochim. Acta Part A Mol. Biomol. Spectrosc.* 118 (2014) 11–16.
- [23] K. Kalantari, A.B.M. Afifi, S. Bayat, K. Shamel, S. Yousefi, N. Mokhtar, A. Kalantari, Heterogeneous catalysis in 4-nitrophenol degradation and antioxidant activities of silver nanoparticles embedded in Tapioca starch, *Arab. J. Chem.* (2017) (Article in press).
- [24] L.B. Talarico, R.G. Zibetti, P.C. Faria, L.A. Scolaro, M.E. Duarte, M.D. Nosedá, C.A. Pujol, E.B. Damonte, Anti-herpes simplex virus activity of sulfated galactans from the red seaweeds *Gymnogongrus griffithsiae* and *Cryptonemia crenulata*, *Int. J. Biol. Macromol.* 34 (2004) 63–71.
- [25] R. Mata, J.R. Nakkala, S.R. Sadras, Biogenic silver nanoparticles from *Abutilon indicum*: their antioxidant, antibacterial and cytotoxic effects in vitro, *Colloids Surfaces B Biointerfaces* 128 (2015) 276–286.
- [26] S. Francis, S. Joseph, E.P. Koshy, B. Mathew, Green synthesis and characterization of gold and silver nanoparticles using *Mussaenda glabrata* leaf extract and their environmental applications to dye degradation, *Environ. Sci. Pollut. Res.* 24 (21) (2017) 17347–17357.
- [27] A.D. Dwivedi, K. Gopal, Biosynthesis of silver and gold nanoparticles using *Chenopodium album* leaf extract, *Colloids Surfaces A Physicochem. Eng. Asp.* 369 (1–3) (2010) 27–33.
- [28] S.K. Das, M.M.R. Khan, A.K. Guha, A.R. Das, A.B. Mandal, Silver-nano hybrid material: synthesis, characterization and application in water purification, *Bioresour. Technol.* 124 (Nov. 2012) 495–499.
- [29] N. Vigneshwaran, A.A. Kathe, P. V. Varadarajan, P.R. Nachane, Balasubramanya, H. Rudrapatna, “Silver – protein (core – shell) nanoparticle production using spent mushroom substrate, *Langmuir* 23 (8) (2007) 7113–7117.
- [30] S.R. Kavitha, M. Umadevi, S.R. Janani, T. Balakrishnan, R. Ramanibai, Fluorescence quenching and photocatalytic degradation of textile dyeing waste water by silver nanoparticles, *Spectrochim. Acta Part A Mol. Biomol. Spectrosc.* 127 (2014) 115–121.
- [31] E.E. Abel, P.R. John Poonga, S.G. Panicker, Characterization and in vitro studies on anticancer, antioxidant activity against colon cancer cell line of gold nanoparticles capped with *Cassia tora* SM leaf extract, *Appl. Nanosci.* (2015) 121–129.
- [32] R.K. Bera, C.R. Raj, A facile photochemical route for the synthesis of triangular Ag nanoplates and colorimetric sensing of H₂O₂, *J. Photochem. Photobiol. A Chem.* 270 (2013) 1–6.
- [33] M. Valko, K. Jomova, C.J. Rhodes, K. Kuca, K. Musilek, Redox- and Non-redox-metal-induced Formation of Free Radicals and Their Role in Human Disease, vol. 90, 2015, pp. 1–37, 1.
- [34] J. Bhaumik, N.S. Thakur, P.K. Aili, A. Ghanghoriya, A.K. Mittal, U.C. Banerjee, Bioinspired nanotheranostic agents: synthesis, surface functionalization, and antioxidant potential, *ACS Biomater. Sci. Eng.* 1 (6) (2015) 382–392.
- [35] S.B. Nimse, D. Pal, Free radicals, natural antioxidants, and their reaction mechanisms, *RSC Adv.* 5 (2015) 27986–28006.
- [36] B. Kumar, K. Smita, L. Cumbal, A. Debut, Synthesis of silver nanoparticles using *Sacha inchi* (*Plukenetia volubilis* L.) leaf extracts, *Saudi J. Biol. Sci.* 21 (6) (2014) 605–609.
- [37] M.K. Swamy, M.S. Akhtar, S.K. Mohanty, U.R. Sinniah, Synthesis and characterization of silver nanoparticles using fruit extract of *Momordica cymbalaria* and assessment of their in vitro antimicrobial, antioxidant and cytotoxicity activities, *Spectrochim. Acta Part A Mol. Biomol. Spectrosc.* 151 (2015) 939–944.
- [38] Y. Wang, J. Wan, R.J. Miron, Y. Zhao, Y. Zhang, “Antibacterial properties and mechanisms of gold–silver nanocages, *Nanoscale* 8 (21) (2016) 11143–11152.
- [39] A. Nabikhan, K. Kandasamy, A. Raj, N.M. Alikunhi, Synthesis of antimicrobial silver nanoparticles by callus and leaf extracts from saltmarsh plant, *Sesuvium portulacastrum* L, *Colloids Surfaces B Biointerfaces* 79 (2) (2010) 488–493.
- [40] S. Basu, P. Maji, J. Ganguly, Biosynthesis, characterisation and antimicrobial activity of silver and gold nanoparticles by *Dolichos biflorus* Linn seed extract, *J. Exp. Nanosci.* 11 (8) (2015) 660–668.
- [41] B.K. Nayak, M.A. Bhat, A. Nanda, Implementation of *Penicillium* sp. as raw material for synthesizing metal nanoparticles for antibiosis, *Mater. Sci. Forum* 760 (2013) 33–38.
- [42] M.A. Bhat, B.K. Nayak, A. Nanda, Evaluation of bactericidal activity of biologically synthesised silver nanoparticles from *Candida albicans* in combination with ciprofloxacin, *Mater. Today Proc.* 2 (9) (2015) 4395–4401.
- [43] A. Nanda, S. Majeed, Improved bactericidal property of silver nanoparticles from *Penicillium pinophilum* (MTTC 2192) in a combined form with carbicillin and moxifloxacin, *Int. J. Pharm. Pharm. Sci.* 6 (2014) 2–5.
- [44] S. Majeed, A. Nanda, K. Thirunavukarasu, Evaluation of antimicrobial activity of biologically synthesized silver nanoparticles from filamentous fungi, *Int. J. PharmTech Res.* 6 (3) (2014) 1049–1053.
- [45] S. Akila, A. Nanda, “In-vivo wound healing activity of silver Nanoparticles : an investigation, *Int. J. Sci. Res.* 3 (7) (2014) 1208–1212.
- [46] M. Lakshminpathy, A. Nanda, Biocatalysts of silver nanoparticles synthesized using an environmental isolate, *Serratia marcescens* S01, *Int. J. Chem. Res.* 5 (3) (2013) 1162–1168.
- [47] M. Latha, M. Sumathi, R. Manikandan, A. Arumugam, N.M. Prabhu, Biocatalytic and antibacterial visualization of green synthesized silver nanoparticles using *Hemidesmus indicus*, *Microb. Pathog.* 82 (2015) 43–49.
- [48] N. Yang, W.-H. Li, Mango peel extract mediated novel route for synthesis of silver nanoparticles and antibacterial application of silver nanoparticles loaded onto non-woven fabrics, *Ind. Crops Prod.* 48 (2013) 81–88.
- [49] D.-Y. Kim, M. Kim, S. Shinde, J.-S. Sung, G. Ghodake, Cytotoxicity and antibacterial assessment of gallic acid capped gold nanoparticles, *Colloids Surfaces B Biointerfaces* 149 (2017) 162–167.
- [50] A.B. Mohseny, I. Machado, Y. Cai, K.-L. Schaefer, M. Serra, P.C.W. Hogendoorn, A. Llombart-Bosch, A.-M. Cleton-Jansen, Functional characterization of osteosarcoma cell lines provides representative models to study the human disease, *Lab. Invest.* 91 (8) (2011) 1195–1205.
- [51] X. Xie, Y.-S. Li, W.-F. Xiao, Z.-H. Deng, H.-B. He, Q. Liu, W. Luo, MicroRNA-379 inhibits the proliferation, migration and invasion of human osteosarcoma cells by targeting EIF4G2, *Biosci. Rep.* 37 (3) (2017). BSR20160542.
- [52] S. Priya Velammal, T.A. Devi, T.P. Amaladhas, Antioxidant, antimicrobial and cytotoxic activities of silver and gold nanoparticles synthesized using *Plumbago zeylanica* bark, *J. Nanostructure Chem.* 6 (3) (2016) 247–260.
- [53] S. Francis, S. Joseph, E.P. Koshy, B. Mathew, Microwave assisted green synthesis of silver nanoparticles using leaf extract of *Elephantopus scaber* and its environmental and biological applications, *Artif. Cells, Nanomedicine, Biotechnol.* 46 (4) (2017) 795–804.
- [54] P. Moteriya, S. Chanda, Synthesis and characterization of silver nanoparticles using *Caesalpinia pulcherrima* flower extract and assessment of their in vitro antimicrobial, antioxidant, cytotoxic, and genotoxic activities, *Artif. Cells, Nanomedicine, Biotechnol.* 45 (8) (2016) 1556–1567.
- [55] P. Singh, Y.J. Kim, C. Wang, R. Mathiyalagan, M. El-Agamy Farh, D.C. Yang, Biogenic silver and gold nanoparticles synthesized using red ginseng root extract, and their applications, *Artif Cells Nanomed Biotechnol* (2015) 1–6, no. January.
- [56] Binil Eldhose, et al., Hepatoprotective effect of *Plumbago indica* root extract on thioacetamide-induced liver damage in rats, *J Pharm Phytochem* 4 (2) (2015) 97–101.



Contents lists available at ScienceDirect

Applied Materials Today

journal homepage: www.elsevier.com/locate/apmt

Review

Status and future scope of plant-based green hydrogels in biomedical engineering

Reza Mohammadinejad^{a,*}, Hajar Maleki^b, Eneko Larrañeta^c, André R. Fajardo^d, Amirala Bakhshian Nik^e, Amin Shavandi^f, Amir Sheikhi^{g,h,i,j,k}, Mansour Ghorbanpour^l, Mehdi Farokhi^m, Praveen Govindhⁿ, Etienne Cabane^{o,p}, Susan Azizi^q, Amir Reza Aref^r, Masoud Mozafari^{s,t,u}, Mehdi Mehrali^v, Sabu Thomasⁿ, João F. Mano^w, Yogendra Kumar Mishra^{x,*}, Vijay Kumar Thakur^{y,z,*}

^a Pharmaceuticals Research Center, Institute of Neuropharmacology, Kerman University of Medical Sciences, Kerman, Iran

^b Institute of Inorganic Chemistry, Department of Chemistry, University of Cologne, Greinstrasse 6, 50939 Cologne, Germany

^c School of Pharmacy, Queens University Belfast, Medical Biology Centre, 97 Lisburn Road, Belfast, BT9 7BL, UK

^d Laboratório de Tecnologia e Desenvolvimento de Materiais Poliméricos e Compósitos - LaCoPol. Centro de Ciências Químicas, Farmacêuticas e de Alimentos, Universidade Federal de Pelotas (UFPeL), 96010-900, Pelotas, RS, Brazil

^e Department of Biomedical Engineering, Florida International University, Miami, FL, 33174, USA

^f BioMatter unit-Biomass transformation Lab (BTL), École interfacultaire de Bioingénieurs (EIB), École polytechnique de Bruxelles, Université Libre de Bruxelles, Avenue F.D. Roosevelt, 50-CP 165/61, 1050, Brussels, Belgium

^g Department of Bioengineering, University of California, Los Angeles, 410 Westwood Plaza, Los Angeles, CA, 90095, USA

^h Center for Minimally Invasive Therapeutics (C-MIT), University of California, Los Angeles, 570 Westwood Plaza, Los Angeles, CA, 90095, USA.

ⁱ California NanoSystems Institute (CNSI), University of California, Los Angeles, 570 Westwood Plaza, Los Angeles, CA, 90095, USA

^j Biomaterials Innovation Research Center, Division of Biomedical Engineering, Department of Medicine, Brigham and Women's Hospital, Harvard Medical School, Cambridge, MA, 02139, USA

^k Harvard-MIT Division of Health Sciences and Technology, Massachusetts Institute of Technology, Cambridge, MA, 02139, USA

^l Department of Medicinal Plants, Faculty of Agriculture and Natural Resources, Arak University, 38156-8-8349, Arak, Iran

^m National Cell Bank of Iran, Pasteur Institute of Iran, Tehran, Iran

ⁿ International Inter-University Centre for Nanoscience and Nanotechnology, Mahatma Gandhi University, Kottayam, India

^o Wood Materials Science, ETH Zürich, Stefano-Franscini-Platz 3, 8093, Zürich, Switzerland

^p Applied Wood Materials, EMPA - Swiss Federal Laboratories for Materials Science and Technology, Überlandstrasse 129, 8600, Dübendorf, Switzerland

^q Department of Bioprocess Technology, Faculty of Biotechnology and Biomolecular Sciences, Universiti Putra Malaysia, UPM Serdang, Selangor, 43400, Malaysia

^r Department of Medical Oncology, Dana-Farber Cancer Institute, Harvard Medical School, Boston, MA, 02215, USA

^s Bioengineering Research Group, Nanotechnology and Advanced Materials Department, Materials and Energy Research Center (MERC), Tehran, Iran

^t Cellular and Molecular Research Center, Iran University of Medical Sciences, Tehran, Iran

^u Department of Tissue Engineering & Regenerative Medicine, Faculty of Advanced Technologies in Medicine, Iran University of Medical Sciences, Tehran, Iran

^v Department of Health Technology, Center for Intestinal Absorption and Transport of Biopharmaceuticals, Technical University of Denmark, 2800 Kgs., Lyngby, Denmark

^w Department of Chemistry, CICECO - Aveiro Institute of Materials, University of Aveiro, Aveiro, 3810-193, Portugal

^x Functional Nanomaterials, Institute for Materials Science, Kiel University, Kaiserstr. 2, D-24143, Kiel, Germany

^y Enhanced Composites and Structures Center, School of Aerospace, Transport and Manufacturing, Cranfield University, Bedfordshire, MK43 0AL, UK

^z Department of Mechanical Engineering, School of Engineering, Shiv Nadar University, Uttar Pradesh, 201314, India

ARTICLE INFO

Article history:

Received 12 January 2019

Received in revised form 11 April 2019

Accepted 13 April 2019

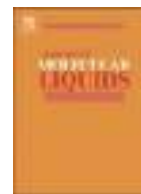
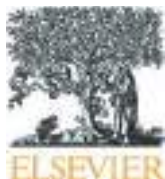
Keywords:

Hydrogels

Green hydrogels

ABSTRACT

Hydrogels are the most iconic class of soft materials, and since their first report in the literature, they have attracted the attention of uncountable researchers. Over the past two decades, hydrogels have become smart and sophisticated materials with numerous applications. This class of soft materials have been playing a significant role in biomedicine due to their tunable and often programmable properties. Hydrogels from renewable polymers have been popularized in biomedical applications as they are often biocompatible, easily accessible, and inexpensive. The challenge however has been to find an ideal plant-based hydrogel for biomedicine that can mimic critical properties of human tissues in terms of structure, function, and performance. In addition, natural polymers can readily be functionalized to engineer their



An insight into the comparative binding affinities of chlorogenic acid functionalized gold and silver nanoparticles with ctDNA along with its cytotoxicity analysis

Riju K. Thomas, Surya Sukumaran, C. Sudarsanakumar *

School of Pure and Applied Physics, Mahatma Gandhi University, Kottayam, Kerala 686560, India



ARTICLE INFO

Article history:

Received 28 November 2018

Received in revised form 25 April 2019

Accepted 2 May 2019

Available online 5 May 2019

Keywords:

CA-AuNPs and CA-AgNPs

Binding energy

LSPR

ITC

Cytotoxicity

ABSTRACT

The binding mechanism of natural drugs and its functionalized metal nanoparticles with DNA have prime importance in the field of nano-toxicology and nano-medicine. The focus of this study was to describe the comparative binding efficiency, structural conformation, mode of binding and thermodynamic parameters due to the complex formation of chlorogenic acid (CHA) capped gold (CA-AuNPs) and silver (CA-AgNPs) nanoparticles with ctDNA, using a series of biophysical analysis. The gold and silver nanoparticles were successfully synthesized by CHA as both capping and reducing agent. The CA-AuNPs and CA-AgNPs were characterized by UV-Visible spectroscopy, XRD, FTIR, DLS and HR-TEM analysis confirmed the formation of stable AuNPs and AgNPs with an average size of 37 and 20 nm respectively. The strength and mode of interaction of CHA functionalized metal nanoparticles with ctDNA were evaluated on the basis of binding parameters extracted from UV-visible absorption, dye displacement fluorescence studies and ITC. The conformational alterations of ctDNA double helix due to its complexation with CA-AgNPs and CA-AuNPs were monitored by Circular dichroism and Fourier transform infrared spectroscopy. The thermodynamic parameters obtained from ITC established the stabilizing forces responsible for the exothermic binding processes. The binding constants obtained from the spectroscopic and calorimetric studies consistently explained the strong binding efficiency of CA-AgNPs than CA-AuNPs with ctDNA. The DNA detection efficiency of CA-AgNPs was comparatively higher than that of CA-AuNPs executed by LOD and colorimetric alterations. The MTT assay on normal human cell lines revealed that CA-AuNPs exhibited mild dose-response suppression on normal human cell lines when compared with CA-AgNPs. These results based on DNA nanoparticles binding mechanism will help for the designing and synthesis of new CHA functionalized nanoparticles possessing better sensing and therapeutic efficacy with minimal side effects.

© 2019 Elsevier B.V. All rights reserved.

1. Introduction

DNA plays an inevitable role as the supreme genetic substance for the biological production of enzymes and proteins in living organisms [1]. Hence, DNA is considered as the main cellular target for interaction studies with naturally occurring/synthetic drugs and its functionalized metal nanoparticles (NPs) having therapeutic potentials for the effective designing of novel drug targets [1–3]. The nanostructured materials had gained renovation with potential applications in medicine, ther-

metal NPs have been identified that they selectively interact and detect biomolecules like DNA; the most important ones are noble metal nanoparticles of gold (Au) and silver (Ag). Such DNA-drug/NPs interactions have been influenced by the size, shape and surface chemistry of the nanostructured materials [3,6]. In specific, apart from the extensive fields of electronics, medicine and optics Au and Ag NPs offer multipurpose application provisions in wide areas of human life such as energy, environmental remediation, water treatment and medical technology [7–9]. Earlier studies also reported the strong complex formation of

Accepted Manuscript

Novel SPR based fiber optic sensor for vitamin A using Au@Ag core-shell nanoparticles doped SiO₂-TiO₂-ZrO₂ ternary matrix

V.P. Prakashan, George Gejo, M.S. Sanu, M.S. Sajna, Thomas Subin, P.R. Biju, Joseph Cyriac, N.V. Unnikrishnan



PII: S0169-4332(19)31047-5
DOI: <https://doi.org/10.1016/j.apsusc.2019.04.055>
Reference: APSUSC 42363
To appear in: *Applied Surface Science*
Received date: 21 December 2018
Revised date: 27 March 2019
Accepted date: 4 April 2019

Please cite this article as: V.P. Prakashan, G. Gejo, M.S. Sanu, et al., Novel SPR based fiber optic sensor for vitamin A using Au@Ag core-shell nanoparticles doped SiO₂-TiO₂-ZrO₂ ternary matrix, *Applied Surface Science*, <https://doi.org/10.1016/j.apsusc.2019.04.055>

This is a PDF file of an unedited manuscript that has been accepted for publication. As a service to our customers we are providing this early version of the manuscript. The manuscript will undergo copyediting, typesetting, and review of the resulting proof before it is published in its final form. Please note that during the production process errors may be discovered which could affect the content, and all legal disclaimers that apply to the journal pertain.



Synthesis, structural and luminescence properties of Dy³⁺ activated GdAlO₃ phosphors by a solid state reaction method under a N₂ atmosphere

SAMIT TIWARI¹, RAUNAK KUMAR TAMRAKAR^{1,*}, KANCHAN UPADHYAY²
and C S ROBINSON¹

¹Department of Applied Physics, Bhilai Institute of Technology (Seth Balkrishan Memorial), Near Bhilai House, Durg (C.G.) 491001, India

²International and Inter University Centre of Nanoscience and Nanotechnology, Mahatma Gandhi University, Kottayam 686560, India

*Author for correspondence (raunak.ruby@gmail.com)

MS received 23 November 2018; accepted 25 February 2019; published online 30 May 2019

Abstract. Dysprosium (Dy³⁺) ion-doped GdAlO₃ nanophosphors were fabricated by using a high temperature solid state reaction method. X-ray diffraction measurements were used to investigate the phase and crystal size of these phosphors. The morphology of the powder was observed by scanning electron microscopy. The band structure of the phosphor was determined by recording the UV absorption spectra and Tauc plot. The optical behaviour of the phosphors was determined by measuring their photoluminescence (PL) spectra. The PL spectra show characteristic blue (489 nm) and green (567 nm) emissions corresponding to the energy level transitions of Dy³⁺.

Keywords. GdAlO₃; Dy³⁺; XRD; photoluminescence; CIE.

1. Introduction

Perovskite compounds behave as the best host materials for the development of various display devices. The perovskite compound has the general formula of ABO₃. Gadolinium aluminate belongs to the perovskite structure-based compound. It has an orthorhombic crystal structure that belongs to the *Pm3m* symmetry group. Perovskites are chemically and thermally stable, which makes them very useful for various applications [1–4]. Doping of Dy³⁺ ions in the GdAlO₃ host makes it useful for white light applications. Dy³⁺ ions are active rare earth ions for the production of white light. Due to this, they are one of the most studied rare earth ions [5,6]. The emission of Dy³⁺ ions can be tuned by varying the host matrix [7,8].

Various preparation methods have been used for the synthesis of GdAlO₃ phosphors doped with various rare earth ions, which include solvothermal, combustion synthesis, solid state

Er³⁺:Yb³⁺-codoped GdAlO₃ phosphors by replacing the oxides of erbium and ytterbium with dysprosium oxide (Dy₂O₃) [9]. To determine the influence of the dopant concentration on the spectral behaviour, phosphors with variable Dy³⁺ concentrations have been prepared by using the above-mentioned method.

3. Results and discussion

3.1 Phase, structure and morphology

Figure 1 shows the X-ray diffraction (XRD) patterns of the sample. The obtained XRD pattern of the sample matches well with the JCPDS file No. 46-0395 [10,11] indicating that the sample has an orthorhombic phase. No other peaks due to Dy³⁺ are observed in the XRD pattern revealing that the sample has a pure phase of GdAlO₃. The average crystal size of the phosphor was determined by using Scherer's formula [12]. The calculated average crystal size was 150 nm.



Structural studies on transition metal ion complexes of polyethylene oxide-natural rubber block copolymers

M. S. Mrudula¹ · Nidhi Tiwari² · Shambhu Nath Jha² · Dibyendu Bhattacharyya² · M. R. Gopinathan Nair¹ 

Received: 29 January 2019 / Accepted: 18 June 2019
© The Polymer Society, Taipei 2019

Abstract

Two shot solution polymerised NR/PEO block copolymer (BC) was used as an absorbent in this study. This polymer has got polyethylene oxide (PEO) immobilised on hydrophobic natural rubber and it was used for complexation studies with the selected 3d transition metal ions. The prepared complexes were subjected to various analytical techniques such as energy dispersive X-ray spectroscopy (EDX), Fourier Transform infrared spectroscopy (FTIR), Raman spectroscopy, X-ray diffraction (XRD) studies, extended X-ray absorption fine structure (EXAFS) analysis and X-ray absorption near edge spectroscopy (XANES). EDX analysis confirms presence of the respective metal ion in each complex. FTIR spectroscopy reveals the 7_2 helical conformation of polyethylene oxide segments in BC which is retained with some deformation upon complexation. The BC-metal ion interaction is confirmed by broadening of the C-O-C triplet peak. XRD analysis revealed that PEO lattice undergoes expansion during complexation in order to accommodate the respective metal ion. From the EXAFS results it was observed that each metal ion shows only one peak that corresponds to the oxygen shell indicating the presence of only one type of metal ion bonding. The EXAFS gives hexa coordinated pattern for Co(II), Ni(II) and Zn(II) complexes while a tetra coordination for the Cu(II) complex. Metal-oxygen distance in a given complex is constant and unique which varies with the metal ion. XANES shows a distorted octahedral symmetry (Oh) with sp^3d^2 hybridisation for the hexa coordinated complexes and a square planar symmetry with dsp^2 hybridisation for the tetra coordinated complex. Feasibility of $1s \rightarrow 3d$ transition confirms +2 oxidation state of the metal ions. The combined result of EXAFS and FTIR shows the best fit structure of the complexes in which metal ions are encapsulated within the PEO helical tunnel.

Keywords NR/PEO block copolymers · Polymer – transition metal ion complex · Structural studies · EXAFS analysis · XANES analysis · EDX analysis

Introduction

Polymer - metal complexes are being extensively studied in recent years due to their wide range of applications in the fields such as catalysis, polymer electrolytes, effluent treatment, ion exchange resin, metal ion removal, hydrometallurgy, etc. [1–4] Among all the polymers studied for this purpose polyethylene oxide (PEO) has a special role due to its ability to form complexes through oxygen donors present as ether

linkages in high density. Easy solubility in various solvents and relatively easy way of chemical modification are added advantages [5–9]. Studies reported on structural aspects of PEO complexation suggest that the mode of complexation has similarity to that of crown ethers [10–13]. However, in contrast, the more flexible PEO ligands are able to wrap bigger ions such as lanthanides in the helical form while the crown ether due to their rigid cavity size are found to coordinate in the out – of – cavity fashion [14, 15]. Over the years



Distribution and risk assessment of trace metals in multifarious matrices of Vembanad Lake system, Peninsular India



M.S. ShyleshChandran^{a,b,*}, E.V. Ramasamy^{a,1}, Mahesh Mohan^{a,1}, Sruthi S. N^{a,1},
K.K. Jayasooryan^{a,1}, Toms Augustine^{a,1}, Kannan Mohan^{a,1}

^a School of Environmental Sciences, Mahatma Gandhi University, Kerala, India

^b National Centre for Earth Science Studies, Thiruvananthapuram, Kerala, India

ARTICLE INFO

Keywords:

Ecological risk assessment
Contamination factor
Incremental lifetime cancer risk
Hazard quotient
Pollution load index

ABSTRACT

Trace metal contamination in aquatic ecosystems is of significant concern in countries like India having a recent industrial history. The present study mainly focuses on the spatial and temporal distribution, occurrence and toxicity of five trace metals (Hg, Cd, Zn, Cu and Pb) in water and sediment matrix of Vembanad Lake system (VLS), India. Mercury analysis was done by using Cold Vapor Atomic Fluorescence Spectrometer, and the other metals were analysed using Volta metric-Trace metal analyser. The spatial distribution of trace metals in the study area showed the following trends, Zn > Pb > Cu > Cd > Hg, Zn > Pb > Cu > Hg > Cd for surface water and bottom water respectively. Health risk assessment on human population associated with trace metals was also calculated to predict their health impacts on human through non-dietary exposure. The trace metals contamination in water and sediments of VLS are potential to cause cancer on human population associated with the system. Ecological risk indices showed that the northern portion of VLS is more contaminated with trace metal than the other part of the system.

1. Introduction

Environmental quality possesses great importance on the survival and well-being of living organisms in the coastal estuaries and inland wetland systems. Pollution stress of such systems mainly through anthropogenic activities is the major challenging problem of the century. These aquatic systems serve as a sink as well as the receptors for the massive quantity of pollutants (Ridgway and Shimmield, 2002; Spencer et al., 2003). The express economic growth, preceding industrialisation and urbanisation leads aquatic environment pollution in coastal wetlands of developing countries. Since 1940's, rapid industrialisation, population exploitation and subsequent urban agglomeration resulted in the enrichment of trace metals in the aquatic environment and trigger various environmental problems in developing countries, especially in India (ShyleshChandran et al., 2019).

When the contaminants reach the aquatic environment, nearly 10% dispersed in water and the rest 90% will be stored in the sedimentary

effects on aquatic biota (Chen et al., 2016; Parween et al., 2017; Patel et al., 2018). The accumulated sediment-bound metals may get mobilized by biochemical or anthropogenic process and may results in bio-concentrate in tissues of aquatic organisms and eventually transmitted to organisms in higher trophic level. Hence, the assessment of spatial and temporal distribution of metals and their risk assessment on the aquatic environment and on human population requisite global attention.

By recognizing the risk of trace metals on entire environment the United States Environmental Protection Agency (USEPA) classified 12 trace metals such as As, Be, Cd, Cr, Cu, Pb, Hg, Ni, Se, Ag, Ti, and Zn as priority pollutants. These priority pollutants especially Hg and Pb may be transformed into organometallic forms and are potential to increase its level of toxicity by reaching to benthic fauna. Trace metal concentration in an aquatic system is mostly influenced by various factors such as sediment texture, mineralogical composition and physical transport (Buccolieri et al., 2006; Marchand et al., 2006). These toxic



Compatibilising action of multiwalled carbon nanotubes in polycarbonate/polypropylene (PC/PP) blends: phase morphology, viscoelastic phase separation, rheology and percolation

Mohammed Arif Poothanari¹ · Priti Xavier² · Suryasarathi Bose² · Nandakumar Kalarikkal^{1,3} · Cibi Komalan⁴ · Sabu Thomas^{1,5}

Received: 15 October 2018 / Accepted: 11 June 2019

© The Polymer Society, Taipei 2019

Abstract

Multiwalled carbon nanotubes were introduced into both dispersed and co-continuous polycarbonate/polypropylene blends through melt compounding in an internal mixer. Both the neat blends and blend nanocomposites showed viscoelastic phase separation process where phase in phase morphologies could be observed due to viscosity disparity and T_g differences between the component polymers. A strong compatibilising action was noticed up on the addition of a small quantity of MWCNT into both dispersed and co-continuous morphologies. Theoretical predictions based on thermodynamic considerations clearly indicated the preferential localisation of MWCNTs in the PC phase. However, because of the viscosity differences between the two polymers, we also found that some of the MWCNTs being localised at the blend interphase and in PP phase. From linear viscoelastic studies rheological percolation was observed at high concentration of the MWCNTs where carbon nanotubes formed a network-like structure leading to solid state behaviour at low frequencies.

Keywords Polycarbonate/polypropylene blends · Co-continuous morphology · Selective localization of MWCNTs

Introduction

Melt blending of polymers is an immensely attractive and inexpensive method of getting novel and different structural materials [1]. We can attain a good cost/performance ratio by the judicious mixing of low-cost polymers with expensive polymers. They can be

miscible or immiscible. The miscibility of polymer blend depends on the thermodynamics of mixing. Most of the blend systems are immiscible due to unfavorable interactions and very low contribution of entropy [2–4]. A wide range of morphologies (dispersed to co-continuous structures) could be obtained by carefully controlling the composition and viscosity ratio of immiscible polymer blends. In recent years, nanoparticles have attracted a lot of interest due to their important role in immiscible and incompatible polymer blends. The nanoparticles are able to change the interaction coefficient between two polymers and thus improve the compatibility between the polymer pairs [5]. The dis-

✉ Sabu Thomas
sabuthomas@mgu.ac.in; sabupolymer@yahoo.com

¹ International and Inter University Centre for Nanoscience and Nanotechnology, Mahatma Gandhi University, Kottavam, Kerala



Contents lists available at ScienceDirect

International Journal of Biological Macromolecules

journal homepage: <http://www.elsevier.com/locate/ijbiomac>

Thermal, biodegradation and theoretical perspectives on nanoscale confinement in starch/cellulose nanocomposite modified via green crosslinker



Preetha Balakrishnan^a, V.G. Geethamma^a, Sreerag Gopi^b, Martin George Thomas^c, Matjaž Kunaver^d, Miroslav Huskić^{d,e}, Nandakumar Kalarikkal^a, Tatiana Volova^f, Didier Rouxel^g, Sabu Thomas^{a,f,g,h,*}

^a International and Inter University Center for Nanoscience and Nanotechnology, Mahatma Gandhi University, Kottayam, Kerala 686560, India

^b Department of Research and Development, ADSO Naturals Pvt. Ltd., 2/5, RMV Second Stage, Bangalore, Karnataka 560094, India

^c University of Pau and Pays de l'Adour IPREM - UMR 5254 UPPA/CNRS - EPCP, Technopole Helioparc - 2, av. Pdt P. Angot, 64 053 PAU Cedex 09, France

^d National Institute of Chemistry, Department of Polymer Chemistry and Technology, Hajdrihova 19, SI-1000 Ljubljana, Slovenia

^e Faculty for Polymer Technology, Ozare 19, 2380 Slovenj Gradec, Slovenia

^f Siberian Federal University, 79 Svobodnyi Av., Krasnoyarsk 660041, Russia

^g UMR CNRS 7198 - Université de Lorraine, France

^h School of Chemical Sciences, Mahatma Gandhi University, Kottayam, Kerala 686560, India

ARTICLE INFO

Article history:

Received 5 February 2019

Received in revised form 9 May 2019

Accepted 13 May 2019

Available online 17 May 2019

Keywords:

Crosslinking

Cellulose nanofiber

Viscoelastic

ABSTRACT

In this research work, we propose a synergistic effect of a green crosslinker and cellulose nanomaterial on the crystallinity, viscoelastic, and thermal properties of starch nanocomposites. A disaccharide derivative was used as a bio crosslinker and nanofiber from pineapple leaf as a reinforcing phase for starch. Sucrose was oxidised using periodate, that can selectively oxidise the vicinal hydroxyl group of sucrose and form tetra aldehyde derivative. Crystallinity of films after crosslinking decreased with successive addition of crosslinker. The melting temperature of films increased because of formation of more dense structure after crosslinking. Morphological investigations were analysed by atomic force microscopy. Polymer chain confinement and mechanics were quantified. The crosslink densities of the films were calculated using two models, phantom model and affine model, using storage modulus data. By using very low amount of crosslinker and nanoreinforcement, the properties of thermoplastic starch were significantly improved.

© 2019 Elsevier B.V. All rights reserved.

1. Introduction

In the creation of high performance advanced polymer nanocomposites, various nanosized fillers are used as reinforcing material. Fine dispersion of nanoparticle within the polymer matrix leads to high performance composites due to high interfacial area which is in the range of molecular dimensions [1].

Starch is one of the most investigated biodegradable materials obtained from renewable resources. It is a resourceful polysaccharide with various positive points like low price, availability, use in food and non-

not truly thermoplastic in nature but can be converted into one, using water and non-aqueous volatile materials called plasticizers (generally polyols like glycerol). However, the hygroscopic nature of starch limits its applications. Also, in addition, retrogradation and crystallization of mobile starch phase leads to change in its thermomechanical properties. Starch is immiscible with other commonly used polymers due to its highly polar nature. Reinforcing with cellulosic fillers in thermoplastic starch improves its property by preserving the biodegradability.

There are several methods reported so far to improve the performance of starch based composites like blending [3–7], crosslinking



Optical Characteristics of Dy³⁺ Ions in Alkali Fluoroborate Glasses for WLEDs

SUBASH GOPI,¹ P. REMYA MOHAN,¹ E. SREEJA,¹
N.V. UNNNIKRISHNAN,¹ CYRIAC JOSEPH,¹ and P.R. BIJU^{1,2}

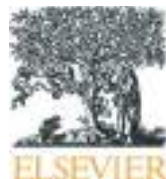
1.—School of Pure and Applied Physics, Mahatma Gandhi University, Kottayam 686560, India.
2.—e-mail: prb.mgu@gmail.com

The aim of this study is to synthesize and characterize an economical alkali fluoroborate glass doped with Dy³⁺ ions using melt quenching technique for white light generation applications. The glasses under investigation are prepared from the precursor mixture keeping the molar composition 10K₂O + 10BaO + 10ZnF₂ + (70-x)B₂O₃ + xDy₂O₃, where $x = 0.1$ mol.%, 0.5 mol.%, 1.0 mol.%, 1.5 mol.% and 2.0 mol.%. Optical characterization techniques such as absorption, photoluminescence excitation, emission and decay analysis were accomplished to validate the use of the prepared glasses for white light emitting diodes. Optical band gap energy and vital Judd–Ofelt (JO) intensity parameters were derived using the absorption spectrum. The JO intensity parameters were used to explore some characteristic radiative parameters of the present glass system. The photoluminescence spectra of the glasses have been recorded at an excitation wavelength of 348 nm and the spectra contain two intense emission bands in the blue (480 nm) and yellow (572 nm) regions and a weak band in the red region (664 nm). With the increase of dopant ion concentration, the intensity of all emission bands marked a gradual increase. The variation of the ratio of integrated intensity of yellow band to blue band (Y/B ratio) with the concentration of Dy₂O₃ is also studied. Color coordinates determined using commission international de l'éclairage (CIE) 1931 suggest that the prepared glass can be a potential material for white light applications. The experimental lifetime values marked a significant decrease with increase in dopant ion concentration and the mechanism responsible for the quenching is identified. Quantum yield is determined experimentally as well as using JO theory.

Key words: Fluoroborate, Judd–Ofelt theory, radiative properties, dipole–quadrupole interaction

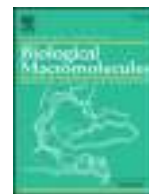
INTRODUCTION

radiation).^{1–3} They can be fabricated either by combining the three primary colors (RGB) or by



Contents lists available at ScienceDirect

International Journal of Biological Macromolecules

journal homepage: <http://www.elsevier.com/locate/ijbiomac>

Quercetin binding to *Spatholobus parviflorus* lectin: Promise of a macromolecular, specific-compound carrier for drug

Surya Sukumaran ^a, Haridas M. ^{b,*}, Sudarsanakumar C. ^{a,*}^a School of Pure and Applied Physics, Mahatma Gandhi University, Kottayam, Kerala 686560, India^b Inter University Centre for Bioscience, Department of Biotechnology and Microbiology, Kannur University, Thalassery Campus, Thalassery 670661, Kerala, India

ARTICLE INFO

Article history:

Received 12 February 2019

Received in revised form 12 April 2019

Accepted 12 April 2019

Available online 13 April 2019

Keywords:

QN

SPL

ssSPL

ITC

Docking

ABSTRACT

Glycan recognition is the most attractive defining feature of lectins, and also they exhibit specific phytochemical interactions at distinct sites without interfering the glycode recognition capability. These additional sites may be viewed as potential drug carrying sites that could be exploited for targeted drug delivery. The pharmacological effects of quercetin (QN) have already been studied. However, its molecular mechanism of interactions with lectin has not yet been addressed. The extending novelty provokes us to unravel the binding profile of QN with *Spatholobus parviflorus* lectin (SPL) using a combination series of biophysical and computational approaches. The UV absorption studies revealed an intense SPL-QN complex formation, indicating a hyperchromic effect. The fluorescence spectroscopic analysis using sugar-free SPL and sugar saturated SPL (ssSPL) revealed that QN binding significantly quenched the intrinsic fluorescence of SPL. The thermodynamic parameters maintained uniformity with the binding stoichiometry ($n = 4$) of both SPL and ssSPL, hence it may be assumed that the sugar binding onto the SPL would not have been influenced with QN binding. The molecular docking analysis also maintained consistency with the in vitro results. It could be concluded from SPL-QN interactions without altering unique carbohydrate specificities, leave SPL unrestricted for other molecular recognition events.

© 2019 Published by Elsevier B.V.

1. Introduction

Traditional polyherbal drug formulations, rich in phytochemicals like alkaloids, flavonoids and phenolic compounds, are generally found to be biologically safe [1–2]. Flavonoids have received more attention as dietary constituents due to their therapeutic significance in modifying eicosanoid biosynthesis in inflammation, preventing platelet aggregation, protecting low-density lipoproteins from oxidation and promoting relaxation of cardiovascular smooth muscles [3]. Flavonoids are a class of naturally occurring, biologically active secondary metabolites containing flavone in various combinations, possessing a broad spectrum of pharmacological and health promoting effects [4,5]. Quercetin (QN) is one such, most abundant dietary flavonol, found predominantly in apples, onions, red grapes, citrus fruits and tea [6]. The QN is chemically known as 3,3',4',5,7-pentahydroxyflavone (Fig. 1) usually

Proteins have emerged as versatile natural/synthetic drug carriers for diagnosis and treatment of many diseases, due to their drug conjugating capability [11]. The interaction studies of QN targeting mostly abundant and highly stable plasma proteins, human serum albumin (HSA) and bovine serum albumin (BSA), by exploiting the emission properties of intrinsic fluorophores, tryptophans and tyrosines, are available in the literature [12–14]. The previous reports focusing on QN affinity towards lysozyme explored by synchronous, steady-state fluorescence technique and molecular simulation have also gained much attention due to its therapeutic effectiveness [15]. The groove-binding mode of QN with calf thymus DNA (ct-DNA) was also investigated by biophysical and molecular simulation means for the designing of DNA-targeted drugs [16]. The biological and pharmacological potentials of QN frame it as a versatile molecule to target binding studies on glycoproteins like lectins. A large number of biological investigations re-



Development of oral-fluid-impervious and fracture-resistant silver-poly (methyl methacrylate) nanoformulations for intra-oral/extra-oral rehabilitation

Sandhya Gopalakrishnan,^{1,2} Indu Raj,^{1,2} Aby Mathew T.,³ Jiji Abraham,^{1,4} Hanna. J. Maria ^{1,4},
Miran Mozetič,⁵ Sabu Thomas,^{1,4} Nandakumar Kalarikkal ^{1,6}

¹International and Inter University Centre for Nanoscience and Nanotechnology, Mahatma Gandhi University, Kottayam 686 560, Kerala, India

²Department of Prosthodontics, Government Dental College, Gandhinagar Post Office, Kottayam 686 008, Kerala, India

³Department of Prosthodontics, Pushpagiri College of Dental Sciences, Pushpagiri Medicity, Perumthuruthy, 686 548, Kerala, India

⁴School of Chemical Sciences, Mahatma Gandhi University, Kottayam 686 560, Kerala, India

⁵Jozef Stefan Institute, Jamova 39, Ljubljana 1000, Slovenia

⁶School of Pure and Applied Physics, Mahatma Gandhi University, Kottayam 686 560, Kerala, India

Correspondence to: N. Kalarikkal (E-mail: nkkalarikkal@mgu.ac.in)

ABSTRACT: Poly(methyl methacrylate) (PMMA) based dental prosthetic materials have an inferior transverse resistance value and a high water-retention capacity. These drawbacks cause frequent prosthesis fractures both inside and outside the mouth, which require the remaking or repair of the prosthesis. The mechanical and physical durability of the polymer matrix can be improved by the incorporation of a multifunctional filler. In this study, we focused on the reinforcing effect of silver nanoparticles (AgNPs) on the flexural properties of PMMA. Apart from that, the transport behavior of water and saliva through this composite matrix was also studied extensively. Morphological analyses with scanning electron microscopy (SEM) and atomic force microscopy imaging techniques confirmed the uniform distribution of nanoparticles in the matrix with an increased surface roughness proportionate to the amount of AgNPs. The flexural strength and modulus were enhanced by the addition of up to 5 wt % AgNPs ($p < 0.05$); we also observed a significant increase in the fracture resistance. The SEM micrographs of the fractured ends of AgNP-reinforced groups had smaller cracks compared to the large multidirectional cracks in the unreinforced group. The diffusion of oral fluid through the composite was investigated in detail as a function of the AgNP content, the nature of the solvent (water or saliva), and the temperature (5, 28, 37, or 60°C). The water and saliva uptake, diffusion, sorption, and permeation constants were investigated and were found to decrease with increasing AgNP loading. The transport properties could have been related to the morphology of the nanocomposites and followed the Korsmeyer–Peppas model. At high concentrations, the AgNPs formed a local filler–filler network in the polymer matrix. This network hindered the transport of water and saliva through the polymer. The outcome deduced from this study confirmed that the reinforced nanocomposites improved the durability of the denture base and could be an effective replacement for the conventional denture base. © 2019 Wiley Periodicals, Inc. *J. Appl. Polym. Sci.* **2019**, *136*, 47669.

KEYWORDS: biomedical applications; kinetics; mechanical properties; nanostructured polymers; theory and modeling

Received 29 September 2018; accepted 1 February 2019

DOI: 10.1002/app.47669

Contents lists available at [ScienceDirect](https://www.sciencedirect.com)

Journal of Luminescence

journal homepage: www.elsevier.com/locate/jlumin

Sm³⁺ doped tetragonal lanthanum molybdate: A novel host sensitized reddish orange emitting nanophosphor

Kukku Thomas, Dinu Alexander, S. Sisira, Linju Ann Jacob, P.R. Biju, N.V. Unnikrishnan, M.A. Ittyachen, Cyriac Joseph*

School of Pure and Applied Physics, Mahatma Gandhi University, Kerala, 686560, India



ARTICLE INFO

Keywords:

Energy transfer
Luminescence
Molybdate
Oriented attachment
Judd-Ofelt analysis

ABSTRACT

A series of trivalent samarium doped lanthanum molybdate nanophosphors were prepared by co-precipitation route. The formation of highly crystalline tetragonal nanocrystals with space group 141/a is identified from powder X-ray diffractogram. The morphology and the oriented attachment mediated growth mechanism of the nanocrystals were recognized from TEM analysis. The strong and broad charge transfer band in the near ultra violet region favours excellent excitation of the nanophosphors and the energy transfer from host matrix to Sm³⁺ ions is established on account of the characteristic emissions of trivalent samarium ions upon host sensitization. The Judd-Ofelt (JO) theoretical analysis was carried out to have an insight into the spectroscopic characteristics of La_{2-x}Sm_x(MoO₄)₃ nanophosphors. The relatively higher value of Ω₂ predicts more asymmetric environment of Sm³⁺ sites in the host lattice, favouring the dominance of electric dipole transitions and the various radiative parameters are evaluated. In spite of the excitation channel, the ⁴G_{5/2} → ⁶H_{9/2} transition of Sm³⁺ observed at 645 nm is the most prominent emission transition. The maximum emission intensity is observed for La_{1.98}Sm_{0.02}(MoO₄)₃ nanophosphors and as the doping concentration exceeds this limit, there will be fall in emission intensity due to concentration quenching effect. A detailed investigation on the decay behaviour of host sensitized and direct excited emission of samarium ions was conducted and the average lifetime values are calculated. The CIE chromaticity co-ordinates calculated for different excitation routes fall in the reddish orange region of CIE diagram and the same for La_{1.98}Sm_{0.02}(MoO₄)₃ nanophosphors are found to be (0.601, 0.394) with a colour purity of 97.21% which disclosed the relevance of La_{2-x}Sm_x(MoO₄)₃ as a potential red phosphor material.

1. Introduction

The exploration of luminescence properties of Ln³⁺ ions embedded in a highly crystalline inorganic host material demand a lot on behalf of their potential applications in the field of display devices, laser sources and lighting. Basically, the Ln³⁺ based luminescence is relied on the sharp emissions spanning the entire visible and near infrared regions with high colour purity, relatively long lifetime (millisecond order) and potentially high quantum yield [1–3]. Specifically, the superiority of rare earth luminescence depends upon the sharp characteristic emissions of these ions emerging from the electronic transitions within partially filled 4f orbitals shielded by filled outer 5s²5p⁶ subshells, re-

blending NUV LED chip with red/green/blue primary colour phosphors [5]. In the present work, our point of interest is to develop a novel red phosphor material with versatile luminescence properties by means of some cost-effective techniques.

Generally, the development of an efficient red phosphor material is traditionally been centered on the photoluminescence properties of trivalent europium ion owing to its high emission intensity along with simple emission spectra. So far less attention has been paid in extracting the luminescence behaviour of trivalent samarium ions with 4f⁵ configuration and numerous closely spaced energy levels which favour non-radiative decay processes. Eventually, the luminescence properties of samarium ions originate from multifold electronic transitions from

Accepted Manuscript

Effect of particle size and dopant concentration on the Raman and the photoluminescence spectra of $\text{TiO}_2:\text{Eu}^{3+}$ nanophosphor thin films

Durgam Komaraiah, Eppa Radha, Jemmy James, Nandakumar Kalarikkal, J. Sivakumar, M.V. Ramana Reddy, R. Sayanna

PII: S0022-2313(18)31550-3

DOI: <https://doi.org/10.1016/j.jlumin.2019.03.050>

Reference: LUMIN 16379

To appear in: *Journal of Luminescence*

Received Date: 22 August 2018

Revised Date: 22 March 2019

Accepted Date: 25 March 2019

Please cite this article as: D. Komaraiah, E. Radha, J. James, N. Kalarikkal, J. Sivakumar, M.V. Ramana Reddy, R. Sayanna, Effect of particle size and dopant concentration on the Raman and the photoluminescence spectra of $\text{TiO}_2:\text{Eu}^{3+}$ nanophosphor thin films, *Journal of Luminescence* (2019), doi: <https://doi.org/10.1016/j.jlumin.2019.03.050>.

This is a PDF file of an unedited manuscript that has been accepted for publication. As a service to our customers we are providing this early version of the manuscript. The manuscript will undergo copyediting, typesetting, and review of the resulting proof before it is published in its final form. Please note that during the production process errors may be discovered which could affect the content, and all legal disclaimers that apply to the journal pertain.



Effect of particle size and dopant concentration on the Raman and the photoluminescence spectra of $\text{TiO}_2:\text{Eu}^{3+}$ nanophosphor thin films

Durgam Komaraiah^a, Eppa Radha^a, Jemmy James^b, Nandakumar Kalarikkal^b, J.Sivakumar^a, M.V.Ramana Reddy^a,
and R.Sayanna^a

^a Department of physics, University College of Science, Osmania University, Hyderabad- 500007, Telangana, India

^b International and Inter University Centre for Nanoscience and Nanotechnology, and Mahatma Gandhi University, Kottayam - 686 560, Kerala, India

Corresponding Author: dkumarou@gmail.com

Abstract: Eu doped TiO_2 nanocrystalline films have been deposited by sol-gel spin coating technique on the glass substrate using titanium (IV) propoxide as a precursor. The obtained films were characterized by X-ray diffractometer (XRD), TEM, EDX, UV-Vis spectrophotometer, Raman spectrometer, and fluorescence spectrometer. As revealed by XRD, and TEM, all the TiO_2 films were a single anatase phase with nanocrystallite structures and hinder the crystal growth with the Eu-doping concentration in deposited films. The images of TEM showed that all the particles have spherical in shape with an average diameter ranging from 6 to 12 nm. The $\text{TiO}_2:\text{Eu}^{3+}$ coatings have higher values of energy gap compared to pure Titania. The Raman spectra shows the characteristic modes of anatase TiO_2 and intensity of modes reduced with an increase of Eu doping concentration. An occurrence of Raman blue shifts was due to reduction of particle size. At 393 nm excitation, the Eu doped TiO_2 nanophosphor thin films showed typical PL emission ${}^5\text{D}_0 \rightarrow {}^7\text{F}_J$ ($J=0, 1, 2, 3, 4, 5$) transitions of Eu^{3+} ions in the visible spectra. The more effective photoluminescence emission was observed for the 7 at. % Eu-doped TiO_2 nanoparticles. The experimental decay times of the ${}^5\text{D}_0$ level through ${}^5\text{D}_0 \rightarrow {}^7\text{F}_2$ transition obtained by exciting at 393nm. The electron-phonon coupling strength (g) of the PSB was estimated from the excitation spectra. Judd-Ofelt (JO) intensity parameters, radiative probabilities were estimated from the emission spectra. The photocatalytic activity (PCA) of Eu-doped TiO_2 nanoparticles showed that the strong photocatalytic activity response, decrease the efficiency of



Full length article

Resolving the structure of organic nano strands self-assembled at a graphite-liquid interface using STM

Loji K. Thomas^{a,c,*}, Nadine Diek^b, Uwe Beginn^b, Michael Reichling^a^a *Fachbereich Physik, Universität Osnabrück, Barbarastr. 7, 49076 Osnabrück, Germany*^b *Institut für Chemie, Universität Osnabrück, Barbarastr. 7, 49076 Osnabrück, Germany*^c *Department of Physics, S.B College, Mahatma Gandhi University, Kerala, India*

ARTICLE INFO

Keywords:

STM
Self-assembly
Hydrogen bond
Strand
Solid-liquid interface
Graphite

ABSTRACT

Scanning tunneling microscopy (STM) at solution-graphite(0001) interface is used to identify nanometer-wide elementary strands of custom-designed amphiphilic benzamides and elucidate their internal structure with sub-molecular resolution. Evidences against graphitic artifacts that often mimic organic strands are provided, thereby unambiguously establishing the molecular origin of these strands. The aliphatic chain lengths are chosen based on bulk studies so as to promote strand architectures and avoid monolayer structures. Two different chain lengths are used to decipher the structural parameters and the results suggest hitherto unknown precursor routes to strand formation on a surface that is different from columnar mesophases in bulk. An on-surface self-assembly into hydrogen-bonded tetramer precursors and their subsequent interaction with other units via van der Waals forces between the dangling alkyl chains is proposed for strand formation on the surface.

1. Introduction

One-dimensional micro- and nano-structures of organic compounds are valuable ingredients in solution-processable organic electronic devices [1–5]. Electron transport through organic structures is the basis for a large number of biological processes as well [6]. Supramolecular self-assembly in solution is a strategy devised by nature to build larger functional ensembles [7]. Several synthetic low-molecular weight (LMW) wedge-shaped and amphiphilic 3,4,5-tris(alkoxy)benzamides are known to self-assemble into columnar mesophases in bulk [8], resulting in self-assembled fibrillar networks in non-polar and semi-polar solvents. Organogelators, due to their tendency to form nanostrands, have aroused much interest in the context of nanoelectronics [9]. It is imperative to decipher the structure of these nanostructures to identify the function they can perform such as their potential use as selective ion-transport channels.

The knowledge about columnar bulk mesophase materials mostly come from X-ray diffraction, scattering and electron microscopy techniques that generally suffice for a macroscopic understanding [10,11].

instance, solution concentration, where denser polymorph usually results from higher solution concentrations [12,13]. The hydrophobic HOPG is an ideal substrate for the investigation of amide moieties-containing compounds such as the ones investigated here. In contrast, hydrophilic substrates, in general, may hinder [14–16] the self-assembling ability of the molecules by forcing them to lie flat on the surface, although deviation from this behavior has also been reported [17]. For a discussion on the influence of substrates on the self-assembly of fibril structures on HOPG and Au, see [18–21]. To elucidate structural details of self-assembled strands on HOPG, we use scanning tunneling microscopy (STM), the only available technique that can resolve structural details at the sub-molecular level.

STM is an efficient technique to probe the structure as well as reactivity in a chemically ‘realistic’ environment- that is at solid-liquid interfaces [22–36]. However, unlike planar surface structures [37,38], the realm of isolated 1-D structures such as nanowires, has been less exploited by this technique. STM imaging of 1-D structures has been successful in imaging films of closely packed strands, edge-on stacks [26,39–41] and innate graphitic structures [42–46], but only few re-



Radio frequency plasma polymerized thin film based on eucalyptus oil as low dielectric permittivity, visible and near-infrared (NIR) photoluminescent material

Beena Mol¹ · Jemy James² · K. K. Anoop¹ · Indra Sulaniya³ · Cyriac Joseph² · M. R. Anantharaman¹ · Junaid Bushiri¹ 

Received: 25 February 2019 / Accepted: 30 May 2019 / Published online: 8 June 2019
© Springer Science+Business Media, LLC, part of Springer Nature 2019

Abstract

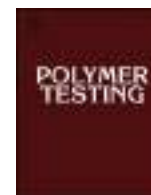
Thin films derived from eucalyptus oil was fabricated on glass and silicon substrate by rf plasma polymerization technique and characterized by FTIR, FESEM, AFM, Ellipsometry, UV–Visible and Photoluminescence spectroscopy. The dielectric constant and dielectric loss of the thin films were estimated using spectroscopic ellipsometry technique. Functional groups related to chromophores present in the eucalyptus oil thin films were identified using FTIR spectroscopy. $\pi-\pi^*$ interband transitions (306 nm) and intramolecular charge transfer (556 nm) was observed from the absorption spectra of the polymerized thin films. The indirect optical band gap estimated using Tauc plot was 3.66 eV, which revealed the semiconducting nature of the thin film. The value of real part of dielectric constant (ϵ') was less than 2.44, which indicated a low dielectric permittivity behaviour of the film in the optical regime. The photoluminescence emission studies and CIE colour coordinates showed that plasma polymerized eucalyptus oil thin films exhibits yellow and IR emission.

1 Introduction

Eco-friendly and biocompatible organic polymer materials have potential applications in the making of phototherapy devices [1], infrared signal processing, telecommunication devices [2, 3], organic solar cell [4, 5], organic light emitting diodes [6] and flat panel TV display screens [7]. To design a luminescent organic polymer material one has to consider intermolecular interactions in the polymer chain since the emission of photons from a polymer film are either due to the interchain excitation or can be from dimers or excimers [8]. Interestingly, organic semiconductor polymers are carbon-rich compounds, their electrical and luminescent properties can be tuned by modifying their structure by chemical doping or by using high energy ion beams [9, 10]. The optical properties of a polymer film arises due to the physical

alignment of transition dipoles in their polymer backbone [11]. Conjugated polymers have multichromophore systems and their photoluminescence emissive properties depend on inter/intramolecular energy transfer between the chromophore units present in the polymer skeleton. Currently, most of the applications are focussed on materials with randomly oriented conjugated chains because of their ability to yield photogenerated charge carriers [12].

Organic thin films are mostly prepared by electrospray process [13], solution processing [14] and solvent-free plasma enhanced deposition [15, 16], electropolymerization [17, 18], dc, ac and rf plasma polymerization [19, 20]. Among the various techniques, rf plasma polymerization gets special attention due to its less infrastructural requirements and easiness in film preparation since polymerization takes place in a single step. This technique is used for the preparation of organic polymer thin films with ultra-low thickness (< 10 nm), which cannot be polymerized



Material Characterisation

Vulcanization kinetics and mechanical properties of organically modified nanoclay incorporated natural and chlorobutyl rubber nanocomposites

Ajesh K. Zachariah^{a,c,*}, Arup Kumar Chandra^b, P.K. Mohammed^b, Sabu Thomas^{c,d}

^a Post Graduate and Research Department of Chemistry, Mar Thoma College, Tiruvalla, Kerala, India

^b R&D Centre, Apollo Tyres, Vadodara, Gujarat, India

^c School of Chemical Sciences, Mahatma Gandhi University, Priyadarsini Hills, Kottayam, Kerala, India

^d International and Interuniversity Centre for Nanoscience and Nanotechnology, Mahatma Gandhi University, Priyadarsini Hills, Kottayam, Kerala, India



ARTICLE INFO

Keywords:

Natural rubber
Chlorobutyl rubber
Nanocomposites
Vulcanization kinetics
Mechanical modeling

ABSTRACT

The curing kinetics, vulcanizate properties, mechanical reinforcement and chemical interactions of organically modified nanoclay filled natural rubber (NR) and chlorobutyl (CIIR) rubbers have been studied. From the vulcanization studies, it is observed that nanoclays are more intercalated in NR matrix rather than CIIR matrix. To understand the exact mechanism operating in the vulcanization behavior of NR and CIIR, autocatalytic model was applied. The vulcanization kinetic studies revealed that the nanoclay distribution at high temperature (190 °C) in CIIR matrix is somewhat intercalated in nature. Highly pronounced reversion behavior was observed in NR matrix. The mechanical reinforcement of vulcanizates was examined using the change in modulus values at 100% and 300% elongation. The mechanical properties were modeled using different kind of models such as Guth-Smallwood, Halpin-Tsai, modified Halpin-Tsai and Mori-Tanaka models. Finally, the dispersion of nanoclay platelets in CIIR and NR matrix was confirmed by the phase images obtained from AFM technique.

1. Introduction

The incorporation of the nanofillers definitely affects the curing kinetics of natural rubber and synthetic rubbers. But, the vulcanization behavior in the presence of organically modified nanoclays and unmodified nanoclays are quite different. Many research groups reported on the behavior of the organically modified nanoclays on the vulcanization behavior of rubber based nanocomposites [1–7]. Vulcanization is mostly favored by the organic modification by quaternary ammonium salts, since the quaternary ammonium salts can accelerate the reaction. The organic modification in nanoclays influence the vulcanization behavior in natural rubber (NR) nanocomposites [1,2] and acrylonitrile rubber (NBR) nanocomposites [3,4]. The vulcanization kinetics of the rubber matrices with different fillers other than nanoclays was also studied. Sui et al. [8] reported the effect of pretreated carbon nanotubes (CNTs) in the vulcanization kinetics and mechanical behavior of natural rubber matrix. Akhlaghi et al. [9] studied the effect of nano ZnO in EPDM matrix on the vulcanization kinetics and mechanical properties. The

nanoclay [10] and TiO₂ [13] on the property improvements of CIIR matrix was examined by Saritha et al. Recently, the vulcanization kinetic studies of rubber systems such as styrene-butadiene rubber (SBR)/zinc dimethacrylate [17], NR/hybrid nanofiller systems [18], NR/efficient vulcanization (EVs) systems have been reported [19]. Estimating the mechanical modulus values and analyzing the swelling pattern is another method to understand the nanofiller interaction with the elastomers. Many works have been reported on the nanofiller interactions with elastomers by considering various above discussed aspects [20,21]. Similarly, many reports [22] pointed out the importance of the Halpin-Tsai [23], Mori-Tanaka [24] and Guth-Smallwood [25,26] models in the interpretation of mechanical behavior of rubber nanocomposites.

In the present article, we try to explore the role of organically modified nanoclay on the vulcanization characteristics and mechanical behavior of natural rubber and chlorobutyl rubber nanocomposites. In particular, the nanoclay interactions with NR and CIIR matrix have been studied. The vulcanization kinetics and mechanical properties of the



Titanium Nanorods Loaded PCL Meshes with Enhanced Blood Vessel Formation and Cell Migration for Wound Dressing Applications

Robin Augustine, Anwarul Hasan,* Noorunnisa Khanam Patan, Anitha Augustine, Yogesh B. Dalvi, Ruby Varghese, Raghunath Narayanan Unni, Nandakumar Kalarikkal, Ala-Eddin Al Moustafa, and Sabu Thomas

Proper management of nonhealing wounds is an imperative clinical challenge. For the effective healing of chronic wounds, suitable wound coverage materials with the capability to accelerate cell migration, cell proliferation, angiogenesis, and wound healing are required to protect the healing wound bed. Biodegradable polymeric meshes are utilized as effective wound coverage materials to protect the wounds from the external environment and prevent infections. Among them, electrospun biopolymeric meshes have got much attention due to their extracellular matrix mimicking morphology, ability to support cell adhesion, and cell proliferation. Herein, electrospun nanocomposite meshes based on polycaprolactone (PCL) and titanium dioxide nanorods (TNR) are developed. TNR incorporated PCL meshes are fabricated by electrospinning technique and characterized by scanning electron microscopy, energy dispersive X-ray spectroscopy, Fourier transform infrared spectroscopy (FTIR) analysis, and X-Ray diffraction (XRD) analysis. In vitro cell culture studies, in ovo angiogenesis assay, in vivo implantation study, and in vivo wound healing study are performed. Interestingly, obtained in vitro and in vivo results demonstrated that the presence of TNR in the PCL meshes greatly improved the cell migration, proliferation, angiogenesis, and wound healing. Owing to the above superior properties, they can be used as excellent biomaterials in wound healing and tissue regeneration applications.

1. Introduction

Impaired or delayed healing of chronic wounds occurs due to several pathogenic abnormalities such as reduced blood vessel formation (angiogenesis), insufficient cell migration, low matrix turnover, infection, and chronic inflammation.^[1] For the effective healing of chronic wounds, suitable wound coverage materials are required to protect the wound bed from pathogenesis and subsequent associated complications. An ideal wound dressing material should have biocompatibility, ability to maintain a moist environment, offer protective barrier function against pathogens, provide enough aeration, and promote epithelization by releasing essential signaling molecules. Recently, emergence of various approaches for the fabrication of novel biomaterial resulted in the development of new biopolymers and synthetic polymers with excellent biocompatibility and biodegradability that can be used for the production of wound dressings.^[2]

Dr. R. Augustine, Dr. A. Hasan, Dr. N. K. Patan
Department of Mechanical and Industrial Engineering
College of Engineering
Qatar University
P. O. Box 2713, Doha, Qatar
E-mail: ahasan@qu.edu.qa

Dr. R. Augustine, Dr. A. Hasan, Prof. A.-E. Al Moustafa
Biomedical Research Centre (BRC)
Qatar University
P. O. Box 2713, Doha, Qatar

A. Augustine, Dr. N. Kalarikkal, Prof. S. Thomas
International & Inter University Centre for Nanoscience & Nanotechnology
Mahatma Gandhi University
Kottayam, Kerala 686560, India

 The ORCID identification number(s) for the author(s) of this article can be found under <https://doi.org/10.1002/mabi.201900058>.

A. Augustine
Department of Chemistry
Bishop Kurialacherry College for Women
Amalagiri, Kottayam, Kerala 686561, India

Dr. Y. B. Dalvi, Dr. R. Varghese
Pushpagiri Research Centre
Pushpagiri Institute of Medical Sciences
Tiruvalla, Kerala 689101, India

Dr. R. N. Unni
RP MedHelix Diagnostics Private limited
Cochin, Kerala 682025, India

Prof. A.-E. Al Moustafa
College of Medicine
Qatar University
P. O. Box 2713, Doha, Qatar

DOI: 10.1002/mabi.201900058



Electrospinning is a simple and affordable technique for the fabrication of nanofibrous or microfibrinous constructs having superior properties suitable for various biomedical applications.^[3,4] Electrospinning help to fabricate porous polymeric meshes that resemble the native architecture of the natural extracellular matrix (ECM).^[5–7] In addition to the morphological similarity to ECM, electrospun meshes have remarkable advantages such as variable pore size, high surface area, and oxygen permeability that make them suitable for wound dressing applications.^[8–10] Moreover, microporous morphology, large surface area, and the ability to facilitate the adhesion and rapid proliferation of cells make electrospun meshes highly advantageous for promoting wound healing.^[7,11] Polycaprolactone (PCL) is a biodegradable and biocompatible polymer approved by US FDA for the use in medical and drug delivery applications.^[12] PCL has been considered to be an appropriate biomaterial for drug delivery systems,^[13] various tissue engineering applications,^[14,15] and wound dressings.^[16] Particularly, electrospun PCL meshes embedded with various active agents could be an excellent candidate for wound dressing applications.^[17]

In the past, metal oxide or metal hydroxide nanoparticles with angiogenic properties such as zinc oxide,^[18] cerium oxide,^[19] yttrium oxide,^[15] and europium hydroxide^[20] nanoparticles were loaded in electrospun polymeric meshes to develop angiogenic and bioactive biomaterials. Among other metal oxide nanostructures, titanium dioxide (TiO₂) nanomaterials have a broad spectrum of desirable properties and it has been used in wide range of applications such as catalysis, sensors, solar cells, and biomedical devices.^[21] Results of *in vitro* and *in vivo* studies have established that TiO₂ nanomaterials can play important role in cell migration and cell proliferation.^[22] In addition, the uptake of TiO₂ nanostructures by cells leads to the activation of macrophages, opening a new path to exploit them to promote cell migration and wound contraction.^[23] Since the photocatalytic reactions taking place on the surface of TiO₂ nanostructures are the major reason for the biological activity, a high surface area-to-volume ratio is of great relevance for increasing the biological response.^[24–27] Several other studies demonstrated that catalytic properties of metal oxide nanoparticles depend on their morphology and those with high aspect ratio show higher catalytic activity.^[24–26] Among the various morphological forms of TiO₂ structures such as nanopowders, nanorods, and nanowires, TiO₂ nanorods (TNR) is a highly promising candidate due to its high aspect ratio.^[28–30] Thus, the use of TiO₂ in the form of nanorods with high aspect ratio would be highly advantageous to provide higher biological activity compared to the spherical nanoparticles.^[31] Studies have shown that TiO₂ nanostructures can effectively deliver reactive oxygen species (ROS) in aqueous conditions.^[21] Generally, ROS can play key roles in molecular and physiological events such as cell migration, cell proliferation, and wound healing.^[32] Although excessive generation of ROS can cause harmful effects, ROS at optimum dose exerts favorable role in angiogenesis and wound healing.^[33] Studies also showed that anodized titanium dioxide nanostructures on implants enhance angiogenesis related cellular responses such as higher endothelial cell adhesion, viability, and proliferation.^[34] However, a detailed investigation on the angiogenic potential of TiO₂ nanostructures yet to be explored using *in ovo* or *in vivo* models. Although the development of PCL

membranes incorporated with TiO₂ nanoparticles had already been reported in the past by various researchers,^[35–37] there is an immense need of studying the angiogenic potential of such membranes. Thus, studying the angiogenic potential of electrospun PCL meshes embedded with TNR could be a novel and interesting direction for the biomaterial research community. Moreover, investigating the potential of TNR in electrospun membranes to promote cell migration will also be an interesting area to be explored in detail.

In addition, unlike spherical TiO₂ nanoparticles, TNR would provide superior catalytic and biological activity due to the higher surface area to volume ratio which has to be further explored. Application of high surface area TNR in the scaffolds would provide additional advantages like superior mechanical properties due to the reinforcement effect of well dispersed TNR in the polymer matrix. Thus, in this study, we report the development of electrospun PCL meshes loaded with TNR as an active agent to promote cell adhesion, cell migration, angiogenesis, and wound healing.

2. Experimental Section

2.1. Synthesis of TNR

The commercial TiO₂ nanoparticle powder with average diameter of 25 nm (Sigma-Aldrich) was used as the precursor for TNR synthesis. In brief, 0.2 g of the precursor was suspended in 20 mL of NaOH (10 mol L⁻¹, Merck) aqueous solution followed by hydrothermal treatment (150 °C) for 24 h. After cooling, the reaction mixture was centrifuged at 12 000 rpm (15 min) and the centrifugate was collected. The obtained TNR centrifugate was washed carefully with water and 0.1 mol L⁻¹ HCl (Merck) aqueous solution, then centrifuged (12 000 rpm, 5 min). This process was repeated several times and lastly in ethanol which was then ultrasonicated to fragment the nanofibers and dried in a hot air oven at 60 °C for 24 h. Finally, the sample was calcined at 400 °C for 2 h and grinded using mortar and pestle.

UV-Visible (VIS) absorbance spectra of TNR particles after dispersing in ethanol by sonication was measured with PerkinElmer, LAMBDA 1050 spectrophotometer between 200 and 600 nm. Perkin-Elmer, spectrum 400 Fourier transform infrared (FTIR) spectrometer was used to obtain FTIR spectrum of samples (400–4000 cm⁻¹). D8-Advance of Bruker, having CuK α radiation with energy 8.04 keV and wavelength 1.54 Å was used to record X-Ray Diffraction (XRD) pattern (2θ range of 30–80°) of synthesized TNR. Transmission electron microscope (TEM, JEOL, JSM-2100) was used to understand the size and shape of TNR. Selected area electron diffraction (SAED) was used to understand the crystallinity and crystallographic planes of TNR.

2.2. Development of Electrospun PCL-TNR Meshes

For the fabrication of nanocomposite meshes, 12% w/v PCL (Mn 80 000–120 000, Sigma-Aldrich) solutions (in acetone, Merck) containing 0.5%, 1%, 2%, and 4% w/w TNR was prepared. Similar concentration of PCL solution without TNR were also prepared. Then, 10 mL of the prepared PCL solutions were electrospun

at a flow rate of 1 mL h⁻¹ as described previously.^[38] The tip to collector distance and the applied voltage were 15 cm and 15 kV, respectively. Spinning was performed for a predetermined time period to get samples with similar thickness (1 ± 0.3 mm).

Hereafter, PCL meshes with a TNR content of 0.5%, 1%, 2%, and 4% w/w referred to as PCL-TNR-0.5%, PCL-TNR-1%, PCL-TNR-2%, and PCL-TNR-4%, respectively.

2.3. Basic Characterization of PCL-TNR Meshes

Gold coated specimens were characterized using scanning electron microscopy (SEM, Hitachi SU6600). The average fiber diameter of each sample was measured from SEM images using ImageJ software. The presence of TNR in PCL mesh was detected using EDS (Oxford Swift ED) which is attached to Nova NanoSEM 450, FEI. FTIR and XRD analyses were performed as described in the case of TNR.

DSC analysis of the samples were performed using Perkin Elmer Pyris 7 DSC instrument in nitrogen atmosphere. The samples (5 mg) were heated from 0 °C to +100 °C at 10 °C min⁻¹ with a 1 min hold at +100 °C, then, cooled at 10 °C min⁻¹ to 0 °C. Subsequently, after 1 min hold at 0 °C, samples were heated from 0 °C to +100 °C at 10 °C min⁻¹. Thermodynamic properties such as enthalpy of melting (ΔH_m), enthalpy of crystallization (ΔH_c), melting temperature (T_m), crystallization temperature (T_c), and degree of crystallinity (X_c) were measured. Crystallinity of the polymer was quantified using Equation (1).

$$\% \text{Crystallinity} = [\Delta H_m] / \Delta H_m^\circ \times 100\% \quad (1)$$

ΔH_m and ΔH_m° are the enthalpy of melting of the samples and enthalpy of melting of 100% crystalline PCL, respectively, ($\Delta H_m = 139.5 \text{ J g}^{-1}$).^[39]

2.4. Uniaxial Tensile Properties of PCL-TNR Nanocomposite Meshes

PCL and PCL-TNR nanocomposite meshes were cut into 6 × 1 cm² dimensions and used for tensile testing. The thickness of the meshes were measured using a digital Vernier caliper and those with more than or less than 1 ± 0.3 mm thickness were neglected from the testing. Instron 5943 extended column universal testing machine was used for testing according to the ASTM D882-2012 standard. A 3 cm gauge distance was kept for mechanical loading. For the testing, 1 kN load cell at a crosshead speed of 1 mm s⁻¹ was used. Five samples were tested in each case and average value (mean ± SD) were reported as the results. Stress versus strain graphs were drawn from the obtained data.

2.5. In Vitro Cell Culture Studies

2.5.1. Cell Lines Used

Mouse 3T3 fibroblasts and immortalized human HaCat keratinocytes were obtained from ATCC (American Type Culture Collection, USA). Human Oral Epithelial Cells (HOEC)

was obtained from donors and immortalized as described in the earlier work.^[40]

2.5.2. Cell Adhesion on the Meshes

3T3 fibroblasts and HOEC were used to assess the morphology of cells grown over the meshes. 3T3 fibroblast cells (passage 37) were seeded on neat PCL and PCL-TNR meshes at 50000 cells per cm² and cultured with Dulbecco's Modified Eagles Media (DMEM, Gibco) supplemented with 10% FBS (Gibco) and 0.1% penicillin-streptomycin solution (Gibco) in 24 well plates.

Similarly, epithelial cells (HOEC, Passage 37) were seeded on the samples (1 × 1 cm size) at a density of 50000 cells per cm² and cultured in 24 well plates. Keratinocyte-SFM (Gibco) with bovine pituitary extract supplement (Gibco) and 1% Penicillin-Streptomycin-Neomycin solution (Gibco) was used for the culturing of HOEC.

After 24 h cell culture, the cell seeded meshes were stained with DAPI (Invitrogen) and Phalloidin (Invitrogen) as per the manufacturer's protocol. Images were taken with a Leica florescent microscope (Leica DMi8 S Platform).

2.5.3. MTT Cell Viability Assay

Cell viability on PCL and PCL-TNR meshes were tested by MTT (3-(4,5-dimethylthiazol-2-yl)-2,5-diphenyl tetrazolium bromide) assay as described in earlier study.^[2] 3T3 fibroblast cells (passage 38) and HaCat keratinocytes (passage 42) were seeded on neat PCL and PCL-TNR meshes at 10000 cells per cm² and cultured with Dulbecco's Modified Eagles Media (DMEM, Gibco) supplemented with 10% FBS (Gibco) and 0.1% penicillin-streptomycin solution (Gibco) in 24 well plates. The cells were allowed to grow for 24 h, 3 days, and 7 days followed by MTT assay. To calculate effect of developed meshes on cell viability, Equation (2) was used.

$$\text{Cell proliferation (\%)} = (\text{OD sample} / \text{OD control}) \times 100 \quad (2)$$

All the experiments were repeated three times and absorbance were measured in triplicates.

2.5.4. Live/Dead Assay

3T3 Fibroblasts and HaCat keratinocytes were seeded on pre-sterilized and pre-wetted meshes at a density of 10000 cells per well in a 24 well plates and cultured under appropriate conditions as described in previous sections. After 3 days of incubation, cell viability on PCL and nanocomposite meshes was assessed using the Live/Dead cell imaging kit (Invitrogen) according to manufacturer's instructions. Live and dead cells were imaged with a fluorescent microscope using FITC and rhodamine filters, respectively.

2.5.5. In Vitro Cell Migration Assay

For determining the effect of PCL-TNR meshes on keratinocyte migration, the in vitro wound contraction assay (scratch

assay) was performed using 3T3 and HaCaT cells as described in our earlier report.^[41] Briefly, cells were cultured in 24 well plates until subconfluence in appropriate media as described in previous sections. Pre-sterilized 1 × 1 cm² sized PCL and PCL-TNR samples were placed on the wounds created on cell culture plates. Control wells were also included. Photographs of wounds were taken soon after the wounding procedure and after 24 h of incubation using inverted microscope (Leica DMi1 Inverted Fluorescent Microscope). Experiments were performed in triplicates. Wound contraction was quantified from the images using Equation (3).

$$\text{Wound contraction(\%)} = (Wd^0 - Wd^t) / Wd^0 \times 100 \quad (3)$$

Whereas Wd^0 is the distance between wound boundaries immediately after wounding procedure and Wd^t is the distance between wound boundaries after time “ t ” of sample treatment.

2.6. Angiogenic Property by Chicken Chorioallantoic Membrane Assay (CAM)

Fertilized eggs were purchased from Arab Qatari for Poultry Production, Shamal road, Farm Street, Qatar and were placed in an egg incubator at 37 °C with 55% humidity. At the 4th day of egg incubation, a small window (1 cm²) was opened in eggshell, exposed the CAM and sterilized meshes (1 cm²) were placed on the CAM. The windows were sealed with transparent adhesive tape and returned to the incubator. After 24 h of treatment, the eggs were reopened, and the CAM were examined for the angiogenesis. Images of CAM were taken with a stereo microscope (Zeiss Stemi 508). Quantification of angiogenesis was performed using AngioQuant software. The results are expressed as mean ± SD of angiogenesis response obtained from four viable embryos for each group.

2.7. In Vivo Studies

2.7.1. Angiogenesis after Subcutaneous Implantation in Guinea Pigs

American satin guinea pigs weighing 200–300 g were selected from the inbred group of animals from the animal house of Pushpagiri Institute of Medical Sciences and Research Centre, Tiruvalla, Kerala, India. Animal experiments were performed with the prior permission from institutional animal ethics committee (No.602/PO/Re/S/2002/CPCSEA) and were conducted strictly adhering to the guidelines of CPCSEA constituted by the Ministry of Environment, Forests and Climate Change, Animal Welfare Division of Government of India in Pushpagiri Institute of Medical Sciences and Research Centre, Tiruvalla, Kerala, India. Animals were provided with standard environmental controlled conditions of 23 ± 5 °C, 12 h light–dark cycle, had free access to standard food and UV sterilized water. The animals were anesthetized by intraperitoneal injection of combination of ketamine hydrochloride (50 mg kg⁻¹) and xylazine (5 mg kg⁻¹).

After anaesthetizing the animals as described above, two surgical incisions approximately 2 cm in length were made on

the dorsal side of the guinea pigs. Each animal received any of the implantation from the following groups: i) PCL, ii) PCL-TNR-0.5%, iii) PCL-TNR-1%, iv) PCL-TNR-2%, and v) PCL-TNR-4%. The wounds were closed with polyamide sutures (Centlon, CNW 3320). After 1 week, the animals were anaesthetized as described before and the meshes were retrieved. Obtained samples were fixed (10% buffered formalin) and embedded in paraffin for histological analysis. The sections were stained with Hematoxylin and Eosin. Experiments were performed in triplicate.

2.7.2. Wound Healing Experiment

Male Sprague Dawley rats (180–260 g) were selected from the inbred animals for the wound healing experiment. The animal breed was obtained from Kerala Veterinary and Animal Sciences University, Mannuthy, India. All the surgical procedures were performed with the approval of institutional animal ethics committee (No.602/PO/Re/S/2002/CPCSEA) by strictly adhering to the guidelines of CPCSEA constituted by the Ministry of Environment, Forests and Climate Change, Animal Welfare Division of Government of India in Pushpagiri Institute of Medical Sciences and Research Centre, Tiruvalla, Kerala, India.

After anaesthetizing the animals as described in previous section, dorsal region of the rats was shaved, wiped with alcohol and two 1.5 × 1.5 cm full thickness skin excision wounds were created. The scaffolds with 1.5 × 1.5 cm dimensions were sutured on the wound. In order to minimize the number of animals, only neat PCL and PCL-TNF-1% meshes were used for the implantation. Decision for the selection of PCL-TNR-1% was made based on the results of in vitro cell culture studies, CAM angiogenesis assay, and in vivo implantation study. The photographs were taken every other day until the 4th week of experiment. The percentage of wound healing was calculated using Equation (4)

$$W\% = [WA^0 - WA^t] / WA^0 \times 100 \quad (4)$$

where $W\%$ is the percentage of wound healing, WA^0 is the area of wound at first day, and WA^t is the area of wound after different days of treatment. Experiments were performed in triplicate.

2.8. Statistical Analysis

The statistical analysis was performed using the un-paired Student's t -test and “One-way ANOVA” were performed using GraphPad Prism. $p < 0.05$ was considered as statistically significantly different than the control groups.

3. Results and Discussions

3.1. Morphological and Physical Properties of TNR

TEM images of the obtained TNR are given in **Figure 1A,B**. In general, the synthesized TNR were in fiber like morphology

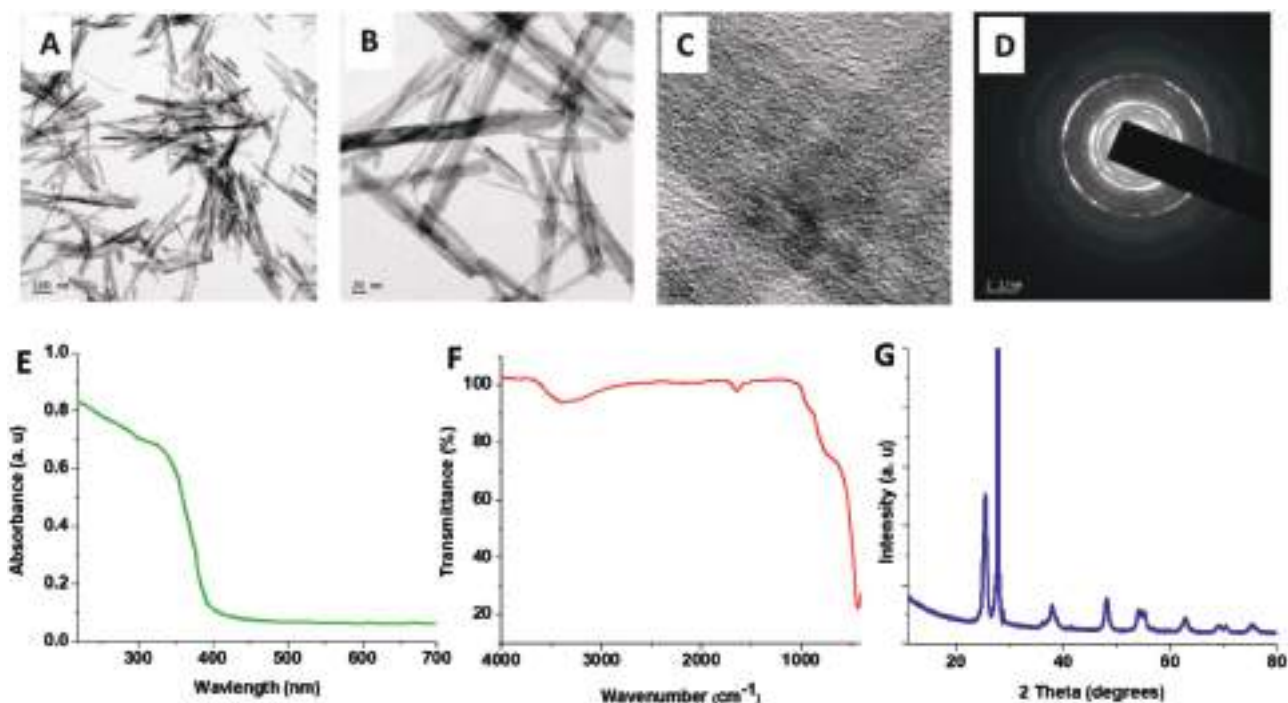


Figure 1. Results of the characterization of TNR for the morphological and physicochemical properties. A,B) TEM images showing the size and morphology of synthesised TNR at two different magnifications. C) HR-TEM image of TNR. D) SAED pattern of TNR. E) UV-Vis spectrum showing the characteristic absorption maximum between 200 and 400 nm. F) FTIR spectrum showing the presence vibrational bands corresponding to the TiO_2 . G) XRD pattern of TNR showing the characteristic diffraction patterns of TiO_2 .

without forming any clusters or agglomerates. TEM images show that the nanorods were of highly elongated morphology and had an average diameter of 26 ± 4 nm. Higher magnification image clearly indicated that each tube was formed by the parallel arrangement of several small nanofibers with average diameter of 2.5 ± 1.5 nm (Figure 1B). HR-TEM image shows each such small fibers further composed of several parallel arranged monocrystalline fiber crystallites (Figure 1C). This lattice-resolved image indicates the anatase phase of TiO_2 with the lattice spacing of 0.35 nm corresponding to the prominent (101) plane. SAED image shows the characteristic diffraction pattern of TiO_2 nanoparticles (Figure 1D). The observed ring patterns confirm that the fibers consisted of nanocrystals. Diffraction pattern of TNR shows the reflections from both the anatase (101) and rutile (101) phases. However, it reveals that the TNR was predominantly composed of single crystalline anatase phase.^[42]

The UV-Vis reflection spectra given in Figure 1E clearly shows the optical properties of the synthesized TNR. The characteristic absorption maxima of TiO_2 nanomaterials can be observed between 200 and 500 nm.^[43] FTIR spectrum of TNR is presented in Figure 1F. The spectrum of the obtained sample shows a broad peak at 3400 cm^{-1} correspond to the stretching vibration of hydroxyl groups from the surface-absorbed water.^[44] The absorption at 1638 cm^{-1} might be related to the bending vibration of hydroxyl groups from the hydrate formed in the presence of water.^[45] Peak from 800 to 400 cm^{-1} with a maxima at 523.88 cm^{-1} show the stretching vibration of $\text{Ti}-\text{O}$.^[45] XRD was used to characterize the synthesized TNR (Figure 1G). XRD pattern of TNR after calcinations at 500°C

for 6 h shows prominent diffraction peaks positioned at $2\theta = 25.5^\circ, 38.0^\circ, 48.2^\circ, 54.5^\circ, 55.3^\circ, 63.06^\circ, 69.2^\circ, 70.4^\circ,$ and 75.2° that are assigned to (101), (104), (200), (105), (211), (204), (116), (220), and (215) planes of anatase phase, respectively.^[46] Other peaks positioned at $2\theta = 27.58^\circ$ and 41.2° are assigned to (110) and (111) planes of rutile phase, respectively.^[47] The broadening of the diffraction peaks was due to the very small size of the TiO_2 nanocrystals in TNR. From the XRD patterns, it can be observed that the TNR are mostly in anatase phase with a negligible quantity of rutile phase.^[48]

3.2. Morphological and Physical Properties of PCL-TNR Nanocomposite Meshes

SEM micrographs are provided in Figure 2A which shows that the fabricated PCL and PCL-TNR nanocomposite meshes were composed of submicron/micro fibers with various diameters. Average diameter of the fibers was calculated from SEM images and the frequency distribution graphs are given in Figure 2B. Higher magnification SEM images of PCL and PCL-TNR meshes are given in Figure S1, Supporting Information. Observed slight variation in fiber morphology and diameter might be due to the variation in electrospinning solution parameters such as conductivity and viscosity (Table S1, Supporting Information). Both PCL and PCL-TNR nanocomposite meshes were highly porous with more than 84% average porosity (Table S2, Supporting Information).

EDS analysis was used to determine the presence of TNR in the fabricated meshes (Figure 2C). EDS spectra of pure

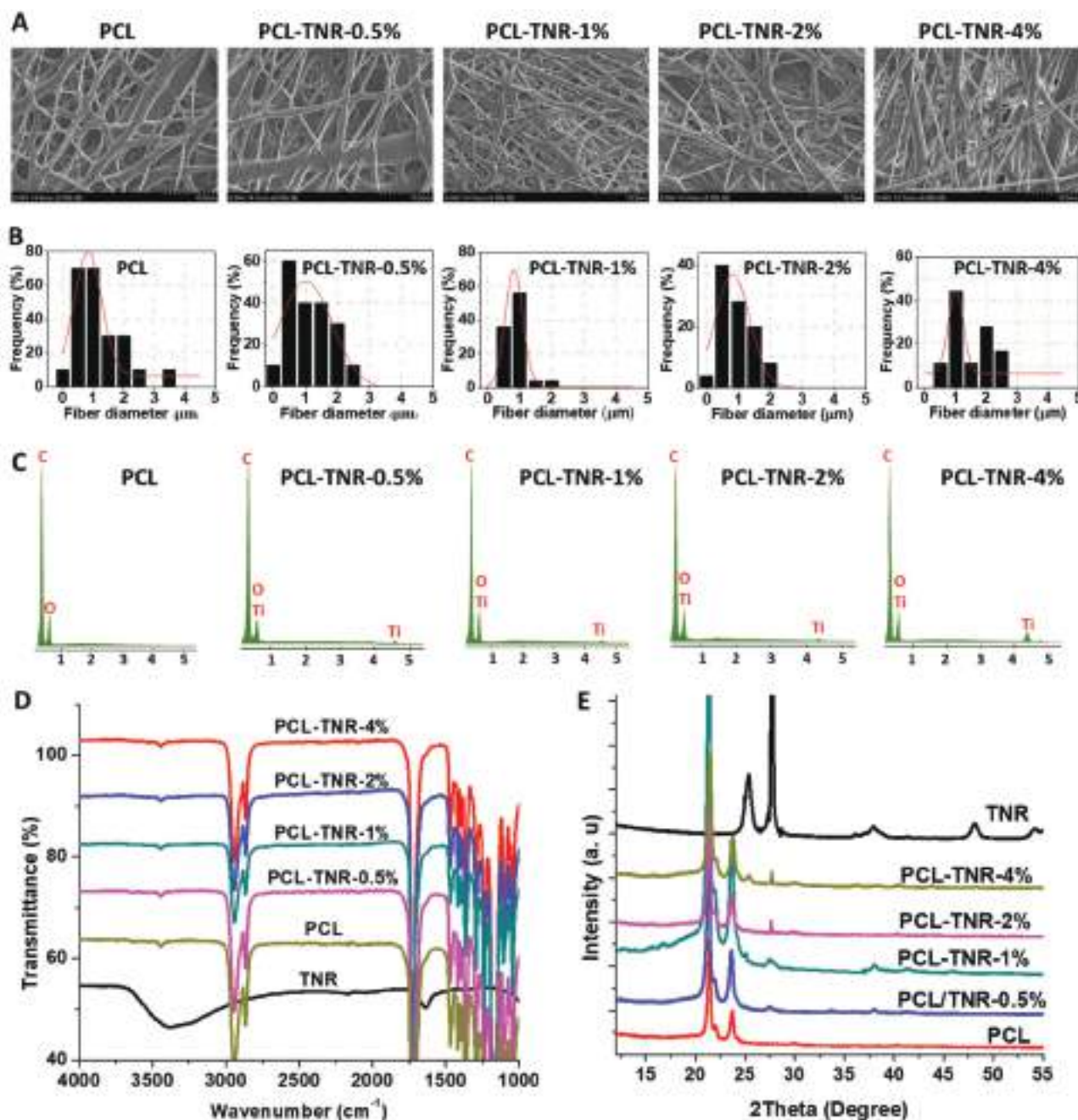


Figure 2. A) Morphology of fabricated PCL and PCL-TNR meshes by SEM analysis showing the formation of random fibers. B) EDS spectra of fabricated meshes showing the presence of Ti element in the nanocomposite meshes. C) FTIR spectra of PCL and PCL-TNR nanocomposite meshes. D) XRD analysis of the samples confirming the presence of TNR in PCL fibers.

PCL shows the elements of carbon and oxygen with sharp and low energy peaks. Appearance of a new peak at 4.508 ($K\alpha$) which indicate the presence of TNR in PCL fibers. The characteristic X-ray energy emitted from TNR are generally observed at 4.508 ($K\alpha$) and 0.452 ($L\alpha$) keV from elemental Ti, and at 0.525 ($K\alpha$) keV from oxygen.^[49] Peaks at 0.452 and 0.525 were very close to each other and was practically difficult to distinguish each other from the spectra of nanocomposite meshes.

The FTIR spectra of pure PCL mesh and PCL/TNR nanocomposite meshes are shown in Figure 2D. The characteristic absorption bands at 2868 and 2941 cm^{-1} are related to C–H stretching vibration of saturated hydrocarbons of PCL.^[50] The intense band at 1721 cm^{-1} corresponds to the stretching vibration of ester carbonyl groups (C=O) of PCL.^[51] The characteristic absorption bands at 1240 cm^{-1} correspond to the C–O–C stretching vibration.^[52] PCL-TNR meshes also showed relatively the same characteristic bands as observed in PCL polymer.

Table 1. Melting point (T_m), crystallization temperature (T_c), melting enthalpy (ΔH_m), and crystallization enthalpy (ΔH_c) of PCL and PCL-TNR meshes.

	T_m [°C]	T_c [°C]	ΔH_m [J g ⁻¹]	ΔH_c [J g ⁻¹]	$X_c\%$ (DSC)	$X_c\%$ (XRD)
PCL	56.6	30.5	77.4	64.3	55.4	33.3
PCL-TNR-0.5%	57.0	30.2	81.7	73.6	58.5	43.5
PCL-TNR-1%	56.4	30.8	78.5	67.2	56.2	43.9
PCL-TNR-2%	57.3	28.5	78.8	65.8	56.2	36.2
PCL-TNR-4%	56.0	29.2	77.8	62.4	55.7	37.5

There was no detectable shift in the peak correspond to the carbonyl groups of PCL which suggest the lack of direct interaction between TNR particles and PCL polymer.^[35]

In the XRD pattern of TNR (Figure 2E), the diffraction peaks were observed at $2\theta = 25.5^\circ, 27.58^\circ, 38.0^\circ, 41.2^\circ, 48.2^\circ, 54.5^\circ, 55.3^\circ, 63.06^\circ, 69.2^\circ, 70.4^\circ,$ and 75.2° corresponding to (101), (110), (104), (111), (200), (105), (211), (204), (116), (220), and (215) planes, respectively.^[53] In the neat PCL spectra, there were two main strong peaks which were observed at 21.4° (110) and 23.75° (200), respectively, showing the crystalline features of the PCL.^[54] TNR loaded PCL meshes were also showed the same peaks corresponding to those observed in neat PCL. XRD analysis confirmed the presence of TNR in PCL fibers, which was evident from the presence of the corresponding diffraction peaks of the TNR in nanocomposite meshes. However, for PCL-TNR-0.5% meshes, many of the diffraction patterns of TNF were very weak to identify from the background diffraction of PCL. Low loading of TNR (0.5 and 1% w/w) in PCL increased the degree of crystallinity of PCL polymer whereas the higher amount of TNR (2 and 4% w/w) decreased the degree of crystallinity of the polymer (Table 1). Several nanostructures can promote polymer crystallization by acting as nucleating agents at an optimal loading.^[55] Observed decreases in degree of crystallinity at higher concentration of TNR might be due to the poor dispersion and subsequent agglomeration of TNR in PCL,

which disturb the crystallization process. Decrease in overall crystallinity of polymers affects the tensile strength, and the results of tensile results agree with this.^[56] Earlier studies also showed that crystallinity of PCL decreases with the addition of higher quantity (above 2% w/w) of nanoparticles such as ZnO in polymer matrix which can be due to the agglomeration of nanoparticles at higher concentration.^[38]

In order to further understand the variation in thermodynamic properties and crystallinity of PCL upon the addition of TNR, DSC analysis was performed. Figure 3A,B shows the DSC thermograms during melting and crystallization of PCL and TNR incorporated PCL meshes. The melting and crystallization temperature of samples with different TNR content were apparently the same (Table 1). The melting temperatures ranged from 56.3 to 57.3 °C and crystallization temperatures ranged from 28.8 to 30.5 °C. The neat PCL meshes showed a T_c of 30.5 °C. Meshes with lower quantity of TNR (PCL-TNR-0.5% and PCL-TNR-1%) did not influence the T_c of the PCL. However, higher quantity (above 1%) of TNR decreased the T_c of the polymer. The neat PCL meshes showed a ΔH_c of 64.3 J g⁻¹ while PCL-TNR-0.5% showed a ΔH_c of 73.6 J g⁻¹, indicating a considerable increase in the enthalpy of crystallization. PCL-TNR-1% showed a ΔH_c of 67.2. The addition of 0.5% to 1% w/w TNR promoted the crystallization by considerably increasing the crystallization enthalpy. However, PCL-TNR-4% possessed a ΔH_c of 62.4 J g⁻¹ pointing a decrease in the enthalpy value of crystallization compared to bare PCL. The addition of 4% w/w TNR hindered the crystallization process by drastically lowering the related enthalpy of crystallization. At higher TNR loading, the PCL chains are strongly adsorbed on the grain surfaces of TNR agglomerates which resulted in the decrease of crystallization enthalpy.^[57] DSC results show that the crystallinity of PCL in PCL-TNR nanocomposites was higher

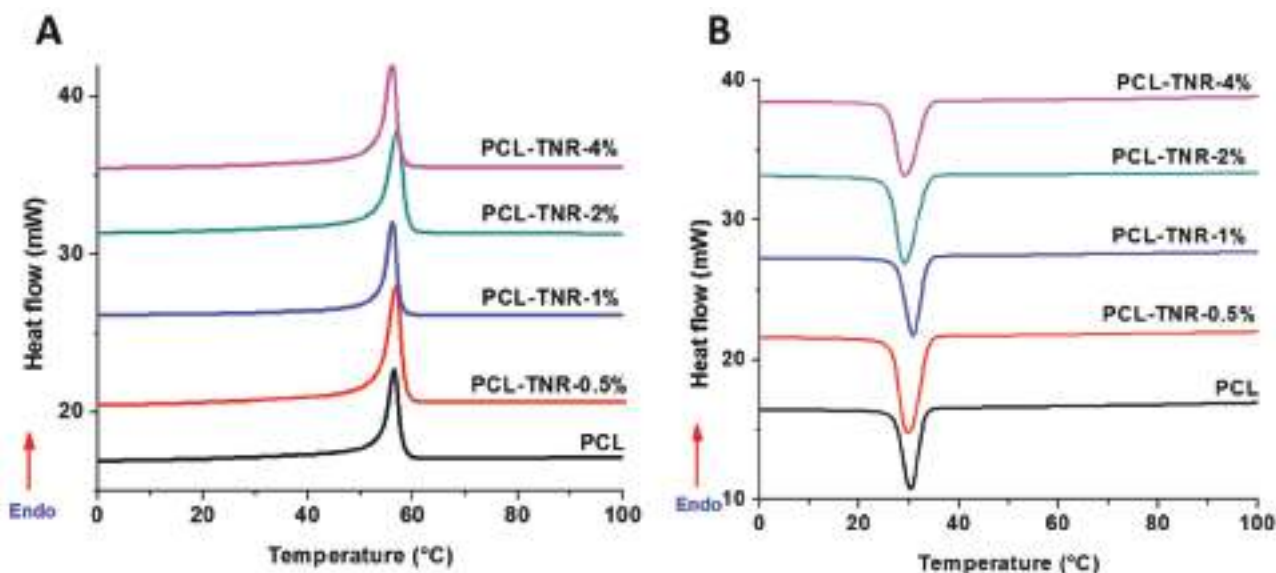


Figure 3. DSC thermograms of A) melting and B) crystallization ramps of neat PCL and PCL-TNR nanocomposite meshes.

than that of neat PCL upto 2% w/w TNR loadings. Loading of higher quantity of TNR resulted in a slight decrease in the ΔH_m compared to PCL-TNR-0.5%, which could be due to the restriction of the PCL crystallization kinetics. The most probable reason might be the multiple interactions formed between the polymer chains and the agglomerated fillers resulted in the restriction of segmental mobility that hindered polymer crystallization.^[58] Degree of crystallinity calculated from XRD also showed a similar trend. Observed difference in absolute values of crystallinity calculated from DSC and XRD might be due to the possible inaccuracy of peak integration or baseline corrections during XRD data analysis. Lincoln et al. also reported that low mobility of polymer chains through nanofillers such as silicate layers can produce significant effect on the crystallization process.^[59]

3.3. Mechanical Properties

A standard wound coverage material should have enough and comparable tensile strength, flexibility, and elasticity to that of the skin. Representative stress–strain curves of PCL and PCL-TNR meshes are shown in Figure 4A. As evident from the stress–strain curves, by incorporating a small amount of TNR, overall tensile properties of the meshes were increased. Detailed information like tensile strength, elongation at break, and modulus are given in Figure 4B–D. PCL meshes possessed a tensile strength of 1.64 ± 0.26 MPa (Figure 4B). The tensile properties of PCL-TNR-0.5% was relatively like bare PCL meshes (1.65 ± 0.13 MPa). However, PCL-TNR-1% possessed a higher tensile strength (1.98 ± 0.18 MPa) than neat PCL meshes ($p < 0.05$). PCL-TNR-2% showed a slight

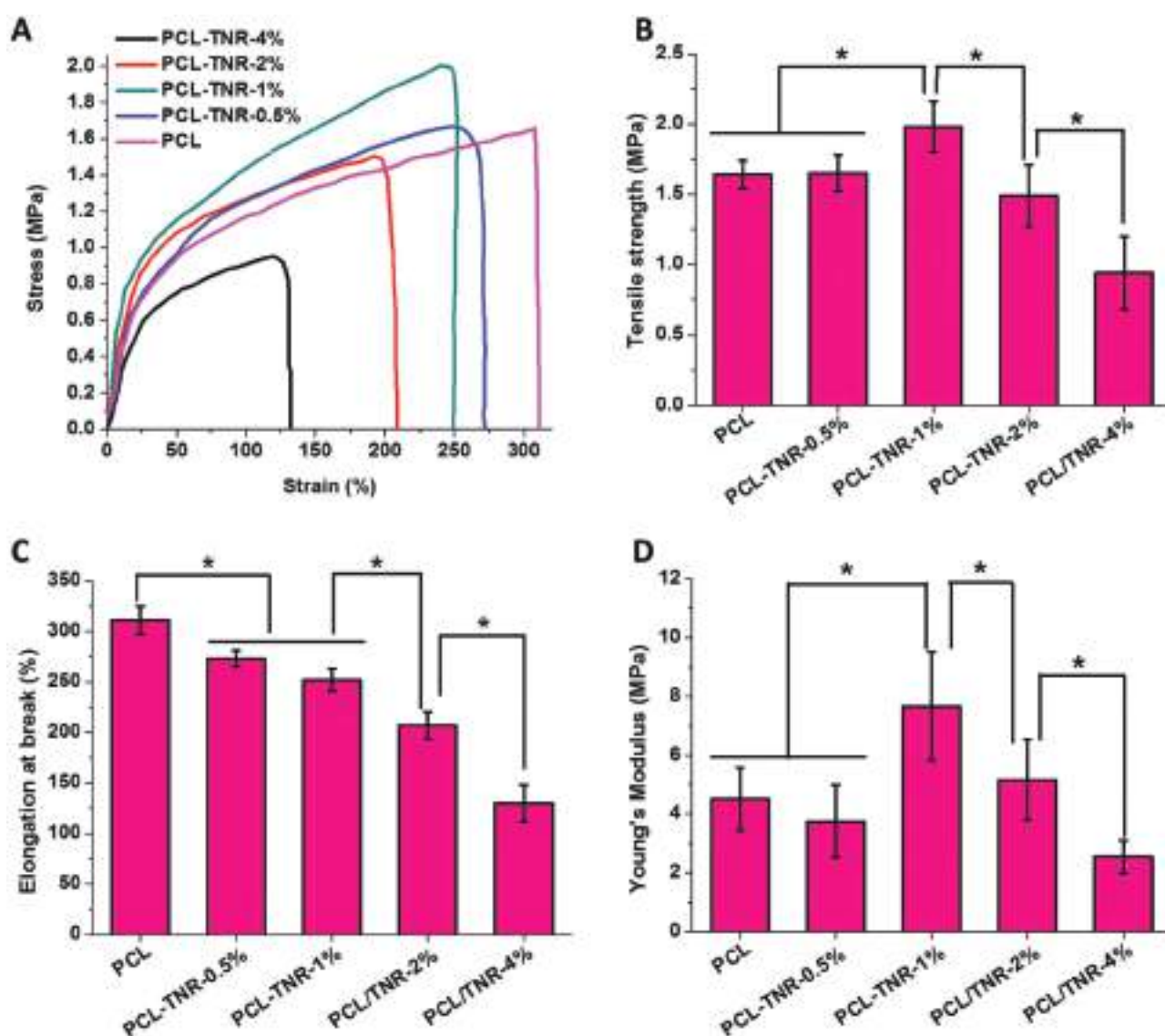


Figure 4. Stress–strain curve showing the effect of TNR on the tensile properties of PCL-TNR meshes. A) Stress–strain curves of bare PCL and PCL-TNR nanocomposite meshes. Graphs showing B) the variation of tensile strength, C) elongation at break, and D) Young's modulus upon the incorporation of TNR.

reduction in tensile strength (1.49 ± 0.22 MPa). However, in the case of PCL-TNR-4%, a considerable decrease of tensile strength was observed (0.94 ± 0.26 MPa). Elongation at break gives an idea about the elasticity of the meshes (Figure 4C). Elongation at break of PCL was $311 \pm 14\%$. We observed a slightly lesser elongation at break for PCL-TNR-0.5% and PCL-TNR-1% meshes ($273 \pm 8\%$). As expected, elongation at break was further decreased in the case of PCL-TNR-2% meshes ($252 \pm 11\%$ and $207 \pm 13\%$, respectively). A large reduction in elongation at break was observed for PCL-TNR-4% meshes. Young's modulus was significantly higher for PCL-TNR-1% (6.67 ± 1.84 MPa) and PCL-TNR-2% (5.16 ± 1.37 MPa) meshes compared to the neat PCL meshes (4.51 ± 1.08 MPa) ($p > 0.05$; Figure 4D).

Tensile strength was high for PCL-TNR nanocomposites upto 1% TNR content of the PCL matrix which is in good agreement with the data presented in earlier reports in the case of electrospun PCL/zinc oxide nanocomposite membranes.^[51] Further increase in TNR loading resulted in the reduction of tensile strength due to the agglomeration of the TNR nanofillers in PCL matrix which might have weekend the polymer–filler interaction and prevented stress transfer between the polymer and the filler.^[60] At the low loading of TNR, polymer matrix could effortlessly transfer the stress to the TNR filler, which increased the tensile strength of the meshes.^[61] Thus, at a lower loading, TNR could disperse uniformly in PCL matrix and resulted in the increase in the interfacial area for stress transfer from the PCL matrix to the TNR and provided good mechanical properties.^[62] Such a higher interaction between the polymer matrix and nanoparticles could be the reason for the enhanced mechanical properties of PCL-TNR nanocomposite meshes. A similar mechanism applies to the elasticity of the meshes. A low concentration of nanofiller does not significantly affect the elongation at break. However, above 2% TNR content resulted in the significant reduction in elongation at break. Agglomerates of TNR formed at higher loadings might have created stress concentration centers during mechanical stretching and behaved as break points.^[63] In general, higher interfacial adhesion between the polymer matrix and filler facilitates efficient load sharing and improvement in the overall mechanical properties of polymer nanocomposites.^[64] Tensile test results of the samples correlate well with the crystallinity results, which showed that the crystallinity decreased at high percentage of TNR due to the agglomeration of them (nanofillers). Ghosal et al. reported the fabrication of PCL-TiO₂ nanocomposite scaffolds and observed that TiO₂ incorporation improved their tensile strength.^[36]

3.4. Cell Adhesion and Proliferation of PCL-TNF Meshes

DAPI and Phalloidin stained images of cells which were cultured for 24 h on PCL and PCL-TNR meshes is given in Figure 5A. On bare PCL meshes and PCL-TNR-0.5%, only a few cells (both 3T3 and HOEC) were observed. In the case of PCL-TNR-1% and PCL-TNR-2%, relatively higher number of cells were observed. Further, the absence of considerable number of dead-floating cells in the culture plates indicate the lack of cell death due to necrosis.^[65]

In order to visualize viable cells on PCL and PCL-TNR nanocomposite meshes, live/dead assay was performed, and the results are given in Figure 5B. Both the controls and bare PCL meshes treated cells showed relatively similar number of live (green) and dead cells (red). Almost all the 3T3 cells which were cultured with the meshes were viable irrespective of TNR content. In contrary, PCL and PCL-TNR meshes treated HaCat cells showed a greater number of dead cells compared to 3T3 cells. However, most cells were green, indicating the highest set of viability and cell proliferation. However, we did not observe considerable variation in relative ratio of live and dead cells, which indicate the nontoxicity of all the tested meshes irrespective of TNR content.

To validate the cytocompatibility of PCL-TNR meshes, cell viability studies were performed at 1st, 3rd, and 7th day using 3T3 fibroblast and HaCat cell lines by MTT assay (Figures 5C and 6D). 3T3 fibroblast cells seeded on all the bare PCL meshes showed more than 85–89% of cell viability compared to the controls throughout the study period (Figure 5C). A similar trend was observed in the case of PCL-TNR-0.5%. Very interestingly, 3T3 cells seeded on PCL-TNR-1% mesh possessed higher cell viability (113–118%) compared to bare PCL meshes and other studied nanocomposite meshes ($p \leq 0.05$). Cells cultured with PCL-TNR-2% meshes showed relatively similar viability (108–117%) as observed for PCL-TNR-1% meshes. There was no significant difference in viability between cells seeded with PCL-TNR-1% and PCL-TNR-2% meshes. In contrast, 3T3 cells cultured with PCL-TNR-4% meshes showed considerably less cell viability than those cultured with PCL-TNR-1% and PCL-TNR-2% meshes ($p \leq 0.05$). However, there was no significant reduction in cell viability compared to the control, bare PCL or PCL-TNR-0.5%. In contrast to the viability results of 3T3 cells, HaCat cells grown in the presence of PCL, PCL-TNR-0.5%, PCL-TNR-1%, and PCL-TNR-2% meshes did not show significant difference from control plates throughout the study period (Figure 5D). PCL-TNR-0.5% samples were also showed a similar trend. The viability of cells cultured with bare PCL meshes (88.4 ± 3.5), PCL-TNR-0.5% (98.9 ± 3.7), and PCL-TNR-1% (92.2 ± 3) nanocomposites were comparable. However, PCL-TNR-4% exhibited the lowest viability compared to all other samples ($p \leq 0.05$) examined in this study. The reduction in cell viability which was observed in the case of PCL-TNR-4% samples might be associated with the release of TNR at a relatively higher rate which might have affected the cell viability by affecting the mitochondrial function.^[66]

3.5. In Vitro Cell Migration Potential of PCL-TNR Meshes

Results obtained from in vitro cell migration assay are shown in Figure 6A–C. After incubation period of 20 h, about $52.4 \pm 0.5\%$ of wounded area was healed in the control well due to the migration and proliferation of 3T3 cells into the scratched area (Figure 6A,B). A relatively similar healing was observed for bare PCL and PCL-TNR-0.5% meshes treated 3T3 cells. Interestingly, a statistically significant ($p \leq 0.05$) improvement in wound closure was observed on PCL-TNR-1% (78.1 ± 0.4) and PCL-TNR-2% (77.7 ± 0.5) treated cells compared to the control, PCL, and PCL-TNR-0.5%. However,

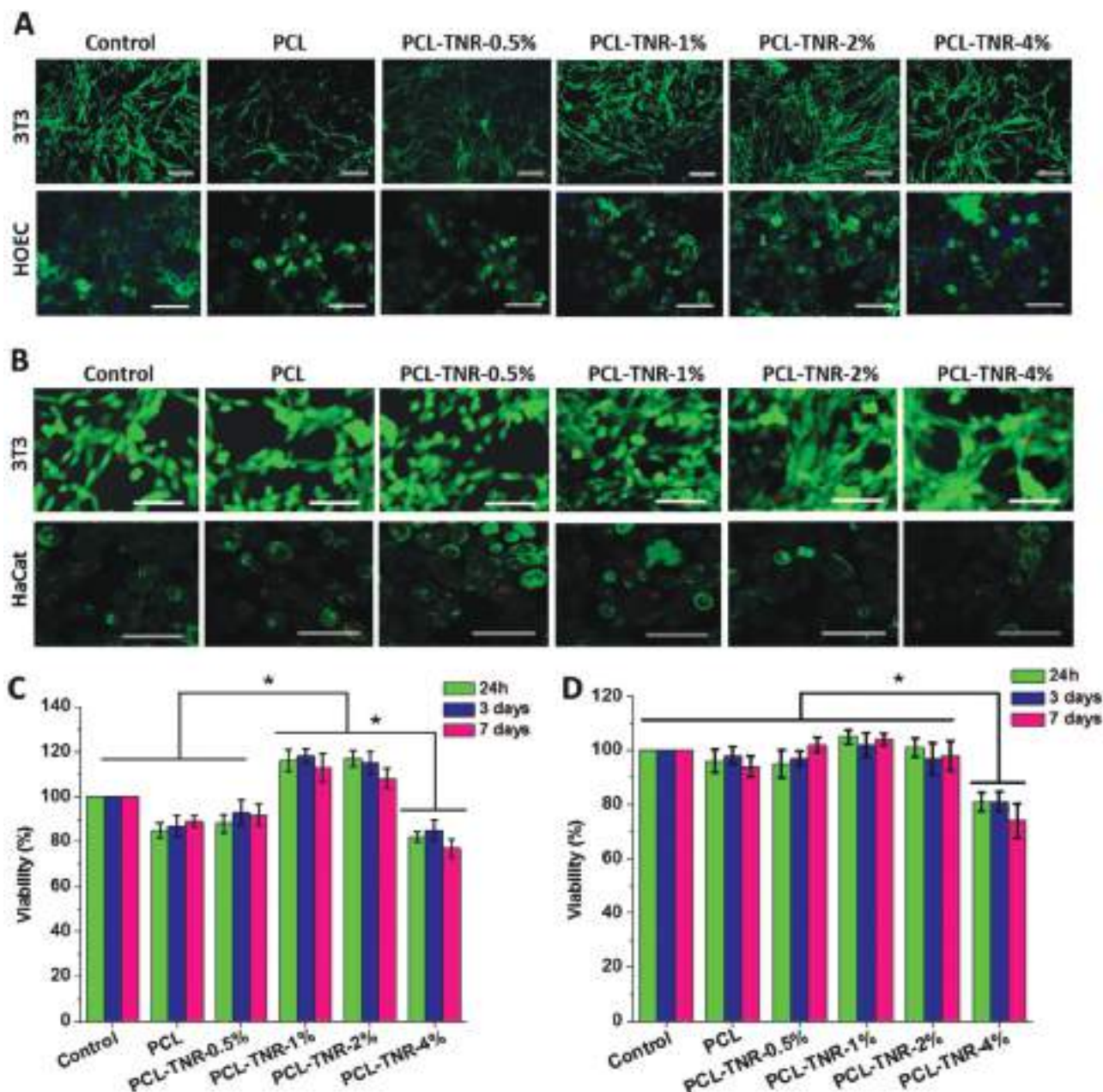


Figure 5. A) Morphology of 3T3 and human oral epithelial cells (HOEC) grown on control cell culture plate, neat PCL meshes, and nanocomposite meshes by DAPI and phalloidin staining. B) Viability of 3T3 fibroblast cells cultured on PCL and PCL-TNR meshes by live/dead assay after 3 days of cell culture. C) Viability of 3T3 fibroblast and D) HaCat cells in the presence of PCL and various PCL-TNR nanocomposite meshes showing the good biocompatibility of the developed meshes.

PCL-TNR-1% and PCL-TNR-2% did not show any significant difference between themselves in wound contraction. In contrast, PCL-TNR-4% meshes slightly retarded the scratch healing compared to the other PCL-TNR groups. Wound healing assay using HaCat keratinocytes also showed a relatively similar trend (Figure 6A,C). After the incubation period of 20 h, about $27.3 \pm 0.3\%$ of wounded area was healed in the control and PCL treated wells due to the migration and proliferation of HaCat cells into the wounded area (Figure 6C). Higher wound healing was observed for PCL-TNR-0.5% meshes treated HaCat cells

($p \leq 0.05$) compared to bare PCL and control groups. Interestingly, a higher wound closure was observed when the scratched areas were treated with PCL-TNR-1% (46.3 ± 0.1), PCL-TNR-2% (44.6 ± 0.4), and PCL-TNR-4% (43.9 ± 0.3) meshes compared to the control, PCL, and PCL-TNR-0.5% ($p \leq 0.05$).

In nutshell, it has been observed that TNR containing PCL meshes promoted the cell migration and wound healing upto 2% w/w in PCL meshes, however, at higher concentration (4% w/w), it inhibited wound healing. Other studies have shown that TiO_2 nanomaterials are able to induce the expression of

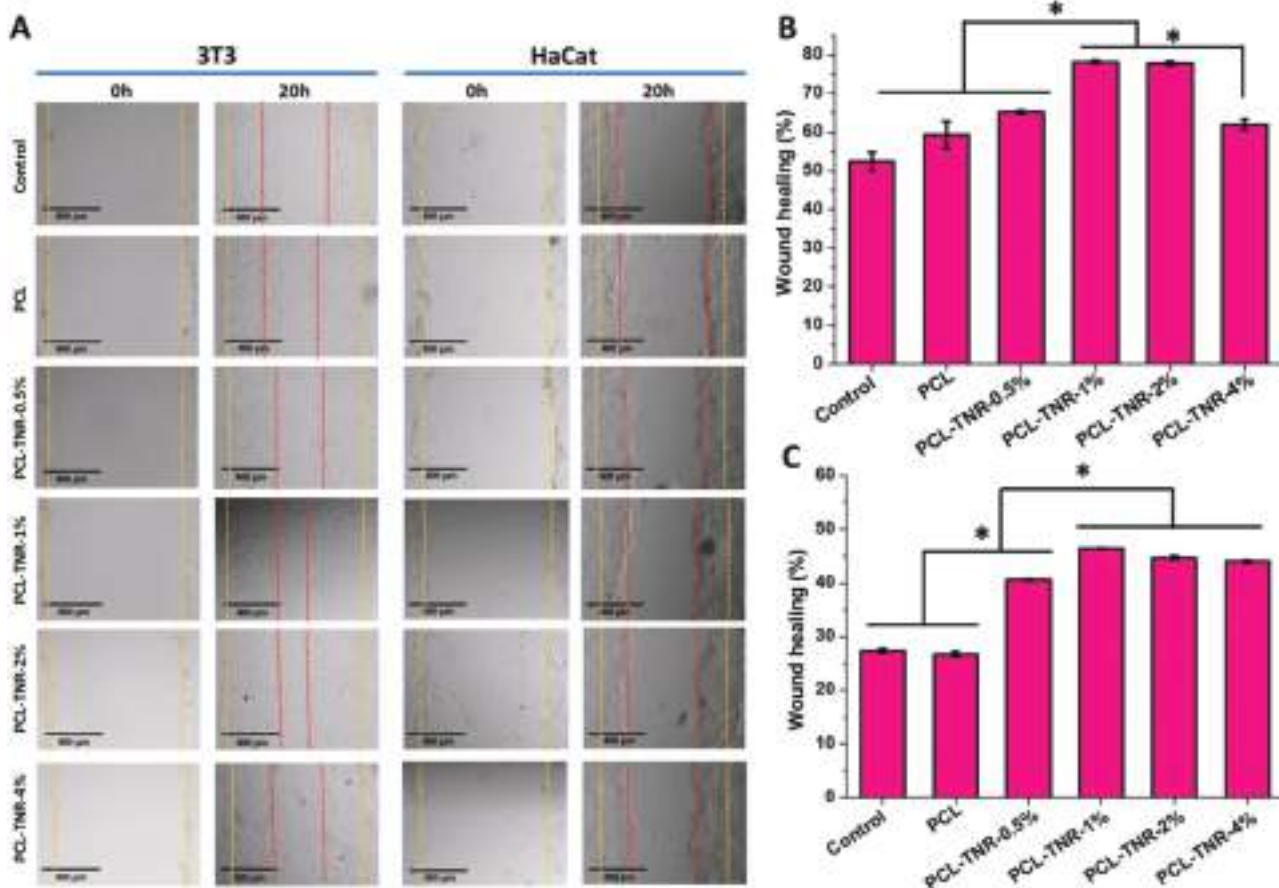


Figure 6. Evaluation of in vitro wound healing performance using 3T3 fibroblast and HaCat keratinocyte cells showing the variation in in vitro cell migration upon treatment with TNR containing PCL meshes. A) Microscopic images showing the scratched area at the beginning of experiment (0 h) and after 20 h of treatment. Percentage of scratch contraction calculated from the distance between cell boundaries before the treatment with the samples and after 20 h of treatment on B) 3T3 and C) HaCat cells.

cytokines such as tumor necrosis factor-alpha (TNF- α),^[67] interleukins,^[68] and this may stimulate cell migration. In addition to TNF and various interleukins, TiO₂ showed a statistically significant increase in the levels of transforming growth factor- β (TGF- β).^[69] Apart from the possible adverse effects expected from the over expression of these cytokines and growth factors, their expression at an optimum level can contribute in cell migration and proliferation.^[70] This could be the reason for the observed higher cell migration in the culture plates treated with 1–2% TNR loaded PCL samples. However, at higher concentrations of TNR, the released TNR can be internalized by the cells and result in the inhibition of cell migration through the inhibitory effect of TGF- β at higher concentration.^[71]

3.6. Chicken Chorioallantoic Membrane (CAM) Angiogenesis Assay

Figure 7 shows the appearance of network of blood vessels growing around the PCL and PCL-TNR meshes. It is evident from **Figure 7A** that PCL-TNR-1% and PCL-TNR-2% meshes have the higher ability to promote angiogenesis compared to other samples. Similarly, PCL-TNR-1% exhibited more

angiogenesis by showing increased number of blood vessels around the membrane. Fold increase in number of blood vessel junction points was significantly higher for PCL-TNR-1% and PCL-TNR-2% meshes (**Figure 7B**). In addition, significantly higher blood vessel diameter was also observed for PCL-TNR-1% and PCL-TNR-2% meshes compared to the control (**Figure 7C**). Fabrication protocol of PCL and PCL-TNR was same except for TNR loading; therefore, it was assumed that the angiogenic property of the meshes was due to the difference in the amount of TNR.

3.7. In Vivo Studies

3.7.1. Angiogenesis after Subcutaneous Implantation in Guinea Pigs

To investigate angiogenesis and cell proliferation in vivo, guinea pig subcutaneous implantation model was used. Implantation of PCL-TNR meshes resulted in significantly higher number of blood capillaries compared to bare PCL meshes from as early as 7 days after implantation (**Figure 8A**). Superior angiogenic response compared to the bare PCL samples was observed in

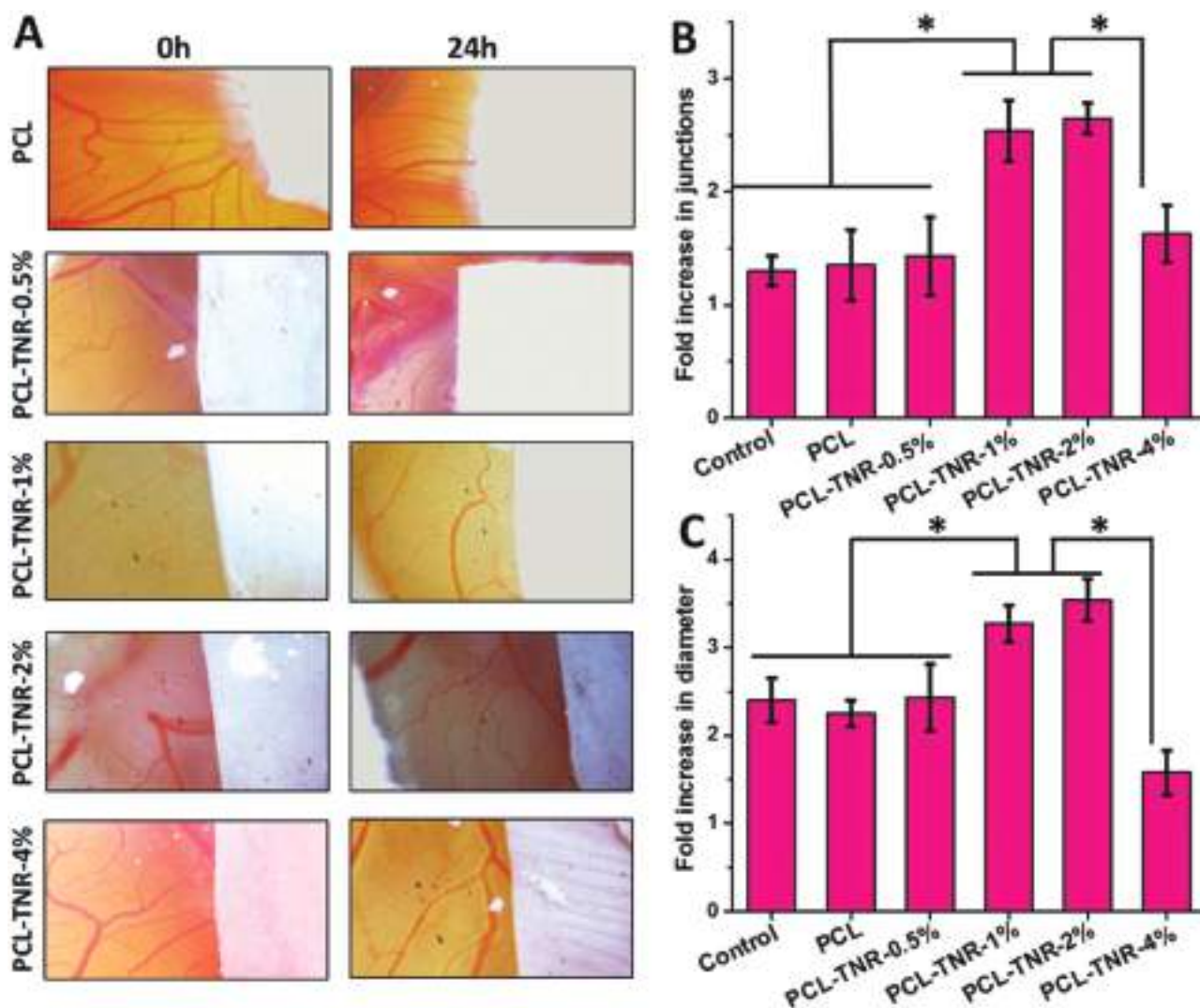


Figure 7. Results of CAM assay showing the formation of blood vessels in the presence of developed meshes. A) Photographs showing the CAM with developed blood vessels. B) Fold increase of blood-vessel junctions and C) diameter of blood vessels were measured using ImageJ software and expressed as mean \pm SD.

the case of PCL-TNR-1% and PCL-TNR-2% meshes. They also showed higher angiogenic response compared to other groups (PCL-TNR-0.5% and PCL-TNR-4%). This *in vivo* data is comparable with the results of the CAM assay (Figure 7). In support to our data, earlier study showed that simultaneous application of ultrasound and TiO₂ nanoparticles promoted neovascularization in mice models.^[72] The most plausible reason for the enhanced wound healing could be due to the ability of TiO₂ nanoparticles to generate ROS in biological system.^[73] As evident from the previous reports, ROS generated^[74] by TNR might have played a major role in angiogenesis; however, its underlying mechanisms remain not well understood. Studies using other metal oxide nanoparticles such as zinc oxide^[75,76] and europium hydroxide^[77] support our present findings. In addition, we performed C-reactive protein (CRP) assay to determine systemic inflammatory response if any caused by implanted meshes. We did not observe any sign of systemic

inflammation irrespective of TNR content in PCL meshes (Figure S2, Supporting Information).

3.7.2. Healing of Full Thickness Excision Wounds in Rats

Generally, a higher rate of wound contraction was observed in PCL-TNR mesh treated wounds as compared to bare PCL treated wounds (Figure 8B,C). However, there was no significant difference in wound contraction between these two treatment groups upto 14 days of the study. For PCL and PCL-TNR groups the contracted wound area was $13.3 \pm 3.2\%$ and $12.5 \pm 4.7\%$, respectively. This trend continued until 14th day of the study. However, on 16th day, PCL-TNR sample implanted wounds showed an effective reduction in the wound size compared to bare PCL implanted wounds. The percentage of wound contraction of the PCL and PCL-TNR implanted wounds were

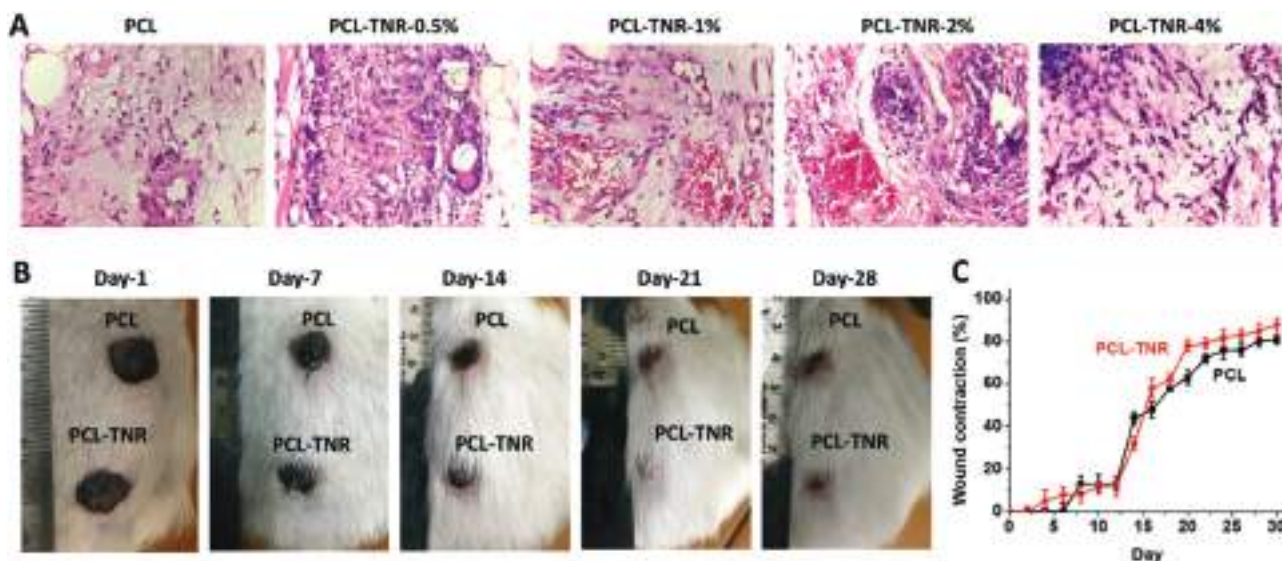


Figure 8. In vivo assessment of PCL-TNR meshes. A) Histology analysis of meshes after in vivo implantation for 7 days showing the formation of blood vessels through implanted meshes. B) Contraction of excision wounds during 4-week study period. C) Percentage of wound contraction during 4-week study period.

48.6 ± 3.9% and 58.4 ± 4.7%, respectively. Difference in the wound healing between blank PCL and PCL-TNR mesh treatment was evident until the end of the study. An increase in epidermal and dermal thickness when compared to bare PCL was observed on PCL-TNR treated healed wounds (Figure S3, Supporting Information). Our results suggest that the application of PCL-TNR meshes shows better healing when compared to bare PCL as the epidermal and dermal thickness might be due to the higher viability and/or proliferation of cells.^[78] Different cell types observed on the healed skin was determined based on a scoring system (Table S3, Supporting Information). Quantification of various cell types indicates that bare PCL implanted wound tissue showed a low tissue response whereas PCL-TNR implanted wounds showed a moderate tissue response (Table S4, Supporting Information).

Overall results clearly demonstrated that TNR provided its beneficial effect on wound healing. TNR packed inside the PCL polymer chains might have facilitated the controlled delivery of ROS to the wound and positively contributed to wound healing. In normal wound healing, ROS could accelerate wound healing by attracting adjacent cells from the wound boundaries toward the center of wound and facilitate faster contraction.^[79] They act as secondary messengers to several cells, which are involved in the repair process, and appear to be important in coordinating the effective tissue repair.^[79] On the other hand, higher amount of ROS lead to the arrest of the cell cycle progression and apoptosis.^[80] Some reports also suggest that titanium dioxide nanomaterials can cause endothelial cell leakiness,^[81] induce oxidative stress and DNA-adduct formation.^[82] Thus, a tight regulation of ROS is crucial for providing their beneficial effects in cell proliferation and wound healing. This can be achieved by entrapping TNR in PCL matrix and facilitating the slow release with the degradation of PCL matrix. Detailed studies are required to find out the rate of release of TNR, extent of generation of ROS and

subsequent activation of key signaling molecules which will be beyond the scope of this specific study. However, owing to the higher angiogenic and wound healing potential of the PCL-TNF microporous meshes, they can be used as a base material for the further development of biomaterials for wound healing applications.

4. Conclusion

In this work, electrospun PCL meshes loaded with various concentrations of TNR were fabricated and characterized. SEM images showed the highly porous and fibrous morphological topography of PCL-TNR meshes. Various physicochemical characterizations such as EDS, XRD, and FTIR analyses confirmed the presence of TNR in PCL meshes. Overall tensile properties of the nanocomposite meshes at optimum TNR content were much higher compared to bare PCL meshes. Fibroblast, epithelial, and keratinocyte cells were able to adhere and proliferate well on the nanocomposite meshes. PCL-TNR-1% and PCL-TNR-2% meshes showed higher cell adhesion and proliferation than other developed samples. The nanocomposite meshes containing 1% and 2% w/w TNR enhanced cell migration and resulted in higher wound contraction in vitro. Both CAM assay and in vivo implantation study demonstrated that TNR containing meshes can enhance angiogenesis in implantation site. In vivo studies in rats demonstrated that TNR loaded PCL meshes provided faster wound healing than the bare PCL meshes. Overall study indicated that PCL-TNR meshes containing about 1–2% w/w TNR can be used for the further development of biodegradable meshes for wound healing applications. However, further investigations on genotoxicity, teratogenicity, and carcinogenicity need to be carried out to rule out the long-term adverse effects of the developed meshes.

Supporting Information

Supporting Information is available from the Wiley Online Library or from the author.

Acknowledgements

This article was made possible by the NPRP9-144-3-021 grant funded by Qatar National Research Fund (a part of Qatar Foundation). The statements made here are totally responsibility of authors.

Conflict of Interest

The authors declare no conflict of interest.

Keywords

angiogenesis, electrospinning, polycaprolactone, TiO₂ nanorods, wound dressings

Received: February 20, 2019

Revised: April 28, 2019

Published online: June 11, 2019

- [1] V. Falanga, *Lancet* **2005**, 366, 1736.
- [2] R. Augustine, A. Augustine, N. Kalarikkal, S. Thomas, *Prog. Biomater.* **2016**, 5, 223.
- [3] R. Rasouli, A. Barhoum, M. Bechelany, A. Dufresne, *Macromol. Biosci.* **2019**, 19, 1800256.
- [4] A. Hasan, R. Waters, B. Roula, R. Dana, S. Yara, T. Alexandre, A. Paul, *Macromol. Biosci.* **2016**, 16, 958.
- [5] I. Jun, H. S. Han, J. R. Edwards, H. Jeon, *Int. J. Mol. Sci.* **2018**, 19, 745.
- [6] A. Hasan, S. Soliman, F. El Hajj, Y. T. Tseng, H. C. Yalcin, H. E. Marei, *Scient. Rep.* **2018**, 8, 8187.
- [7] A. Hasan, A. Memci, N. Annabi, M. Hossain, A. Paul, M. R. Dokmeci, F. Dehghani, A. Khademhosseini, *Acta Biomater.* **2014**, 10, 11.
- [8] A. Hasan, B. Byambaa, M. Morshed, M. I. Cheikh, R. A. Shakoar, T. Mustafy, *J. Tissue. Eng. Regen. Med.* **2018**, 12, 1448.
- [9] P. Zahedi, I. Rezaeian, S. O. Ranaei-Siadat, S. H. Jafari, P. Supaphol, *Adv. Powder Technol.* **2010**, 21, 77.
- [10] R. Ahmed, M. Tariq, I. Ali, R. Asghar, P. Noorunnisa Khanam, R. Augustine, A. Hasan, *Int. J. Biol. Macromol.* **2018**, 120, 385.
- [11] R. Augustine, F. Sarry, N. Kalarikkal, S. Thomas, L. Badie, D. Rouxel, *Nano-Micro Lett.* **2016**, 8, 282.
- [12] S. Jo, S. M. Kang, S. A. Park, W. D. Kim, J. Kwak, H. Lee, *Macromol. Biosci.* **2013**, 13, 1389.
- [13] U. Capasso Palmiero, L. Morosi, M. Lupi, M. Ponzio, R. Frapolli, M. Zucchetti, P. Ubezio, M. Morbidelli, M. D'Incalci, E. Bello, D. Moscatelli, *Macromol. Biosci.* **2018**, 18, 1800164.
- [14] M. S. Kim, I. Jun, Y. M. Shin, W. Jang, S. I. Kim, H. Shin, *Macromol. Biosci.* **2010**, 10, 91.
- [15] R. Augustine, Y. B. Dalvi, V. K. Nath, R. Varghese, V. Raghuvveeran, A. Hasan, S. Thomas, N. Sandhyarani, *Mater. Sci. Eng. C* **2019**, 109801.
- [16] K. Wang, W. Zheng, Y. Pan, S. Ma, Y. Guan, R. Liu, M. Zhu, X. Zhou, J. Zhang, Q. Zhao, Y. Zhu, L. Wang, D. Kong, *Macromol. Biosci.* **2016**, 16, 608.
- [17] C. H. Jang, Y. B. Cho, M. G. Yeo, G. H. Kim, *Macromol. Biosci.* **2013**, 13, 660.
- [18] R. Augustine, E. A. Dominic, I. Reju, B. Kaimal, N. Kalarikkal, S. Thomas, *RSC Adv.* **2014**, 4, 24777.
- [19] R. Augustine, Y. B. Dalvi, P. Dan, N. George, D. Helle, R. Varghese, S. Thomas, P. Menu, N. Sandhyarani, *ACS Biomater. Sci. Eng.* **2018**, 4, 4338.
- [20] R. Augustine, S. K. Nethi, N. Kalarikkal, S. Thomas, C. R. Patra, *J. Mater. Chem. B* **2017**, 5, 4660.
- [21] F. Han, V. S. R. Kambala, M. Srinivasan, D. Rajarathnam, R. Naidu, *Appl. Catal., A* **2009**, 359, 25.
- [22] Y. Hou, K. Cai, J. Li, X. Chen, M. Lai, Y. Hu, Z. Luo, X. Ding, D. Xu, *Int. J. Nanomed.* **2013**, 8, 3619.
- [23] P. Martin, S. J. Leibovich, *Trends Cell Biol.* **2005**, 15, 599.
- [24] X. Zhang, S. Xu, G. Han, *Mater. Lett.* **2009**, 63, 1761.
- [25] A. Othman, A. Karimi, S. Andreescu, *J. Mater. Chem. B* **2016**, 4, 7178.
- [26] J. H. Park, S. Kim, A. J. Bard, *Nano Lett.* **2006**, 6, 24.
- [27] J. Lim, D. Park, S. S. Jeon, C. W. Roh, J. Choi, D. Yoon, M. Park, H. Jung, H. Lee, *Adv. Funct. Mater.* **2018**, 28, 1704796.
- [28] F. Gao, H. Dai, H. Pan, Y. Chen, J. Wang, Z. Chen, *J. Colloid Interface Sci.* **2018**, 513, 693.
- [29] Y. C. Tu, H. Lim, C. Y. Chang, J. J. Shyue, W. F. Su, *J. Colloid Interface Sci.* **2015**, 448, 315.
- [30] Y. Zhang, J. Bai, L. Zhou, D. Liu, F. Liu, X. Liang, Y. Gao, F. Liu, X. Yan, G. Lu, *J. Colloid Interface Sci.* **2019**, 536, 215.
- [31] V. C. Anitha, A. Goswami, H. Sopha, D. Nandan, M. B. Gawande, K. Cepe, S. Ng, R. Zboril, J. M. Macak, *Appl. Mater. Today* **2018**, 10, 86.
- [32] M. J. Jackson, *Free Radical Biol. Med.* **2008**, 44, 132.
- [33] H. M. Kimmel, A. Grant, J. Ditata, *Wounds a Compend. Clin. Res. Pract.* **2016**, 28, 264.
- [34] E. Beltrán-Partida, B. Valdéz-Salas, A. Moreno-Ulloa, A. Escamilla, M. A. Curiel, R. Rosales-Ibáñez, F. Villarreal, D. M. Bastidas, J. M. Bastidas, *J. Nanobiotechnol.* **2017**, 15, 10.
- [35] S. Nandagopal, R. Augustine, S. C. George, V. P. Jayachandran, N. Kalarikkal, S. Thomas, *Polym.-Plast. Technol. Eng.* **2016**, 55, 1785.
- [36] K. Ghosal, A. Manakhov, L. Zajíčková, S. Thomas, *AAPS PharmSciTech* **2017**, 18, 72.
- [37] M. S. deS. B. Monteiro, M. I. B. Tavares, *Adv. Nanopart.* **2018**, 07, 11.
- [38] R. Augustine, H. N. Malik, D. K. Singhal, A. Mukherjee, D. Malakar, N. Kalarikkal, S. Thomas, *J. Polym. Res.* **2014**, 21, 347 (1).
- [39] P. Morouço, S. Biscaia, T. Viana, M. Franco, C. Malça, A. Mateus, C. Moura, F. C. Ferreira, G. Mitchell, N. M. Alves, *Biomed Res. Int.* **2016**, 2016, 1.
- [40] A. E. Al Moustafa, W. D. Foulkes, N. Benlimame, A. Wong, L. Yen, J. Bergeron, G. Batist, L. Alpert, M. A. Alaoui-Jamali, *Oncogene* **2004**, 23, 350.
- [41] R. Augustine, A. Hasan, V. K. Yadu Nath, J. Thomas, A. Augustine, N. Kalarikkal, A. E. Al Moustafa, S. Thomas, *J. Mater. Sci.: Mater. Med.* **2018**, 29, 205.
- [42] Z. Peining, A. S. Nair, Y. Shengyuan, S. Ramakrishna, *Mater. Res. Bull.* **2011**, 46, 588.
- [43] S. H. Yoo, J. M. Kum, G. Ali, S. H. Heo, S. O. Cho, *Nanoscale Res. Lett.* **2012**, 7, 142.
- [44] T. Peng, D. Zhao, K. Dai, W. Shi, K. Hirao, *J. Phys. Chem. B* **2005**, 109, 4947.
- [45] Y. Zhao, C. Li, X. Liu, F. Gu, H. Jiang, W. Shao, L. Zhang, Y. He, *Mater. Lett.* **2007**, 61, 79.
- [46] V. J. Babu, A. S. Nair, Z. Peining, S. Ramakrishna, *Mater. Lett.* **2011**, 65, 3064.
- [47] S. Suphankij, W. Mekprasart, W. Pecharapa, *Energy Procedia* **2013**, 34, 751.
- [48] J. L. Gole, J. D. Stout, C. Burda, Y. Lou, X. Chen, *J. Phys. Chem. B* **2004**, 108, 1230.
- [49] J. A. Rengifo-Herrera, D. A. Marín-Silva, E. Mendoza-Portillo, A. N. Pinotti, L. R. Pizzio, *Mol. Catal.* **2018**, 448, 1.

- [50] T. Elzein, M. Nasser-Eddine, C. Delaite, S. Bistac, P. Dumas, *J. Colloid Interface Sci.* **2004**, 273, 381.
- [51] R. Augustine, N. Kalarikkal, S. Thomas, *Int. J. Polym. Mater. Polym. Biomater.* **2016**, 65, 28.
- [52] R. Augustine, N. Kalarikkal, S. Thomas, *Polym.-Plast. Technol. Eng.* **2016**, 55, 518.
- [53] D. Di Camillo, F. Ruggieri, S. Santucci, L. Lozzi, *J. Phys. Chem. C* **2012**, 116, 18427.
- [54] K. Sowthari, S. A. Suthanthiraraj, *eXPRESS Polym. Lett.* **2013**, 7, 495.
- [55] T. Urushihara, K. Okada, K. Watanabe, A. Toda, E. Tobita, N. Kawamoto, M. Hikosaka, *Polym. J.* **2007**, 39, 55.
- [56] O. Ero-Phillips, M. Jenkins, A. Stamboulis, *Polymers* **2012**, 4, 1331.
- [57] G. Jimenez, N. Ogata, H. Kawai, T. Ogihara, *J. Appl. Polym. Sci.* **1997**, 64, 2211.
- [58] D. Homminga, B. Goderis, I. Dolbnya, H. Reynaers, G. Groeninckx, *Polymer* **2005**, 46, 11359.
- [59] D. M. Lincoln, R. A. Vaia, Z. G. Wang, B. S. Hsiao, *Polymer* **2001**, 42, 1621.
- [60] G. S. Góis, N. C. Nepomuceno, C. H. A. França, Y. M. B. Almeida, E. P. Hernández, J. E. Oliveira, M. P. Oliveira, E. S. Medeiros, A. S. F. Santos, *Polym. Compos.* **2019**, 40, E399.
- [61] M. A. Ashraf, W. Peng, Y. Zare, K. Y. Rhee, *Nanoscale Res. Lett.* **2018**, 13, 212.
- [62] M. Kokabi, M. Sirousazar, Z. M. Hassan, *Eur. Polym. J.* **2007**, 43, 773.
- [63] X. Ma, Y. Zare, K. Y. Rhee, *Nanoscale Res. Lett.* **2017**, 12, 621.
- [64] A. K. Naskar, J. K. Keum, R. G. Boeman, *Nat. Nanotechnol.* **2016**, 11, 1026.
- [65] P. V. AshaRani, G. L. K. Mun, M. P. Hande, S. Valiyaveetil, *ACS Nano* **2009**, 3, 279.
- [66] C. Beer, R. Foldbjerg, Y. Hayashi, D. S. Sutherland, H. Autrup, *Toxicol. Lett.* **2012**, 208, 286.
- [67] R. Wan, Y. Mo, X. Zhang, S. Chien, D. J. Tollerud, Q. Zhang, *Toxicol. Appl. Pharmacol.* **2008**, 233, 276.
- [68] A. S. Yazdi, G. Guarda, N. Riteau, S. K. Drexler, A. Tardivel, I. Couillin, J. Tschopp, *Proc. Natl. Acad. Sci. USA* **2010**, 107, 19449.
- [69] C. M. Nogueira, W. M. de Azevedo, M. L. Zaidan Dagli, S. H. Toma, A. Z. de, A. Leite, M. L. Lordello, I. Nishitokukado, C. L. Ortiz-Agostinho, M. I. Seixas Duarte, M. A. Ferreira, A. M. Sipahi, *World J. Gastroenterol.* **2012**, 18, 4729.
- [70] E. Y. Yang, H. L. Moses, *J. Cell Biol.* **1990**, 111, 731.
- [71] H. L. Moses, E. Y. Yang, J. A. Pietsenpol, *Cell* **1990**, 63, 245.
- [72] K. Osumi, S. Matsuda, N. Fujimura, K. Matsubara, M. Kitago, O. Itano, C. Ogino, N. Shimizu, H. Obara, Y. Kitagawa, *J. Biomed. Mater. Res., Part B* **2017**, 105, 2344.
- [73] P. P. Fu, Q. Xia, H. M. Hwang, P. C. Ray, H. Yu, *J. Food Drug Anal.* **2014**, 22, 64.
- [74] M. Ushio-Fukai, R. W. Alexander, *Mol. Cell. Biochem.* **2004**, 264, 85.
- [75] R. Augustine, E. A. Dominic, I. Reju, B. Kaimal, N. Kalarikkal, S. Thomas, *RSC Adv.* **2014**, 4, 51528.
- [76] R. Augustine, P. Dan, A. Sosnik, N. Kalarikkal, N. Tran, B. Vincent, S. Thomas, P. Menu, D. Rouxel, *Nano Res.* **2017**, 10, 3358.
- [77] R. Augustine, S. K. Nethi, N. Kalarikkal, S. Thomas, C. R. Patra, *J. Mater. Chem. B* **2017**, 5, 4660.
- [78] F. Anjum, N. A. Agabalyan, H. D. Sparks, N. L. Rosin, M. S. Kallos, J. Biernaskie, *Sci. Rep.* **2017**, 7, 10291 (1).
- [79] C. Dunnill, T. Patton, J. Brennan, J. Barrett, M. Dryden, J. Cooke, D. Leaper, N. T. Georgopoulos, *Int. Wound J.* **2017**, 14, 89.
- [80] F. Atashi, A. Modarressi, M. S. Pepper, *Stem Cells Dev.* **2015**, 24, 1150.
- [81] M. I. Setyawati, C. Y. Tay, S. L. Chia, S. L. Goh, W. Fang, M. J. Neo, H. C. Chong, S. M. Tan, S. C. J. Loo, K. W. Ng, J. P. Xie, C. N. Ong, N. S. Tan, D. T. Leong, *Nat. Commun.* **2013**, 4, 1673.
- [82] K. Bhattacharya, M. Davoren, J. Boertz, R. P. F. Schins, E. Hoffmann, E. Dopp, *Part. Fibre Toxicol.* **2009**, 6, 17.

Free volume defects and transport properties of mechanically stable polyhedral oligomeric silsesquioxane embedded poly(vinyl alcohol)-poly(ethylene oxide) blend membranes

Valiya Parambath Swapna,^a Padinharu Madathil Gopalakrishnan Nambissan,^b Selvin P Thomas,^c Abitha Vayyaprontavida Kaliyathan,^d Thomasukutty Jose,^e Soney C George,^e Sabu Thomas^d and Ranimol Stephen^{a*}

Abstract

Polymer membrane based gas transport and pervaporation processes are fast growing areas in separation technology and have received wide attention as areas of 'clean technology'. Mechanically stable novel polyhedral oligomeric silsesquioxane (POSS) embedded poly(vinyl alcohol) (PVA)/poly(ethylene oxide) (PEO) blend membranes were prepared by solution blending followed by casting. The addition of carboxymethyl cellulose enhanced the interfacial activities of the PVA and PEO blends. The peripheral organic substituent on POSS plays a key role in achieving compatibility with polymers whereas the rigid Si–O–Si core of POSS imparts high mechanical strength. Compared to PVA membrane, poly(ethylene glycol) and octa(tetramethylammonium) functionalized POSS embedded PVA/PEO membranes exhibit 680% and 580% enhancement in Young's modulus as well as 130% and 140% improvement in tensile strength respectively. The Einstein, Kerner and Frankel–Acrivos models were applied to compare the experimental and theoretical Young's modulus of PVA-PEO/POSS membranes. The presence of an ethylene oxide tail on POSS as well as PEO in the blend membrane enhances the CO₂ affinity of the membrane. The presence of a hydrophilic functional group on the POSS improves the hydrophilicity of the membrane and produces more binding sites for water molecules in the membrane during the pervaporation separation of a tetrahydrofuran–water azeotropic mixture. The transport properties of the membrane are further elucidated by means of free volume defect analysis carried out by positron annihilation lifetime spectroscopy and coincidence Doppler broadening spectroscopy.

© 2019 Society of Chemical Industry

Keywords: polyvinyl alcohol (PVA); PVA-PEO; pervaporation; THF–water azeotropic mixture; polyhedral oligomeric silsesquioxane (POSS); gas transport; CO₂ selectivity; positron annihilation

INTRODUCTION

In the last few decades, polymer membrane based separation technologies have attracted considerable industrial and research attention as prominent paradigms for gas and liquid mixture separation. Polymer membranes are of considerable interest

* Correspondence to: R Stephen, Department of Chemistry, St Joseph's College (Autonomous), Devagiri, Calicut, Kerala 673 008, India.
E-mail: ranimolstephen@gmail.com



Single phased white light emitting Dy³⁺/Sm³⁺ co-doped CePO₄ nanocrystals for white light applications

S. Sisira¹ · Linju Ann Jacob¹ · Kamal P. Mani¹ · P. R. Biju¹ · N. V. Unnikrishnan¹ · Cyriac Joseph¹

Received: 13 December 2018 / Accepted: 7 May 2019 / Published online: 14 May 2019
© Springer Science+Business Media, LLC, part of Springer Nature 2019

Abstract

Excitation dependent color tunable dysprosium and samarium co-doped cerium phosphate nanocrystals were synthesized via sol gel method. X-ray diffractograms confirmed that all the samples crystallized in monoclinic form. Morphology of the samples resembling a custard apple surface was demonstrated by FESEM analysis. The structural characterization carried out via FTIR and XPS analysis displayed the monoclinic CePO₄ lattice as a good host providing minimum quenching environment. Luminescence characterizations were done in detail as a function of Dy³⁺ and Sm³⁺ doping concentrations by means of photoluminescence spectroscopy. Energy transfer from Ce³⁺ to Dy³⁺ and Sm³⁺ in CePO₄ was established via the analysis of excitation spectra. The possibility of simultaneous activation of Dy³⁺ and Sm³⁺ ions was utilized to generate white light. Excitation dependent luminescence measurements were also carried out to explore the yellow-white-orange-red color tunability of synthesized samples for different excitations. The codoping of Sm³⁺ with Dy³⁺ is found to be more suitable for generating white light with CIE values close to the standard white and stands as a potential candidate in the field of white light applications.

1 Introduction

White light emitting diodes (WLEDs) based on single phased full-color emitting phosphors have attracted much attention in recent years as a possible alternative to the existing lighting technologies owing to their high efficiency [1–3]. Therefore the synthesis and characterization of new single phased white light emitting phosphors is one of the focus tasks in solid state lighting technology. Since rare earth ions are often considered to be excellent activators as they emit over the entire spectral range it cannot be neglected the role of rare earth ions when deals with the single phased white light emitting phosphors [2, 3]. Among various rare earth activated luminescence materials those materials doped with Dy³⁺ have drawn much interest owing to the white emission which is obtained by adjusting the yellow to blue intensity ratio value [4–6]. Therefore, nowadays, many

GdAl₃(BO₃)₄ etc. are some of the materials which are used for the white light generation by doping Dy³⁺ ions [7, 9, 10]. However, due to the scarcity of red component in Dy³⁺ it is very difficult to attain the standard white emission in Dy³⁺ singly doped systems exactly [11, 12]. The possible method to surpass this constraint is the addition of a red component together with the blue and yellow components of Dy³⁺ [11, 12]. Samarium (III) ions emitting strong orange-red/red color are often used to synthesize red emitting materials [13]. Hence Sm³⁺ can be chosen to co-dope with Dy³⁺ to overcome the scarcity of red component for generating white light with high quality.

Among various rare earth based compounds rare earth orthophosphates stand out owing to their wide range of applications in the field of optoelectronics, especially for the fabrication of LEDs [14–16]. LaPO₄, GdPO₄, YPO₄, and CePO₄ are well accepted potential candidates due to



TOPICAL REVIEW

Biomolecular assisted synthesis and mechanism of silver and gold nanoparticles

RECEIVED
12 February 2019REVISED
27 May 2019ACCEPTED FOR PUBLICATION
12 June 2019PUBLISHED
21 June 2019Sreeparna Samanta¹, Shivankar Agarwal^{1,2}, Kishore Kumar Nair^{3,4} , Richard Anthony Harris⁴ and Hendrik Swart⁴¹ TERI-Deakin Nano Biotechnology Centre, The Energy and Resources Institute (TERI), New Delhi—110003, India² Indian Council of Medical Research (ICMR), IJMR Unit, V Ramalingaswami Bhawan, Ansari Nagar-AIIMS, 110029-Delhi, India³ School of Environmental Sciences, Mahatma Gandhi University, Kottayam 686560, India⁴ Department of Physics, University of Free State, Bloemfontein 9300, South AfricaE-mail: sreeparna9@gmail.com and kknair9@gmail.com

Keywords: gold, silver, nanoparticles, plant-mediated synthesis, biomechanism

Abstract

Gold (Au) and silver (Ag) nanoparticles (NPs) are useful nanomaterials. For these NPs various synthesis methods including chemical, physical and biological have been used. Biological methods have some advantages for the synthesis of Au and Ag NPs, such as the use of non-toxic chemicals, lower energy consumption, improved cost effectiveness and stable NP production. A large number of biological methods using culturable micro-organism, including bacteria, fungi and algae as well as plants have been explored as methodology for Au and Ag NP production. Since nanotechnology-based applications require the use of specified shape, size, surface charge and stability of NPs, a major problem associated with biologically synthesized Au and Ag NPs is that these NPs display variability in all these factors. This is a major drawback of biologically synthesized Au and Ag NPs compared to the physico-chemically synthesized NPs. Some organisms exhibit distinct metabolic pathways and produce biological macromolecules that enable them to withstand metal ions stress. Therefore, determining the molecular mechanics involved may enable the control of the shape, size, surface charge and stability of biologically synthesized Au and Ag NPs. This review article focuses on the biomolecular mechanism of Au and Ag NPs synthesis using different biological entities. A comprehensive study of these biomolecular mechanisms of Au and Ag NPs will be helpful for scientists and researchers for the fabrication of desired shape, size, surface charges and stability of Au and Ag NPs.

1. Introduction

Engineered nanoparticles (NPs) open up new horizons to many areas of science and nanotechnology. These engineered nanoparticles gained the attention of many researchers to explore their applications as antibacterial agents, sunscreen, self-cleaning glass, biosensors, paints, electronics, drug delivery tools and many others [1–4]. Noble metal NPs such as silver and gold are one of the most researched subjects due to its remarkable optical and physicochemical properties with wide range of applications in various fields of research. Less toxic and the



Green Silver Nanoparticles Based Multi-Technique Sensor for Environmental Hazardous Cu(II) Ion

Maria Sebastian¹ · Archana Aravind¹ · Beena Mathew¹

Published online: 12 February 2019
© Springer Science+Business Media, LLC, part of Springer Nature 2019

Abstract

In the present work, we report green synthesized unmodified silver nanoparticles from *Moringa oleifera*'s bark extract (AgNP-MO) as multifunctional sensor for hazardous Cu(II) ion with high selectivity. The optical and fluorescent sensing of Cu(II) ion in presence of AgNP-MO was investigated and optimized. The intensity of SPR absorption band of AgNP-MO dramatically reduced with Cu(II) ion concentration as a result of complex formation, and it could be recognized by naked eye with a visual detection. The electrochemical activity of silver nanoparticles was explored for the sensing of Cu(II) ion by AgNP-MO-modified platinum electrode (AgNP-MO/PE). The Cu(II) ion selectivity of the developed system was investigated by both techniques. The applicability of developed electrochemical sensor was checked with water samples collected from Vembanad Lake, Kumarakom, Kottayam, Kerala, and electroplating industry. The limit of detection of a developed sensor for Cu(II) ion detection was found at 0.530 μM . The antibacterial activity of silver nanoparticles from *Moringa oleifera* was checked against with two waterborne bacteria extracted from the same lake water sample. To the best of our knowledge, there are no reports for the electrochemical sensing of Cu(II) ion by AgNP-MO/PE. We expect our present approach to have multifunctional applications in various areas.

Keywords Silver nanoparticle · Cu(II) ion · Optical · Fluorescent · Sensing · Electrochemical

1 Introduction

Among transition metals, Cu(II) ion plays an important role in different physiological processes [1, 2]. Cu(II) ion is the main essential trace metal in our human body and a main component of several enzyme systems [3]. But at higher concentrations, Cu(II) ion produces high toxicity that exhibits neurodegenerative diseases. Results from a number of studies from Europe, Canada, and the USA indicate that copper levels in drinking water can range from ≤ 0.005 to > 30 mg/l [4, 5]. Moreover, overdose produces many health diseases including liver damage [6], cellular toxicity [7], gastrointestinal disturbance, and even kidney damage. There are lots of traditional methods for the detection of Cu(II) ion, which includes mass spectroscopy [8], fluorescent spectroscopy [9], atomic absorption

highly expensive instruments, complicated sample preparations, and much more time.

In this situation, fabricating eco-friendly and high output technique to sense Cu(II) ion with high selectivity has great importance for various applications [11–17]. Nowadays, optical sensors have got great attention in the field of metal ion sensing due to the convenient direct visual observation without any costly instruments [18–26]. Existing optical sensors for Cu(II) ion detection includes dyes like rhodamine B, polymers like IIP (ion imprinted polymer), composites like PMMA poly(methyl methacrylate)/CB (carbon black) etc. But recently, metal nanoparticle-based optical sensors have gotten much more attention because of their unique optical and physical properties [27–30]. Surface plasmon resonance [31] and surface



Surface Plasmon Assisted Luminescence Enhancement of Ag NP/NWs-Doped SiO₂-TiO₂-ZrO₂:Eu³⁺ Ternary System

Prakashan V. P.¹ · Sajna M. S.¹ · Gejo G.¹ · Sanu M. S.¹ · Saritha A. C.¹ · Biju P. R.¹ · Cyriac J.¹ · Unnikrishnan N. V.¹

Received: 3 July 2018 / Accepted: 27 August 2018 / Published online: 10 September 2018
© Springer Science+Business Media, LLC, part of Springer Nature 2018

Abstract

Non-hydrolytic sol-gel process was employed to prepare Eu³⁺-doped and silver nanoparticles/nanowires (Ag NP/NWs) co-doped SiO₂-TiO₂-ZrO₂ ternary matrix. XRD, TEM, and SAED analyses revealed that the matrix is of amorphous nature even the crystalline nanoparticles/nanowires are embedded. The formation of ternary matrix is further evidenced by the characteristic peaks in FTIR spectrum and EDS analysis. The emission intensity is enhanced by sixfold for Ag NPs and eightfold for Ag NWs embedded matrix and is probably due to Surface Plasmon Coupled Emission (SPCE). Above the critical concentration of 1 wt.% Ag NP and 1.5 wt.% Ag NW, the emission intensity starts to diminish because of quenching effects. CIE chromaticity studies confirm that the addition of Ag NP/NWs into Eu³⁺-doped ternary matrix does not alter the color coordinates and purity of the present system. These Eu³⁺-Ag NP/NWs-doped ternary systems could be used as a promising material for efficient red light emitting sources, bio-detection, and plasmonic sensor applications.

Keywords Sol-gel · Surface Plasmon Resonance · Surface Plasmon Coupled Emission · Luminescence

Introduction

Sol-gel-derived optically transparent matrices doped with trivalent rare earths are attaining a great deal of interest among researchers for several years due to their versatile features [1, 2]. Compared to binary oxides of SiO₂, TiO₂, and ZrO₂, the respective ternary oxides have attracted many industrial applications due to their superior properties like increased rates of spectrum intensity, energy transfer, photostability, fluorophore decay rate, and multiphoton excitation [3–6]. In recent years, much more interest has been devoted to enhance the optical properties of these systems by co-doping with other rare earths, transition metals, metal nanoparticles, semiconductor materials, etc. Co-doping of metal nanoparticles with rare-earth ions has received much attention because of its Surface Plasmon Resonance (SPR) effects [7].

The collective oscillations of conduction electrons of noble metal nanoparticles with incident light otherwise referred to as

devices, sensors, surface-enhanced Raman scattering, nanosized optics etc. [8–12]. Recent research has revealed that metallic particles can be structured and characterized at the nanolevel and this in turn has renewed interest in Surface Plasmons [13]. Enhanced local fields and fluorescence may result from the strong incident light scattering by the metal nanoparticles. Among the metallic nanoparticles, silver nanoparticles with a Surface Plasmon Resonance at around 420 nm of the visible spectrum have gained much interest in the past few years. These particles when incorporated into a solid dielectric matrix, the refractive index mismatches between them, which leads to extraordinary optical properties for these materials [14]. By changing the size and shape of nanoparticles as well as the dielectric medium in which the nanoparticle is incorporated, the Localized Surface Plasmon Resonance (LSPR) can be tuned which in turn influences the optical performance of rare-earth-doped systems [11]. Increased energy transfer rate, quantum yield, decrease in life time etc. in the co-

Accepted Manuscript

Administration of probiotic *Paenibacillus polymyxa* HGA4C induces morphometric, enzymatic and gene expression changes in *Oreochromis niloticus*

Sebastian Jose Midhun, Damodaran Arun, Sahadevan Neethu, A. Vysakh, E.K. Radhakrishnan, Mathew Jyothis



PII: S0044-8486(19)30553-8
DOI: <https://doi.org/10.1016/j.aquaculture.2019.04.061>
Reference: AQUA 634095
To appear in: *aquaculture*
Received date: 6 March 2019
Revised date: 22 April 2019
Accepted date: 22 April 2019

Please cite this article as: S.J. Midhun, D. Arun, S. Neethu, et al., Administration of probiotic *Paenibacillus polymyxa* HGA4C induces morphometric, enzymatic and gene expression changes in *Oreochromis niloticus*, *aquaculture*, <https://doi.org/10.1016/j.aquaculture.2019.04.061>

This is a PDF file of an unedited manuscript that has been accepted for publication. As a service to our customers we are providing this early version of the manuscript. The manuscript will undergo copyediting, typesetting, and review of the resulting proof before it is published in its final form. Please note that during the production process errors may be discovered which could affect the content, and all legal disclaimers that apply to the journal pertain.

Administration of probiotic *Paenibacillus polymyxa* HGA4C induces morphometric, enzymatic and gene expression changes in *Oreochromis niloticus*

Sebastian Jose Midhun^a, Damodaran Arun^b, Sahadevan Neethu^a, A. Vysakh^a, E.K.

Radhakrishnan^a, Mathew Jyothis^{a,*}

^a School of Biosciences, Mahatma Gandhi University, Kottayam, India

^b Department of Animal Science, Central University of Kerala, Kasaragod, India

*Corresponding author

Dr. Jyothis Mathew, Professor, School of Biosciences, Mahatma Gandhi University, Kottayam,

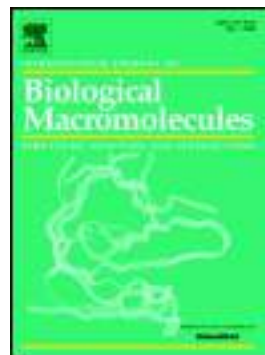
India

Email: prof.dr.jyothismathew@gmail.com

Accepted Manuscript

Novel processing parameters for the extraction of cellulose nanofibres (CNF) from environmentally benign pineapple leaf fibres (PALF): Structure-property relationships

Lakshmipriya Ravindran, M.S. Sreekala, Thomas Sabu



PII: S0141-8130(18)36509-7
DOI: <https://doi.org/10.1016/j.ijbiomac.2019.03.134>
Reference: BIOMAC 11964
To appear in: *International Journal of Biological Macromolecules*
Received date: 27 November 2018
Revised date: 9 February 2019
Accepted date: 20 March 2019

Please cite this article as: L. Ravindran, M.S. Sreekala and T. Sabu, Novel processing parameters for the extraction of cellulose nanofibres (CNF) from environmentally benign pineapple leaf fibres (PALF): Structure-property relationships, *International Journal of Biological Macromolecules*, <https://doi.org/10.1016/j.ijbiomac.2019.03.134>

This is a PDF file of an unedited manuscript that has been accepted for publication. As a service to our customers we are providing this early version of the manuscript. The manuscript will undergo copyediting, typesetting, and review of the resulting proof before it is published in its final form. Please note that during the production process errors may be discovered which could affect the content, and all legal disclaimers that apply to the journal pertain.